516

USNDC-1
EANDC(US)-168"U"
INDC(USA)-43"U"

Reports to...

THE U.S. NUCLEAR DATA COMMITTEE

Meeting at

LOS ALAMOS SCIENTIFIC LABORATORY

23-25 MAY 1972

Compiled by...

H. E. Jackson, Secretary, USNDC

Physics Division

U of C-AUA-USAEC

Argonne National Laboratory

Printed in the United States of America
Available from
National Technical Information Service
U.S. Department of Commerce
5285 Port Royal Road
Springfield, Virginia 22151
Price: Printed Copy $3.00; Microfiche $0.95

REPORTS TO THE U.S. NUCLEAR DATA COMMITTEE

LOS ALAMOS SCIENTIFIC LABORATORY

23—25 MAY 1972

Compiled by

H. E. Jackson, Secretary

USNDC

ARGONNE NATIONAL LABORATORY

PREFACE

The reports in this document were submitted to the United States Nuclear Data Committee (USNDC) at the meeting at Los Alamos, New Mexico, May 23—25, 1972. The reporting laboratories are those having a substantial effort in measuring neutron and nuclear cross sections of relevance to the U. S. applied nuclear energy program. The material contained in these reports is to be regarded as comprised of informal statements of recent developments and preliminary data. Appropriate subjects are listed as follows:

1. Microscopic neutron cross sections relevant to the nuclear energy program, including shielding. Inverse reactions where pertinent are included.

2. Charged particle cross sections, where they are relevant to 1) above, and where relevant to developing and testing nuclear models.

3. Gamma-ray production, radioactive decay, and theoretical developments in nuclear structure which are applicable to nuclear energy programs.

4. Proton and alpha-particle cross sections, at energies of up to 1 GeV, which are of interest to the space program.

These reports cannot be regarded as a complete summary of the nuclear research efforts of the AEC. A number of laboratories, whose research is less programmatically oriented do not submit reports; neither do the submitted reports reflect all the work related to nuclear cross sections in progress at the submitting laboratory. Budgetary limitations have made it mandatory to follow more strictly the subject guidelines described above and therefore to restrict the size of this document.

Persons wishing to make use of these data should contact the individual experimenter for further details. The data which appear in this document should be quoted only by permission of the contributor and should be referenced as private communication, and not by this document number.

This compilation has been produced almost completely from master copies prepared by the individual contributors listed in the Table of Contents. It is a pleasure to acknowledge their help in the preparation of these reports.

H. E. Jackson
Secretary, USNDC
Argonne National Laboratory
Argonne, Illinois 60439

TABLE OF CONTENTS

Recent Reports submitted to the predecessor of the USNDC, the AEC Nuclear Cross Sections Advisory Committee include the following:

November 1971 Meeting at Brookhaven National Laboratory	NCSAC- 42 EANDC(US)-165U INDC(USA)- 36U
May 1971 Meeting at Duke University	NCSAC- 38 EANDC(US)-156U INDC(USA)- 30U
December 1970 Meeting at Lawrence Radiation Laboratory	NCSAC- 33 EANDC(US)-150U INDC(US)- 25U
May 1970 Meeting at Argonne National Laboratory	NCSAC- 31 EANDC(US)-143U INDC(US)- 22U
September 1969 Meeting at Rice University	WASH-1136 EANDC(US)-122U INDC(US)- 14U
April 1969 Meeting at Oak Ridge, Tennessee	WASH-1127 EANDC(US)-120U INDC(US)- 10U
October 1968 Meeting at Columbia University	WASH-1124 EANDC(US)-111U INDC(US)- 9U
April 1968 Meeting at Los Alamos, New Mexico	WASH-1093 EANDC(US)-105U INDC(US)- 2U
October 1967 Meeting at Idaho Falls, Idaho	WASH-1079 EANDC(US)-104U INDC(US)- 12U
April 1967 Meeting at Brookhaven, New York	WASH-1074 EANDC(US)- 99U INDC(US)- 9U

The following is an index to measurements in USNDC-1 pertinent to entries listed in NCSAC-35, "Compilation of Requests for Nuclear Cross Section Measurements", (March 1971). A CINDA-type index, prepared by L. T. Whitehead, of the Division of Technical Information, follows on page vii.

NCSAC-35 REQUEST NO.	MATERIAL	X-SECTION	USNDC-1 PAGE NO.
6	He-3	Total	111
7	He-3	Elastic	114
10	Li-6	Total	175
17	Li-7	Total	119
22	Be	Elastic	232
28,29	B-10	N, alpha	77
31,32,33	C	Elastic	5,166,232
35	C	Total $\bar{g}$ Prod.	144
37	C-12	Polariz	166,234
38,39	N	Elastic	232
43	O	Elastic	142,232
44	O	Emission	142
50	F	Elastic	5
51	F	Emission	5
54	Na	Total	59
59	Na	Reson Params	59
84	V	Elastic	6
85	V	Emission	6
97	Fe	Elastic	6, 167
99	Fe	Emission	6
107	Fe-54	N, Gamma	175
111	Fe-58	N, Gamma	175
118	Ni	Elastic	6
119	Ni	Emission	6
155	Zr	N, Gamma	8, 94
156	Zr	Res. Int	8, 94
253	Sm-152	Res. Int	1
278	Gd-154	$\bar{G}_n$	40
290	Gd-158	$\bar{G}_n$	40
292	Gd-160	$\bar{G}_n$	40

NCSAC-35 REQUEST NO.	MATERIAL	X-SECTION	USNDC-1 PAGE NO.
302	Tm	N, Gamma	94
321	Ta	N, Gamma	94, 176
322	Ta	Total $\bar{g}$ Prod.	144
336	Au	N, Gamma	94, 176
343	Pb-208	N, Gamma	136
362	U-233	Nu bar	183
367	U-233	Res Par	70
387	U-235	Fission	145
387,388,389, 390	U-235	Fission	2,111,145
395	U-235	Nu bar	183
397	U-235	Delay N	2
412	U-238	Elastic	7
413,414	U-238	Emission	7
417	U-238	Fission	2
420	U-238	Delay N	2
421, 422	U-238	N, Gamma	8,94,176
427	U-238	Res Par	67,167
444	Pu-239	Elastic	7
445	Pu-239	Emission	7
453	Pu-239	Delay N	7
464	Pu-240	Fission	175
471	Pu-240	Res Par	175
528	Cf-249	Fission	162
534	Cf-252	Nu	19

ELEMENT S	A	QUANTITY	TYPE	ENERGY MIN	ENERGY MAX	DOCUMENTATION REF	VOL	PAGE	DATE	LAB	COMMENTS	SERIAL NO.
H	001	N,GAMMA	EXPT-PROG	THR		USNDC-1	L23		5/72	NBS	ARNOLD+. SEARCH FOR 2-PHOTON CAPTURE	62675
D	002	GAMMA N	EXPT-PROG	7.0 6	3.0 7	USNDC-1	237		5/72	YAL	FIRK+. NO DATA. NEUT POL. TBP NP	62791
HE	003	TOTAL XSECT	EXPT-PROG		3.0 7	USNDC-1	111		5/72	LAS	SEAGRAVE+. TO BE DONE	62657
HE	003	DIFF ELASTIC	EXPT-PROG	8.0 6	1.2 7	USNDC-1	198		5/72	DKE	LISOWSKI+.POLARIZD NEUTS. NO DATA	62546
HE	003	DIFF ELASTIC	EXPT-PROG	7.9 6	2.4 7	USNDC-1	114		5/72	LAS	DROSG+. ANG DIST SHOWN FOR 5 ES	62659
HE	003	POLARIZATION	EXPT-PROG	8.0 6	1.2 7	USNDC-1	198		5/72	DKE	LISOWSKI+.POLARIZD NEUTS. NO DATA	62545
HE	004	TOTAL XSECT	EXPT-PROG		3.0 7	USNDC-1	111		5/72	LAS	SEAGRAVE+. TO BE DONE	62656
HE	004	TOTAL XSECT	EXPT-PROG	7.0 5	3.0 7	USNDC-1	175		5/72	RPI	GOULDING+. TO BE COMPLETED.NO DATA	62734
HE	004	DIFF ELASTIC	EVAL-PROG		2.0 7	USNDC-1	195		5/72	DKE	STAMMBACH+.NO DATA.SEE NP A180 225	62755
HE	004	POLARIZATION	EVAL-PROG		2.0 7	USNDC-1	195		5/72	DKE	STAMMBACH+.NO DATA.SEE NP A180 225	62756
LI	006	TOTAL XSECT	EXPT-PROG	7.0 5	3.0 7	USNDC-1	175		5/72	RPI	GOULDING+. ANAL TBC. NO DATA GIVEN	62733
LI	007	TOTAL XSECT	EVAL-PROG	5.0 5	2.5 7	USNDC-1	119		5/72	LAS	BATTAT+.NO DATA GIVN.TBP LA-4851	62664
B	010	DIFF ELASTIC	EXPT-PROG	1.4 6	4.8 6	USNDC-1	164		5/72	OHO	HAUSLADEN+. TBC. NO DATA GIVEN	62725
B	010	DIFF ELASTIC	EXPT-PROG	2.6 6		USNDC-1	165		5/72	OHO	COX+.18-123DEG C-M. TABLE	62726
B	010	POLARIZATION	EXPT-PROG	2.6 6		USNDC-1	165		5/72	OHO	COX+.18-123DEG C-M. TABLE	62727
B	010	N,ALPHA	EXPT-PROG	1.0 3	1.0 6	USNDC-1	77		5/72	GA	FRIESENHAHN+. LINAC. NO DATA GIVEN	62564
B	011	DIFF ELASTIC	EXPT-PROG	2.2 6	5.0 6	USNDC-1	163		5/72	OHO	NELSON+. 20-160DEG. TBC. NO DATA GVN	62724
C		TOTAL XSECT	EXPT-PROG	4.0 3	2.0 6	USNDC-1	121		5/72	NBS	MENKE+. PRELIMINARY MEAST.NO DATA	62673
C		TOTAL XSECT	EXPT-PROG	1.5 6	3.5 6	USNDC-1	5		5/72	ANL	SMITH+. NO DATA GIVEN	62779
C		DIFF ELASTIC	EXPT-PROG	6		USNDC-1	83		5/72	GA	HARRIS+. INTEGRAL EXPT IN PROGR.NDG	62562
C		DIFF ELASTIC	EXPT-PROG	1.5 6	3.5 6	USNDC-1	5		5/72	ANL	SMITH+. NO DATA GIVEN	62780
C		DIFF ELASTIC	EXPT-PROG	7.4 6	9.5 6	USNDC-1	232		5/72	ABD	BUCHER+. 2.7-150EG. 6ES. TABLE	62786
C		NONEL GAMMAS	EXPT-PROG	6		USNDC-1	83		5/72	GA	HARRIS+. INTEGRAL EXPT IN PROGR.NDG	62563
C		NONEL GAMMAS	EXPT-PROG	7.0 3	2.0 7	USNDC-1	144		5/72	ORL	MORGAN+. NO DATA. SEE ORNL-TM-3702	62752
C	012	DIFF ELASTIC	EXPT-PROG	2.6 6		USNDC-1	166		5/72	OHO	KNOX+. TABLE PHASE SHIFTS	62728
C	012	DIFF ELASTIC	EXPT-PROG	2.0 6	5.0 6	USNDC-1	234		5/72	YAL	FIRK+. DIFF POL 30-150DEG CURVES	62790
C	012	POLARIZATION	EXPT-PROG	2.6 6		USNDC-1	166		5/72	OHO	KNOX+. NO DATA GIVEN	62729
C	012	POLARIZATION	EXPT-PROG	2.0 6	5.0 6	USNDC-1	234		5/72	YAL	FIRK+. DIFF POL 30-150DEG CURVES	62789
N		DIFF ELASTIC	EXPT-PROG	6		USNDC-1	83		5/72	GA	HARRIS+. INTEGRAL EXPT IN PROGR.NDG	62561
N		DIFF ELASTIC	EXPT-PROG	7.4 6	9.5 6	USNDC-1	232		5/72	ABD	BUCHER+. 2.7-150EG. 6ES. TABLE	62787
N		NONEL GAMMAS	EXPT-PROG	6		USNDC-1	83		5/72	GA	HARRIS+. INTEGRAL EXPT IN PROGR.NDG	62560
O		DIFF ELASTIC	EXPT-PROG	4.3 6	8.6 6	USNDC-1	142		5/72	ORL	KINNEY+. ANG DIST GVN.SEE ORNLTM4780	62750
O		DIFF ELASTIC	EXPT-PROG	7.4 6	9.5 6	USNDC-1	232		5/72	ABD	BUCHER+. 2.7-150EG. 6ES. TABLE	62788
O		DIFF INELAST	EXPT-PROG	4.3 6	8.6 6	USNDC-1	142		5/72	ORL	KINNEY+. NO DATA GVN.SEE ORNL-TM4780	62751
O	016	TOTAL XSECT	EXPT-PROG	2.0 5	5.8 6	USNDC-1	132		5/72	ORL	JOHNSON+. R-MATRIX PARAMS. CURVE	62736
O	016	RESON PARAMS	EXPT-PROG	1.7 6		USNDC-1	132		5/72	ORL	GALLOWAY+. EO#1651+-1 KEV	62737
F	019	TOTAL XSECT	EXPT-PROG	1.0 5	1.5 6	USNDC-1	5		5/72	ANL	SMITH+. MEASTS COMPLETE. NO DATA GVN	62705
F	019	DIFF ELASTIC	EXPT-PROG	1.0 5	1.5 6	USNDC-1	5		5/72	ANL	SMITH+. MEASTS COMPLETE. NO DATA GVN	62706
F	019	DIFF INELAST	EXPT-PROG	1.0 5	1.5 6	USNDC-1	5		5/72	ANL	SMITH+. MEASTS COMPLETE. NO DATA GVN	62707
NA	023	TOTAL XSECT	EXPT-PROG	1.0 1	3.6 5	USNDC-1	59		5/72	COL	RAHN+. TRANS. CURVE SHOWN	62601
NA	023	RESON PARAMS	EXPT-PROG	2.8 3	5.3 4	USNDC-1	59		5/72	COL	RAHN+. 2RESON. J L WT VALUES GIVEN	62602
NA	023	NONEL GAMMAS	EXPT-PROG	4.8 6	7.5 6	USNDC-1	144		5/72	ORL	DICKENS. NO DATA.SEE ORNL-TM-3737	62754
SI	028	TOTAL XSECT	EVAL-PROG	1.5 6	2.0 6	USNDC-1	191		5/72	DKE	CHOI+. R-MATRIX ANAL NBS DATA. CURVE	62759
CL	036	SPECT NGAMMA	EXPT-PROG	THR		USNDC-1	18		5/72	ANL	THOMAS+. ABSOL GAMMA INTENSITY MEASD	62645
CA	040	RESON PARAMS	EXPT-PROG	2.0 4	2.9 5	USNDC-1	59		5/72	COL	RAHN+. L J WN GIVN FOR 9 RESON	62604
CA	040	STRNTH FNCTN	EXPT-PROG	2.0 4	2.9 5	USNDC-1	59		5/72	COL	RAHN+. SO AND S1 VALUES GIVEN	62606
CA	044	RESON PARAMS	EXPT-PROG	1.1 4	1.0 5	USNDC-1	59		5/72	COL	RAHN+. L J WN GIVN FOR 4RESON	62605
CA	044	STRNTH FNCTN	EXPT-PROG	1.1 4	1.0 5	USNDC-1	59		5/72	COL	RAHN+. SO AND S1 VALUES GIVEN	62607

ELEMENT S A	QUANTITY	TYPE	ENERGY MIN	ENERGY MAX	DOCUMENTATION REF VOL PAGE DATE	LAB	COMMENTS	SERIAL NO.
TI	TOTAL XSECT	EXPT-PROG	1.0 5	3.0 6	USNDC-1 5 5/72	ANL	SMITH+. ANAL TO BE COMPLETED.NO DATA	62708
TI	DIFF ELASTIC	EXPT-PROG	1.0 5	3.0 6	USNDC-1 5 5/72	ANL	SMITH+. ANAL TO BE COMPLETED.NO DATA	62709
TI	DIFF INELAST	EXPT-PROG	1.0 5	3.0 6	USNDC-1 5 5/72	ANL	SMITH+. ANAL TO BE COMPLETED.NO DATA	62710
V	DIFF ELASTIC	EXPT-PROG	1.5 6	3.0 6	USNDC-1 6 5/72	ANL	SMITH+. NEW VALUES AVAILABLE. NDG	62711
V	DIFF INELAST	EXPT-PROG	1.5 6	3.0 6	USNDC-1 6 5/72	ANL	SMITH+. NEW VALUES AVAILABLE. NDG	62712
CR 051	SPECT NGAMMA	EXPT-PROG	THR		USNDC-1 18 5/72	ANL	THOMAS+. ABSOL GAMMA INTENSITY MEASD	62642
CR 053	SPECT NGAMMA	EXPT-PROG	THR		USNDC-1 18 5/72	ANL	THOMAS+. ABSOL GAMMA INTENSITY MEASD	62643
CR 054	SPECT NGAMMA	EXPT-PROG	THR		USNDC-1 18 5/72	ANL	THOMAS+. ABSOL GAMMA INTENSITY MEASD	62644
FE	TOTAL XSECT	EXPT-PROG	2.4 4		USNDC-1 178 5/72	RPI	BLOCK+.ARMCO IRON. TRANS. CURVE	62792
FE	DIFF ELASTIC	EXPT-PROG	1.5 6	3.8 6	USNDC-1 6 5/72	ANL	SMITH+. MEASTS COMPLETE. NO DATA GVN	62713
FE	DIFF ELASTIC	EXPT-PROG	1.0 4	6.0 5	USNDC-1 167 5/72	RPI	ZUHR+. 6ANGS 45-60DEG.10PC RSLN.CRVS	62730
FE	SCATTERING	EXPT-PROG	2.2 5	6.0 5	USNDC-1 167 5/72	RPI	ZUHR+. 8ES.6ANGS. 10PC RESOL. CURVES	62732
FE	DIFF INELAST	EXPT-PROG	1.5 6	3.8 6	USNDC-1 6 5/72	ANL	SMITH+. MEASTS COMPLETE. NO DATA GVN	62714
FE 054	N,GAMMA	EXPT-PROG	8.0 3	3.0 4	USNDC-1 175 5/72	RPI	HOCKENBURY+. CAPT YLD. NO DATA GIVEN	62557
FE 058	N,GAMMA	EXPT-PROG	NDG		USNDC-1 175 5/72	RPI	HOCKENBURY+. NO DATA GIVEN.	62802
CO 059	TOTAL XSECT	EXPT-PROG	3.0 5	1.5 7	USNDC-1 105 5/72	LOK	FISHER+. POLARZD TARGET.TO BE DONE	62654
CO 059	DIFF ELASTIC	EXPT-PROG	1.5 6	3.0 6	USNDC-1 6 5/72	ANL	SMITH+. RESULTS AVAILBL.NO DATA GIVN	62715
CO 059	DIFF INELAST	EXPT-PROG	1.5 6	3.0 6	USNDC-1 6 5/72	ANL	SMITH+. RESULTS AVAILBL.NO DATA GIVN	62716
NI	DIFF ELASTIC	EXPT-PROG	1.5 6	3.0 6	USNDC-1 6 5/72	ANL	SMITH+. RESULTS AVAILBL.NO DATA GIVN	62717
NI	DIFF INELAST	EXPT-PROG	1.5 6	3.0 6	USNDC-1 6 5/72	ANL	SMITH+. RESULTS AVAILBL.NO DATA GIVN	62718
NI 061	N,GAMMA	EXPT-PROG	NDG		USNDC-1 175 5/72	RPI	HOCKENBURY+. NO DATA GIVEN.	62801
NI 064	N,GAMMA	EXPT-PROG	NDG		USNDC-1 175 5/72	RPI	HOCKENBURY+. NO DATA GIVEN.	62800
NI 064	SPECT NGAMMA	EXPT-PROG	THR		USNDC-1 36 5/72	BNL	COCHAVI+. CORRELATN WITH (D,P) REACT	62573
CU	TOTAL XSECT	EXPT-PROG	2.5 3	6.0 4	USNDC-1 59 5/72	COL	RAHN+. TRANSMISSION. CURVES	62603
CU	DIFF ELASTIC	EXPT-PROG	1.5 6	3.0 6	USNDC-1 6 5/72	ANL	SMITH+. RESULTS AVAILBL.NO DATA GIVN	62719
CU	DIFF INELAST	EXPT-PROG	1.5 6	3.0 6	USNDC-1 6 5/72	ANL	SMITH+. RESULTS AVAILBL.NO DATA GIVN	62720
GE 072	DIFF INELAST	EXPT-PROG	NDG		USNDC-1 6 5/72	ANL	SMITH+. SIGS FOR 691KEV 0+ LVL. NDG	62544
SR	TOTAL XSECT	EVAL-PROG	NDG		USNDC-1 191 5/72	DKE	MALAN+. NO DATA GIVEN	62757
SR	RESON PARAMS	EVAL-PROG		8.5 5	USNDC-1 191 5/72	DKE	MALAN+. NO DATA GIVEN	62758
Y 089	DIFF ELASTIC	EXPT-PROG	8.0 5	1.4 6	USNDC-1 10 5/72	ANL	ELWYN+. WEAK STRUCTURE SEEN	62635
Y 089	POLARIZATION	EXPT-PROG	8.0 5	1.4 6	USNDC-1 10 5/72	ANL	ELWYN+. NO DATA GIVEN	62636
Y 089	N,GAMMA	EXPT-PROG	1.0 2	1.0 6	USNDC-1 94 5/72	LRL	CZIRR+. TO BE COMPLETED. NO DATA GVN	62549
ZR	N,GAMMA	EXPT-PROG	1.0 2	1.0 6	USNDC-1 94 5/72	LRL	CZIRR+. TO BE COMPLETED. NO DATA GVN	62552
ZR	N,GAMMA	EXPT-PROG	4.0 5	1.5 6	USNDC-1 8 5/72	ANL	POENITZ. SCINT TANK.ANAL TBC. NDG	62684
ZR 091	RESON PARAMS	EXPT-PROG	1.8 2	1.5 3	USNDC-1 141 5/72	ORL	MUGHABGHAB+. J VALUES FOR 7 RESCN	62748
NB 093	RESON PARAMS	EXPT-PROG	3.6 1	9.4 1	USNDC-1 25 5/72	BNL	CHRIEN+.CHANNEL SPIN ADMIXT.TBL+CURV	62631
NB 093	RESON PARAMS	EXPT-PROG	PILE		USNDC-1 18 5/72	ANL	BOLLINGER+.SPIN-CUTOFF PARAM MEAST	62639
NB 093	N,GAMMA	EXPT-PROG	4.0 5	1.5 6	USNDC-1 8 5/72	ANL	POENITZ. SCINT TANK.ANAL TBC. NDG	62682
NB 093	SPECT NGAMMA	EXPT-PROG	PILE		USNDC-1 18 5/72	ANL	BOLLINGER+.SPIN-CUTOFF PARAM MEAST	62638
MO	N,GAMMA	EXPT-PROG	4.0 5	1.5 6	USNDC-1 8 5/72	ANL	POENITZ. SCINT TANK.ANAL TBC. NDG	62683
MO 092	TOTAL XSECT	EXPT-PROG	3.0 5	1.5 6	USNDC-1 7 5/72	ANL	SMITH+. NO DATA GIVEN. TBP	62688
MO 092	RESON PARAMS	EXTH-PROG		2.5 4	USNDC-1 27 5/72	BNL	WASSON+. VALENCE MODEL CFD XPT. CRVS	62632
MO 092	RESON PARAMS	EXPT-PROG		1.0 5	USNDC-1 134 5/72	ORL	WASSON+. CAPT+TRANS MEASTS.NO DATA	62739
MO 092	RESON PARAMS	EXPT-PROG		1.6 4	USNDC-1 136 5/72	ORL	SLAUGHTER+. 17RESON SEEN FROM CAPT.	62747
MO 092	DIFF ELASTIC	EXPT-PROG	3.0 5	1.5 6	USNDC-1 7 5/72	ANL	SMITH+. NO DATA GIVEN. TBP	62689
MO 092	DIFF INELAST	EXPT-PROG	3.0 5	1.5 6	USNDC-1 7 5/72	ANL	SMITH+. NO DATA GIVEN. TBP	62690
MO 092	SPECT NGAMMA	EXTH-PROG		1.0 5	USNDC-1 27 5/72	BNL	WASSON+. VALENCE MODEL CFD XPT. CRVS	62633
MO 092	SPECT NGAMMA	EXPT-PROG	6.0 3	5.0 4	USNDC-1 134 5/72	ORL	WASSON+. GAMM YLD CURVES GIVEN	62738

ELEMENT S	A	QUANTITY	TYPE	ENERGY MIN	ENERGY MAX	DOCUMENTATION REF	VOL	PAGE	DATE	LAB	COMMENTS	SERIAL NO.
MO	092	SPECT NGAMMA	EXPT-PROG	1.0 1	1.0 5	USNDC-1	136		5/72	ORL	SLAUGHTER+. GE(LI) DET. LINAC. NDG	62746
MO	094	TOTAL XSECT	EXPT-PROG	3.0 5	1.5 6	USNDC-1	7		5/72	ANL	SMITH+. NO DATA GIVEN. TBP	62691
MO	094	DIFF ELASTIC	EXPT-PROG	3.0 5	1.5 6	USNDC-1	7		5/72	ANL	SMITH+. NO DATA GIVEN. TBP	62692
MO	094	DIFF INELAST	EXPT-PROG	3.0 5	1.5 6	USNDC-1	7		5/72	ANL	SMITH+. NO DATA GIVEN. TBP	62693
MO	096	TOTAL XSECT	EXPT-PROG	3.0 5	1.5 6	USNDC-1	7		5/72	ANL	SMITH+. NO DATA GIVEN. TBP	62694
MO	096	DIFF ELASTIC	EXPT-PROG	3.0 5	1.5 6	USNDC-1	7		5/72	ANL	SMITH+. NO DATA GIVEN. TBP	62695
MO	096	DIFF INELAST	EXPT-PROG	3.0 5	1.5 6	USNDC-1	7		5/72	ANL	SMITH+. NO DATA GIVEN. TBP	62696
MO	098	TOTAL XSECT	EXPT-PROG	3.0 5	1.5 6	USNDC-1	7		5/72	ANL	SMITH+. NO DATA GIVEN. TBP	62697
MO	098	DIFF ELASTIC	EXPT-PROG	3.0 5	1.5 6	USNDC-1	7		5/72	ANL	SMITH+. NO DATA GIVEN. TBP	62698
MO	098	DIFF INELAST	EXPT-PROG	3.0 5	1.5 6	USNDC-1	7		5/72	ANL	SMITH+. NO DATA GIVEN. TBP	62699
MO	100	TOTAL XSECT	EXPT-PROG	3.0 5	1.5 6	USNDC-1	7		5/72	ANL	SMITH+. NO DATA GIVEN. TBP	62700
MO	100	DIFF ELASTIC	EXPT-PROG	3.0 5	1.5 6	USNDC-1	7		5/72	ANL	SMITH+. NO DATA GIVEN. TBP	62701
MO	100	DIFF INELAST	EXPT-PROG	3.0 5	1.5 6	USNDC-1	7		5/72	ANL	SMITH+. NO DATA GIVEN. TBP	62702
PD		TOTAL XSECT	EXPT-PROG	3.0 5	1.5 6	USNDC-1	6		5/72	ANL	SMITH+. NO DATA GIVN. TBP	62721
PD		DIFF ELASTIC	EXPT-PROG	3.0 5	1.5 6	USNDC-1	6		5/72	ANL	SMITH+. NO DATA GIVN. TBP	62722
PD		DIFF INELAST	EXPT-PROG	3.0 5	1.5 6	USNDC-1	6		5/72	ANL	SMITH+. NO DATA GIVN. TBP	62723
PD	108	RESON PARAMS	EXPT-PROG	3.0 0		USNDC-1	38		5/72	BNL	MUGHABGHAB+. RESON#P3/2	62609
PD	108	SPECT NGAMMA	EXPT-PROG	3.0 0		USNDC-1	38		5/72	BNL	MUGHABGHAB+. RESON#P3/2	62608
CD		N,GAMMA	EXPT-PROG	4.0 5	1.5 6	USNDC-1	8		5/72	ANL	POENITZ. SCINT TANK.ANAL TBC. NDG	62686
CD	110	TOTAL XSECT	EXPT-PROG	NDG		USNDC-1	40		5/72	COL	RAINWATER+. ANAL TO BE COMPL.NO DATA	62611
CD	111	RESON PARAMS	EXPT-PROG	2.7 2	1.0 4	USNDC-1	134		5/72	ORL	WASSON+. CAPT MEAST. LINAC. NO DATA	62741
CD	111	N,GAMMA	EXPT-PROG	2.7 2	1.0 4	USNDC-1	134		5/72	ORL	WASSON+. LINAC. NO DATA GIVEN	62740
CD	112	TOTAL XSECT	EXPT-PROG	NDG		USNDC-1	40		5/72	COL	RAINWATER+. ANAL TO BE COMPL.NO DATA	62612
CD	114	TOTAL XSECT	EXPT-PROG	NDG		USNDC-1	40		5/72	COL	RAINWATER+. ANAL TO BE COMPL.NO DATA	62613
CD	116	TOTAL XSECT	EXPT-PROG	NDG		USNDC-1	40		5/72	COL	RAINWATER+. ANAL TO BE COMPL.NO DATA	62614
IN		N,GAMMA	EXPT-PROG	1.0 2	1.0 6	USNDC-1	94		5/72	LRL	CZIRR+. TO BE COMPLETED. NO DATA GVN	62553
IN		N,GAMMA	EXPT-PROG	2.4 4		USNDC-1	176		5/72	RPI	BLOCK+.LINAC.TOF.FE-FILTERED BEAM	62795
TE		SPECT NGAMMA	EXPT-PROG		3	USNDC-1	30		5/72	BNL	MUGHABGHAB+. P-WAVE RESON CAPT. CURV	62582
TE	126	RESON PARAMS	EXPT-PROG		3	USNDC-1	30		5/72	BNL	MUGHABGHAB+. P-WAVE RESON FROM CAPT	62580
TE	128	RESON PARAMS	EXPT-PROG		3	USNDC-1	30		5/72	BNL	MUGHABGHAB+. P-WAVE RESON FROM CAPT	62581
TE	130	RESON PARAMS	EXPT-PROG		3	USNDC-1	30		5/72	BNL	MUGHABGHAB+. P-WAVE RESON FROM CAPT	62579
BA	130	RES INT ABS	EXPT-PROG	2.0 1	3.0 3	USNDC-1	95		5/72	LRL	BROWNE+. LINAC. VALUE GIVEN	62651
BA	130	N,GAMMA	EXPT-PROG	2.0 1	3.0 3	USNDC-1	95		5/72	LRL	BROWNE+. LINAC. CURVES	62650
LA	139	RESON PARAMS	EXPT-PROG	1.0 4	2.1 4	USNDC-140			5/72	COL	RAINWATER+. G*WN GIVN FOR 29 RESON	62599
LA	139	STRNTH FNCTN	EXPT-PROG	1.0 4	2.1 4	USNDC-140			5/72	COL	RAINWATER+. SO VALUE GIVEN	62600
CE	140	TOTAL XSECT	EXPT-PROG	NDG		USNDC-1	40		5/72	COL	RAINWATER+. ANAL TO BE COMPL.NO DATA	62617
ND	150	SPECT NGAMMA	EXPT-PROG	THR		USNDC-1	118		5/72	LAS	SMITH+. NO DATA GIVEN	62660
PM	147	N,GAMMA	EXPT-PROG	PILE		USNDC-1	1		5/72	AGN	HARKER+. CFRMF MEAST. VALUE GIVEN	62771
SM	144	SPECT NGAMMA	EXPT-PROG	PILE		USNDC-1	19		5/72	ANL	SMITHER+. NO DATA GIVEN	62625
SM	147	RESON PARAMS	EXPT-PROG	3.4 0		USNDC-1	36		5/72	BNL	GELLETLY+. J PI GIVEN FROM CAPT	62575
SM	147	SPECT NGAMMA	EXPT-PROG	3.4 0		USNDC-1	36		5/72	BNL	GELLETLY+. SM148 LEVELS	62574
SM	148	SPECT NGAMMA	EXPT-PROG	PILE		USNDC-1	19		5/72	ANL	SMITHER+. NO DATA GIVEN	62626
SM	149	SPECT NGAMMA	EXPT-PROG	4.0-3	9.8-2	USNDC-1	37		5/72	BNL	KANE+. HIGH-E GAMMAS. NO DATA GIVEN	62576
SM	150	SPECT NGAMMA	EXPT-PROG	PILE		USNDC-1	19		5/72	ANL	SMITHER+. SM151 LVLS SHOWN	62627
SM	152	N,GAMMA	EXPT-PROG	PILE		USNDC-1	1		5/72	AGN	HARKER+. CFRMF MEAST. VALUE GIVEN	62769
SM	152	SPECT NGAMMA	EXPT-PROG	PILE		USNDC-1	19		5/72	ANL	SMITHER+. CURVES	62628
SM	154	N,GAMMA	EXPT-PROG	PILE		USNDC-1	1		5/72	AGN	HARKER+. CFRMF MEAST. VALUE GIVEN	62770
SM	154	SPECT NGAMMA	EXPT-PROG	PILE		USNDC-1	19		5/72	ANL	SMITHER+. NO DATA GIVEN	62629

ELEMENT S	A	QUANTITY	TYPE	ENERGY MIN	ENERGY MAX	DOCUMENTATION REF	VOL	PAGE	DATE	LAB	COMMENTS	SERIAL NO.
EU	151	SPECT NGAMMA	EXPT-PROG	4.0-3	4.6-1	USNDC-1	37		5/72	BNL	KANE+. HIGH-E GAMMAS. NO DATA GIVEN	62577
GD	154	RESON PARAMS	EXPT-PROG	1.2 1	9.9 2	USNDC-1	40		5/72	COL	RAINWATER+. TRANS. WN WG GIVEN	62676
GD	154	STRNTH FNCTN	EXPT-PROG	1.2 1	9.9 2	USNDC-1	40		5/72	COL	RAINWATER+. SO VALUE GIVEN	62591
GD	158	RESON PARAMS	EXPT-PROG	2.2 1	1.0 4	USNDC-1	40		5/72	COL	RAINWATER+. TRANS. WN WG AVG D GIVEN	62677
GD	158	STRNTH FNCTN	EXPT-PROG	1.2 1	9.9 2	USNDC-1	40		5/72	COL	RAINWATER+. SO VALUE GIVEN	62592
GD	160	RESON PARAMS	EXPT-PROG	2.2 2	9.9 3	USNDC-1	40		5/72	COL	RAINWATER+. TRANS. WN WG AVG D GIVEN	62678
GD	160	STRNTH FNCTN	EXPT-PROG	1.2 1	9.9 2	USNDC-1	40		5/72	COL	RAINWATER+. SO VALUE GIVEN	62593
DY	160	TOTAL XSECT	EXPT-PROG	NDG		USNDC-1	40		5/72	COL	RAINWATER+. ANAL TO BE COMPL.NO DATA	62618
DY	160	RESON PARAMS	EXPT-PROG	NDG		USNDC-1	40		5/72	COL	RAINWATER+. ANAL TBC. NO DATA GIVEN	62594
DY	161	TOTAL XSECT	EXPT-PROG	NDG		USNDC-1	40		5/72	COL	RAINWATER+. ANAL TO BE COMPL.NO DATA	62619
DY	161	RESON PARAMS	EXPT-PROG	NDG		USNDC-1	40		5/72	COL	RAINWATER+. ANAL TBC. NO DATA GIVEN	62597
DY	162	TOTAL XSECT	EXPT-PROG	NDG		USNDC-1	40		5/72	COL	RAINWATER+. ANAL TO BE COMPL.NO DATA	62620
DY	162	RESON PARAMS	EXPT-PROG	NDG		USNDC-1	40		5/72	COL	RAINWATER+. ANAL TBC. NO DATA GIVEN	62595
DY	162	N,GAMMA	EXPT-PROG	THR	3.0 2	USNDC-1	24		5/72	BNL	COLE+. DIRECT CAPT. NO DATA. TBC	62630
DY	163	TOTAL XSECT	EXPT-PROG	NDG		USNDC-1	40		5/72	COL	RAINWATER+. ANAL TO BE COMPL.NO DATA	62621
DY	163	RESON PARAMS	EXPT-PROG	0	2	USNDC-1	28		5/72	BNL	SLAUGHTER+.SEARCH FOR WIDTH CORRELAT	62583
DY	163	RESON PARAMS	EXPT-PROG	NDG		USNDC-1	40		5/72	COL	RAINWATER+.GAMMA GVN FOR 106EV DOUBLT	62598
DY	163	RESON PARAMS	EXPT-PROG	1.6 1	2.5 2	USNDC-1	141		5/72	ORL	SLAUGHTER+. J VALUES FOR 29 RESCN	62749
DY	163	SPECT NGAMMA	EXPT-PROG	0	2	USNDC-1	28		5/72	BNL	SLAUGHTER+. RESON CAPT.WIDTH CORRELT	62634
DY	164	TOTAL XSECT	EXPT-PROG	NDG		USNDC-1	40		5/72	COL	RAINWATER+. ANAL TO BE COMPL.NO DATA	62622
DY	164	RESON PARAMS	EXPT-PROG	NDG		USNDC-1	40		5/72	COL	RAINWATER+. ANAL TBC. NO DATA GIVEN	62596
HO	165	N,GAMMA	EXPT-PROG	1.6 2	1.0 6	USNDC-1	94		5/72	LRL	CZIRR+. TO BE COMPLETED. NO DATA GVN	62547
HO	165	N,GAMMA	EXPT-PROG	4.0 5	1.5 6	USNDC-1	8		5/72	ANL	POENITZ. SCINT TANK.ANAL TBC. NDG	62685
TM	169	N,GAMMA	EXPT-PROG	1.0 2	1.0 6	USNDC-1	94		5/72	LRL	CZIRR+. TO BE COMPLETED. NO DATA GVN	62554
LU		N,GAMMA	EXPT-PROG	1.0 2	1.0 6	USNDC-1	94		5/72	LRL	CSIRR+. TO BE COMPLETED. NO DATA GVN	62555
LU		N,GAMMA	EXPT-PROG	1.0 2	1.0 6	USNDC-1	94		5/72	LRL	CZIRR+. TO BE COMPLETED. NO DATA GVN	62556
TA	181	TOTAL XSECT	EXPT-PROG	NDG		USNDC-1	40		5/72	COL	RAINWATER+. ANAL TO BE COMPL.NO DATA	62623
TA	181	NONEL GAMMAS	EXPT-PROG	7.0 3	2.0 7	USNDC-1	144		5/72	ORL	MORGAN+. NO DATA. SEE ORNL-TM-3702	62753
TA	181	N,GAMMA	EXPT-PROG	1.0 2	1.0 6	USNDC-1	94		5/72	LRL	CZIRR+. TO BE COMPLETED. NO DATA GVN	62551
TA	181	N,GAMMA	EXPT-PROG	2.4 4		USNDC-1	176		5/72	RPI	BLOCK+.LINAC.TOF.FE-FILTERED BEAM	62794
W		TOTAL XSECT	EVAL-PROG	2.0 4	2.2 7	USNDC-1	120		5/72	LAS	DEVANEY+. NO DATA GVN. TBP LA-4928	62665
W	182	TOTAL XSECT	EVAL-PROG	2.0 4	2.2 7	USNDC-1	120		5/72	LAS	DEVANEY+. NO DATA GVN. TBP LA-4928	62667
W	183	TOTAL XSECT	EVAL-PROG	2.0 4	2.2 7	USNDC-1	120		5/72	LAS	DEVANEY+. NO DATA GVN. TBP LA-4928	62666
W	184	TOTAL XSECT	EVAL-PROG	2.0 4	2.2 7	USNDC-1	120		5/72	LAS	DEVANEY+. NO DATA GVN. TBP LA-4928	62668
W	186	TOTAL XSECT	EVAL-PROG	2.0 4	2.2 7	USNDC-1	120		5/72	LAS	DEVANEY+. NO DATA GVN. TBP LA-4928	62669
RE	188	SPECT NGAMMA	EXPT-PROG	THR		USNDC-1	118		5/72	LAS	SHERA. NO DATA GIVEN	62661
OS	189	RESON PARAMS	EXPT-PROG	6.6 0	1.9 2	USNDC-1	127		5/72	NRL	NAMENSON+. J ASSIGNMENT FOR 38 RESCN	62735
AU	197	TOTAL XSECT	EXPT-PROG	NDG		USNDC-1	40		5/72	COL	RAINWATER+. ANAL TO BE COMPL.NO DATA	62624
AU	197	N,GAMMA	EXPT-PROG	1.0 2	1.0 6	USNDC-1	94		5/72	LRL	CZIRR+. TO BE COMPLETED. NO DATA GVN	62548
AU	197	N,GAMMA	EXPT-PROG	2.4 4		USNDC-1	176		5/72	RPI	BLOCK+.LINAC.TOF.FE-FILTERED BEAM	62796
AU	197	SPECT NGAMMA	EXPT-PROG	PILE		USNDC-1	16		5/72	ANL	BOLLINGER+. SEARCH FOR PYGMY RESCN	62637
AU	198	SPECT NGAMMA	EXPT-PROG	THR		USNDC-1	18		5/72	ANL	THOMAS+. ABSOL GAMMA INTENSITY MEASD	62640
TL	203	TOTAL XSECT	EXPT-PROG	NDG		USNDC-1	40		5/72	COL	RAINWATER+. ANAL TO BE COMPL.NO DATA	62615
TL	205	TOTAL XSECT	EXPT-PROG	NDG		USNDC-1	40		5/72	COL	RAINWATER+. ANAL TO BE COMPL.NO DATA	62616
PB		DIFF ELASTIC	EXPT-ABST	3.5 6	5.0 6	BAP 4	103P6		3/59	TXN	30-140 DEG	62588
PB	204	N2N REACTION	EXPT-PROG	8.4 6	1.5 7	BNL-653(N-3)			2/61	LRL	EXCITATION FUNCTION NO DATA GIVEN	62589
PB	204	N,GAMMA	EXPT-PROG	2.5 3	6.0 5	USNDC-1	136		5/72	ORL	ALLEN+. LINAC. CURVE	62742
PB	206	DIFF INELAST	EXPT-JOUR	2.0 6	8.0 6	PR	159	969	7/67	LAS	CRANBERG+.EXC FN TO 4.5MEV ANG DIST	62590

ELEMENT S	A	QUANTITY	TYPE	ENERGY MIN	ENERGY MAX	DOCUMENTATION REF	VOL	PAGE	DATE	LAB	COMMENTS	SERIAL NO.
PB	206	N,GAMMA	EXPT-PROG	2.5 3	6.0 5	USNDC-1	136		5/72	ORL	ALLEN+. LINAC. CURVE	62743
PB	207	TOTAL XSECT	EXPT-PROG	NDG		USNDC-1	95		5/72	LRL	PHILLIPS+. TOF SPECTRA SHOWN	62649
PB	207	N,GAMMA	EXPT-PROG	2.5 3	6.0 5	USNDC-1	136		5/72	ORL	ALLEN+. LINAC. CURVE	62744
PB	208	N,GAMMA	EXPT-PROG	2.5 3	6.0 5	USNDC-1	136		5/72	ORL	ALLEN+. LINAC. CURVE	62745
TH	232	TOTAL XSECT	EXPT-PROG	1	3	USNDC-1	67		5/72	COL	RAHN+. RESON PARAMS GIVEN(P-WAVE)	62578
TH	232	RESON PARAMS	EXPT-PROG	5.9 1	2.9 3	USNDC-1	67		5/72	COL	RAHN+. P-WAVE G*WN GIVEN FOR 62RESGN	62570
TH	232	PHOTO-FISSN	EXPT-PROG	5.0 6	1.0 7	USNDC-1	87		5/72	GA	GOZANI+. BREMSSTRAHLUNG. YLD CURVES	62584
U	233	RESON PARAMS	EXPT-PROG	1.5 0	3.0 1	USNDC-1	70		5/72	COL	RAHN+. PARAMS GIVN FOR 38 RESON	62572
U	233	NU	EXPT-PROG	NDG		USNDC-1	183		5/72	RPI	REED+. TO BE DONE	62764
U	233	RES INT FISS	EXPT-PROG	4.1-1	1.2 3	USNDC-1	70		5/72	COL	RAHN+. 32 E INTERVLS. CFD OTHER XPTS	62568
U	235	TOTAL XSECT	EXPT-PROG	5.0 5	1.5 7	USNDC-1	121		5/72	NBS	SCHWARTZ+. ANAL TBC. NO DATA GIVEN	62670
U	235	RESON PARAMS	EVAL-PROG	NDG		USNDC-1	1		5/72	AGN	SMITH. MULTILEVEL PARAMS.NO DATA GVN	62768
U	235	FISSION	EXPT-PROG	8.0 0	1.0 4	USNDC-1	145		5/72	ORL	PEREZ+. LINAC. CURV. CFD ENDF/B	62559
U	235	FISSION	EXPT-PROG	1.0 6	6.0 6	USNDC-1	111		5/72	LAS	HANSEN+. ABSOL MEAST.TO BE COMPL.NDG	62658
U	235	FISSION	EXPT-PROG	9.0 5	5.0 6	USNDC-1	2		5/72	ANL	MEADOWS. REL TO U238.CURV. TBP NSE	62776
U	235	FISSION	EXPT-PROG	2.0 6	3.0 6	USNDC-1	2		5/72	ANL	POENITZ+. REL TO U235.TBL.TBP JNE	62778
U	235	FISSION	EVAL-PROG	0.	6.0 1	USNDC-1	145		5/72	ORL	DE SAUSSURE. SEE ORNL-TM-3707.CURVE	62785
U	235	NU	EXPT-PROG	NDG		USNDC-1	183		5/72	RPI	REED+. TO BE COMPLETED.NO DATA GIVEN	62763
U	235	DELAYD NEUTS	EXPT-PROG	FAST		USNDC-1	2		5/72	ANL	COX. TOTAL DELAYED YLD TO BE MEASD	62772
U	235	SPECT FISS G	EXPT-PROG			USNDC-1	94		5/72	LRL	BROWNE+. GAMS BEFORE ISOM FISS. NDG	62647
U	235	SPECT FISS G	EXPT-PROG	THR		USNDC-1	152		5/72	ORL	PLEASONTON+. CURVES. TBP PR	62782
U	235	FRAG SPECTRA	EXPT-PROG	THR		USNDC-1	122		5/72	NBS	SCHRODER. FRAG/ALPHA KE CORRELATNS	62674
U	235	PHOTO-FISSN	EXPT-PROG	5.0 6	1.0 7	USNDC-1	87		5/72	GA	GOZANI+. BREMSSTRAHLUNG. YLD CURVES	62585
U	235	FISS PROD GS	EXPT-PROG	THR		USNDC-1	77		5/72	GA	SUND+. TABLE. 20NS-1MUS AFTER FISSN	62565
U	235	N,GAMMA	EXPT-PROG	8.0 0	1.0 4	USNDC-1	145		5/72	ORL	PEREZ+. LINAC. CURV. CFD ENDF/B	62558
U	235	N,GAMMA	EVAL-PROG	0.	6.0 1	USNDC-1	145		5/72	ORL	DE SAUSSURE. SEE ORNL-TM-3707.CURVE	62784
U	236	FISSION	EXPT-PROG	5.0 5	8.0 6	USNDC-1	148		5/72	ORL	ROSLER+. CURVES. SEE PL JAN. 4,1972	62783
U	238	TOTAL XSECT	EXPT-PROG	1	3	USNDC-1	67		5/72	COL	RAHN+. RESON PARAMS GIVEN(P-WAVE)	62569
U	238	TOTAL XSECT	EXPT-PROG	5.0 5	1.5 7	USNDC-1	121		5/72	NBS	SCHWARTZ+. ANAL TBC. NO DATA GIVEN	62671
U	238	TOTAL XSECT	EXPT-PROG		3.0 6	USNDC-1	7		5/72	ANL	SMITH+. NO DATA GIVEN	62703
U	238	TOTAL XSECT	EXPT-PROG	5.0 5	3.0 7	USNDC-1	167		5/72	RPI	HAYES+.LINAC. CURVES	62731
U	238	TOTAL XSECT	EXPT-PROG	5.0 3	5.6 3	USNDC-1	182		5/72	RPI	BYOUN+. EFFECTIVE AVERAGE SIG GIVEN	62761
U	238	RESON PARAMS	EXPT-PROG	1.0 1	2.9 3	USNDC-1	67		5/72	COL	RAHN+. P-WAVE G*WN GIVEN FOR 74RESGN	62571
U	238	STRNTH FNCTN	EXPT-PROG	1.0 3	7.0 4	USNDC-1	182		5/72	RPI	BYOUN+. S0 AND S1 VALUES GIVEN	62762
U	238	DIFF ELASTIC	EXPT-PROG		3.0 6	USNDC-1	7		5/72	ANL	SMITH+. NO DATA GIVEN	62704
U	238	NONEL GAMMAS	EVAL-PROG	3.0 0		USNDC-1	39		5/72	BNL	PEARLSTEIN+. EVALUATN COMPLETED. NDG	62610
U	238	FISSION	EXPT-PROG	9.0 5	5.0 6	USNDC-1	2		5/72	ANL	MEADOWS. REL TO U235.CURV. TBP NSE	62775
U	238	FISSION	EXPT-PROG	2.0 6	3.0 6	USNDC-1	2		5/72	ANL	POENITZ+. REL TO U235.TBL.TBP JNE	62777
U	238	DELAYD NEUTS	EXPT-PROG	FAST		USNDC-1	2		5/72	ANL	COX. TOTAL DELAYED YLD TO BE MEASD	62773
U	238	PHOTO-FISSN	EXPT-PROG	5.0 6	1.0 7	USNDC-1	87		5/72	GA	GOZANI+. BREMSSTRAHLUNG. YLD CURVES	62586
U	238	N,GAMMA	EXPT-PROG	1.0 2	1.0 6	USNDC-1	94		5/72	LRL	CZIRR+. TO BE COMPLETED. NO DATA GVN	62550
U	238	N,GAMMA	EXPT-PROG	4.0 5	1.5 6	USNDC-1	8		5/72	ANL	POENITZ. SCINT TANK.ANAL TBC. NDG	62687
U	238	N,GAMMA	EXPT-PROG	2.4 4		USNDC-1	176		5/72	RPI	BLOCK+.LINAC.TOF.FE-FILTERED BEAM	62797
U	238	SPECT NGAMMA	EXPT-PROG	THR		USNDC-1	118		5/72	LAS	JURNEY+. ANAL TBC. NO DATA GIVEN	62662
U	239	SPECT NGAMMA	EXPT-PROG	THR		USNDC-1	18		5/72	ANL	THOMAS+. ABSOL GAMMA INTENSITY MEASD	62641
PU	239	TOTAL XSECT	EXPT-PROG	5.0 5	1.5 7	USNDC-1	121		5/72	NBS	SCHWARTZ+. ANAL TBC. NO DATA GIVEN	62672
PU	239	TOTAL XSECT	EXPT-PROG		1.5 6	USNDC-1	7		5/72	ANL	SMITH+. NO DATA GIVEN. TBP JNE	62679
PU	239	DIFF ELASTIC	EXPT-PROG		1.5 6	USNDC-1	7		5/72	ANL	SMITH+. NO DATA GIVEN. TBP JNE	62680

ELEMENT S A	QUANTITY	TYPE	ENERGY MIN	ENERGY MAX	DOCUMENTATION REF	VOL	PAGE	DATE	LAB	COMMENTS	SERIAL NO.
PU 239	DIFF INELAST	EXPT-PROG		3.0 6	USNDC-1	7		5/72	ANL	SMITH+. TO BE COMPLETED. NO DATA	62681
PU 239	DELAYD NEUTS	EXPT-PROG	FAST		USNDC-1	2		5/72	ANL	COX. TOTAL DELAYED YLD TO BE MEASD	62774
PU 239	PHOTO-FISSN	EXPT-PROG	5.0 6	1.0 7	USNDC-1	87		5/72	GA	GOZANI+. BREMSSTRAHLUNG. YLD CURVES	62587
PU 239	FISS PROD GS	EXPT-PROG	THR		USNDC-1	77		5/72	GA	SUND+. TABLE. 20NS-1MUS AFTER FISSN	62566
PU 240	RESON PARAMS	EXPT-PROG	7.5 2	1.0 4	USNDC-1	175		5/72	RPI	HOCKENBURY+. FISSION WIDTHS.NO DATA	62798
PU 240	FISSION	EXPT-PROG	7.5 2	3.0 4	USNDC-1	175		5/72	RPI	HOCKENBURY+. SUB-THRESHOLD FISSION	62799
PU 240	SPECT NGAMMA	EXPT-PROG	THR		USNDC-1	119		5/72	LAS	JURNEY.GE(LI)+NAI PAIR SPECTR. NDG	62663
PU 242	SPECT FISS G	EXPT-PROG			USNDC-1	94		5/72	LRL	BROWNE+. GAMS BEFORE ISOM FISS. NDG	62648
CF 249	FISSION	EXPT-PROG	3.2-1	1.5 6	USNDC-1	162		5/72	ORL	BEMIS+.LINAC+TOF.PEAK SIG .71EV RES	62781
CF 252	NU	EXPT-PROG	SPON		USNDC-1	19		5/72	ANL	DE VOLPI. FINAL VALUE GIVEN.	62646
CF 252	SPECT FISS G	EXPT-PROG	SPON		USNDC-1	78		5/72	GA	GOZANI+. ENERGY/MULTIPLICITY CORREL	62567
CF 253	FISSION	EXPT-PROG	THR		USNDC-1	98		5/72	LRL	WILD+. VALUE GIVEN	62653
FM 257	FISSION	EXPT-PROG	THR		USNDC-1	98		5/72	LRL	WILD+. VALUE GIVEN	62652
FM 257	NU	EXPT-PROG	SPON		USNDC-1	110		5/72	LAS	VEESER+. TO BE DONE	62655
MANY	STRNTH FNCTN	EVAL-PROG			USNDC-1	189		5/72	RPI	TURINSKY+. A#20-220.P-WAVE. CURVE	62760
STEEL	TOTAL XSECT	EXPT-PROG	2.4 4		USNDC-1	178		5/72	RPI	OBLOCK.TYPE C1018.TRANS. CURVE	62793

AEROJET NUCLEAR COMPANY

A. CROSS SECTIONS EVALUATIONS

1. Multilevel Parameters for ^{235}U (J. R. Smith)

Multilevel fitting of ^{235}U resonance data is in progress. This program uses the same interpretation of the experimental data as was used in deriving single-level parameters plus smooth files for ENDF/B, Version III.[1] The new fit uses Reich-Moore multilevel parameters. The two matched fits will form the basis of single-level vs multilevel comparison studies.

B. INTEGRAL CROSS SECTION MEASUREMENTS IN THE CFRMF (Y. D. Harker, J. R. Berreth, E. H. Turk and J. W. Rogers)

Capture cross section measurements for different materials have been measured in the Coupled Fast Reactivity Measurement Facility (CFRMF). Earlier reports to NCSAC have described the CFRMF, spectral measurements and previous cross section determinations.[2] Since the last report the main efforts of the FBR Physics Constants Program have been directed toward the installation of the electromagnetic mass separator for use in sample preparation and dosimetry measurements in the CFRMF as a part of the Interlaboratory LMFBR Reaction Rate Program. The ILRR program is a multi-laboratory effort to establish neutron standard source fluxes over the energy region of interest in fast reactor physics. The CFRMF is currently being studied and will become a standard source for the energy region from 1 keV to 1 MeV.

Recent capture cross section measurements have been completed on ^{152}Sm, ^{154}Sm and ^{147}Pm. These values are 0.367, 0.145 and 0.938 barns, respectively and are based upon an effective cross section for gold in the CFRMF of 0.5 barns.

---

1. J. R. Smith and R. C. Young, "U-235 Resolved Resonance Parameters for ENDF/B, Version III", ANCR-1044 (1971).

2. R. E. Chrien, "Reports to the AEC Nuclear Cross Sections Advisory Committee", Dec. 1, 1970, BNL-50276 (T-603), NCSAC-33; May 1, 1971, BNL-50298, NCSAC-38; and November 1971, NCSAC-42.

ARGONNE NATIONAL LABORATORY

A. FAST NEUTRON PHYSICS

1. Fission

a. Total Delayed Neutron Yield from Fissile and Fissionable Nuclides (S. A. Cox)

A program for the measurement of the total delayed neutron yield from fissile and fissionable nuclides has been initiated. Because the Fast Neutron Generator at Argonne provides very high neutron source intensities combined with lower background than other facilities, it is expected that the measurements will result in a significant improvement in accuracy. Initial measurements will be made with ^{235}U, ^{238}U and ^{239}Pu.

(NCSAC—35, Req. No. 399)

b. The ^{238}U to ^{235}U Fission Cross Section Ratio from 1 to 5 MeV (J. W. Meadows)

Measurements of the ^{238}U to ^{235}U fission cross section ratio were carried out in the 2 to 3 MeV region using two methods to determine the relative masses. The energy dependence of the ratio was measured from 1 to 5 MeV and normalized to the results at 2.5 MeV. Fast ion chambers and the time-of-flight technique were used to reduce the background. The results are shown in Fig. A-1 and A-2. A paper has been submitted to Nuclear Science and Engineering.

(NCSAC-35, Req. No. 417)

c. The Fission Cross Section Ratio of ^{238}U to ^{235}U at 2.0, 2.5 and 3.0 MeV (W. P. Poenitz and R. J. Armani)

These measurements described in NCSAC-41, 42 were concluded. A paper was accepted for publication by J. Nucl. Energy. The final values are summarized in Tab. 1. The errors given in this table were obtained by applying statistical error evaluation to statistical quantities only. Using the usually applied error evaluations for all contributing uncertainties would reduce the given errors by about a

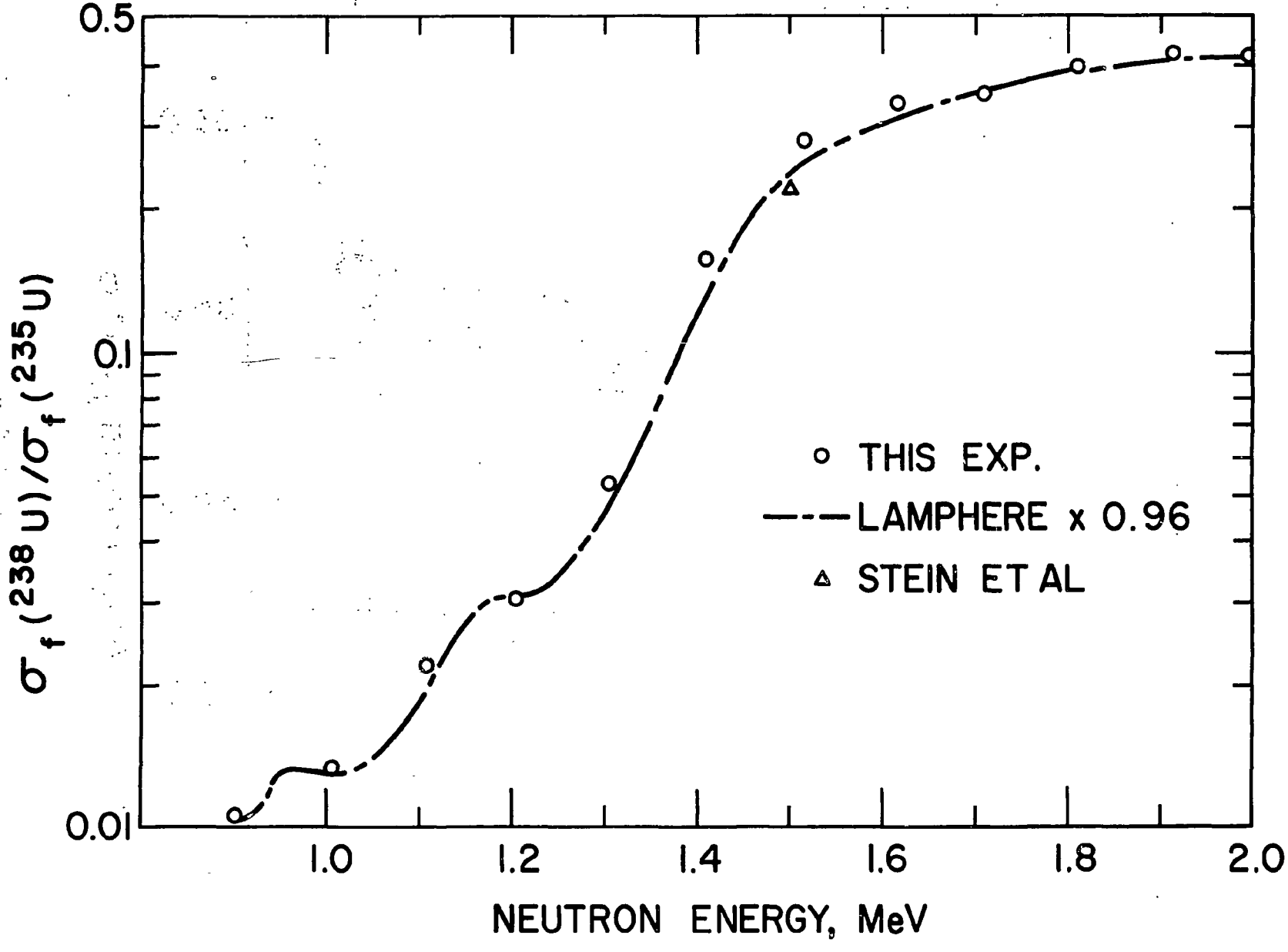
0.5
0.1
0.01
$\sigma_f(^{238}U)/\sigma_f(^{235}U)$
1.0
1.2
1.4
1.6
1.8
2.0
NEUTRON ENERGY, MeV
THIS EXP.
LAMPHERE x 0.96
STEIN ET AL

Figure A-1

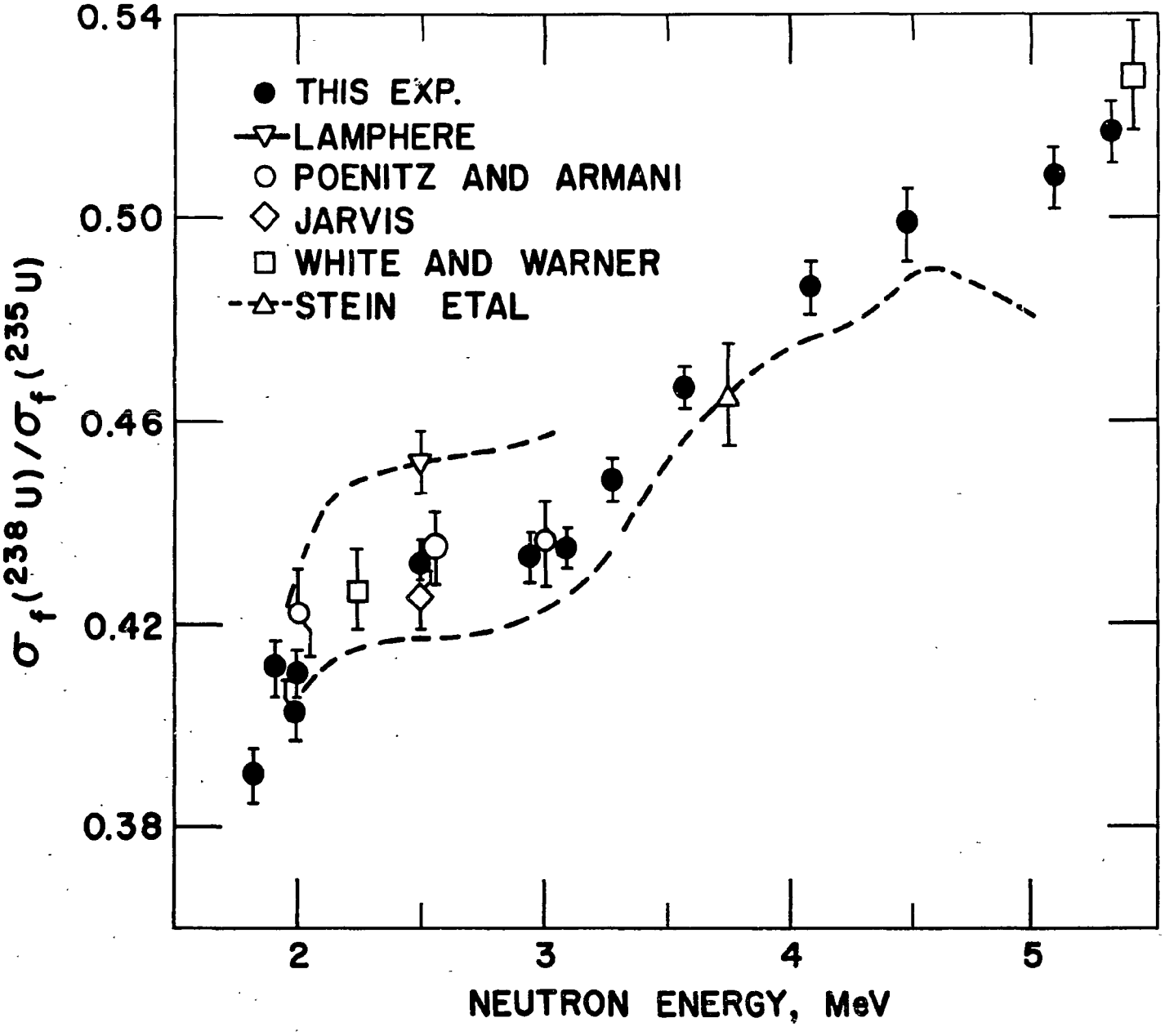
0.54
0.50
0.46
0.42
0.38
THIS EXP.
LAMPHERE
POENITZ AND ARMANI
JARVIS
WHITE AND WARNER
STEIN ETAL
$\sigma_f(^{238}U)/\sigma_f(^{235}U)$
2
3
4
5
NEUTRON ENERGY, MeV

Figure A-2

factor 2.

(NCSAC—35, Req. No. 417)

TABLE A-1. Results for $\sigma_f(^{238}U)/\sigma_f(^{235}U)$

En (MeV)	Ratio
2.0	0.422 ± 0.009*
2.5	0.435 ± 0.007
3.0	0.436 ± 0.008*

*Normalized at 2.5 MeV

2. Neutron Scattering and Total Cross Section Program (A. Smith, P. Guenther, D. Smith, J. Whalen)

a. Carbon

New results are available in the range 1.5—3.5 MeV including eleastic scattering and total cross sections. Measurements are generally made at 100 keV incident energy intervals and 20 scattering angles.

(NCSAC—35, Req. No. 32)

b. Flourine

Total and elastic and inelastic scattering cross sections are complete over the incident neutron energy range 0.1—1.5 MeV.

(NCSAC—35, Req. No. 51)

c. Titanium

Total and elastic and inelastic scattering cross sections measurements are complete over the incident energy range 0.1—1.5 MeV. These values have been used to update the ENDF file. Additional

values are available to incident energies of 3.0 MeV. Interpretations based upon the statistical R-Matrix are in progress.

d. Vanadium

New elastic and inelastic scattering values are available in the energy range 1.5—3.0 MeV.

(NCSAC—35, Req. Nos. 84, 85)

e. Iron

Extensive measurements of elastic and inelastic scattering cross section in the energy range 1.5—3.8 MeV are complete.

(NCSAC—35, Req. Nos. 97, 99)

f. Cobalt, Nickel, Copper

Selected measurements of elastic and inelastic scattering cross sections are available in the energy range 1.5—3.0 MeV.

(NCSAC—35, Req. Nos. 118, 119)

g. Germanium-72

Detailed inelastic excitation cross sections have been measured for the 691 keV 0+ state. The results are of use in flux monitoring using GeLi detectors.

h. Niobium

Detailed total, and elastic and elastic scattering cross sections are available in the incident neutron energy range 1.5—3.8 MeV.

(NCSAC—35, Req. Nos. 203, 205)

i. Palladium

A report of measured total and elastic and inelastic scattering cross sections to 1.5 MeV has been submitted for publication. (See also ANL-7869)

j. Molybdenum 92, 94, 96, 98, and 100

Measurements of total and elastic and inelastic scattering cross sections to energies of 1.5 MeV are complete and a report has been prepared for publication.

(NCSAC—35, Req. Nos. 220, 221)

k. Uranium 238

Detailed measurements of total and elastic scattering cross sections to 3.0 MeV have been completed. Some concurrent knowledge of the inelastic scattering process was obtained.

(NCSAC—35, Req. Nos. 412, 413, 414)

l. Plutonium 239

Measurements of total and elastic scattering cross sections to 1.5 MeV are complete and a paper reporting the work has been submitted to Jour. Nucl. Energy. Measurement of the inelastic cross sections continues and the work has been extended to an incident neutron energy of 3.0 MeV.

(NCSAC—35, Req. Nos. 444, 445, 446)

3. Polarization in the Elastic Scattering of Neutrons from Medium and Heavy Weight Elements (A. Cox and E. E. Dowling Cox)

A paper with the above title has been submitted for publication. The abstract follows.

A systematic study of the differential elastic neutron scattering cross section and associated polarization for ~1 MeV neutrons is presented for 29 elements from titanium to uranium. The data for each element are averaged over an incident neutron energy range of 200 to 500 keV and compared with predictions of the optical model and Hauser-Feshbach theories. The optical model parameters which best fit the differential scattering data and polarizations exhibit a clear mass number dependence. The real potential well depth (V) decreases monatonically from ~48 MeV at A = 60 to ~43 MeV at A = 238. The imaginary potential well depth (W) has a value of ~14 MeV at

A = 60, goes through a minimum of ~10 MeV at A = 140 and then rises to a value of ~16 MeV at A = 238. The spin-orbit well depth V_{so} is essentially constant at ~6 MeV with an indication of a rise to ~7 MeV for A>140. When V, W, and V_{so} are averaged over the mass number the results agree very well with the generalized parameter set as proposed by Moldauer.

4. Capture Cross Section Measurements (W. P. Poenitz)

The capture cross sections of Nb, Mo, Zr, Ho, Cd and ^{238}U were measured with the large liquid scintillator tank (NCSAC—42, p. 21) in the energy range 400—1500 keV. The neutron flux was determined with a Grey Neutron Detector using vanadium sulfate-solution as a neutron capture medium. Both the high energetic capture γ-rays of vanadium and the 2.2 MeV capture γ-ray of hydrogen were detected. The detector was absolutely calibrated with Cf-252 sources and relatively with measurements relative to the $^{6}Li(n,\alpha)$ and $^{197}Au(n,\gamma)$ cross sections. The data are being analyzed.

(NCSAC—35, Req. Nos. 421, 422, 155, 207, 222)

5. Neutron Sources:—Neutron Yield From the $^{7}Li(p,n^{3}He)^{4}He$ Reaction (J. W. Meadows and D. L. Smith)

The $^{7}Li(p,n^{3}He)^{4}He$ three-body breakup reaction yields significant numbers of neutrons for $E_p \geq 5$ MeV. At higher proton energies a broad distribution of neutrons is observed in addition to the two mono-energetic groups from the $^{7}Li(p,n)^{7}Be, ^{7}Be^{*}$ reactions. The yield of breakup neutrons relative to the mono-energetic groups has been measured at zero degrees using time-of-flight techniques. The results are summarized in Fig. A-3 which gives the percentage of all neutrons from proton bombardment of ^{7}Li which are attributed to the $^{7}Li(p,n^{3}He)^{4}He$ reaction. The spectrum of emitted neutrons has also been determined. This work has been formally completed and will be published shortly as an ANL report.

6. Thick Target Neutron Yields from Proton and Deuteron Bombardment of ^{9}Be (F. T. Kuchnir,* L. S. Skaggs,* A. J. Elwyn, and F. P. Mooring)

A t.o.f. technique in conjunction with the pulsed beam from the ANL tandem accelerator has been used to measure the energy

*Argonne Cancer Research Hospital, Chicago, Illinois.

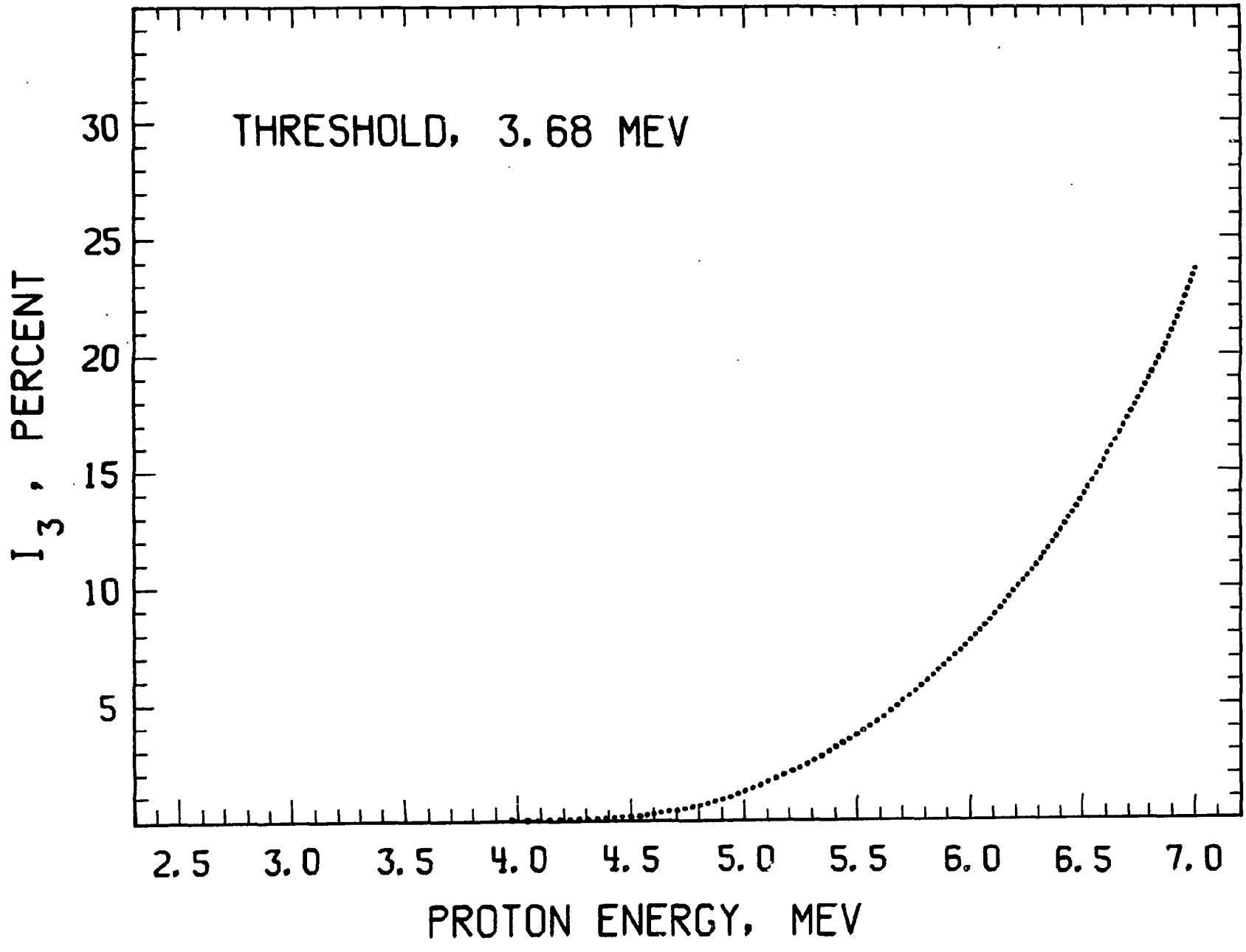
THRESHOLD, 3.68 MEV
I_3, PERCENT
30
25
20
15
10
5
2.5
3.0
3.5
4.0
4.5
5.0
5.5
6.0
6.5
7.0
PROTON ENERGY, MEV

Figure A-3

spectra and angular distributions of neutrons produced in the b mbardment of a thick ^{9}Be target with deuterons of 8 and 16 MeV, and protons of about 15 MeV. Neutrons were detected by a 2" diameter by 1" thick stilbene scintillator at flight paths of 2 and 3 meters and at various angles between 0° and 150°. Preliminary results indicate that in the deuteron bombardment the neutrons are distributed in a continuous spectrum that peaks at the average energy of 3.2 MeV (for 8-MeV deuterons) and ~6 MeV (for 16-MeV deuterons). The neutron yields in the deuteron-induced reactions are strongly peaked in the forward direction. For the case of proton bombardment, the neutrons show a typical evaporation spectrum (peaking at ~1 MeV), and the angular distributions are isotropic. In general the neutron yields are considerably less in the case of protons than for deuteron bombardment. Further analysis is in progress. The experimentally observed neutron-energy spectra and angular distributions will be used in order to optimize the collimator and shielding design for a neutron radiation-therapy facility in conjunction with a medical cyclotron at the Argonne Cancer Research Hospital.

7. Possible Resonant Structure in the Elastic Scattering of ~1 MeV Neutrons by Y (A. J. Elwyn, J. E. Monahan,* S. A. Cox,** J. Adams,† and C. Chen†)

Analysis is essentially completed of the measured differential cross sections and polarization in the elastic scattering of 0.8—1.4 MeV neutrons by ^{89}Y. The data which show relatively weak intermediate-width structure have been interpreted in terms of an optical-potential plus resonance model. The results are consistent with the existence of both 1^- and 1^+ resonances with 40—50-keV widths in the neutron energy region between 1 and 1.2 MeV. The 1^- states can probably be interpreted as parents of the $T_>$-components of the E1 giant resonance near 21 MeV excitation in ^{90}Zr observed[1] in the ^{89}Y(p, γ)^{90}Zr reaction. The existence of 1^- states in ^{90}Y in this region of excitation have recently been predicted.[2]

---

* Also at Ohio University, Athens, Ohio.

** Applied Physics Division, Argonne Natl. Laboratory.

† Ohio University, Athens, Ohio.

[1] P. Axel, D. M. Drake, S. Whetstone and S. S. Hanna, Phys. Rev. Lett. 19, 1343 (1967); M. Hasinoff, G. A. Fisher, H. M. Kuan and S. S. Hanna, Phys. Lett. 30B, 337 (1969).

[2] S. Ramavataram, B. Goulard and J. Bergeron, Nucl. Phys. (to be published).

8. Detectors, Accelerators and Facilities

a. The Black Neutron Detector (W. P. Poenitz)

The response and spectra for incident mono-energetic neutrons were investigated with Monte Carlo calculations for this newly designed detector (See ANL-7915). Optimum dimensions for a Black Neutron Detector suitable for the use with neutrons up to 10 MeV were derived from these calculations and a detector was built. The efficiency of this detector is shown in Fig. A-4. At a first glance, the structure in the efficiency curve appears disturbing if a smooth efficiency is required. However, the structure is very small and thus of minor practical importance. The uncertainty of the calculated efficiency is small due to the insensitivity even to large changes in the cross sections and parameters of the detector. With conservative estimates of the uncertainties of the detector efficiency are 0.3% at 1 MeV, 0.5% at 2.5 MeV, and 0.7% at 4 MeV.

The detector has been used in absolute and shape measurements of the ^{235}U cross section which are presently being evaluated.

b. Fast Neutron Generator

This device is basically a tandem accelerator of the Dynamitron type, having the merits of entirely electrical operation, good stability and high beam power capability. The machine is pulsed (nsec) and sustains DC positive ion beams of up to 200 micro-amps at energies to 8 MeV. It is the only machine of its type in routine research operation. We are pleased to report that operation has generally exceeded specification for over 9,000 hours and that during this period the down time has been minimal and due to minor component failures. In a very sense an essentially developmental machine has proven very satisfactory during this relatively long period of operation.

c. High Intensity Negative Ion Injector

The Fast Neutron Generator is presently source limited in the context of intensity. A new high intensity negative-ion injection system, designed to increase the beam currents by about $\times$ 10, is now under bench test. The basic components were made commercially (Cyclotron Corp.) and are being matched to the Generator. The operation will be in both pulsed and DC modes.

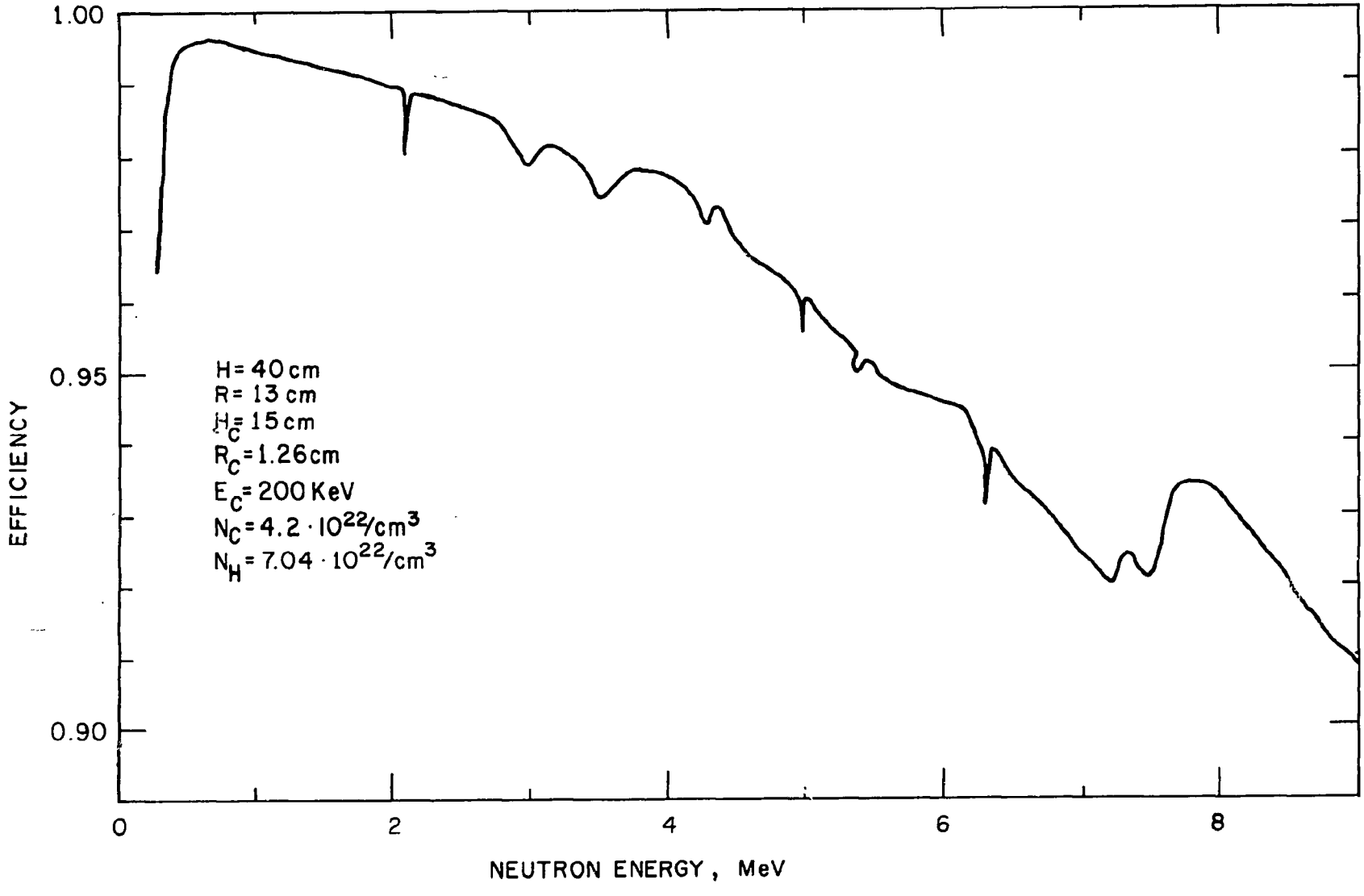
1.00
0.95
0.90
EFFICIENCY
H = 40 cm
R = 13 cm
H_C = 15 cm
R_C = 1.26 cm
E_C = 200 KeV
$N_C = 4.2 \cdot 10^{22}/cm^3$
$N_H = 7.04 \cdot 10^{22}/cm^3$
0
2
4
6
8
NEUTRON ENERGY, MeV

Figure A-4

d. 100 Meter Flight Tube

Long neutron flight paths are conventionally employed in conjunction with white neutron sources. They also are of merit when used with mono-energetic pulsed sources as the superior time resolution improves the available resolutions and the control of source energy permits precise background determinations. With these advantages a 100 meter flight tube is being installed at the Fast Neutron Generator. All materials are on site and about 40 meters are presently under vacuum test. The facility will be particularly useful in conjunction with the new high intensity injector (b, above).

B. PHOTONUCLEAR PHYSICS

1. $^{208}Pb(\gamma, n)^{207}Pb$ and the Giant M1 Resonance (R. E. Toohey and H. E. Jackson)

A short paper with the following abstract has been submitted for publication in the Phys. Rev.

Photoneutron resonances and their angular distributions have been studied in a high resolution measurement of the $^{208}Pb(\gamma, n)^{207}Pb$ reaction near threshold. The angular distributions observed for photoneutron resonances tend to confirm the conclusions of earlier experiments which suggest the existence of a giant M1 resonance in ^{208}Pb.

2. Photoneutron Resonances from $^{29}Si(\gamma, n)^{28}Si$ (H. E. Jackson and R. E. Toohey).

Analysis of photoneutron resonance yields and angular distributions in ^{29}Si for neutron energies of 10 keV to 1.4 MeV has been completed. The time of flight spectrum for neutron emission at 90° is shown in Fig. B-1. The data suggest (1) the localization of resonance strength at the same excitation as proposed by Newson[1] for a neutron doorway in $^{28}Si + n$, (2) a strong correlation between the partial widths for the corresponding resonances in the two channels, and (3) the presence of a strong background cross section which produces a pronounced interference asymmetry in the shape of a resonance in the (γ, n)

[1] H. W. Newson, in Statistical Properties of Nuclei, edited by J. B. Garg (Plenum Press, New York, 1972), p. 309.

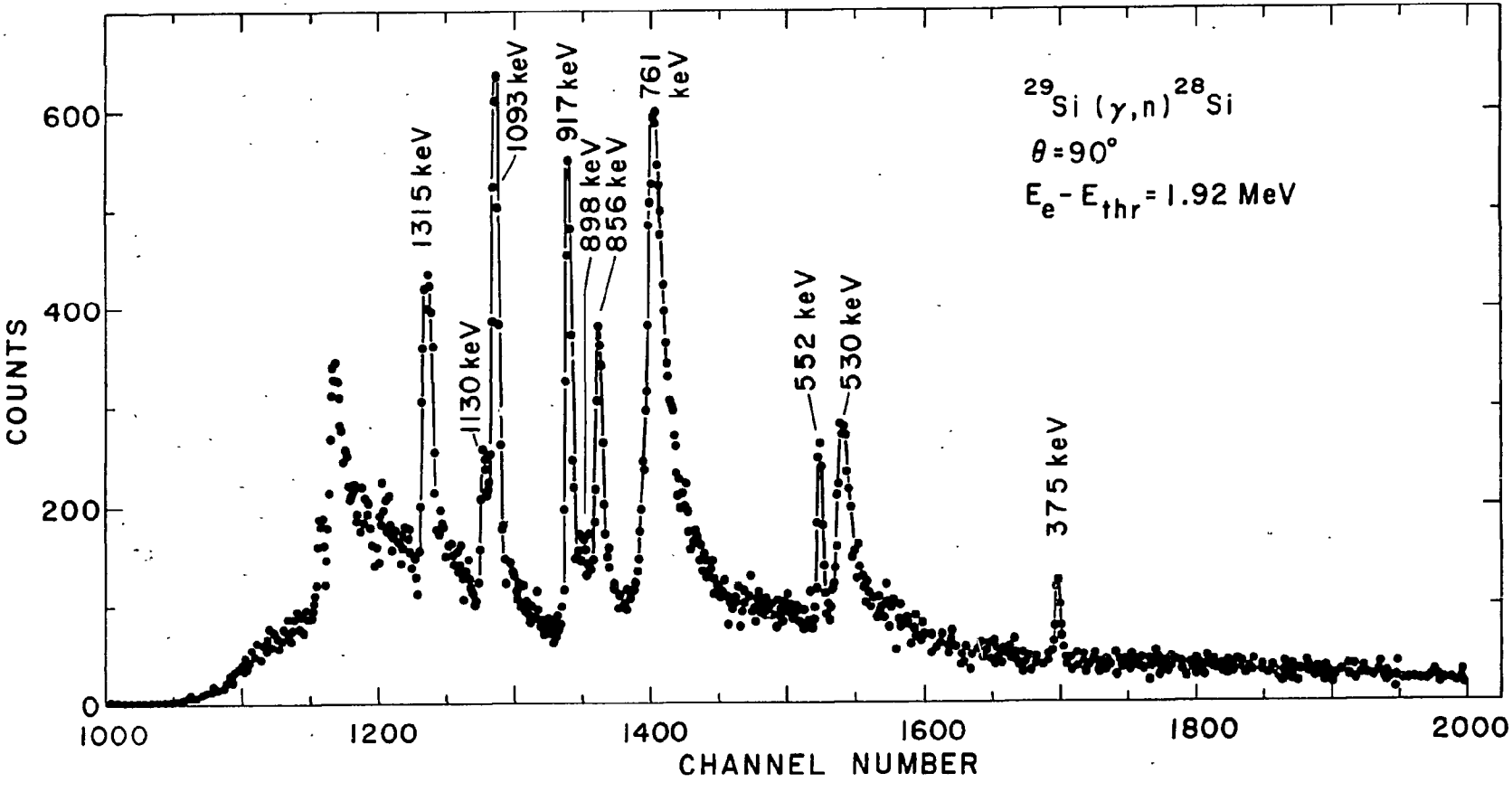
$^{29}Si\ (\gamma,n)\ ^{28}Si$
$\theta = 90°$
$E_e - E_{thr} = 1.92$ MeV
1315 keV
1130 keV
1093 keV
917 keV
898 keV
856 keV
761 keV
552 keV
530 keV
375 keV
COUNTS
CHANNEL NUMBER
0
200
400
600
1000
1200
1400
1600
1800
2000

Figure B-1

channel at 761 keV. Lane[2] has predicted such a nonresonant cross section as a direct consequence of the existence of strong correlations in partial widths. The three effects observed could be attributed to the presence of an isolated common doorway state consisting of a $2p_{\frac{3}{2}}$ neutron coupled to the ^{28}Si ground state.

---

[2] A. M. Lane, Phys. Lett. 31B, 344 (1970).

3. Possible Doorway-State Effects in the ^{207}Pb(γ, n) Threshold Reaction (K. L. Nelson, H. E. Jackson, and R. E. Toohey)

Recently[1] the Livermore group presented evidence for an E1 doorway in the reaction ^{207}Pb + γ near threshold. The result was explained as a $s_{\frac{1}{2}}$ doorway arising from a strong $s_{\frac{1}{2}}$ resonance coupled to the ^{206}Pb ground state. Because a corresponding doorway was observed in ^{206}Pb + n and the partial neutron and ground state radiation widths were found to be correlated the result was interpreted as evidence for a doorway common to both channels. We have repeated this measurement with improved resolution and over an expanded range of energies in an attempt to span completely the region in which doorway was expected. The results weaken the support for earlier interpretations. In particular throughout the energy region small energy descrepancies raise doubts concerning the parities of photoneutron resonances previously interpreted as s-wave. Of greater significance, the inclusion of three additional resonances above 600 keV in the analysis of the degree of correlation between the partial resonance widths decreases the correlation coefficient from a large positive value to a small negative value. New measurements of increased resolution and intensity are planned.

4. ^{91}Zr(γ, n)^{90}Zr and the Valency Model (R. E. Toohey and H. E. Jackson)

A series of threshold photoneutron measurements on the stable Zr isotopes is in progress. The ground state radiation widths for approximately 25 resonances below 200 keV in ^{91}Zr have been obtained, yielding the rather high average value of 200 meV. This

---

[1] R. J. Baglan, C. D. Bowman, and B. L. Berman, Phys. Rev. C3, 2475 (1971).

corresponds to a preliminary value for the E1 strength function, $\Gamma_{\gamma_0}/D = 3 \times 10^{-5}$. These radiation widths will be correlated with neutron widths obtained from total cross-section measurements on ^{90}Zr performed in collaboration with Good, Harvey, et al. at ORELA. The correlation analysis will test the valency model for threshold photoneutron reactions near the N = 50 closed shell. The data will also be investigated for evidence of p-wave doorway states.

C. REACTOR NEUTRON PHYSICS

1. Search for the "Pygmy Resonance" in $^{197}Au(n, \gamma)^{198}Au$

(L. M. Bollinger, G. D. Loper*, and G. E. Thomas)

Thermal and resonance neutron capture γ-ray spectra from the reaction $^{197}Au(n, \gamma)^{198}Au$ were measured with a Ge(Li) spectrometer at the internal target facility at the reactor CP-5 and compared with those of $^{181}Ta(n, \gamma)^{182}Ta$ in a search for the "pygmy resonance" at about 5.5 MeV. The energy dependence of the average intensity of transitions from many initial states to various final states for both ^{182}Ta and ^{198}Au in the energy region 4.8 to 6.5 MeV, as obtained by the average-resonance-capture method, is in good agreement with what is expected from the giant resonance model. The γ-ray strength functions for the two reactions are equal within ±30%. There is no evidence in the resonance-capture data for $^{197}Au(n, \gamma)^{198}Au$ for an anomalous "bump", and the data are consistent with the simple statistical model. The Fig. C-1 is a plot of average reduced radiation widths versus gamma-ray energy for resonance capture in Au and Ta, averaged over intervals of final states. From the thermal-capture data, the γ-ray strengths of tantalum and gold as determined from absolute transition intensities are found to be equal within the errors. Also, the apparent gross structure in the thermal-capture spectrum for gold does not exhibit fluctuations greater than can be accounted for by the Porter-Thomas distribution. There is no anomaly in the level density of the final states of gold or tantalum, and all the evidence of this experiment leads to the conclusion that the "pygmy resonance" in $^{197}Au(n, \gamma)^{198}Au$ does not exist.

---

* Faculty Research Participant, Wichita State University.

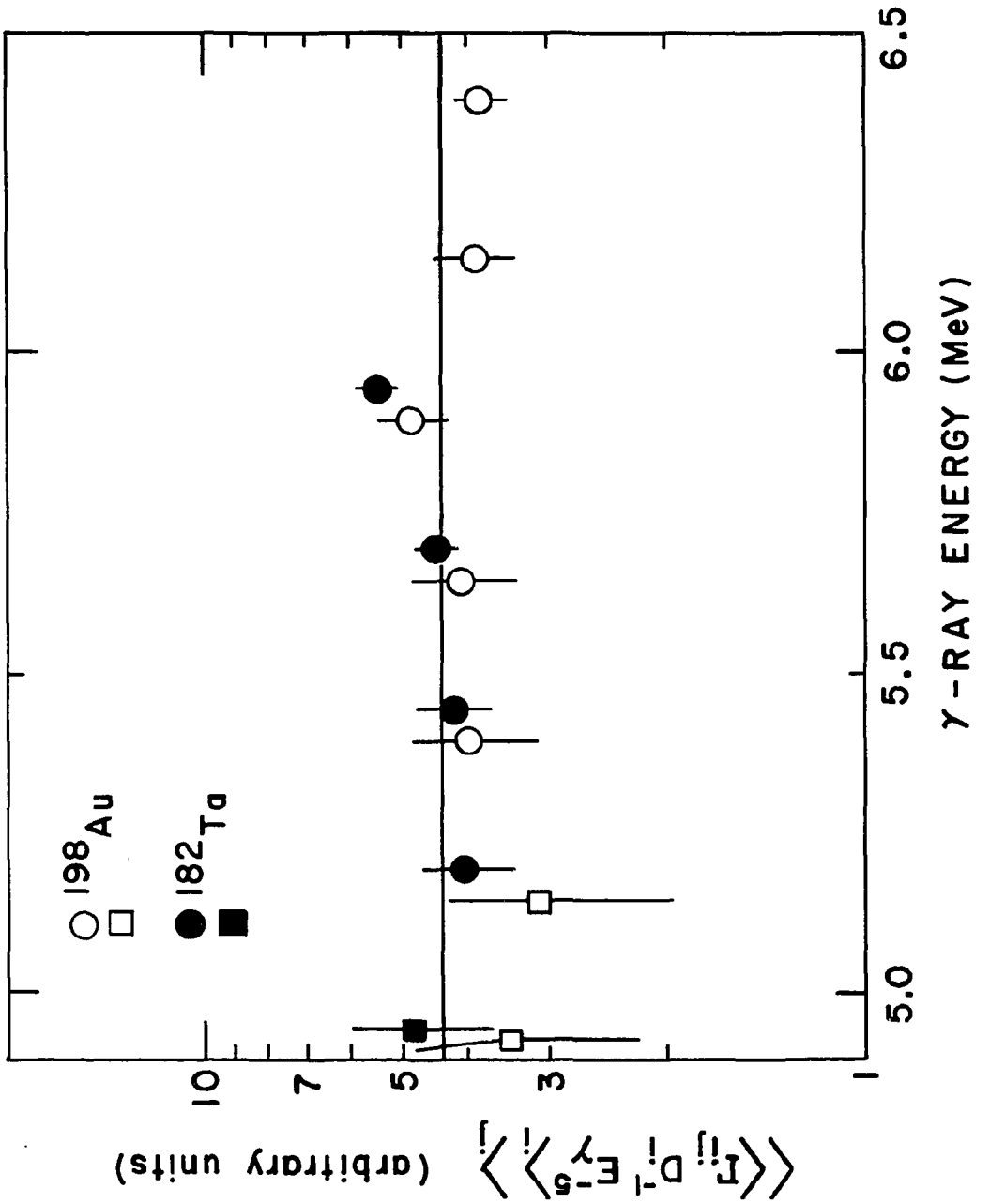
6.5
6.0
5.5
5.0
γ-RAY ENERGY (MeV)
198Au
182Ta
10
7
5
3
1
(arbitrary units)

Figure C-1

2. Determination of the Spin-Cutoff Parameter from Neutron-Capture γ-Rays (L. M. Bollinger, G. D. Loper*, and G. E. Thomas)

The reaction $^{93}Nb(n, \gamma)^{94}Nb$ has been studied by the average-resonance-capture technique at the internal target facility at the reactor CP-5. In this reaction, s-wave capture followed by transitions to final states with $J^{\pi} = 3^-$, 4^-, 5^-, and 6^- and p-wave capture followed by transitions to final states with $J^{\pi} = 2^+$, 3^+, 4^+, 5^+, 6^+, and 7^+ is observed. The intensities for positive parity states do not satisfy the simple relationships observed for many nuclides studied previously; e.g., the intensity for the 7^+ (79-keV) state is 3.7 times as strong as for the 2^+ (334-keV) state, whereas equal intensities were expected. The anomaly may be explained by the large departure of the level density from a 2J + 1 law and the fact that p-wave capture dominates. Assuming that the neutron strength function is independent of J, the observed intensity ratio $I(7^+)/I(2^+)$ yields the reasonable value $\sigma_m = 3.4 \pm 0.5$ for the spin-cutoff parameter. If this value is used, then γ-ray strength functions for all states fall smoothly on the tail of the giant resonance. This regular behavior raises doubts about the reality of the correlation between (n, γ) and (d, p) strengths reported by Rimawi et al.

3. Determination of Absolute Intensities of Thermal-Neutron Captive γ-Rays from ^{198}Au, ^{239}U, $^{51,53,54}Cr$, and ^{36}Cl (G. E. Thomas, G. D. Loper*, and L. M. Bollinger)

The high sensitivity of the internal-target facility at the reactor CP-5 makes it feasible to measure easily the thermal-neutron capture γ-ray spectra of small samples of materials with low cross sections. This characteristic allows accurate values of absolute intensities to be measured rapidly by comparing, in the spectrum for a composite sample, the intensities of transitions for the material of interest with those from capture in low cross-section standards such as lead and carbon. The results obtained are reproducible within 2%, and the overall uncertainty is believed to be only about ±5%.

The absolute intensities of ^{239}U are to appear in a paper entitled $^{238}U(n, \gamma)^{239}U$ and States of ^{239}U. Those from ^{198}Au, $^{51,53,54}Cr$, and ^{36}Cl will be useful secondary standards.

---

*Permanent address: Wichita State University.

The result obtained for $^{197}Au(n,\gamma)^{198}Au$ is $I_\gamma = 3.74 \pm 0.2$ γ's/100 neutrons for the 6.319-MeV transition, and the sum of intensities of transitions with $E_\gamma > 6.1$ MeV is 19.6 ± 1.0 γ's/100 neutrons captured. This latter value is 58% greater than that reported by Groshev et al.[1]

---

[1] L. V. Groshev et al., Nuclear Data A5, 370 (1969).

4. Final Value for Neutron Yield from ^{252}Cf (A. De Volpi)

Publication of a paper on thermal neutron absorption in cavity walls[1] culminates our program to determinate an accurate and precise value for the total neutron yield in spontaneous fission of ^{252}Cf. A slight revision of our previously published result[2] is effected by our investigation of central cavity absorption in the manganese bath. The final value is 3.729 ± 0.015 neutrons/fission, which is 0.1% greater than the previous report. The value is final in the sense that no further experimental work on this project is anticipated.

5. Average Resonance Neutron Capture in the Odd Sm Isotopes (R. K. Smither, D. Bushnell, and D. Buss)

The "average resonance neutron capture" gamma ray spectra for the reactions $^{144}Sm(n,\gamma)^{145}Sm$, $^{148}Sm(n,\gamma)^{149}Sm$, $^{150}Sm(n,\gamma)^{151}Sm$, $^{152}Sm(n,\gamma)^{153}Sm$, and $^{154}Sm(n,\gamma)^{155}Sm$ have been measured using separated isotope samples in the Argonne (n, γ) facility at the CP-5 research reactor. The results from the $^{152}Sm(n,\gamma)^{153}Sm$ reaction are shown in Fig. C-2. Each point corresponds to a primary gamma transition whose relative intensity divided by E_γ^5 is plotted vertically and its gamma energy, E_γ, is plotted horizontally. The relative gamma intensities divide into three groups. The highest one corresponding to E1 transitions, the middle group to M1 transitions, and the lowest group to E2 transitions following s-wave capture plus E1 transitions following p-wave capture. The bars with arrows are upper limits on transitions to

---

[1] A. De Volpi, "Thermal Neutron Absorption in Neutron Sources and Cavity Walls Centered in Moderating Solutions", J. Nucl. Energy 26: 75-89 (1972).

[2] A. De Volpi, "Neutron Yield of ^{252}Cf Based on Absolute Measurements of the Neutron Rate and Fission Rate", Phys. Rev. C1: 683-694 (1970).

known levels whose spin and parity would require M2, E3, and high multipole transitions. A horizontal line indicates an E_γ^5 dependence for the average gamma strength. The E_γ^5 fits the data for M1 and E2 (+ E1 following p-wave capture) but not the E1 data. The line drawn through the E1 data in Fig. C-2 has an E_γ^7 dependence. A similar energy dependence for the E1 group appears in the $^{150}Sm(n, \gamma)^{151}Sm$ results. Although the analysis of the data on the $^{144}Sm(n, \gamma)^{145}Sm$, $^{148}Sm(n, \gamma)^{149}Sm$, and $^{154}Sm(n, \gamma)^{155}Sm$ reactions has not been completed, their spectra appear to give similar results. The previously published results for the $^{149}Sm(n, \gamma)^{150}Sm$ and $^{147}Sm(n, \gamma)^{148}Sm$ reactions show an E_γ^5 dependence for the E1 group as well as for the M1 and E2 groups so the higher power E1 energy dependence is associated with only the odd isotopes of Sm.

The separation of gamma strengths into groups depending on the multipole of the transition makes it possible to assign parities to the corresponding levels and limit the spin of the level to one or two choices. This work is being used in connection with the corresponding low energy (n, γ) spectra taken with the Argonne 7.7 m bent crystal spectrometer to develop the level schemes of the odd Sm isotopes. Some of the detail in ^{151}Sm is shown in Fig. C-3. The level scheme appears quite similar to that of ^{153}Sm, consisting of many over-lapping rotational bands.

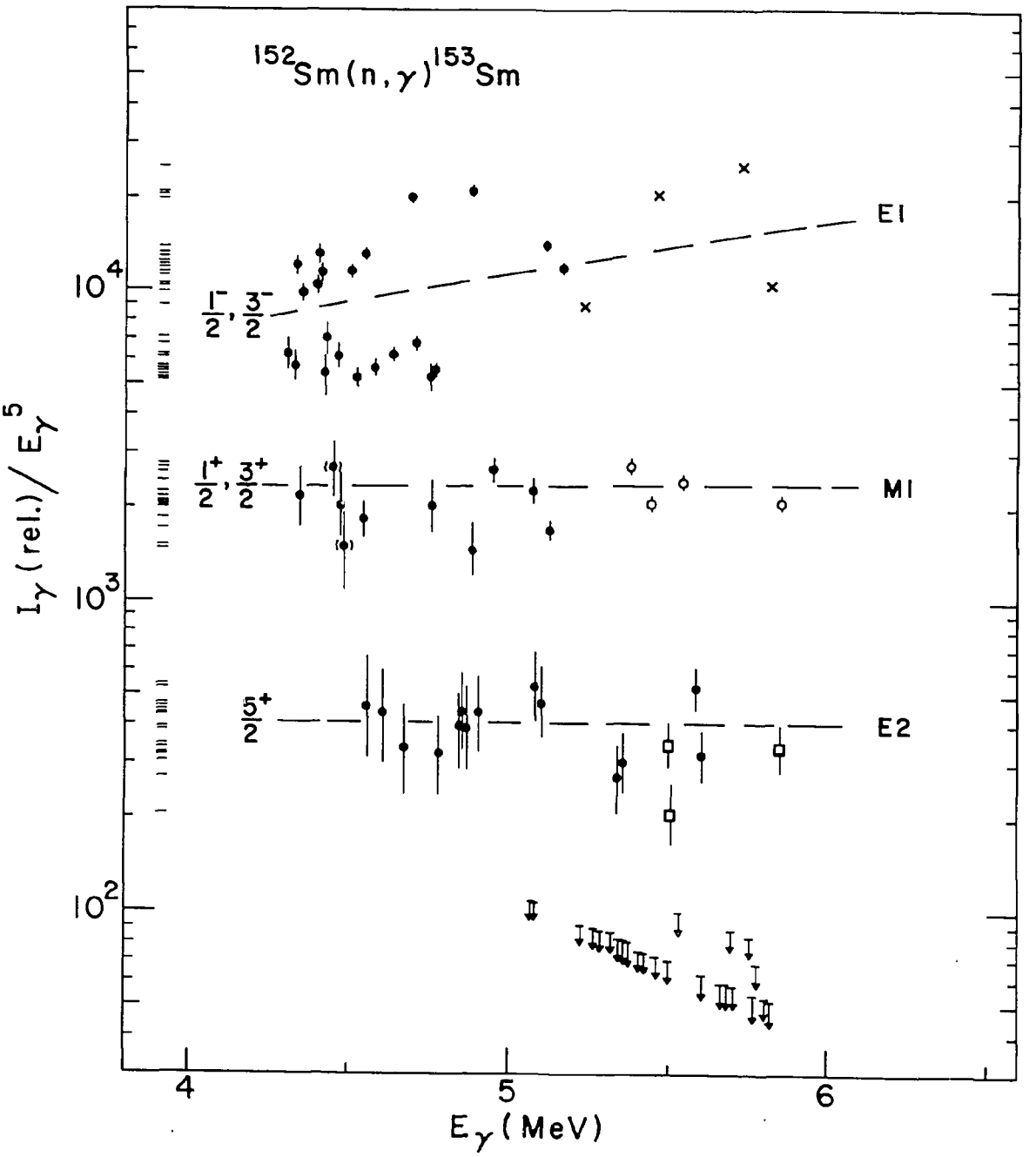
$^{152}Sm(n,\gamma)^{153}Sm$
E1
M1
E2
$\frac{1^-}{2}, \frac{3^-}{2}$
$\frac{1^+}{2}, \frac{3^+}{2}$
$\frac{5^+}{2}$
10^4
10^3
10^2
I_γ (rel.) / E_γ^5
4
5
6
E_γ (MeV)

Figure C-2

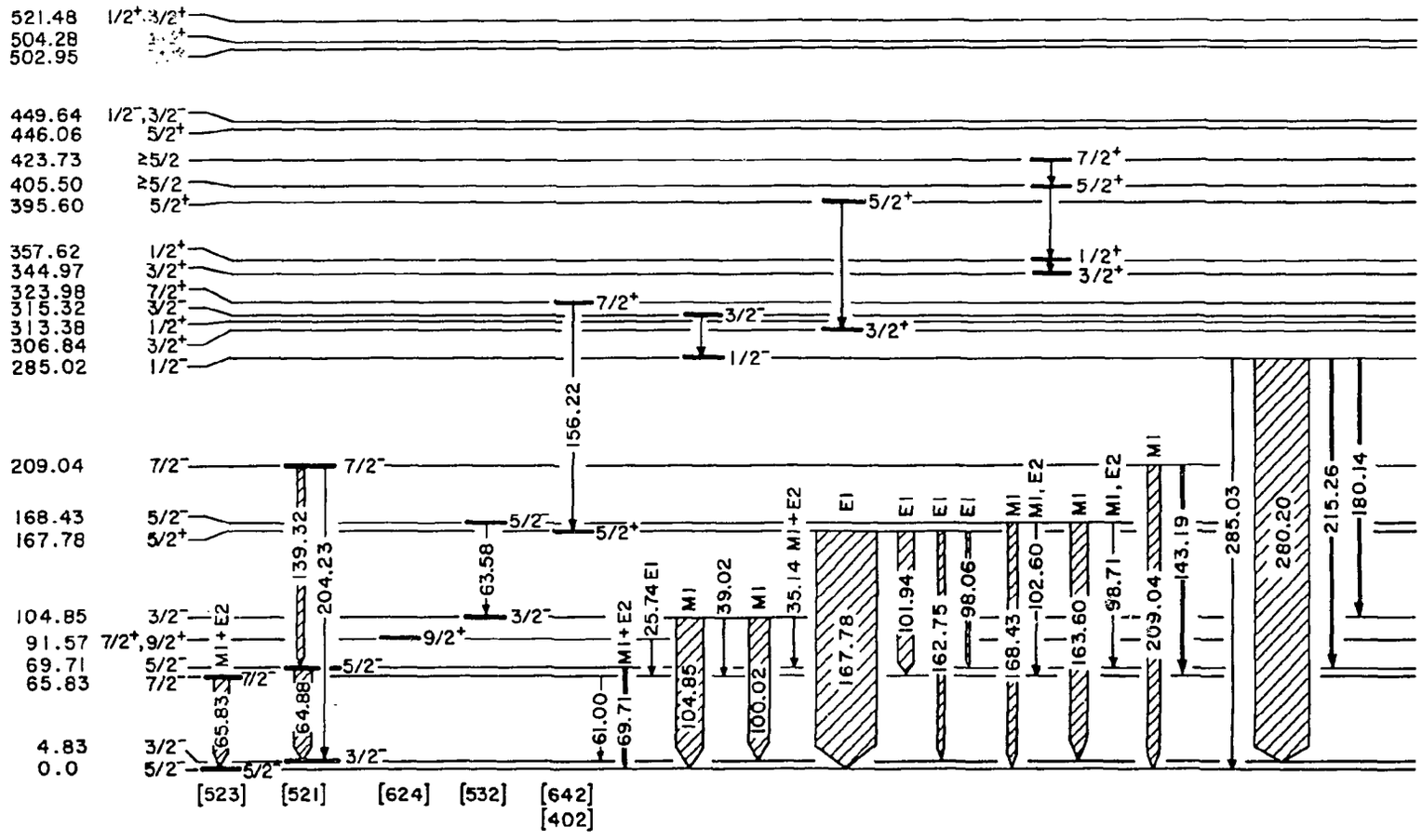
521.48
504.28
502.95
449.64
446.06
423.73
405.50
395.60
357.62
344.97
323.98
315.32
313.38
306.84
285.02
209.04
168.43
167.78
104.85
91.57
69.71
65.83
4.83
0.0
[523]
[521]
[624]
[532]
[642]
[402]
156.22
139.32
204.23
63.58
25.74 E1
104.85
39.02
100.02
35.14 M1+E2
167.78
101.94
162.75
98.06
68.43
102.60
163.60
98.71
209.04
43.19
285.03
280.20
215.26
180.14
65.83
64.88
61.00
69.71

Figure C-3

BROOKHAVEN NATIONAL LABORATORY

A. NEUTRON PHYSICS

1. Fast Chopper (R. E. Chrien, O. A. Wasson,* G. W. Cole, S. F. Mughabghab,† and M. R. Bhat†)

a) Instrumental Developments

A redesign of the collimation system used at H-2 beam tube (Fast Chopper) has been completed. The aim is to decrease the severe collimation of the beam in the vertical direction from the present value of $\sim$ 7 minutes to about 20 minutes of arc. The result should be an increase in the effective beam current on target by about a factor of two, at the expense of additional shielding requirements around the beam pipe.

Further tests on circuitry to handle the high instantaneous counting rates sometimes associated with neutron capture time-of-flight experiments have been carried out. An electronic filter using a trapezoidal weighting function has been shown by Radeka[1] to be essential in maintaining good resolution at high rates in large coaxial germanium detectors. Radeka's circuit, which also employs pile-up inspection circuitry is now in routine use. The effect of the circuit is shown in Fig. A-1. Pile-up effects are particularly important to evaluate in connection with a comparison of resonance to off-resonance capture spectra, where rate-dependent count losses could introduce serious systematic errors in the energy variation of partial radiative cross sections. We have introduced the practice of injecting a free-running (time-uncorrelated) pulser into the amplifier continuously in order to monitor rate dependent effects. Fortunately, many of the earlier experiments involved sufficiently low counting rates. For example, a check was carried out on cobalt, and it was shown that pile-up effects in the experiment of Wasson et al.,[2] on direct capture in cobalt, were negligible. This, however, was not the case in

---

* On leave from BNL at Oak Ridge National Laboratory

† Department of Applied Science, BNL

1 V. Radeka, BNL 16245; also IEEE Trans. Nuc. Sci. N519, 419 (1972)

2 O. A. Wasson, M. R. Bhat, R. E Chrien, M. A. Lone, and M. Beer, Phys. Rev. Letters 17, 1220 (1966)

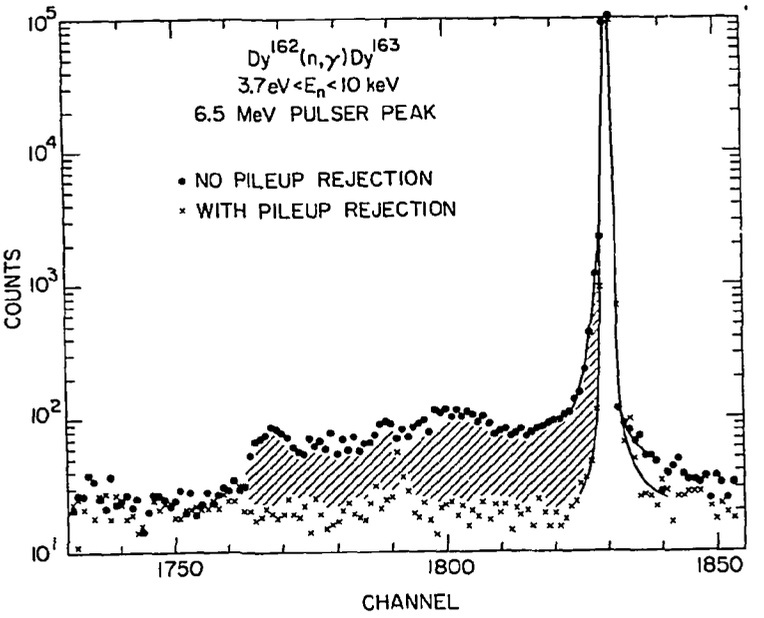

Fig. A-1. Performance of pile-up rejection circuit in Dy-162 direct capture experiment.

gold,[3] and this suggests that the resonance-resonance interference effects previously reported require considerable modification.

b) Experimental

1. Search for direct capture in Dy-162(n,γ)Dy-163
(G. W. Cole, S. F. Mughabghab, and R. E. Chrien)

The existence of a significant direct reaction amplitude for neutron capture has been demonstrated for only a limited number of nuclei such as U-238 and Co-59. We might expect a significant direct amplitude to be present near the 4s giant resonance in the s-wave neutron strength function, since single-particle admixtures in the capturing wave function are larger there. Dy-162 is a likely candidate for two reasons: 1) unusually large total radiation widths have been reported[4], and 2) the final state at 351 keV in Dy-163 is strongly populated in (d,p) stripping. A sample of 115 grams of 96.26% $(Dy\text{-}162)_2O_3$ was studied from thermal to 300 eV

[3] O. A. Wasson, R. E. Chrien, M. R. Bhat., M. A. Lone, and M. Beer, Phys. Rev. 173, 1170 (1968)

[4] S. F. Mughabghab and R. E. Chrien, Phys. Rev. C-1, 1850 (1970)

at the HFBR fast chopper, and the intensity variation of several lines, including that feeding the 351 keV state, has been studied over this energy range. The variation cannot be fitted using known resonance parameters, and the transition shows virtually complete destructive interference in the thermal region. Analysis is continuing in an attempt to evaluate possible bound state contributions in the positive energy region. If such possible contributions are ignored a direct amplitude, contributing between 0.1 and 1.0 barn at 1 eV, can be deduced from the data. Further measurements to higher neutron energies are in progress.

2. Channel spin admixtures in Nb-93 resonances
(R. E. Chrien, M. R. Bhat, G. W. Cole)

Gamma rays from $\ell \neq 0$ resonances show anisotropic angular distributions with respect to the neutron beam direction provided that the resonance spin is $> \frac{1}{2}$. Assuming dipole transitions, such angular distributions have the form $a+b\sin^2\theta$, where θ is the angle between photon omission and the incident beam.

For cases of non-zero target spin, one can in general expect contributions from different channel spins in forming a compound state of a given angular momentum J. The angular distribution parameters a and b are a function of relative channel spin admixture. The question of relative spin admixtures would be important, for example, for the question of the necessity of including a spin-spin term in the interaction Hamiltonian.

For the specific case of Nb-93 (spin $9/2)^+$, resonances of spin 4^- or 5^- could be formed from contributions s = 4 or 5 coupled to ℓ=1. If we denote the relative weight of channel spin 5, for example, by α, then:

$$\alpha = \frac{w_5}{w_4\ w_5} ,$$

where w_5, w_4 represent the neutron widths approprite to channel spins 5 and 4 respectively. The ratio $I(90^o)/I(135^o)$, plotted as a function of α is shown in Fig. A-2 for the transitions $5^- \rightarrow 5^+$, $5^- \rightarrow 4^+$, and $5^- \rightarrow 6^+$, as seen in the 5^- resonance at 35.8 eV.

We expect the individual channel width distributions to follow a Porter-Thomas distribution. Assuming equal strength functions for both channel spins, the variable α would consequently follow a beta-variate distribution of the first kind with parameters $(\frac{1}{2},\frac{1}{2})$. This distribution has a functional form $f(x) = 1/\pi(x(1-x))^{\frac{1}{2}}$ with a mean of $\frac{1}{2}$ and variance 1/8, as shown in Fig.A-3. Only three

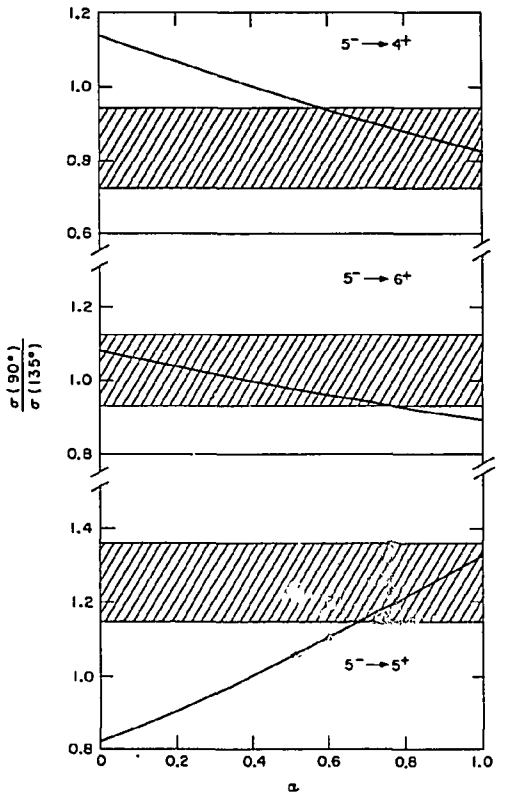

Fig. A-2. Ratio of intensities at 90° to 135° for three transitions in the 35.8 eV resonance of Nb-93, plotted as a function of $\alpha = w_5/(w_4+w_5)$

resonances could be examined with sufficient precision to establish α in the present experiment. Table A-1 summarizes the results obtained for α. Within the very limited statistics the results are entirely consistent with the assumed statistical distribution for α. It would be of considerable interest to extend these results to a sample of many resonances in order to check the dependence of strength function on channel spin.

TABLE A-1

Channel Spin Admixtures in Nb-93

Er(eV)	J^{π}	$\alpha = w_5/w_4+w_5$
35.8	5^-	0.70±.08
42.2	4^-	0.27±.17
94.3	4^-	.84±.13

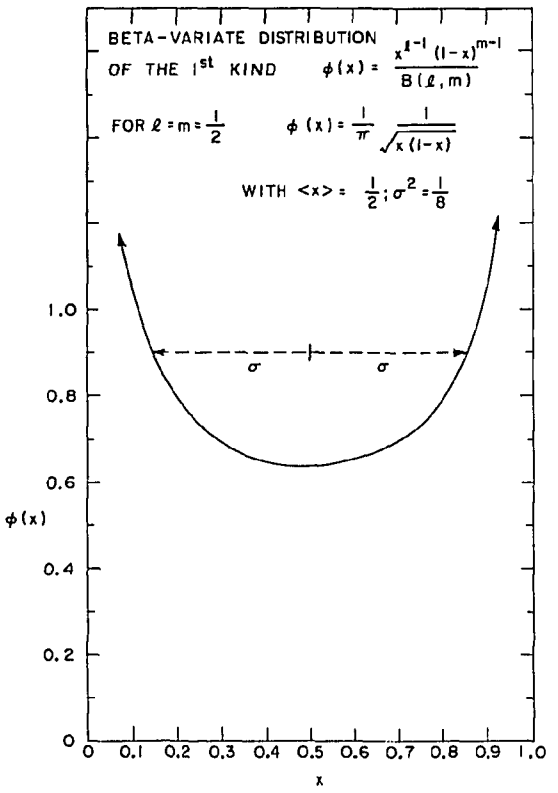

Fig. A-3. The probability density function for $\alpha = w_5/w_4+w_5$, assuming a Porter-Thomas distribution for individual widths for each channel spin in Nb-93

3. Test of the valence neutron transition model for Mo-92
(O. A. Wasson, G. G. Slaughter,* S. F. Mughabghab, R. E. Chrien)

Neutron capture γ-ray spectra for resonances in Mo-92 up to 100 keV have been obtained using ORELA. Resonances above 25 keV were not resolved, while 23 resonances below 25 keV were resolved. Nineteen of the resonances have tentatively been assigned to ℓ=1, and four to ℓ=0 neutron capture. Total cross section data have also been obtained at ORELA to aid in interpretation of the results in terms of the valence neutron model of Lynn.[5]

Some of these resonances fit the model very well. In Fig. A-4 a comparison of the predicted and observed $p_{3/2}$ spectra are

---

[5] E. Lynn, "Theory of Neutron Resonance Reactions", Clarendon Press, Oxford (1968)

* Oak Ridge National Laboratory

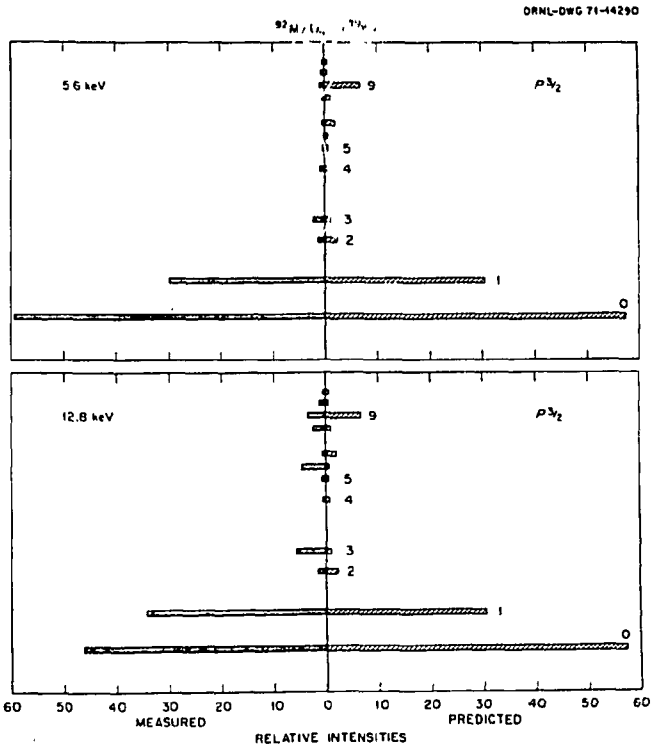

Fig. A-4. The 5.6 and 12.8 keV Mo-92 resonances compared to valence model predictions.

shown for the 5.6 and 12.8 keV resonances. In Fig. A-5 the 2.33 keV, 3.06 keV, and 23.9 keV resonances are compared to the p1/2 model predictions. Some of the resonance spins and parities, however, are still in doubt, and many of the neutron widths are poorly known. A detailed comparison with the model awaits completion of total cross section analyses and angular distribution measurements; it is quite clear, however, from the strong appearance of the 7129 keV γ-ray to the first excited state ($\frac{1}{2}$+) of Mo-93 in almost all resonances, that a statistical decay hypothesis is not tenable.

4. Search for width correlations in Dy-163(n,γ)Dy-164 (G. G. Slaughter, S. F. Mughabghab, O. A. Wasson, R. E. Chrien)

Measurements on capture spectra from resonances in dysprosium-163 have been completed at ORELA. This work was undertaken to extend measurements done at the HFBR fast chopper which reported correlations between neutron and partial radiative widths.[6]

[6] S. F Mughabghab, R. E. Chrien and O. A. Wasson, Phys. Rev. Letters 25, 1670 (1970)

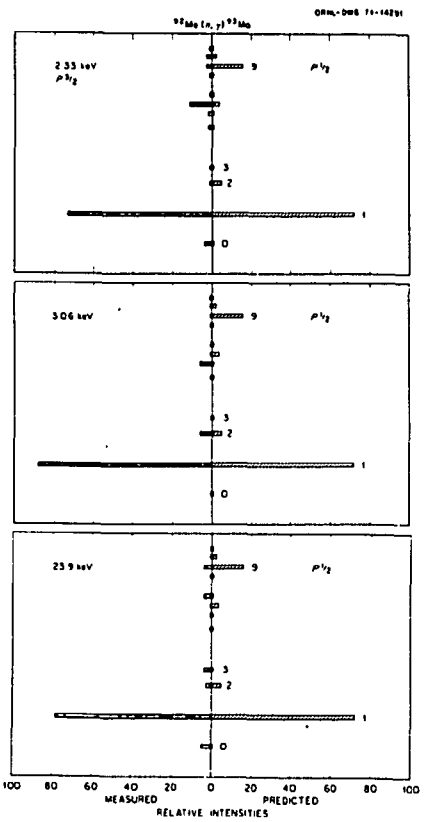

Fig. A-5. The 23.9 keV p-1/2 resonance spectrum compared to the valence model prediction. Spectra from the 2.33 keV p-3/2 (?) and 3.06 keV p-1/2 resonances are also shown.

In the newer data several previously unresolved resonances have been separated and resonances to several hundred electron volts have been identified according to spin. For 9 J=3 resonances whose neutron widths are known, the preliminary results are as follows:

a) $< \rho > = -0.15$, averaged over the 5 low-lying rotational states of Dy-164. These states are not populated in the (d,p) reaction

b) $< \rho > = +0.24$, averaged over the 3 2-quasiparticle neutron states lying near 2 MeV in Dy-164. These states are strongly populated in the (d,p) reaction.

Whether these results represent significant non-zero correlations will not be ascertained until neutron widths for many more resonances become available.

5. Search for p-wave neutron resonances in tellurium isotopes (S. F. Mughabghab, G. W. Cole, R. E. Chrien, O. A. Wasson, M. R. Bhat)

The γ-ray spectra in a natural tellurium target have been measured at the BNL-HFBR chopper in an effort to identify p-wave resonances for the region of mass number A=125. The effort is part of a systematic attempt to study p-wave neutron capture and the predictions of the valence neutron model in the region below and above the 3p strength function giant resonance. The following conclusions were obtained:

a) At least one, if not both, of the resonances near 424 and 435 eV of Te-128 is due to p-wave neutron capture. The conclusion is based on observing a very strong transition to the ground state of Te-129 (see Fig. A-6), which is a $d_{3/2}$ state. From the known

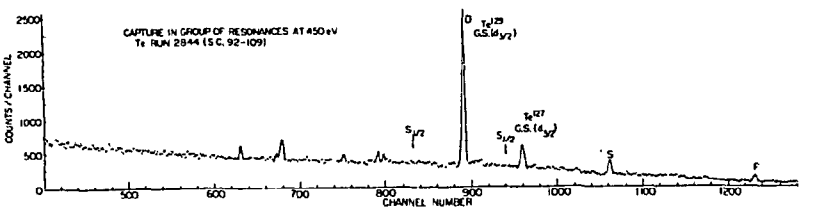

Fig. A-6. Capture spectrum for resonances of tellurium near 430 eV. Te-128 is expected to be the dominant contributor to this spectrum.

M-1 strengths in the tellurium isotopes, it seems unlikely that this transition has M-1 character. If it is E-1, then one or both of the resonances is p-wave.

b) For both Te-126 and Te-128 targets the $d_{3/2}$ ground state transition is intense, while the $s_{1/2}$ 1st excited state is absent or very weakly populated.

c) For the Te-130 resonance at 1710 eV, and for the Te-128 resonance at 941 eV transitions to $p_{1/2}$ states in the residual nucleus are absent, suggesting that these resonances are p-wave. The calculated branching ratios for $d_{3/2}$ and $s_{1/2}$ final states are in accord with the valence neutron model.

Further measurements on neutron widths, spin, and parity assignments are required, however, to verify the suppositions based on the γ-ray spectra alone.

7. Boron density profiles by $B^{10}(n,\alpha)$ (G. W. Cole, J. F Ziegler,* and J. E. E. Baglin†)

A problem of continuing interest in the physics of semiconductor devices in the determination of impurity concentration profiles in various substrates. While several techniques have been developed for such measurements, none has been applicable to studies of boron distributions. Since boron is the nearly-universal p-type dopant, determinations of its concentration profile in semiconductors is of some importance.

Experiments carried out at the H-1 beam port of the High Flux Beam Reactor have for the first time yielded an accurate determination of boron density profiles in silicon. The high cross-section of the $B^{10}(n,\alpha)$ reaction (3700b at thermal) is exploited. A 1.4 cm diameter beam of $\sim 3\times10^{8}$ cm^{-2}-sec^{-1} thermal neutrons irradiates the silicon wafer to be studied; a silicon surface barrier detector detects the α-particles and Li^{7} ions produced in the $B^{10}(n,\alpha)$ reaction. The energy of the detected particle is a direct indication of the depth at which it was produced in the silicon wafer.

---

* Thomas J. Watson Research Center, IBM, Yorktown Heights, N. Y.

† Iowa State University, Ames, Iowa

Figure A-7 shows the spectrum obtained from a calibration target containing a surface layer of 10^{16} atoms-cm^{-2} of B^{10}. The peak on the far right is due to α-particles leaving Li^7 in the ground state; the next peak to the left is due to α particles leaving Li^7 in its 479 keV excited state (94% branching). The 1470 keV α-particles from this excited state branch are the ones used for depth analysis. The two peaks at the left are due to the two Li^7 ion groups. The spectrum is free of background in the region of the 1470 keV peak. Counting time to obtain this spectrum was 5 min.

The first problem studies using this technique was the distribution of boron in the base of the NPN bipolar transistor. In the fabrication of these devices, a boron base region is introduced into the silicon by diffusion, followed by an arsenic emitter

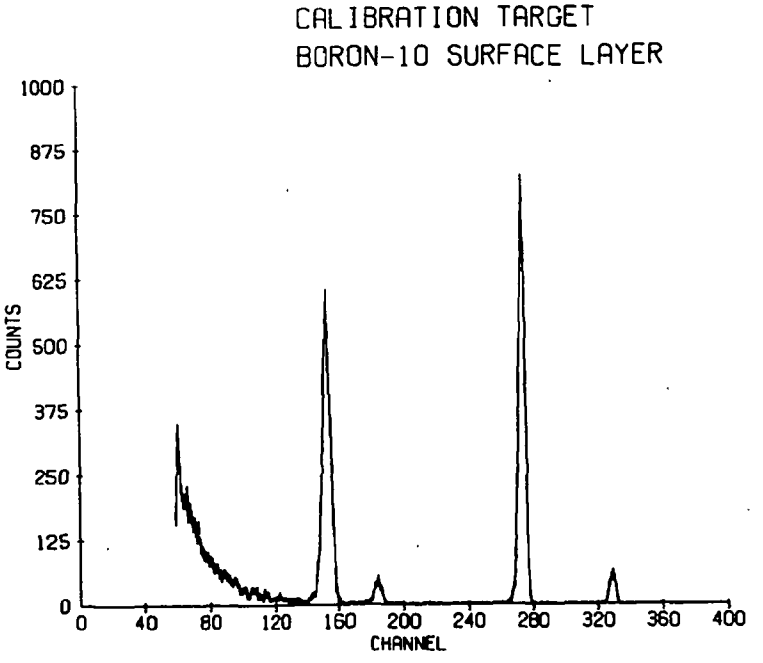

Fig. A-7. Calibration for the boron profile method. The peaks represent ground state and first excited α-particle transitions and corresponding Li-7 recoils.

layer at much higher concentration. Figure A-8 shows the results obtained for such a sample, where the arsenic concentration has been determined by other means. It is obvious that the addition of the arsenic layer has caused rearrangement of the previously smooth boron profile; the sharp dip in boron concentration at $\sim$ 850 μm does not appear in a sample which has been processed in the same fashion but has had no arsenic added. These results are of considerable significance in the understanding of such devices.

A possible explanation for this effect is a mechanism involving ion-pairing effects between the n-type arsenic and the p-type boron. In an attempt to measure this effect, we studied the diffusion constant of boron in silicon, with and without the presence of arsenic. Boron was ion implanted in two silicon targets, one of which contained a uniform arsenic doping. The two samples were then annealed at a high temperature for 120 min.

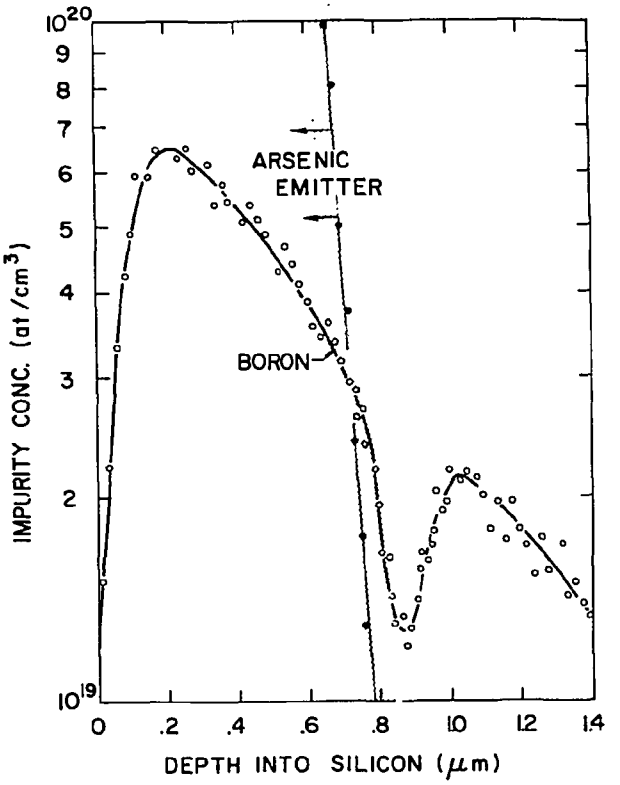

Fig. A-8. Boron profile for a sample simulating a bipolar transistor configuration. The diffusion of arsenic has caused a rearrangement in the previously smooth boron profile.

Figure A-9 shows the raw data for the boron profiles measured after this processing. In the silicon sample without arsenic, the gaussian boron profile has become completely spread out by the annealing; in the arsenic-doped wafer, however, little diffusion of the boron has occurred even though the annealing was severe. The surface of the wafer (zero energy loss for the 1470 keV α-particle) is near channel 280. From these results the existence of a strong interaction between the boron and arsenic dopants is evident.

The same technique has been applied to quantitative determinations of the diffusion constant of boron in silicon, and to the effects of annealing on ion-implanted density distributions in silicon. The method is not restricted to silicon substrates, but can be used in any matrix for which the α-particle energy loss is known.

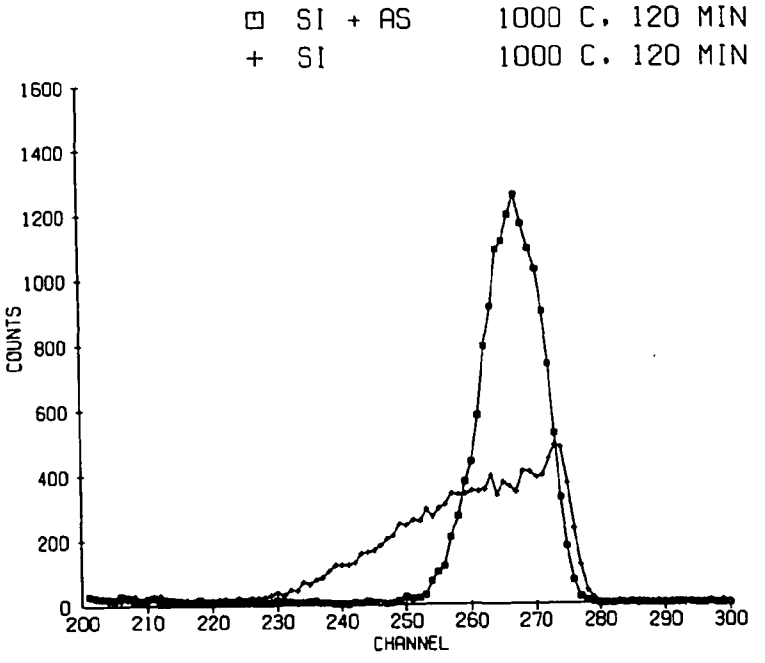

Fig. A-9. Boron profile in an annealed sample with and without arsenic doping. The presence of the arsenic inhibits boron diffusion.

2. Nuclear Structure

a. Higher Excited States of Hf^{179}, $W^{183,184}$ (R. F. Casten, W. R. Kane)

The low lying levels of these nuclei have been thoroughly investigated by charged particle reactions. However, many of the strongest transitions in such reactions occur to states at higher excitation energies (1.5 - 2.2 MeV) and spin and/or orbital assignments have not previously been made. In order to do this and thereby to study the fractionation of the single particle Nilsson picture at these energies the (n,γ) reaction has been performed at several resonance energies leading to the final nuclei listed above. Both primary capture radiation and lower energy γ transitions have been observed. Several new levels have been located, a number of discrepancies among previous (n,γ) studies clarified and a number of firm or tentative spin assignments made.

With this information it is possible to place lower limits on the number of rotational bands present and tabulate the (d,p) strength seen to levels of a given spin. Comparison of the results for Hf^{179} and W^{183} shows that while both final nuclei exhibit considerable fragmentation all of the expected (d,p) strength is found in Hf^{179} while only about half is observed in W^{183}. This is in spite of the fact that inspection of a Nilsson diagram gives the expectation that this strength should lie even lower in W^{183} than in Hf^{179}. A similar analysis has been carried out for W^{184} where in particular several 1^+ states are known. The study of these should be of interest to theorists who have recently been studying the properties of collective 1^+ modes in deformed nuclei.[1]

Finally, the W^{184} information is particularly timely since a number of experiments* leading to this nucleus have just been completed or are in progress at several laboratories. By comparing the various final state populations in the different experiments considerable information about the parentage of these levels can be extracted.

b. Study of the $Ni^{64}(n,\gamma)$ Reaction (S. Cochavi,** W. R. Kane)

The question of the relation between the (n,γ) and (d,p) reactions has been of considerable interest since it was recognized

---

* Among these are the (d,p), (d,d'), (^{3}He,α), (p,t), and (t,p) reactions as well as new decay data and the present (n,γ) work.

** Present address: Tel-Aviv University, Israel.

1 I. Hamamoto, Nucl. Phys. A177, 484 (1971).

a number of years ago that a close correspondence exists between the strengths of individual transitions in the two processes. This is especially evident in the mass region $25 \leq A \leq 70$ where the intensities of primary transitions in the (n,γ) reaction to low-lying p-shell states of the product nucleus are highly correlated with the strengths of individual proton groups for the (d,p) reaction to the same final states. The existence of strong transitions in the (n,γ) reaction to final states which possess large neutron widths in the (d,p) reaction is usually viewed as evidence that the neutron capture process takes place not only through compound nucleus formation but through a direct capture mechanism as well. While there are a score or more of nuclei in the $25 \leq A \leq 70$ mass region which exhibit strong correlations between the (n,γ) and (d,p) reactions there are three examples for which the correlation is small or absent. The product nuclei are Fe^{57}, Ni^{63}, and Zn^{65} respectively. Since the light isotopes of nickel, Ni^{59} and Ni^{61}, display very strong (n,γ)-(d,p') correlations, it is clearly of interest to investigate the two reactions leading to final states of Ni^{65}.

In new work carried out at the BNL High Flux Beam Reactor the gamma rays emitted after thermal neutron capture in Ni^{64} have been studied with both singles and coincidence measurements. Five primary transitions from the capture state to final states known to have $\ell_n=1$ in the (d,p) reaction were observed. A comparison of the strengths of corresponding transitions in the (d,p) reaction gives a correlation coefficient of 0.8, indicating a very strong correlation between the (n,γ) and (d,p) reactions leading to final states in Ni^{65}. The absence of this correlation for Ni^{63} thus does not reflect a trend with increasing neutron number, and Fe^{57}, Ni^{63}, and Zn^{65} thus remain as isolated examples of nuclei which do not follow the pattern of a strong correspondence between the (n,γ) and (d,p) reactions.

The results obtained also provided a number of new facts concerning the energy levels of Ni^{65}. The branching of low energy transitions gave probable spin and parity assignments for four of the final states observed, and a measurement of the lifetime of the 63 keV first excited state and a determination of the internal conversion coefficient of the corresponding ground state transition yielded its spin and parity. New results were also obtained on the decay of Ni^{65} to Cu^{65}.

c. Spins of Levels in Sm^{148} (W. Gelletly,† W. R. Kane)

Because of the interference from neutron capture in Sm^{149}, where the thermal capture cross section is extraordinarily large

† Present address: Schuster Laboratories, University of Manchester, England.

(41,800 barns) very little information can be obtained on the level structure of Sm^{148} from the study of thermal neutron capture, even in highly enriched samples. However, it has been possible recently, by the use of the average resonance capture method, to reduce by a large factor the dominance of Sm^{149} and thus to observe the gamma rays from neutron capture in Sm^{147}. In this way a considerable body of new information was obtained on the energy levels of Sm^{148}. The spectroscopic information provided by the average resonance capture method is necessarily incomplete, however, leaving a residual ambiguity in the knowledge of the spins of the final states populated.

With new studies of the gamma rays from the capture of neutrons in the 3.4 eV resonance of Sm^{147}, many of the ambiguities in the existing information in Sm^{148} have been removed and additional new facts disclosed. The neutron beam for this experiment was provided by a crystal monochromator at the BNL HFBR. With the use of targets enriched in Sm^{147}, it was possible to observe the capture gamma rays of Sm^{147} with essentially no interference from those of Sm^{149}. Since capture in the 3.4 eV resonance leads initially to a state with unique spin and parity, the interpretation of the gamma-ray spectrum is comparatively simple. The existence of a strong transition from the capture state to the first 2+ state of Sm^{148} confirmed that the spin and parity of the 3.4 eV resonance are 3-. The information from the gamma-ray spectrum then established the spins and parities of a number of additional levels. In particular, the assignment of the second 2+ level in Sm^{148} was confirmed. Three previously unobserved energy levels were disclosed.

d. Influence of Bound Levels on Intensities of Gamma Rays from Capture of Low Energy Neutrons in Sm^{149} and Eu^{151} (W. R. Kane, R. F. Casten, S. Cochavi)

Because of the influence of a bound level in Sm^{149}, the branching ratio in the $Sm^{149}(n,\alpha)Nd^{146}$ reaction of transitions to levels in Nd^{146} at thermal energy and below is very sensitive to the neutron energy. It was recently demonstrated that this branching ratio depends not only upon the neutron energy but also upon the temperature and chemical state of the target, i.e., that chemical binding effects, similar to the well-known effects pointed out by Lamb for resonance neutron capture, influence the effective energy of the interaction. This effect evidently may be useful in studying the dynamics of samarium atoms in various lattices.

Since the cross section of Sm^{149} for the (n,γ) reaction is a factor $\sim 10^6$ greater than that for the (n,α) reaction, it appeared worthwhile to determine if the high energy gamma rays from neutron capture in Sm^{149} also exhibit a similar dependence on neutron energy.

Such an effect would be expected since the bound resonance of Sm^{149} has 3- spin and parity, permitting E1 transitions to low-lying 2+ states of Sm^{150}, while the first positive energy resonance at 0.0976 eV has 4- spin and parity. With the use of a monoenergetic neutron beam from the crystal monochromator at the BNL HFBR, the high energy capture gamma rays of Sm^{149} were examined at several neutron energies between 0.004 and 0.0976 eV. Contrary to the situation for the (n,α) reaction, no significant changes with neutron energy were observed in the gamma-ray spectra. In particular, no transitions to known 2+ states were observed.

A more favorable case for the observation of high energy gamma rays whose intensities are sensitive to neutron energy is Eu^{151}. Eu^{151} has resonances at 0.32 and 0.46 eV and a bound state at -0.0036 eV, all of which contribute to the cross section near thermal energy. The results of a number of runs for neutron energies between 0.004 and 0.46 eV showed that the intensities of certain high energy gamma rays vary strongly with neutron energy. For example, the ratio of intensities of one pair of strong gamma rays varies by a factor of ~ 20 between 0.004 and 0.46 eV neutron energy. Eu^{151} thus also has potential utility in studies of lattice dynamics through neutron capture.

e. Test of Valence Neutron Model in $Pd^{108}(n,\gamma)Pd^{109}$ (S. F. Mughabghab,‡ W. R. Kane, R. F. Casten)

Intensities of γ-rays from neutron capture in Pd^{108} have been measured at the 2.96 eV resonance with the HFBR monochromator. Off resonance contributions near 2.0 eV and at thermal were also measured. Transitions to the ground state (E_γ = 6154±1 keV) and excited states at 910.5 and 981 keV, all $d_{5/2}$ states, establish the resonance as $p_{3/2}$. A strong transition to a level at 433 keV indicates that the $g_{7/2}$ state at 426 keV, assigned in (d,p) work, is probably a doublet.[2] The population of low-lying states with large spectroscopic factors is reasonably well predicted by the valence neutron model, except for the ground state transition, which is weakly populated.

---

‡ Dept. of Applied Science, BNL.

2 B. L. Cohen et al., Phys. Rev. 176, 1401 (1968).

B. NATIONAL NEUTRON CROSS SECTION CENTER (S. Pearlstein, M. R. Bhat, H. R. Connell, D. E. Cullen, M. K. Drake, D. I. Garber, M. D. Goldberg, P. Hlavac, R. E. Kinsey, T. J. Krieger, B. A. Magurno, V. M. May, S. F. Mughabghab, O. Ozer, A. Prince, J. R. Stehn, H. Takahashi)

A Request Bookkeeping System for the computerized experimental data library, CSISRS, has been designed to take note of additions and corrections to the file, and to keep record of queries and retrievals made from the file. It will be able to keep a profile of continuing interests for each individual and to make retrievals of new data which suit his profile.

The first large scale application of this Bookkeeping system will be to the USNDC's Compilation of Requests for Nuclear Cross Section Measurements. The requesters in that compilation have been profiled and will be informed of the existence and types of new CSISRS data related to their requests.

The third version of the recommended Evaluated Nuclear Data File, ENDF/B-III, has been distributed. It covers 124 different materials, including 61 which are individual or combined fission products, and photon production cross sections for 12 materials.

Preparations are under way to publish a new compilation of experimental neutron data. This successor to BNL-325 will consist of two volumes: one of recommended thermal cross sections and resonance parameters, the other of energy dependent data in condensed and graphical form. The technical work on the resonance parameters volume is more than half completed.

The ENDF/A Library has been expanded to include the United Kingdom Nuclear Data Library (UKNDL), the Karlsruhe Neutron Microscopic Cross Section Data File (KEDAK), the library for 198 fission product nuclides prepared by J. L. Cook (Australian Atomic Energy Commission), and the SAND-II Library of dosimetry data prepared by W. McElroy (Hanford Engineering Development Laboratory).

An evaluation of neutron-induced gamma-ray production cross sections for ^{238}U has been completed. This effort was done in conjunction with efforts to develop suitable nuclear model techniques for predicting secondary gamma ray spectra resulting from neutron interactions.

An evaluation of neutron absorption cross sections of krypton and xenon isotopes is under way to explore the possibility of locating leaky fuel elements in reactors by "tagging" them with various mixtures of isotopes of these gases.

COLUMBIA UNIVERSITY

I. NEUTRON SPECTROSCOPY

A. Neutron Resonance Cross Section Measurements (J. Rainwater, F. Rahn, H. Liou, G. Hacken, M. Slagowitz, W.W. Havens, Jr., S. Wynchank)

Recently our attention has been concentrated on the analysis of the data obtained during the two preceding experimental runs. The data on the Er, Eu, and Sm isotopes have been published in the Physical Review (Phys. Rev. C 5, 974 (1972)), as well as the paper on the statistical tests for single level populations to neutron spectroscopy data (Phys. Rev. C 5, 1002 (1972)). Papers are being prepared on the W, In, La, Yb, and Lu isotopes. Our results for the minima in the total cross section in Fe has been published in Nuclear Science and Engineering (N.S.&E. 47, 372 (1972)). The paper on resonance integrals of the rare earth isotopes Sm, Eu, Gd, Er, Yb, Lu, and W has been accepted by Nuclear Science and Engineering for publication and it will probably be published in June 1972. The data for the separated isotopes of Cd, Tl, Ce, and Dy, as well as for the natural elements Au and Ta are being evaluated.

The Nevis cyclotron modification is nearing completion, with an initial test proton beam expected by the end of this year. Final shimming of the floating iron pole pieces has been finished, and testing of the support structure for the tuning iron is in progress, with the insertion and testing of the RF copper ground skin about to start. Work has started on the electrostatic system to deflect the proton beam into a lead target for the production of neutrons.

A short catalogue of resonance energies suitable for the calibration of time of flight neutron spectrometers is being prepared. Table A1 gives resonance energies of some selected prominent sharp neutron resonances in readily available isotopes useful for this purpose. These resonance energies should be helpful in eliminating possible energy shifts in neutron spectroscopy data which may arise in neutron velocity selector results. The most common shift is due to difficulties in determining the zero point on the timing scale, in which case all calculated energies will be inaccurate by a quantity that varies monotonically with energy.

The work of the analysis of the ^{154,158,160}Gd data taken in 1968 and 1970 is nearing completion. Figure A1 shows examples of our data for these isotopes. We obtained individual parameter results up to 1 keV in ^{154}Gd and 10 keV in ^{158,160}Gd. Table A2 lists the parameters E_0, Γ_n, and in favorable cases Γ_γ for these isotopes, along with

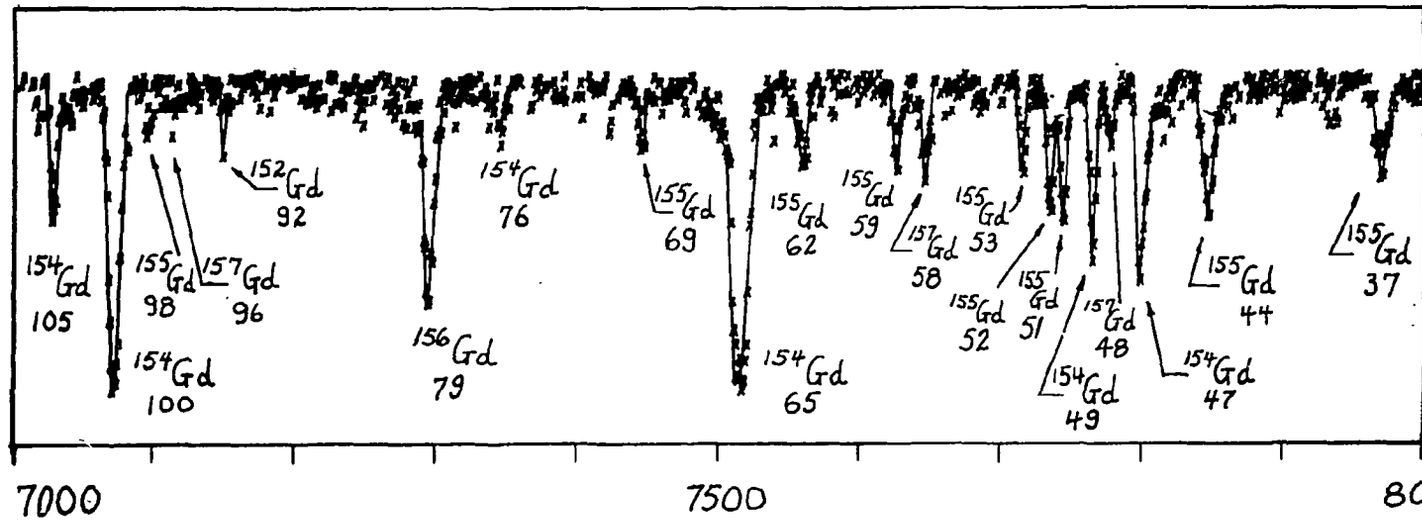

Fig. A1. Transmission of ^{154}Gd sample with (1/n)=344 barns/atom. This sample was ∿45% enriched in ^{154}Gd, ∿30% in ^{155}Gd, and had significant amounts of ^{156}Gd and ^{157}Gd present. This figure shows the isotopic identification of the prominent resonances, with their energy parameter in eV. Less prominent resonances, not indicated for reasons of clarity, are due mainly to ^{155}Gd.

TABLE A1

Isotope	E_n(KeV)	ΔE_n(KeV)	Reference
Na^{23}	53.15	0.03	17
	298.5	1.0	17
Al^{27}	5.907	0.003	12
	119.8	0.3	12
	222.9	0.4	12
	255.7	0.5	12
	365.5	0.7	12
	435.5	1.0	12
	524.9	1.3	12
	646.9	1.7	12
S^{32}	202.2	2.4	12
	380.3	3.0	12
	591.7	8.0	12
Cl (unassigned)	14.81	0.02	12
	26.67	0.03	12
	113.8	0.2	12
Ca^{40}	20.47	0.02	12
	89.40	0.13	12
	133.8	0.3	16
	146.4	0.3	12
	170.9	0.4	16
	295.1	0.8	12
	640.9	1.0	15
	694.6	1.0	15
	758.0	1.0	15

TABLE A1

Isotope	E_n(KeV)	E_n(KeV)	Reference
Ti^{47}	3.074	0.004	11
	10.510	0.014	11
Ti (unassigned)	11.040	0.016	11
	11.460	0.017	11
Mn^{55}	17.80	0.02	12
	30.30	0.04	12
	41.09	0.05	12
	53.40	0.08	12
	81.59	0.08	12
Fe^{56}	27.91	0.02	12
	73.96	0.07	12
	83.63	0.09	12
	129.53	0.14	12
	168.96	0.26	12
	188.0	0.3	12
	318.1	0.6	12
	435.5	1.0	12
Co^{59}	8.049	0.005	12
	10.692	0.010	12
	13.268	0.010	12
	31.34	0.03	12
	41.49	0.06	12
	56.39	0.04	12
	66.28	0.06	12
	84.29	0.09	12
	142.3	0.1	12

TABLE A2

Neutron Resonance Parameters of ^{154}Gd

E_0 (eV)	ΔE_0	Γ_n (meV)	$\Delta\Gamma_n$	Γ_γ (meV)	$\Delta\Gamma_\gamma$
11.58	.02	.39	.06		
22.33	.06	11.5	1.0		
47.07	.07	2.8	.4		
49.50	.07	1.6	.2		
65.06	.05	21.	3.		
76.12	.08	1.1	.3		
100.68	.11	29.	4.0	80.	15.
105.61	.12	4.5	.3		
124.00	.15	115.	17.	85.	10.
139.18	.18	124.	16.	91.	10.
148.43	.20	33.	5.		
164.48	.23	105.	7.	73.	9.
170.35	.12	5.0	1.5		
201.61	.15	11.7	2.5		
211.02	.17	35.	5.		
224.01	.18	18.	3.		
252.77	.22	12.	2.		
257.46	.23	34.	5.		
269.16	.24	28.	4.		
331.71	.34	14.	2.		
333.76	.33	13.5	3.		
364.83	.38	7.	4.		
396.53	.43	95.	8.	65.	10.
407.56	.45	45.	9.		
444.73	.26	120.	15.	76.	11.
447.05	.27	94.	8.	69.	9.
467.95	.28	125.	15.	86.	9.
486.20	.31	69.	10.	75.	15.
511.52	.34	91.	12.	83.	13.
515.98	.32	50.	7.	80.	15.
551.76	.35	55.	7.	85.	15.
589.83	.43	152.	20.	115.	30.
625.50	.42	240.	35.	80.	10.
640.32	.44	61.	14.	90.	15.
684.65	.49	55.	10.		
687.11	.49				
773.97	.59	148.	12.	105.	15.
795.02	.61	35.	8.		
808.70	.63	195.	30.	95.	15.
811.86	.64	75.	20.		

TABLE A2 (cont.)

Neutron Resonance Parameters of ^{154}Gd

E_0 (eV)	ΔE_0	Γ_n (meV)	$\Delta\Gamma_n$	Γ_γ (meV)	$\Delta\Gamma_\gamma$
836.31	.33	540.	70.	104.	15.
845.32	.34	370.	50.	96.	15.
858.95	.35	265.	40.	97.	15.
897.42	.36	310.	40.	92.	12.
910.82	.37	63.	9.	84.	13.
916.87	.37	405.	50.	98.	10.
966.71	.41	275.	40.	105.	10.
985.50	.43	157.	28.	83.	14.

TABLE A2 (cont.)

Neutron Resonance Parameters of ^{158}Gd

E_0(eV)	ΔE_0	Γ_n(meV)	$\Delta\Gamma_n$	Γ_γ(meV)	$\Delta\Gamma_\gamma$
22.30	.02	6.0	.7	96.	10.
101.08	.09	1.0	.2		
242.73	.17	46.	7.	105.	12.
277.15	.20	16.	2.		
344.76	.28	155.	15.	93.	8.
409.07	.36	265.	20.	110.	10.
503.31	.25	270.	20.	115.	10.
588.49	.31	56.	6.	112.	14.
692.86	.40	790.	100.	98.	10.
847.30	.54	1550.	200.	105.	12.
869.3	.5	3.3	1.6		
917.13	.31	460.	30.	88.	10.
1076.97	.37	270.	20.	70.	15.
1219.90	.47	850.	100.	110.	14.
1294.70	.25	430.	60.	112.	12.
1351.34	.28	25.	15.		
1427.61	.30	660.	50.	108.	14.
1458.84	.31	1070.	80.	135.	30.
1584.35	.33	360.	40.	93.	10.
1740.	1.	3.0	1.5		
1776.55	.41	480.	50.	128.	14.
1876.10	.44	265.	55.	102.	10.
*1911.	1.	1.5	1.0		
1944.68	.47	650.	120.	99.	10.
1990.60	.49	610.	120.	107.	13.
2113.	2.	8.9	4.0		
2243.40	.59	165.	35.	85.	17.
2317.33	.61	650.	80.	155.	25.
2361.	2.	7.6	4.0		
2386.66	.64	1115.	90.	117.	20.
2564.25	.71	350.	100.	135.	18.
2585.36	.72	80.	15.	70.	20.
2654.39	.75	225.	30.	95.	17.
*2706.	2.	2.4	1.5		
2795.73	.81	605.	30.	130.	25.
2868.78	.84	4200.	600.		
2933.82	.87	790.	40.	91.	13.
3071.	3.	42.	15.		
3094.15	.94	65.	25.		
3165.10	.98	220.	30.		

*p wave or spurious level

TABLE A2 (cont.)

Neutron Resonance Parameters of ^{158}Gd

E_0(eV)	ΔE_0	Γ_n(meV)	$\Delta\Gamma_n$	Γ_γ(meV)	$\Delta\Gamma_\gamma$
3325.	3.	16.	8.		
3479.28	1.13	3400.	600.		
3535.	3.	21.	12.		
3586.21	1.18	770.	100.		
3624.14	1.20	40.	20.		
3684.	3.	24.	12.		
3768.10	1.26	2950.	300.		
3936.99	1.35	1500.	240.		
3982.70	1.38	4000.	800.		
4180.42	1.48	570.	40.		
4223.	4.	30.	15.		
4299.86	1.54	445.	80.		
4468.	4.	55.	20.		
4501.24	1.65	360.	70.		
4621.00	1.73	2050.	300.		
4796.15	1.81	1650.	200.		
4894.03	1.88	420.	80.		
4985.29	1.93	1100.	250.		
5029.93	1.97	100.	50.		
5113.00	2.00	50.	30.		
5196.10	2.06	30.	20.		
5334.18	2.16	360.	160.		
5414.01	2.18	910.	230.		
5611.23	2.30	6200.	1500.		
5680.93	2.35	1900.	500.		
5759.11	2.40	1600.	400.		
5993.42	2.56	1500.	300.		
6112.05	2.62	125.	50.		
6193.99	2.67	770.	195.		
6343.48	2.76	2050.	500.		
6376.81	2.79	2300.	600.		
6782.87	3.05	700.	200.		
6807.42	3.08	350.	150.		
6878.78	3.13	100.	50.		
7266.17	3.39	100.	50.		
7445.83	3.52	250.	70.		
7548.94	3.60	270.	80.		
7610.37	3.64	2950.	750.		
7676.25	3.76	5500.	1400.		
7854.23	3.84	1650.	450.		

TABLE A2 (cont.)

Neutron Resonance Parameters of ^{158}Gd

E_0 (eV)	ΔE_0	Γ_n (meV)	$\Delta\Gamma_n$	Γ_γ (meV)	$\Delta\Gamma_\gamma$
7936.85	3.87	600.	200.		
8010.94	3.93	300.	200.		
8235.46	4.07	1550.	400.		
8288.92	4.13	650.	200.		
8368.01	4.20	3700.	900.		
8660.54	4.72	850.	210.		
8740.54	4.48	6200	1550.		
8867.21	4.57	1250.	300.		
9362.64	4.96	5800.	1500.		
9437.50	5.00	135.	80.		
9513.27	5.10	2100.	500.		
9626.00	5.18	2500.	630.		
9767.26	5.28	550.	250.		
9949.51	5.44	580.	260.		
9979.75	5.59	140.	80.		

TABLE A2 (cont.)

Neutron Resonance Parameters of ^{160}Gd

E_0(eV)	ΔE_0	Γ_n(meV)	$\Delta\Gamma_n$	Γ_γ(meV)	$\Delta\Gamma_\gamma$
221.96	.14	49.	5.	120.	17.
*421.9	.5	1.5	.7		
447.9	.5	15.	6.		
478.89	.46	320.	40.	125.	15.
*571.81	.30	6.	4.		
*707.5	1.	3.8	2.		
752.59	.45	8.	4.		
904.93	.30	3100.	360.		
**1025.	1.	2.8	1.5		
1240.94	.48	3050.	360.	85.	18.
*1291.	1.	5.	2.5		
1417.91	.30	880.	100.	115.	15.
**1632.	1.	3.3	1.6		
*1695.	1.	6.	3.		
1808.35	.42	6500.	450.		
1828.9	1.2	200.	100.		
*1874.	1.	5.	3.		
1959.79	.48	250.	40.		
2268.92	.60	1450.	100.		
2396.29	.65	5500.	750.		
2516.92	.69	4500.	1000.		
*2555.	2.	16.5	8.		
2640.21	.75	3200.	800.		
2813.22	.82	510.	120.		
*2899.32	0.85	50.	30.		
**3174.	3.	27.5	13.		
3343.	3.	25.	12.		
3454.68	1.11	200.	100.		
*3563.	3.	40.	15.		
*3598.	3.	45.	20.		
3717.93	1.24	1400.	300.		
3870.20	1.32	1300.	300.		
3931.58	1.35	550.	130.		
4517.82	1.66	6100.	1500.		
4639.	4.	20.	10.		
**4667.	4.	15.	10.		
4794.	4.	50.	20.		
5018.23	2.05	2000.	500.		
5251.92	2.09	1200.	300.		
5482.27	2.23				

*p wave or spurious level
**probably spurious level

TABLE A2 (cont.)

Neutron Resonance Parameters of ^{160}Gd

E_0(eV)	ΔE_0	Γ_n(meV)	$\Delta\Gamma_n$	Γ_γ(meV)	$\Delta\Gamma_\gamma$
5836.48	2.44	1950.	500.		
5927.89	2.50	3500.			
6390.78	2.80	2550.	650.		
6504.19	2.88	11500.	2500.		
6792.07	3.06	6300.	1600.		
6832.10	3.10	1480.	500.		
6900.65	3.20	400.	250.		
7303.64	3.43	1950.	500.		
7379.42	3.47	5600.	1400.		
7691.00	3.69	4300.	1100.		
7840.91	3.81	3100.	750.		
8305.48	4.15	3200.	750.		
8465.27	4.27	2500.	600.		
8693.70	4.44	2700.	6500.		
9095.60	4.77	3700.	900.		
9518.37	5.11	2400.	600.		
9662.38	5.20	2200.	550.		
9852.	6.				

preliminary ℓ assignments. These values have been revised from the ones we presented in our last report. Figure A2 shows the curves of N(E) versus E and the histogram of adjacent level spacings for ^{154}Gd. A good fit to a straight line is obtained to 300 eV, giving a Δ_{exp}=0.22, compared with theoretical Δ_{DM}=0.28±0.11 expected in the Dyson-Mehta theory of adjacent level spacings. The Wigner distribution gives good agreement with the histogram of adjacent spacings in this energy interval, with a correlation coefficient of adjacent spacings of $\rho(S_iS_{i+1}) = -0.6\pm0.3$ versus the $\rho \simeq -0.27$ predicted by the Orthogonal Ensemble (O.E.) theory. From Figure A3 we determine our value of the strength function. The slope of the line drawn to $\Sigma\Gamma_n^0$ versus E gives our "best choice" value of $S_0 = (2.0\pm0.4)\times10^{-4}$ for this isotope. We found $\langle\Gamma_\gamma\rangle$ = 88 meV for 25 levels in ^{154}Gd, with few values of Γ_γ more than 20% from the average. A χ^2 variance analysis gives ν = 151 degrees of freedom, mainly due to experimental uncertainties in the individual Γ_γ values.

Examples of our ^{158}Gd and ^{160}Gd results are presented in Figure A4. Figure A5 shows the level densities and Wigner plots for the ^{158,160}Gd isotopes. Good fits to a straight line for the level spacing are obtained up to ∿4 keV for these isotopes. In ^{158}Gd, we obtain Δ_{exp} = 0.29 (versus $\Delta_{DM} = 0.38\pm0.11$) and a $\rho(S_iS_{i+1}) = -0.14\pm0.15$; while for ^{160}Gd we obtain Δ_{exp} = 0.32 (versus $\Delta_{DM} = 0.30\pm0.11$) and a $\rho(S_iS_{i+1}) = -0.33\pm0.17$. The experimental average spacing of s levels is $\langle D\rangle = 86\pm4$ eV and 202±27 eV respectively. The $\sigma(k)$ of the spacings distributions for k spacings is much lower than implied by Bohigas and Flores' Two Body Random Matrix Theory, and is in general agreement with Wigner Gaussian Orthogonal Ensemble. Figures A6 and A7 show determinations of S_0 for ^{158}Gd and ^{160}Gd respectively. We find $S_0 = (1.5\pm0.2)\times10^{-4}$ and $(1.8\pm0.4)\times10^{-4}$ in these isotopes, with $\langle\Gamma_\gamma\rangle$ = 105 meV (n = 27) and 111 meV (n = 4).

The transmission-cross section data processing is nearly complete for the isotopes ^{160}Dy, ^{162}Dy, and ^{164}Dy and is nearly complete for ^{161}Dy and ^{163}Dy. The data is presently being evaluated for resonance energies and resonance parameters. We have found that the important resonance near 106 eV in ^{163}Dy is a doublet with resonance energies at 105.88±0.10 and 107.18±0.10 eV. These two levels have $g\Gamma_n$ values of 33±5 and 14±5 meV respectively.

The analysis of the ^{139}La data has been extended. The new level parameters in the energy interval 10 to 21 keV are given in Table A3. The strength function was determined to be 0.62×10^{-4} for this isotope in the 0-21 keV region.

When neutron reduced widths Γ_n are evaluated for N adjacent "single population" resonances for an isotope, it is customary to express the

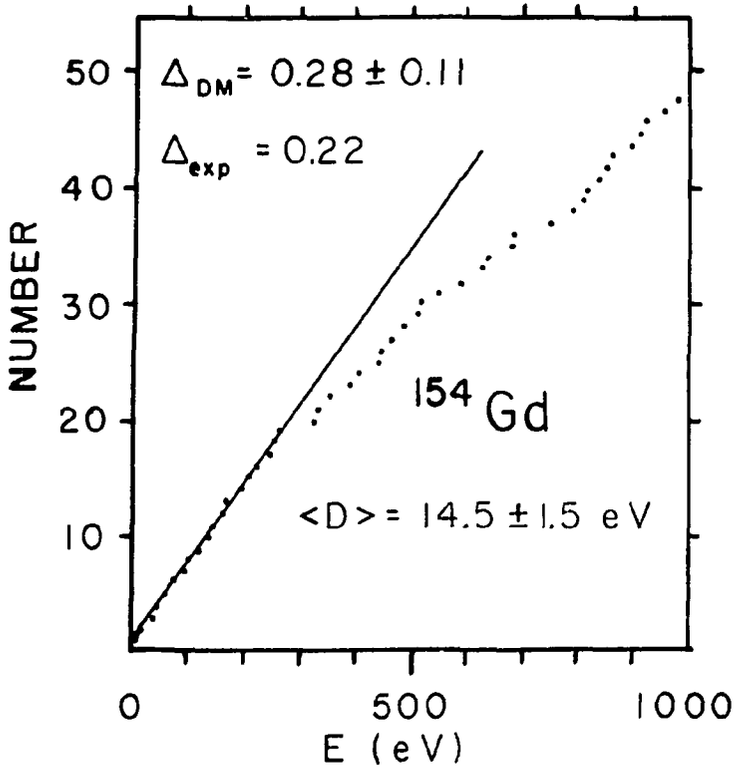

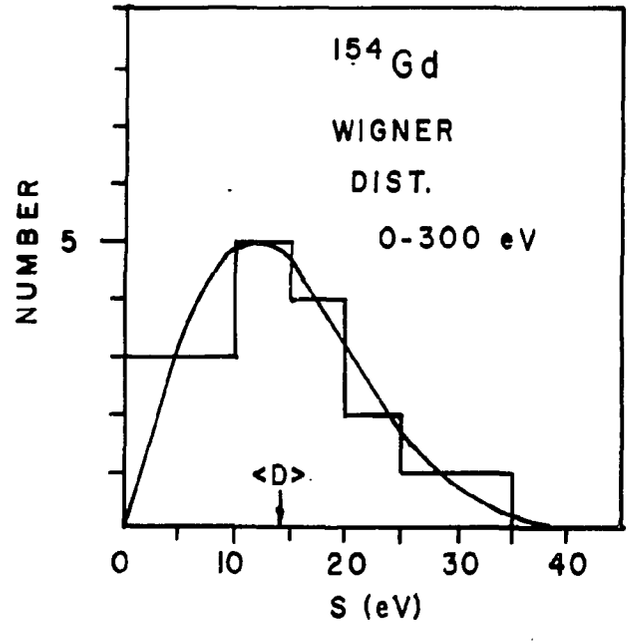

Fig. A2. (a) Number of levels versus E observed in ^{154}Gd. The sharp decrease in N(E) above 300 eV is due mainly to our inability to make isotopic assignments of many weaker levels above this energy due to the presence of significant amounts of other Gd isotopes.

(b) The observed histogram of nearest neighbor spacings in ^{154}Gd and the theoretical Wigner distribution in the energy interval 0-300 eV over which we believe all, or nearly all, s-wave resonances have been identified.

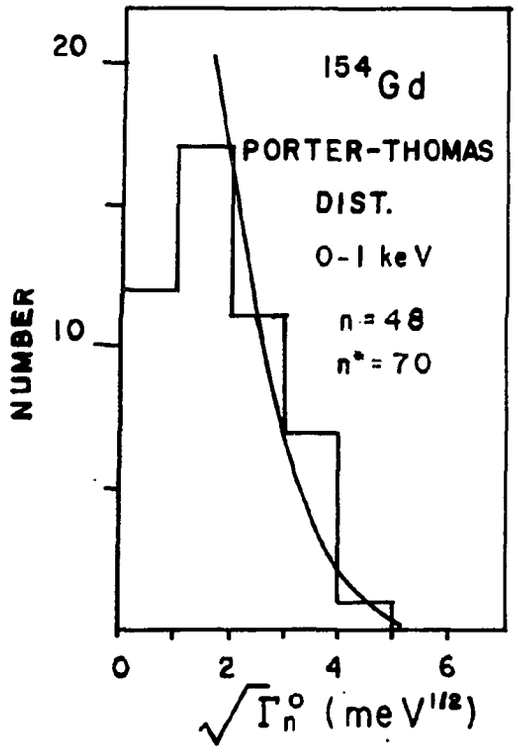

Fig. A3. (a) Histogram of reduced neutron widths for ^{154}Gd observed in energy interval 0-1 keV. The Porter-Thomas curve is also shown for n*=70 levels indicated from the level density in the lower energy interval 0-300 eV over which a good Δ_{exp} was obtained.

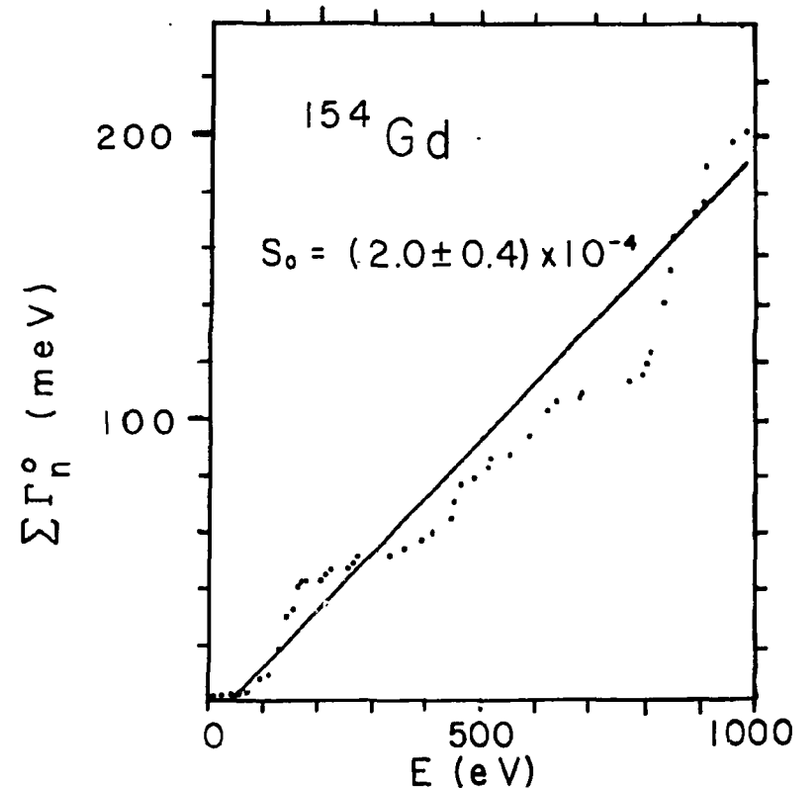

(b) $\Sigma\Gamma_n^0$ versus E. The slope of the straight line determines the s strength function, S_0.

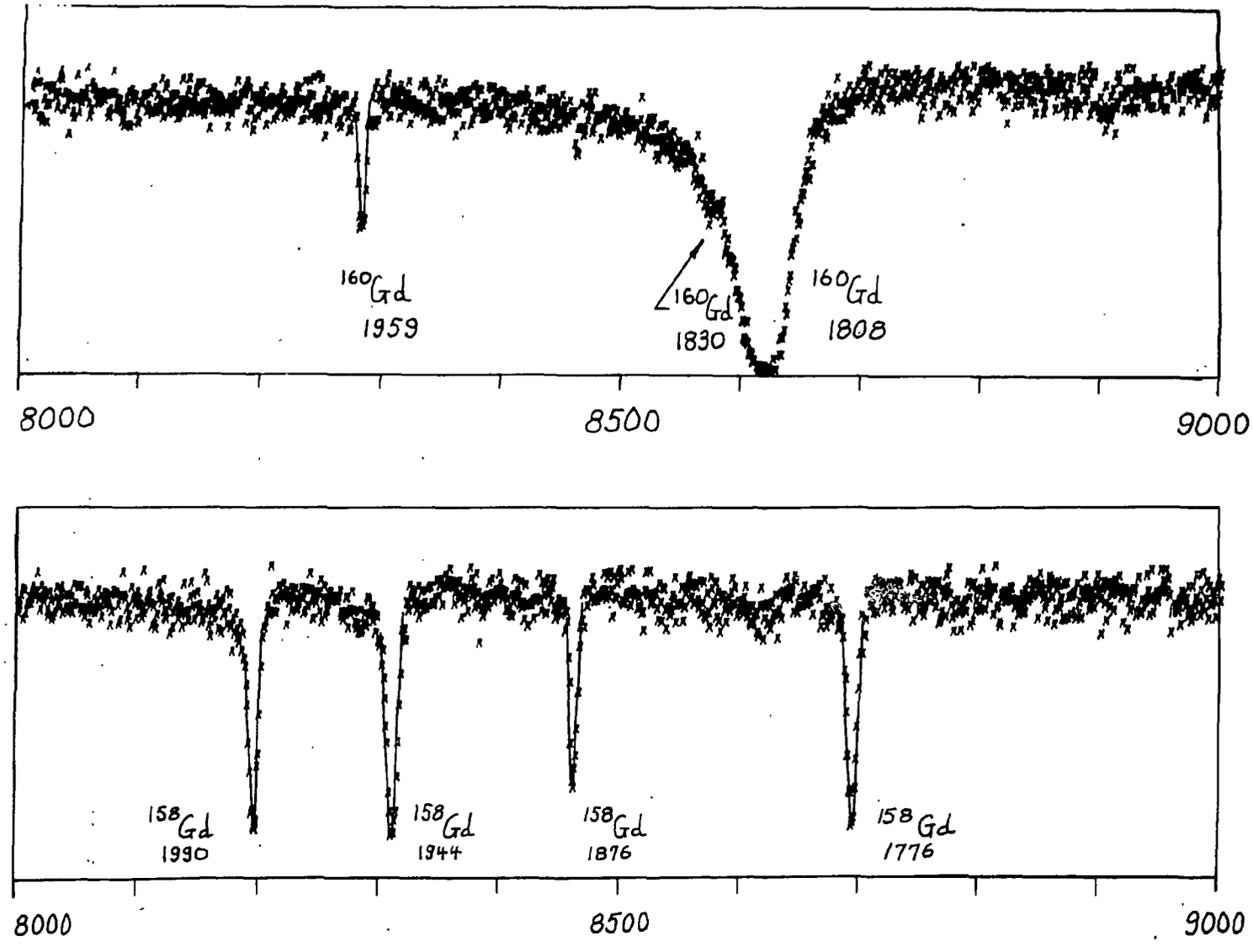

Fig. A4. Examples of our ^{158}Gd (lower plot) and ^{160}Gd (upper plot) results. These plots show transmission histograms for (1/n)=240 and 184 barns/atom respectively, with isotopic enrichments of 99% and 98%. As seen in this figure, almost no "showing through" of even the strongest resonances from the other Gd isotopes occurs.

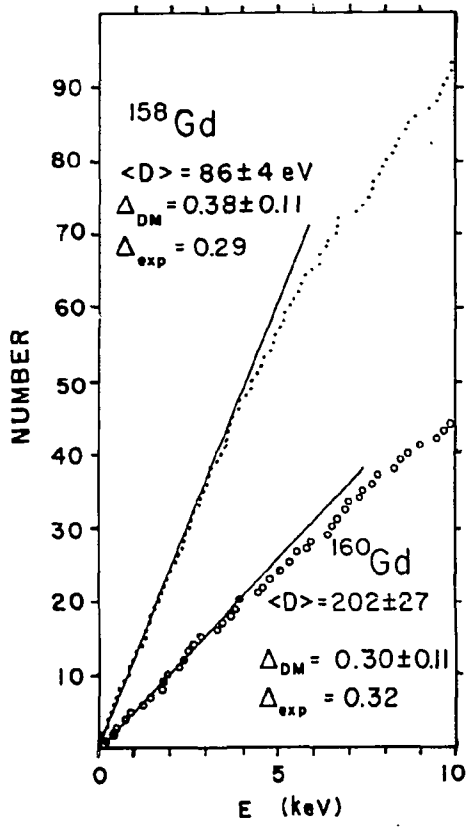

Fig. A5. (a) Number of observed levels versus E for ^{158}Gd and ^{160}Gd. Only S levels are shown. Few, if any, levels are thought to have been missed below 4 keV. Two weak levels in ^{158}Gd and 13 weak levels in ^{160}Gd were observed in the "D only" data, which we tentatively assign as p wave.

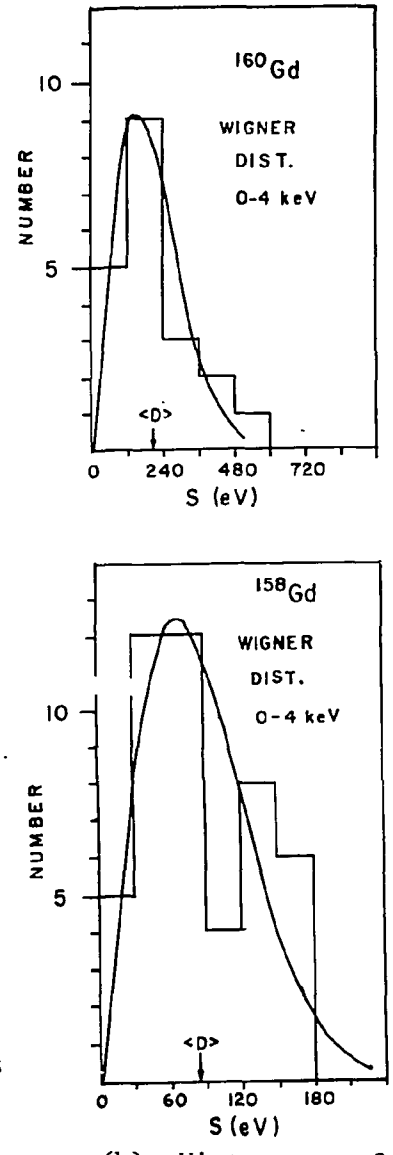

(b) Histograms of observed level spacings & Wigner distributions for ^{158}Gd and ^{160}Gd in the energy interval 0-4 keV. Relatively good fits to the data are obtained.

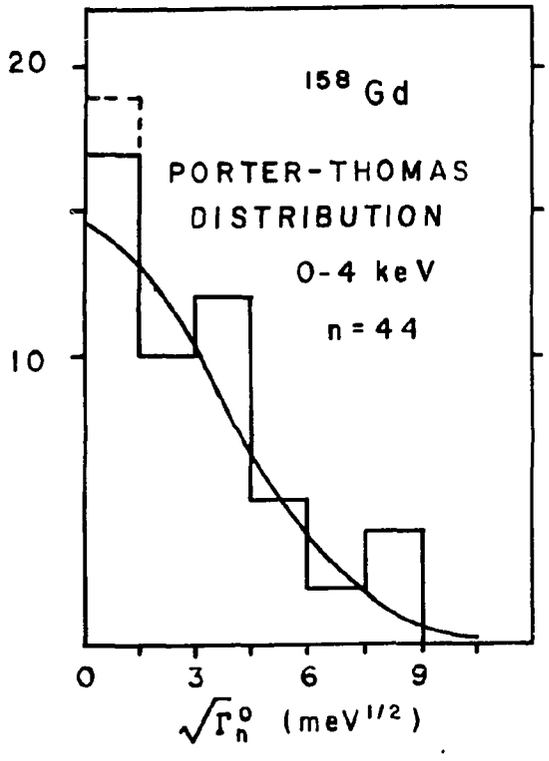

Fig. A6 (a) Porter-Thomas distribution compared to the observed distribution of reduced neutron widths. The P-T distribution has been normalized to S_0 and the level density in the 0-4 keV energy region.

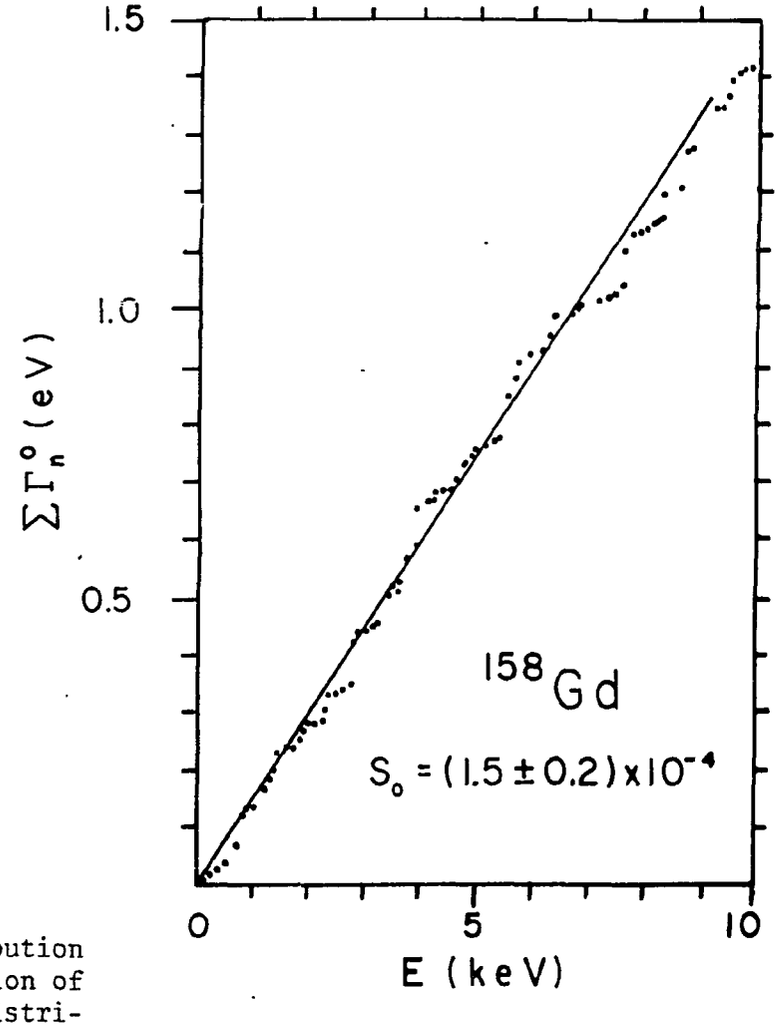

(b) $\Sigma\Gamma_n^0$ versus E for ^{158}Gd. The slope gives $S_0=(1.5\pm0.2)\times10^{-4}$ as the experimental s strength function.

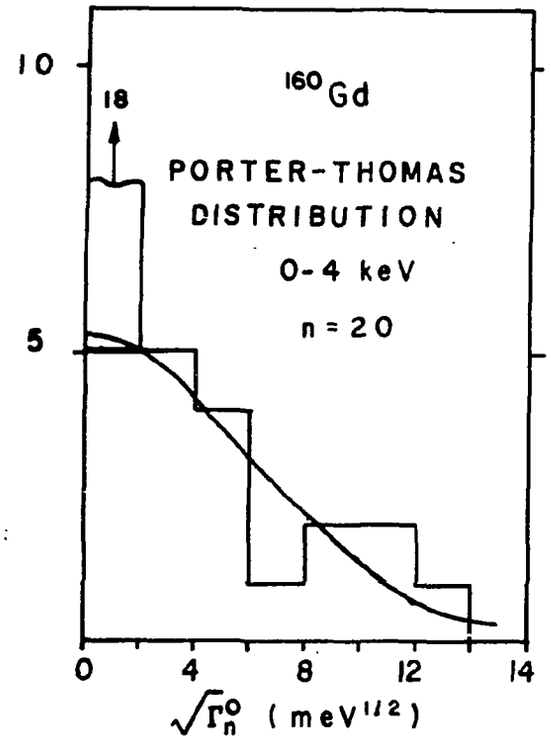

Fig. A7 (a) Porter-Thomas distribution and observed reduced neutron widths in the interval 0-4 keV. There are 13 additional "very weak" levels observed which appear in the first histogram box which are likely to be p waves or spurious levels.

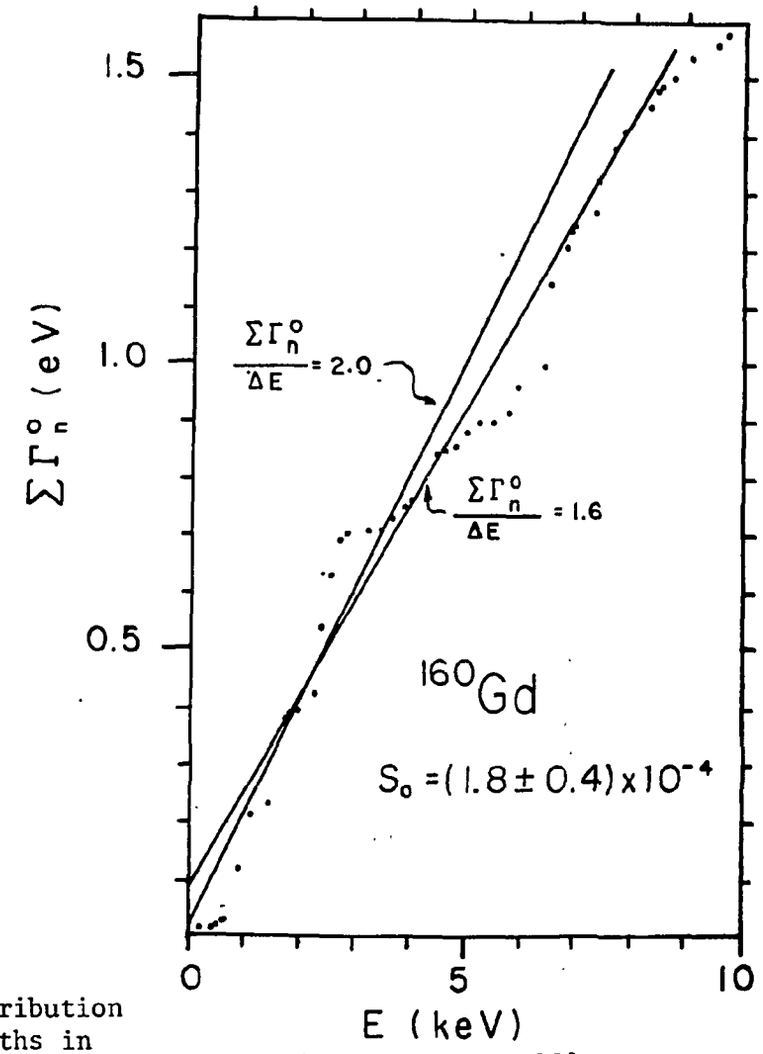

(b) $\Sigma\Gamma_n^0$ versus E for ^{160}Gd. The two lines shown give nearly extreme possibilities of S that are consistent with our data. Our best choice is $S_0=(1.8\pm0.4)\times10^{-4}$, which gives a somewhat stronger weighting to the 0-4 keV energy region.

TABLE A-3

Neutron Resonance Parameters of ^{139}La

	E_0 (eV)	$g\Gamma_n$ (meV)		E_0 (eV)	$g\Gamma_n$ (meV)
1	10375	540	16	14217	2050
2	10580	415	17	14584	2700
3	10731	220	18	14890	3000
4	11170	1500	19	15142	810
5	11518	1600	20	15206	4300
6	11908	200	21	16273	8000
7	11989	600	22	17207	6500
8	12134	1300	23	17891	5000
9	12404	430	24	18565	8000
10	12673	1200	25	18880	4000
11	13124	3500	26	19023	2500
12	13280	760	27	20227	10000
13	13396	1300	28	20465	5100
14	13492	820	29	21017	(15000)
15	14125	450			

fractional uncertainty in the s strength function, S_0, as $\pm(2.27/n)^{1/2}$ or $\pm(2/n)^{1/2}$, where n is the number of levels. It is assumed that the Γ_n^0 values follow a Porter-Thomas single channel distribution with a common $\langle\Gamma_n^0\rangle$ for the interval, with no correlation between the different Γ_n^0. If the spacing distribution follows the Wigner formula for the nearest neighbor spacings, but with no correlations, the $(2.27/n)^{1/2}$ fractional uncertainty applies for large n. For spacings following a statistical Orthogonal Ensemble (O.E.) behavior, the fractional uncertainty in $\langle D\rangle$ is $\sim 1/n$, so the fractional uncertainty in S_0 is $\sim(2/n)^{1/2}$ for large n. For small n, the situation is more complicated. We have used Monte Carlo methods with a Porter Thomas distribution for Γ_n^0, and O.E. for spacings, to establish the upper and lower bound values for S_0, divided by $\overline{S_0} \equiv \overline{\Gamma_n^0}/\overline{D}$ (the ratio of the measured averages of Γ_n^0 and D). The method of confidence intervals was used.

The distribution functions, ρ, for $\overline{S_0}/\langle S_0\rangle$ generated by Monte Carlo methods for the O.E. case are shown in Figure A8. We denote the best choice value as C_N. The results of the analysis showed that smooth curves for C_N and the upper and lower limits of the distribution functions that lie within one standard deviation, $\rho_{0.8413^+}$ and $\rho_{0.1587^-}$, are well fitted by:

$$C_N = 1.0 + 0.858/n - 1.18/n^2 + 1.28/n^3$$

$$\rho_{0.8413^+} = 1.0 + 7.73/(n+1.39) - 39.7/(n+1.39)^2 + 139/(n+1.39)^3$$

$$\rho_{0.1587^-} = 1.0 - 10.7/(n+16.7) + 249/(n+16.7)^2 - 3020/(n+16.7)^3$$

The figure and empirical formulae are intended for easy use by experimentalists in presenting the results of measurements. No attempt has been made to fold in the contributions due to experimental uncertainties in the measured quantities. A simple quadrature method might be suitable.

B. Cross Section and Resonance Parameters A<80 (F. Rahn, J. Rainwater, W.W. Havens, Jr., M. Slagowitz, U. Singh)

Transmission measurements of the total neutron cross section of natural sodium samples were run during the 1968 and 1970 experimental series. The measurements covered the energy region of 10 eV to greater than 350 keV. The full width half maximum resolution of the data was approximately 0.2 nsec/meter. Our previous results on sodium were limited by resolution and background effects to energies below 100 keV. Our present data is an attempt to increase the energy interval so that it extends into the region where other recent measurements have been made at higher energies.

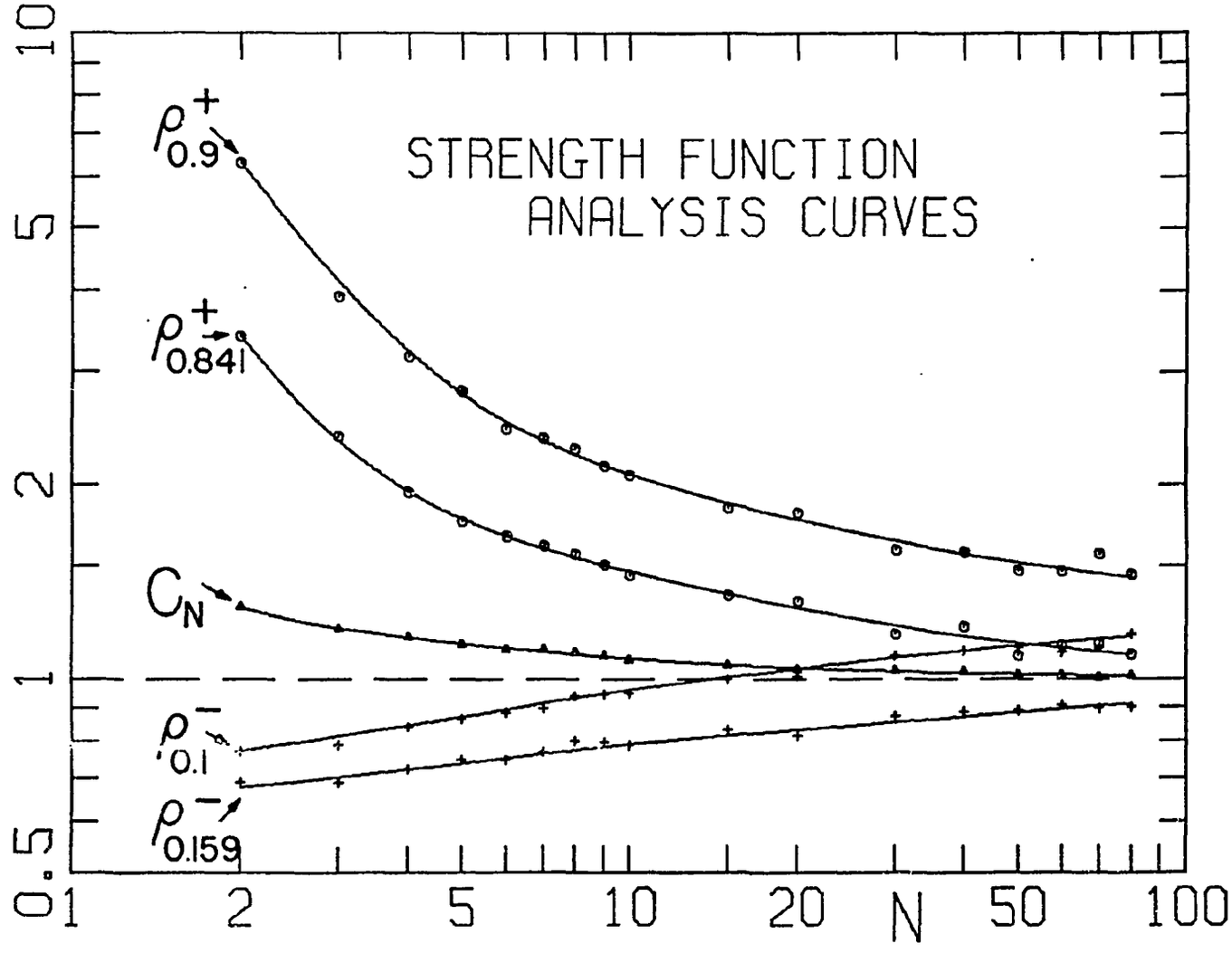

Fig. A-8. Monte Carlo results for C_N and ρ_A^+ and ρ_A^- for determining a "best choice" and (±) uncertainties for the "true" strength function S_0 in terms of the observed averages $\overline{\Gamma^0}_n/\overline{D}$. We suggest using "true" $S_0 = C_N(\overline{\Gamma^0}_n/\overline{D})$ with asymmetric (±) fractional uncertainties ρ_A^+/ρ_A^- times $(2/n)^{1/2}$.

Our samples had a range of inverse thickness (1/n) values between 4.8 and 550 barns/atom. The background associated with our data presented special problems above 20 keV, where it was found to be especially dependent on the neutron energy. In order to assure an accurate normalization of the data, we used Fe and Co in the filter technique, which directly yields the total cross section of sodium at points in the energy spectrum where these materials have sharp resonance structure. In this manner we have determined the sodium cross section near the 376 Fe resonance to be 3.46 barns.

Figure B1 shows our results in the 20 to 360 keV region. The measured total cross section as shown in this figure and the "true" cross section differ by an amount which depends on the thickness of our samples and resolution effects. The resolution effects, important where the cross section is rapidly varying, is a function of the transmission, T(E). The resonance parameters of the first two levels, obtained by an R-matrix analysis, are as follows: the 2.850 keV level is assigned J=1, ℓ=0 with Γ=388 eV, and the 53.15 keV level can be fit with J=2, ℓ=1 and Γ=1228 eV. These R-matrix parameters are consistent with peak cross sections of $\sigma_0 \simeq 390$ and 37 barns respectively, and the shapes of these resonances. There is general agreement of our total cross section values with the Karlsruhe data in the region where the data sets overlap, 280 to 360 keV. Our values are slightly higher overall, and do not go as deep in the minimum close to 296 keV, which may be due to the lower resolution of our data in this region.

Measurements of the total cross section of natural copper and ^{63}Cu were also made during 1968 and 1970, for a series of thicknesses (1/n)=4.6 to 458 barns/atom. Figure B2 shows our results from 60 to 2 keV. The filter materials Co, Fe, Ta, Cl, and U were used to assure a proper normalization of the data. Work is beginning on the resonance parameter analysis, which will include area and shape formulisms, to determine the energies and neutron widths of the observed levels, isotopic identification, and attempt to assign their ℓ and J values.

The resonance parameters for the Ca isotopes A=40 and A=44 are presented in Table B1. Values of the spin J and orbital angular momentum ℓ were determined by an R-matrix fit of the data in the energy region 0 to 300 keV, and Γ_n values also obtained. The data was further processed by an area analysis to find $g\Gamma_n$ for the weaker levels in these isotopes. The preliminary values of the strength functions for these isotopes were estimated to be: $S_0 = 3.12\times10^{-4}$, $S_1 = 0.33\times10^{-4}$ (for ^{40}Ca) and $S_0 = 0.02\times10^{-4}$ and $S_1 = 1.68\times10^{-4}$ (for ^{44}Ca).

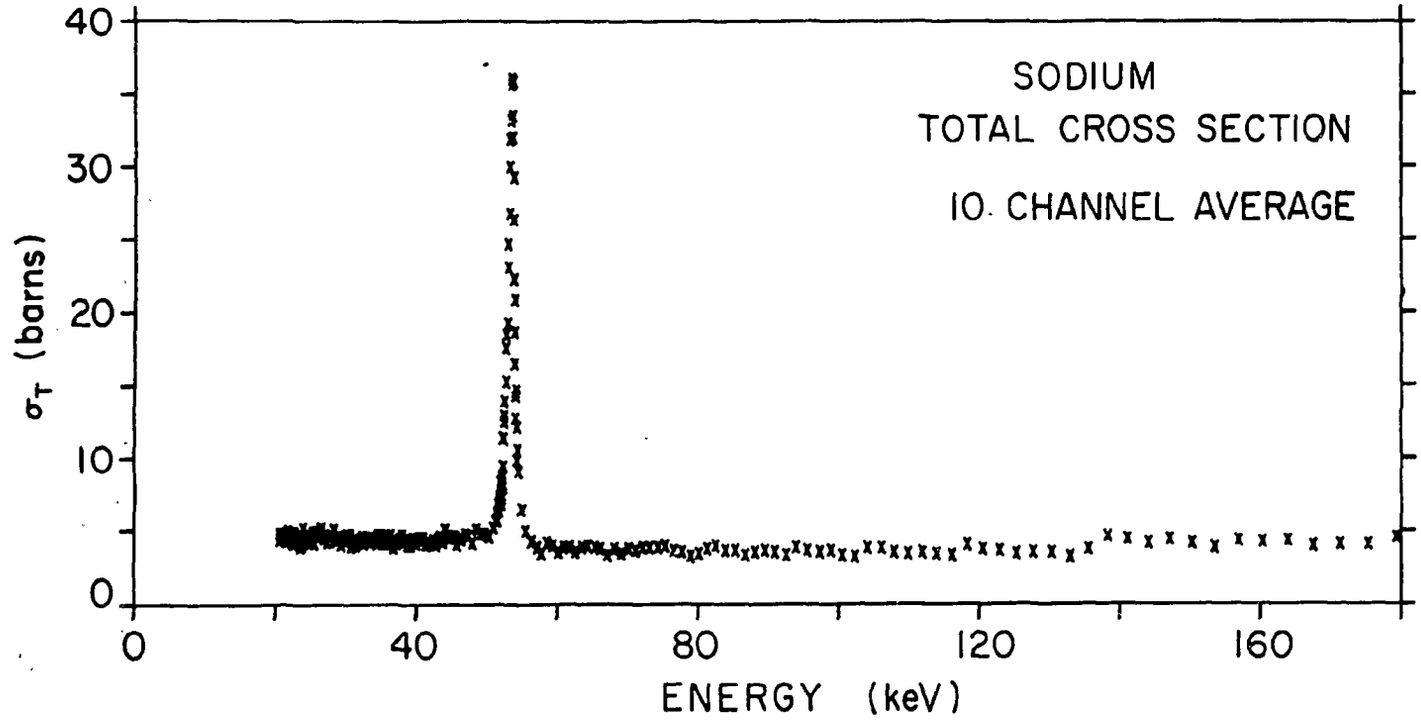

Fig. B1. Total cross section of natural sodium from 20 to 360 keV. This experimental σ_T is subject to effects which are dependent on the thickness of our samples and the resolution of the NVS time of flight spectrometer.

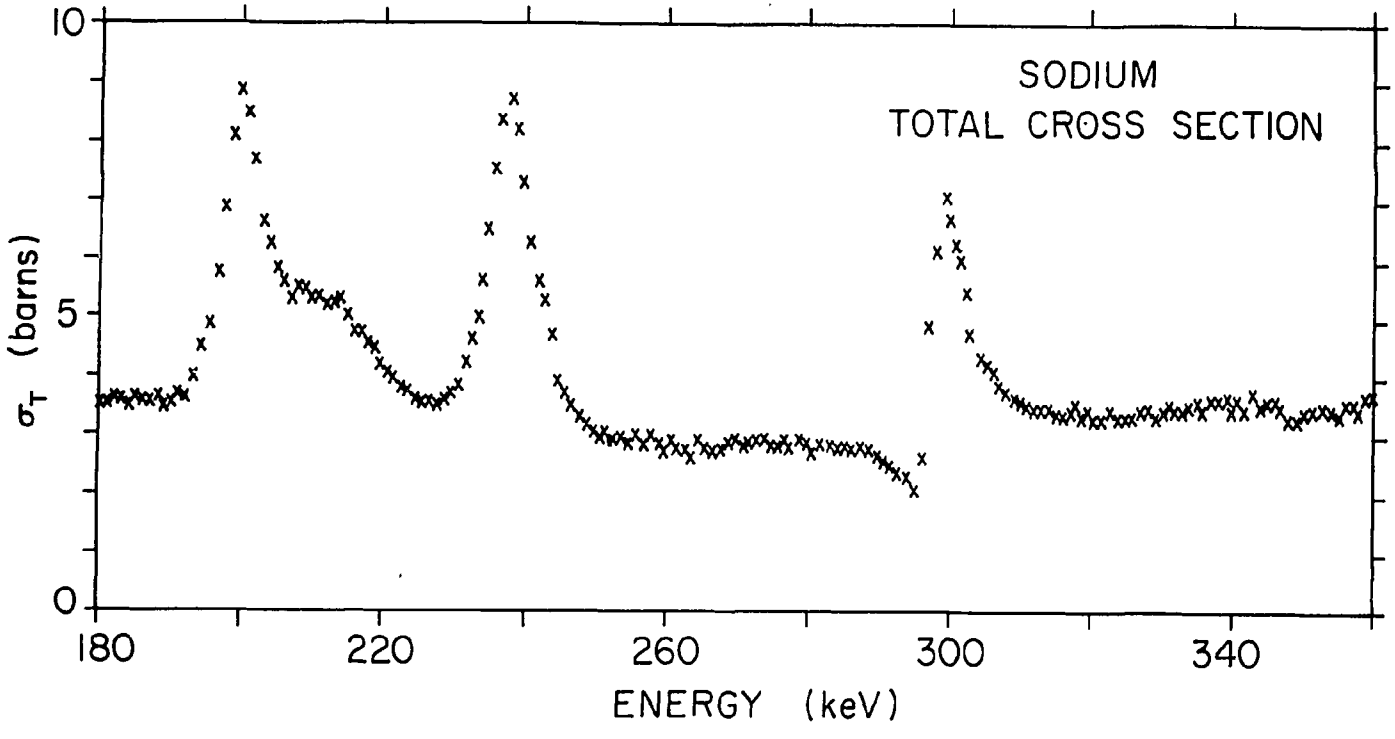

Fig. B1 (continued). Total cross section of natural sodium, 20-360 keV.

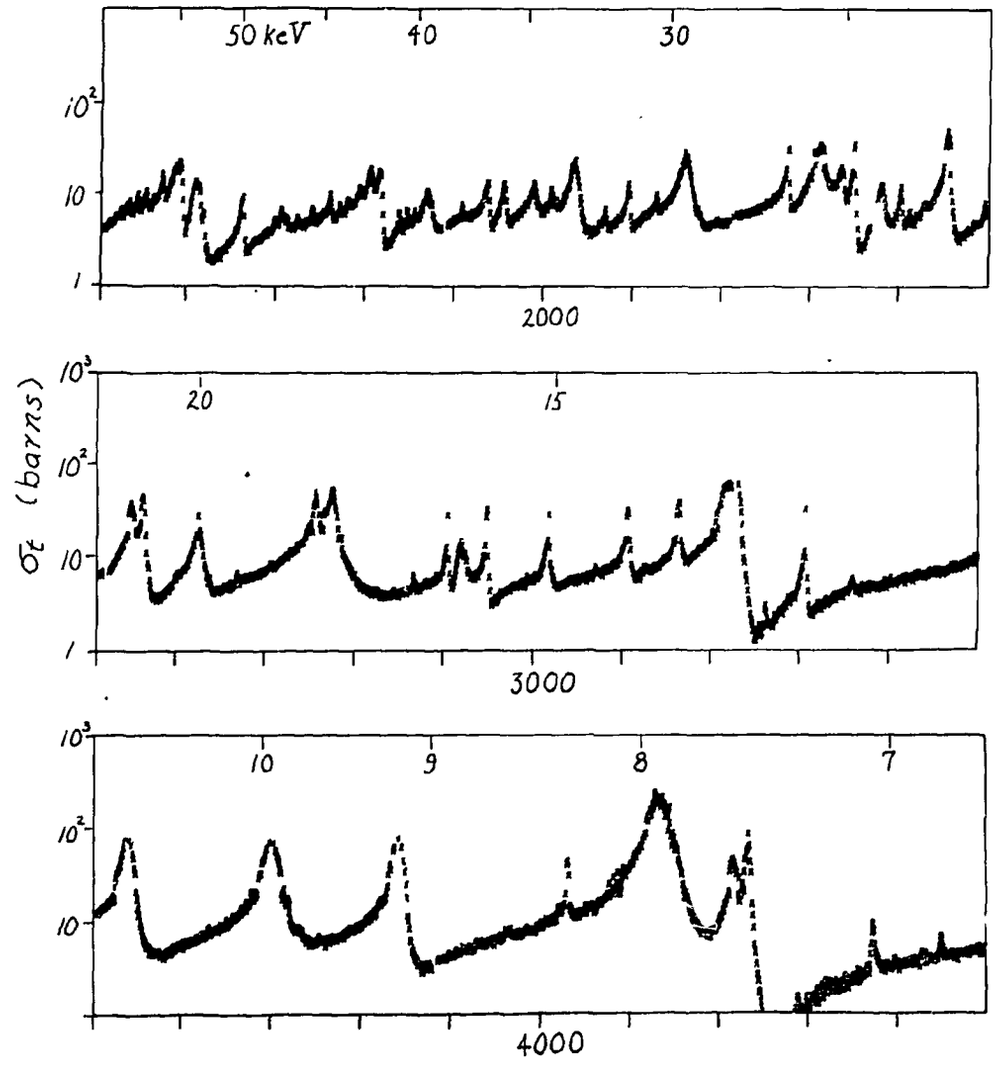

Fig. B2. The total cross section of natural copper in the energy interval 60 - 2.5 keV.

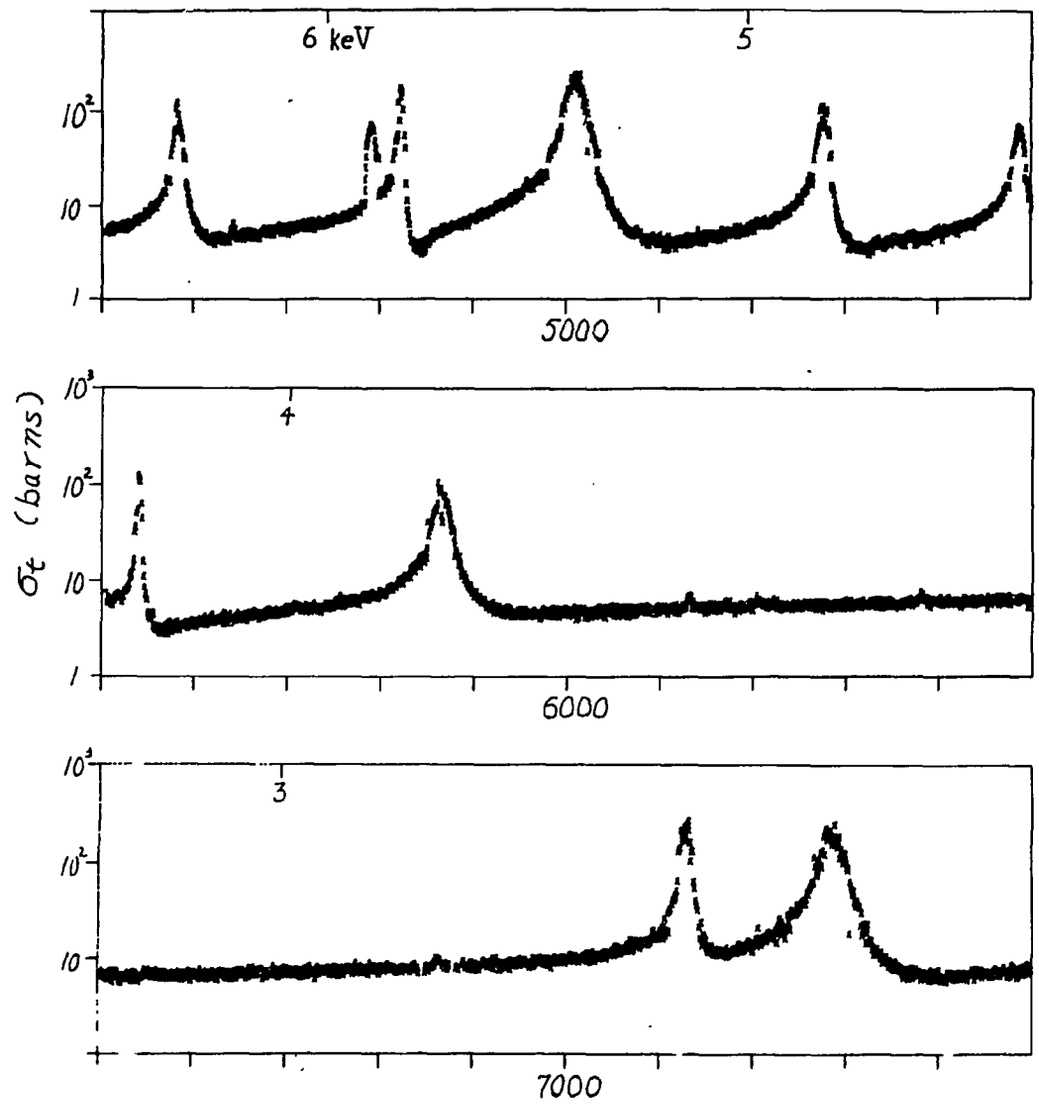

Fig. B2 (continued). Total cross section of natural copper in the energy interval 60 to 2.5 keV.

TABLE B-1

Ca (Resonance Parameters)

E_0 (keV)	Shape				Area		
	A	ℓ	J	Γ_n (eV)	A	ℓ	$g\Gamma_n$ (eV)
10.834±0.010	44	1	3/2	12	44	1	(22±5)
20.427±0.023	40	1	1/2	5	40	1	(8±2)
42.075±0.062	44	0	1/2	130	44	0	(35±5)
51.27±0.16	44	1	3/2	570	44	1	(700±100)
88.84±0.17	40	1	1/2	150	40	1	(150±20)
101.18±0.21	44	1	3/2	630	44	1	(800±100)
131.87±0.31	40	0	1/2	3220			
145.3±0.35	40	1	1/2	140	40	1	(160±20)
169.38±0.44	40	0	1/2	2460			
211.5±0.60	40	1	1/2	140	40	1	(170±20)
217.5±0.60	40	0	1/2	6900			
244.5±0.8	40	0	1/2	18300			
292.58±0.97	1	1	1/2	1340			

C. Cross Section and Resonance Parameters of ^{232}Th and ^{238}U (F. Rahn, H. Liou, J. Rainwater, W.W. Havens, Jr., M. Slagowitz, S. Wynchank).

Tables C1 and C2 give resonance parameters for levels we identify as p levels in ^{232}Th and ^{238}U. The calculation of the $g\Gamma_n^l$ values requires that an effective nuclear radius R be chosen. This gives a "barrier energy" E_1 where the neutron wave length λ equals R. We use $R=1.41\ A^{1/3}$ fermi, giving E_1=276 keV and 270 keV for ^{232}Th and ^{238}U respectively. The statistical spin factor g is included, and is unity except for $P_{3/2}$ levels where it is equal to 2. The information from the $g\Gamma_n^l$ values for these levels permits us to make rough estimates for the p wave strength functions S_1 for the two isotopes. In making such estimates it must be noted that (a) most of the p levels are too weak for us to observe, (b) the fractional uncertainties in these $g\Gamma_n^l$ values are relatively large, (c) these weak levels are mainly seen using our thickest samples where a significant fraction of the energy range is not satisfactory for observing weak p levels due to the effects of the strong s levels, and (d) an examination of our data shows that we have a greatly reduced efficiency for detecting p levels above 400 eV in ^{232}Th and 1200 eV in ^{238}U.

We assume that the "true" p level density is three times that for s levels (due to statistical factors) and the $\langle g\Gamma_n^l\rangle$ is the same for $P_{1/2}$ and $P_{3/2}$ levels. An estimate is made of the effective energy interval ΔE_1, available not too near the strong s levels, and the strength function implied by the number of levels observed having $g\Gamma_n^l$ values greater than a given $g\Gamma_n^l$. We found $S_1=(0.9^{+0.5}_{-0.3})\times10^{-4}$ for ^{232}Th and $(1.43^{+0.30}_{-0.27})\times10^{-4}$ for ^{238}U. The uncertainties in these values were determined by using distinctly too few and too many levels to be consistent with our data.

From our analysis of total cross section data, including shape fitting of various well isolated s resonances, we were able to arrive at values of R', the optical model potential scattering radius. Interference contributions from more than one resonance are significant in these isotopes, except in the vicinity of a few single isolated resonances, notably the 221 eV level in ^{232}Th and 347 eV level in ^{238}U. At these energy regions, we examined the behavior of σ_T, particularly at the interference minima and in the wings where σ is sensitive to R', and resolution effects are relatively unimportant. We found that R'=9.1±0.3 f. for ^{232}Th and 9.6±0.3 f. for ^{238}U.

TABLE C-1. Neutron Resonance parameters for assigned p levels in ^{232}Th.

E_0 (eV)	ΔE_0	$g\Gamma_n^1$ (meV)	$\Delta g\Gamma_n^1$	E_0 (eV)	ΔE_0	$g\Gamma_n^1$ (meV)	$\Delta g\Gamma_n^1$	E_0 (eV)	ΔE_0	$g\Gamma_n^1$ (meV)	$\Delta g\Gamma_n^1$	E_0 (eV)	ΔE_0	$g\Gamma_n^1$ (meV)	$\Delta g\Gamma_n^1$
58.84	0.07	3.6	1.8	380.40	0.33	4.0	1.3	1217.3	0.4	3.9	1.4	1897.1	0.4	6.5	2.6
90.08	0.08	3.2	1.6	402.62	0.36	3.0	1.5	1223.8	0.4	2.6	1.2	2015.4	0.4	2.4	1.3
128.21	0.12	8.5	2.0	533.55	0.27	4.9	1.7	1233.3	0.4	4.8	1.7	2055.5	0.5	1.5	0.8
145.72	0.15	14.1	3.0	535.45	0.27	7.1	2.0	1260.8	0.5	3.7	1.3	2158.5	0.5	5.5	2.3
178.62	0.21	6.9	2.2	660.66	0.37	3.2	1.3	1261.7	0.5	5.6	1.8	2170.1	0.5	7.9	2.9
202.41	0.25	2.8	1.4	771.7	0.4	1.9	1.0	1287.84	0.25	3.0	1.3	2206.8	0.5	5.6	2.4
210.87	0.26	1.8	0.9	846.7	0.5	1.6	0.8	1345.65	0.27	5.3	2.0	2307.2	0.5	7.6	2.9
219.30	0.28	1.7	0.9	869.3	0.5	7.7	2.8	1349.44	0.27	4.4	1.6	2329.5	0.6	4.9	2.1
242.23	0.16	2.1	1.1	919.26	0.30	2.9	1.4	1384.59	0.29	1.6	0.9	2427.4	0.6	5.5	2.4
290.12	0.21	2.2	1.1	934.24	0.31	1.9	0.9	1441.30	0.30	6.1	2.5	2434.6	0.6	6.8	3.0
302.30	0.23	5.2	2.2	1021.38	0.35	2.9	1.3	1469.27	0.31	1.4	0.8	2462.5	0.6	8.0	3.2
309.20	0.24	3.0	1.4	1043.74	0.37	5.3	2.0	1509.56	0.32	16.6	3.4	2604.0	0.7	3.3	1.7
321.47	0.25	1.9	1.0	1073.73	0.39	1.6	0.8	1610.47	0.36	3.5	1.5	2803.4	0.8	8.5	3.5
338.26	0.26	2.6	1.3	1115.9	0.4	8.0	2.4	1689.65	0.38	5.9	2.1	2843.2	0.8	2.7	1.4
361.47	0.31	3.2	1.6	1132.7	0.4	2.2	1.1	1767.1	0.4	5.5	2.2	2861.2	0.8	14.5	5.0
												2870.4	0.8	2.7	1.5
												2932.0	0.8	2.7	1.5

TABLE C-2. Neutron resonance parameters for assigned p levels in ^{238}U.

E_0 (eV)	ΔE_0	$g\Gamma_n^1$ (meV)	$\Delta g\Gamma_n^1$	E_0 (eV)	ΔE_0	$g\Gamma_n^1$ (meV)	$\Delta g\Gamma_n^1$	E_0 (eV)	ΔE_0	$g\Gamma_n^1$ (meV)	$\Delta g\Gamma_n^1$	E_0 (eV)	ΔE_0	$g\Gamma_n^1$ (meV)	$\Delta g\Gamma_n^1$
10.22	0.01	14.6	3.0	337.19	0.27	2.2	1.1	846.9	0.4	11.0	3.3	1256.5	0.4	1.2	0.9
19.50	0.02	4.3	1.8	351.75	0.30	3.3	1.5	890.6	0.3	8.0	2.7	1371.6	0.3	3.2	1.7
45.19	0.07	1.8	0.9	354.66	0.31	1.2	0.8	909.5	0.3	12.7	3.5	1381.6	0.3	3.1	1.6
63.54	0.08	3.2	1.4	407.64	0.36	2.7	1.4	932.3	0.3	2.9	1.6	1410.5	0.3	2.0	1.2
83.57	0.08	1.4	0.7	439.71	0.39	4.7	2.1	940.1	0.3	2.9	1.5	1416.3	0.3	8.9	2.7
89.19	0.08	28.8	3.5	488.20	0.40	11.2	3.4	964.9	0.3	1.8	1.1	1549.8	0.3	5.3	2.3
121.61	0.11	1.2	0.7	498.93	0.25	2.0	1.1	976.8	0.3	5.3	1.9	1646.1	0.3	3.9	2.1
124.30	0.12	2.3	1.2	523.21	0.26	4.5	2.0	985.6	0.3	2.6	1.4	1744.9	0.4	7.3	2.6
152.42	0.16	5.7	2.2	542.34	0.28	1.1	0.8	1014.4	0.3	13.2	3.0	1912.6	0.4	1.6	1.0
158.89	0.17	0.9	0.7	606.12	0.33	4.5	2.2	1031.1	0.3	8.1	2.7	2175.1	0.5	3.9	2.0
173.11	0.19	3.0	1.3	624.80	0.34	17.3	3.8	1062.3	0.3	5.4	2.5	2288.9	0.6	2.2	1.2
202.30	0.25	3.7	1.5	668.40	0.37	3.9	1.8	1067.6	0.3	7.7	2.1	2798.1	0.8	3.7	1.9
214.97	0.27	3.4	1.4	677.50	0.39	10.6	3.1	1071.0	0.3	2.4	1.3	2907.1	0.8	2.6	1.5
242.60	0.16	10.6	2.4	712.49	0.40	3.6	1.5	1081.0	0.3	5.3	2.5	2922.1	0.8	6.8	2.7
253.88	0.18	6.6	2.0	729.4	0.4	9.4	2.9	1094.4	0.4	9.6	2.9				
255.37	0.19	4.0	1.7	743.2	0.4	3.9	1.6	1102.7	0.4	14.6	3.5				
257.10	0.19	1.3	0.8	756.0	0.4	5.7	2.6	1147.0	0.4	2.1	1.1				
275.76	0.20	4.7	2.1	808.2	0.4	4.7	2.3	1154.8	0.4	2.8	1.4				
282.29	0.21	3.5	1.5	815.3	0.4	2.3	1.2	1217.9	0.4	2.5	1.4				
294.96	0.22	1.6	0.9	832.4	0.4	2.9	1.5	1237.9	0.4	2.5	1.3				

D. Fission Cross Section of ^{233}U (J.P. Felvinci and E. Melkonian)

Increasing interest in thermal breeder reactors warrants a second (and critical) look at the ^{233}U cross sections. We reported earlier[1] that when the fission fragment energy distribution was subdivided into groups, the resulting partial fission cross sections showed significant variation. Suggestions were made that some of the differences observed in fission cross sections among several experimenters could be due to the different bias in the detection of the fission fragments.

In this report we present $\sigma_0\Gamma_F$ values for the fission resonances. The experiment which we report on was performed in the Spring of 1970 at the Nevis (NVS) synchrocyclotron. The details of the experiment were reported earlier[1]. Both time-of-flights and fission fragment energies were measured simultaneously and recorded event-by-event on magnetic tape. The energy resolution was good enough to subdivide the fission cross section into partial fission cross sections corresponding to different energy groups.

In this report we present in Table D1 the $\sigma_0\Gamma_F$ values calculated from fitting the experimental data to a single level Breit-Wigner formula. The results are compared with values given in BNL-325. In Table D2 the G and H values calculated from the Adler-Adler formalism are given and are compared with other published results. The errors quoted include both statistical and possible fitting errors. Table D3 gives the fission resonance integrals

$$\int_{E_1}^{E_2} \sigma_F \frac{dE}{E}$$

over GAM (1/4 lethargy) intervals and they are compared with existing data. Table D4 summarizes the fission resonance integrals for different energy intervals corresponding to other experimenters' values.

We analyzed resonances in detail up to 30 eV and will continue to analyze them at higher energies. Since the fits to resonances above 30 eV involve matching at the boundary to the fits below 30 eV, it is possible that some resonance parameters just below 30 eV will be slightly changed. We believe that the change will be within the errors quoted.

The $\sigma_0\Gamma_F$ values from the fit to the Doppler and resolution broadened single-level Breit-Wigner formula show reasonable agreement with Nifenecker's results for the large resonances, but are quite different

TABLE D1

Resonance Parameters of ^{233}U (single level fits)

E_0	Γ_T	NVS $\sigma_0\Gamma_F$(eVb)	Saclay[1]
1.55	600	127.95±2.55	
1.79	240	161.07±1.68	301
2.16	180	22.69±1.07	
2.28	70	39.98±0.84	54
3.30	550	20.73±1.58	
3.60	180	27.07±0.95	45
4.75	800	55.61±3.35	63.5
5.88	300	25.29±1.37	43.5
6.44	500	44.72±2.17	
6.79	150	104.85±1.81	130
7.46	200	1.56±0.87	8.3
8.69	650	4.86±1.83	5.3
9.33	350	19.66±1.44	13.8
10.35	350	169.79±2.71	163
11.20	350	18.04±1.63	
11.69	200	5.79±1.18	
12.22	500	18.13±2.19	16.9
12.73	300	113.41±2.62	122
13.66	320	31.02±1.88	37
15.34	240	61.03±2.15	47
15.84	250	10.57±2.98	
16.13	200	25.18±2.18	107
16.50	300	61.32±2.40	12.8
17.93	200	14.52±1.45	14.7
18.47	250	16.90±1.81	9.1
18.91	300	99.49±2.78	97
20.52	400	51.99±2.45	51.5
21.75	200	51.10±2.73	32.4
22.28	480	180.90±4.92	199
22.89	760	18.16±4.09	
23.67	500	29.72±2.77	33
25.20	380	38.24±2.63	43.7
25.86	360	7.33±2.07	5.1
26.54	480	21.35±2.68	8.3
27.55	400	5.26±2.25	26
28.17	220	10.69±1.89	27
29.00	480	56.25±3.43	64
29.54	200		

1. Nifenecker, H. Jour. de Physique 25, 877 (1964).

TABLE D2

Resonance Parameters of ^{233}U (multilevel fits)

μ (eV)		ν (eV)		G_f(beV$^{3/2}$)		H_f(beV$^{3/2}$)	
NVS	ORNL[1]	NVS	ORNL[1]	NVS	ORNL[1]	NVS	ORNL[1]
1.55	1.43	0.30	0.29	78.15±2.71	50.86	4.33±2.87	-18.87
1.79	1.78	0.12	0.12	104.05±1.93	114.26	-7.30±1.47	-0.23
2.28	2.29	0.05	0.05	39.60±0.71	42.74	14.76±0.56	18.48
3.30	3.37	0.275	0.35	18.98±2.31	28.12	1.01±2.24	-13.61
3.60	3.63	0.09	0.08	24.32±1.22	22.02	1.30±1.15	6.80
4.75	4.61	0.40	0.40	62.28±4.09	62.53	1.51±3.76	-35.08
5.88	5.80	0.15	0.15	28.83±2.21	20.14	-1.34±2.35	-17.06
6.44		0.25		52.28±4.61		6.70±4.86	
6.79	6.80	0.075	0.09	140.36±2.91	176.62	1.72±2.51	31.33
7.46	7.47	0.10	0.10	3.57±1.39	6.78	-1.17±1.38	-0.67
8.68	8.69	0.32	0.28	6.19±3.97	22.67	-2.85±3.68	4.82
9.33	9.14	0.175	0.15	23.62±3.07	17.48	-3.51±3.09	-20.48
10.35	10.35	0.175	0.16	266.03±5.37	275.89	14.40±4.18	0.42
11.20	11.30	0.175	0.20	31.42±4.27	33.41	5.06±4.02	8.67
11.69		0.10		10.15±3.18		0.63±3.02	
12.22		0.25		30.74±7.45		5.78±6.97	
12.73	12.76	0.15	0.17	206.74±6.16	238.89	3.22±6.50	49.43
	13.45		0.20		41.96		14.53
13.66	13.65	0.16	0.14	59.34±3.97	44.99	0.89±3.34	-26.72
15.34	15.28	0.12	0.12	115.92±5.17	119.77	-5.06±4.79	-35.47
15.84		0.125		19.24±7.99		16.10±8.34	
16.13	16.13	0.10	0.22	58.63±8.86	101.25	-7.61±8.07	-4.79
16.50	16.52	0.15	0.13	127.05±7.47	94.54	3.09±6.76	26.62
17.93	17.93	0.10	0.12	35.81±3.96	43.16	-1.46±3.69	4.22
18.47	18.42	0.125	0.21	42.07±5.79	58.68	-15.12±6.49	1.83
18.91	18.86	0.15	0.15	204.74±7.65	216.24	-15.29±6.49	-46.49
20.52	20.53	0.20	0.20	100.30±6.66	111.51	9.41±5.93	6.53
21.75	21.85	0.10	0.13	102.85±8.62	130.22	16.71±8.23	86.08
22.28	22.23	0.24	0.24	453.40±19.88	532.22	31.96±17.96	-77.59
22.89	22.94	0.38	0.38	78.15±19.98	96.58	5.27±21.07	3.64
23.67	23.54	0.25	0.32	80.43±9.67	65.49	-11.39±9.73	-94.87
25.20	25.13	0.19	0.19	98.97±9.05	80.77	-1.65±8.14	-38.01
25.86	26.19	0.18	0.18	16.57±9.07	-0.73	-1.80±8.59	16.46
26.54	26.57	0.24	0.24	58.96±10.49	70.76	6.28±9.76	19.32
27.55	27.18	0.20	0.77	12.01±8.73	14.32	-12.52±7.94	-42.57
28.17	28.31	0.11	0.11	16.63±7.45	13.54	2.84±6.77	14.45
29.00	29.05	0.24	0.27	140.35±15.08	176.58	30.93±12.61	48.21
29.54	29.60	0.10	0.08	14.79±7.74	12.87	13.62±6.07	10.80

1. de Saussure, G., et al. Nuclear Data for Reactors, Vol. II, 757 (1970). IAEA, Vienna.

TABLE D3

Comparison of Resonance Integrals for ^{233}U

Energy Interval (eV)	Weston et al.[1]	Brooks[2]	Nifenecker[3]	Moore et al.[4]	Cao et al.[5]	NVS
0.414-0.532	33.34	35.14		34.20	34.77	35.05
0.532-0.683	30.54	32.29		31.47	32.14	30.75
0.683-0.876	28.84	30.84		29.53	30.61	30.15
0.876-1.126	34.76	37.17		35.54	36.99	36.00
1.126-1.445	56.61	53.87		54.63	59.48	59.00
1.445-1.855	138.23	139.95		140.54	137.32	136.00
1.855-2.382	97.56	95.55	97.63	92.02	99.64	95.15
2.382-3.059	14.55	15.22	13.18	17.19	14.70	16.55
3.059-3.927	26.14	25.54	23.11	25.82	24.73	26.80
3.927-5.043	20.41	20.07	17.92	19.82	18.94	21.85
5.043-6.475	22.10	22.07	19.92	20.83	20.57	25.80
6.475-8.313	35.09	30.98	33.44	31.55	33.56	34.70
8.313-10.67	30.48	28.59	28.43	25.85	28.00	32.10
10.67-13.70	27.61		26.98	23.17	26.55	28.30
13.70-17.59	18.99		19.30	16.36	19.62	20.40
17.59-22.59	32.47		30.87	23.21	30.57	33.80
22.59-29.07	16.76		17.53	15.12	17.50	16.96
29.07-37.03	15.18		15.54	11.77	15.08	15.00
37.03-47.83	6.76		7.27	5.90	8.46	6.86
47.83-61.42	11.29		10.91	8.23	13.17	11.40
61.42-78.86	9.77			7.14	11.44	9.83
78.86-101.3	8.74			6.51	7.83	8.80
101.3-130.0				8.09		8.73
130.0-166.9				4.70		5.60
166.9-214.4	5.82			4.07	5.54	5.61
214.4-275.2	5.51			4.59	5.57	5.87
275.2-353.4	5.42			4.51	4.73	5.05
353.4-453.8	3.65			3.77	3.50	3.50
453.8-582.6	3.54			2.80	3.31	3.30
582.6-748.1	3.84			3.17	3.40	3.80
748.1-960.5	3.26				2.72	3.00
960.5-1223	2.44				2.00	2.15

1. Weston, L.W., et al. ORNL-TM-2140 and Nucl.Sci.Eng. 39, 1 (1968).
2. Brooks, F.D., et al. AERE M-1709 (1966).
3. Nifenecker, H. Journ. de Physique 25, 877 (1964).
4. Moore, M.S., et al. Phys. Rev. 118, 714 (1960).
5. Cao, M.G., et al. Nuclear Data for Reactors, Vol. I, 419 (1970), IAEA, Vienna.

TABLE D4

Comparison of Resonance Integrals for ^{233}U

Energy Interval (eV)	Weston et al.[1]	Brooks[2]	Nifen-ecker[3]	Moore et al.[4]	Cao et al.[5]	NVS
0.414-10.67	568.65	567.28		559.00	571.45	579.90
1.85-61.42	375.41		362.03		371.9	385.67
0.414-101.2	716.24			676.4	721.17	731.25
166.9-748	27.78			22.91	25.87	27.13
0.414-1223	762.5					777.86

1. Weston, L.W., et al. ORNL-TM-2140 and Nucl.Sci.Eng. 39, 1 (1968).
2. Brooks, F.D., et al. AERE M-1709 (1966).
3. Nifenecker, H. Journ. de Physique 25, 877 (1964).
4. Moore, M.S., et al. Phys. Rev. 118, 714 (1960).
5. Cao, M.G., et al. Nuclear Data for Reactors, Vol. I, 419 (1970), IAEA, Vienna.

for wide or very close resonances. In these cases naturally the exact resonance energy assumed and the width used is quite critical. Several minor changes in the resonance parameters kept the values within the quoted errors.

It might be pointed out that in the single level formalism a level at 2.16 eV is necessary for a good fit, but this can be removed in the Adler-Adler form. The additional level at 6.44 eV and 12.22 eV cannot be removed, as no interference term in the multilevel fit will give a good result. Inspection of the Weston et al.[3] results and the calculation of de Saussure[7] shows that they have also some excess area in these regions, though these are accentuated in our experiment. We believe again that these are wide levels having wider mass and energy distribution and thus slightly biased against in ionization chamber experiments. The level at 11.69 eV has an especially high ratio of low energy to medium energy fragments[1] and also a higher proportion of high energy γ-rays[2]. We also note the changing ratio of areas between the 21.75 and 22.28 eV level in different pulse height cuts.

Inspection of the resonance integrals in different intervals in Table D3 reveals some discrepancies between our results and past experiments. We seem to be on the high side in the energy interval of 4 - 6.5 eV which is a region of small, wide levels and again in the region of 8.3 - 25 eV. At higher energies our results seem to be close to those of Weston et al.[3] but are above the results of Moore et al.[4] and Cao et al.[5]

The cross sections were calculated by assuming the energy dependence of the flux to be $\phi(t) = E^{0.60}dt$. This was confirmed by comparison with other experiments in the same run and also by Monte-Carlo calculations. The background was assumed to consist of a part which varies as the neutron flux and a fairly constant one. Normalization was obtained by comparing the cross sections at 1 eV, 20 keV, and the peak cross sections at several resonances with those of Weston et al.[1] Discrepancies between peak values at several resonances were noted and attributed to possible pulse height effects in the fission chamber they used.

We have observed in the past that our "background" is higher for the low energy fission fragments. We have ruled out admixture of α-particles as our bias was set around 35 MeV above the α-particles but below the fission fragments. Our conclusion is that some wide levels which contribute more to the "background" have a larger proportion of low energy fission fragments (also very high energy fragments) and thus are possibly discriminated against in other experiments.

References

1. Felvinci, J.P. and Melkonian, E. Proc. Third Conf. on Neutron Cross Sections and Technology, Vol. II, 855. Knoxville, Tennessee. 1971

2. Felvinci, J.P. and Melkonian, E. NYO-72-227, p.12. 1969.

3. Weston, L.W., et al. ORNL-TM-2140 and Nucl. Sci. Eng. 39, 1 (1968).

4. Moore, M.S., et al. Phys. Rev. 118, 714 (1960).

5. Cao, M.G., et al. Nuclear Data for Reactors, Vol. I, 419 (1970). IAEA, Vienna.

6. Nifenecker, H. Journ. de Physique 25, 877 (1964).

7. de Saussure, G., et al. Nuclear Data for Reactors, Vol. II, 757 (1970). IAEA, Vienna.

GULF RADIATION TECHNOLOGY
A Division of Gulf Energy and Environmental Systems
San Diego, California

A. NEUTRON CROSS SECTIONS

1. Linac Measurements of the $^{10}B(n,\alpha)$ Cross Sections

(S. J. Friesenhahn, A. D. Carlson, V. J. Orphan and M. P. Fricke)

The $^{10}B(n,\alpha)^7Li$ and $^{10}B(n,\alpha_1\gamma)^7Li$ cross section data have been taken and the analysis of these measurements is almost complete. The neutron flux spectrum was measured with hydrogen and methane gas proportional counters. The hydrogen proportional counter data extend from ~1 to 50 keV and the methane proportional counter data cover the range from 13 to 1000 keV. Rate of rise gamma-ray discrimination was employed and the linear signals were digitized in two ADC's with gains differing by a factor of 16 to allow a very large dynamic range. For each of the measurements a precision pulser was employed to determine electronic non-linearity effects.

The 478-keV gamma ray from the $^{10}B(n,\alpha_1\gamma)^7Li$ reaction was detected with an 80cc Ge(Li) detector. For these measurements the signal to background ratio was excellent and a statistical precision of 1-2% was achieved.

The $^{10}B(n,\alpha)^7Li$ events were detected in BF_3 counters and also in a large ion chamber constructed with thin self-supporting films. The gas in the BF_3 counters contains 10% methane which allows a $^{10}B(n,\alpha)^7Li$ cross section determination from a comparison of the alpha and proton recoil pulse height distributions. (This work pertinent to request Nos. 28 and 29 in NCSAC-35.)

B. FISSION PHYSICS

1. Isomeric Gamma Rays for Times Less Than One Microsecond After $^{235}U(n,F)$ and $^{239}Pu(n,F)$

(R. E. Sund, V. V. Verbinski, and Hans Weber)

Measurements of the isomeric gamma-ray energy spectra

from the thermal-neutron fission of ^{235}U and ^{239}Pu were performed at Gulf Radiation Technology with a Ge(Li) detector for times between 20 nsec and ~1 μsec after fission. A total of 69 resolved gamma-ray peaks with different energies and half lives were observed; 36 of these gamma-ray peaks had not been seen in previous delayed gamma-ray measurements. No gamma rays were positively identified above ~1314 keV, although measurements were made to much higher energies. The analyzed results for the resolved peaks are shown in Table B-1. Also shown are the Livermore ^{252}Cf results[1] for those gamma rays which appear to correspond in both energy and half-life to the peaks observed from ^{235}U or ^{239}Pu.

The total energy of the resolved peaks from this experiment, when integrated over all time, is 163 and 164 keV/fission for ^{235}U and ^{239}Pu, respectively. Roughtly 40% of the total energy of the resolved peaks is from gamma rays in the 1100-1340-keV region. Isomers in ^{134}Te and ^{136}Xe contribute most of these high-energy gamma rays. The continuum of unresolved gamma rays were also analyzed for both ^{235}U and ^{239}Pu.

2. On the Correlation Between Energy Spectra and Multiplicity Of Prompt Fission Gamma Rays (Tsahi Gozani and D. G. Costello)

The existence and the degree of correlation between multiplicity and the energy distribution of prompt neutrons and gamma rays emitted from fission is useful in understanding some aspects of the fission process, especially events after the scission point. The existence of such a correlation may appreciably influence the calculations of the absolute detection efficiency of coincidence detectors such as the Fission Multiplicity Detector (FMD).[3]

In the case of prompt neutron emission from the spontaneous fissioning of ^{252}Cf, there is a strong indication[4] that there is no

---

[1]W. John, F. W. Guy and J. J. Wesolowski, Phys. Rev. C2 1451 (1970).

[2]R. B. Walton and R. E. Sund, Phys. Rev. 178, 1894 (1969).

[3]T. Gozani and D. G. Costello, Trans. Am. Nucl. Soc. 13, 746 (1970).

[4]H. R. Bowman, et al., Phys. Rev. 129, 5 (1962) and Phys. Rev. 129, 5 (1963).

Table B-1

DELAYED GAMMA-RAY RESOLVED PEAKS OBSERVED IN THE PRESENT ^{235}U AND ^{239}Pu MEASUREMENTS

For comparison the Livermore ^{252}Cf results[1] are shown for those gamma rays which appear to correspond in both energy and half life to the peaks observed from ^{235}U or ^{239}Pu. The errors given for the ^{235}U and ^{239}Pu gamma-ray intensities do not include possible systematic uncertainties of ~ ±10% and ~ ±15%, respectively.

PRESENT RESULTS												LIVERMORE RESULTS			
^{235}U						^{239}Pu						^{252}Cf			
E_γ (keV)	$T_{1/2}$ (nsec)	$\pm\Delta T_{1/2}$ (%)	$T_{1/2}$ Ref.	I_γ (photons/fission)	$\pm\Delta I_\gamma$ (%)	E_γ (keV)	$T_{1/2}$ (nsec)	$\pm\Delta T_{1/2}$ (%)	$T_{1/2}$ Ref.	I_γ (photons/fission)	$\pm\Delta I_\gamma$ (%)	E_γ (keV)	A[a]	$T_{1/2}$ (nsec)	I_γ (photons/fission)
85.0	16.		1	0.0116	35	85.3	16.		1	0.0244	35	85.6	105^{+1b}_{-0}	16	0.0012
85.1	140.		1	0.0056	27	85.5	140.		1	0.0077	27	86.3	108^{+1}_{-0}	140	0.0054
91.3	120.		1	0.0025	29	91.3	120.		1	0.00169	26	90.0 91.2	108+1,-0 132±0	120 120	0.0022 0.00075
91.3	15.		1	0.0021	35	91.3	15.		1	0.0039	35	90.2 90.5 91.5	108±0 142±0 101+0,-1	15 15 19	0.0013 0.00089 0.00076
						102.8	15.		1	0.0038	14	102.8 103.5	105±0 111+0,-1	15 14	0.0038 0.0059
						102.8	200.		1	0.0099	29	103.2	150^{+0}_{-1}	200	0.0011
						106.6	20.		1	0.0018	60	105.0 106.0	146±2 142±2	20 20	0.0023 0.0029
109.1	11.9	10	1	0.0095	40	109.4	10.7	12		0.0079	40				
115.3	175.	4		0.0103	7	115.3	175.	5		0.0089	7	115.0	134±0	162	0.0061
121.6	360.		1	0.0101	7	121.4	360.		1	0.0094	7	121.4	99^{+1}_{-0}	360	0.0048
121.8	22.		1	0.00219	15	121.7	22.		1	0.0034	17	122.0	99^{+1}_{-0}	22	0.0025
125.0	81.6	14		0.00216	14	125.0	79.2	16		0.0033	15	125.1	134±0[c]	115	0.00176
130.5	375.	3		0.0089	9	130.1	340.		1	0.0077	25	129.8	99^{+1}_{-0}	340	0.0029
						130.5	19.		1	0.0012	30	130.5	146±0	19	0.0032
141.5	360.		1	0.00415	5	141.3	360.		1	0.0025	11	140.9	96^{+1}_{-0}	360	0.00084
142.3	55.		1	0.0368	4	142.1	55.		1	0.0188	4	140.9 142.0	104·0 91^{+1}_{-0}	62 55	0.0016 0.0036

Table B-1 (Continued)

PRESENT RESULTS												LIVERMORE RESULTS			
^{235}U						^{239}Pu						^{252}Cf			
E_γ (keV)	$T_{1/2}$ (nsec)	$\pm\Delta T_{1/2}$ (%)	$T_{1/2}$ Ref.	I_γ (photons/ fission)	$\pm\Delta I_\gamma$ (%)	E_γ (keV)	$T_{1/2}$ (nsec)	$\pm\Delta T_{1/2}$ (%)	$T_{1/2}$ Ref.	I_γ (photons/ fission)	$\pm\Delta I_\gamma$ (%)	E_γ (keV)	A^a	$T_{1/2}$ (nsec)	I_γ (photons/ fission)
						153.8	143.	12		0.0021	11	153.6	108±0	110	0.0077
162.4	97.1	4		0.0073	5							{163.0 {163.5	133+0,-1 152±0	110 82	0.0018 0.00011
167.4	240.		1	0.0032	15	167.1	240.		1	0.00042	12	167.1	96^{+1}_{-0}	240	0.0015
167.7	13.		1	0.0072	30	167.7	13.		1	0.0028	30	167.7	146^{+1}_{-0}	13	0.0073
169.	1100.		1	0.0027	21	170.5	1100.		1	0.0039	19	170.5	98±0	1100	0.0020
181.2	127.	20		0.0011	36	181.0	127.	20		0.0024	38				
181.5	28.0	10		0.0013	30	181.6	28.0	10		0.0026	32				
186.5	1166.	15		0.0017	30	186.1	1000.	30		0.0013	42	186.4	98±1[c]	650	0.0005
191.7	115.	10		0.0023	25	191.8	162.	33		0.0010	40	191.1	94^{+0}_{-1}	110	0.00029
197.3	3400.		2	0.0082	15	197.3	3400.		2	0.0152	15	197.3	136	2800	0.0060
204.0	3000.		1	0.0064	9	204.0	3000.		1	0.0034	11	204.0	98±1	3000	0.0013
204.3	24.		1	0.0408	15	204.2	24.		1	0.0238	15	204.3	95±2	24	0.0062
217.4	94.	10		0.0036	10	217.3	128.	25		0.0015	25	217.2	93±0	70	0.00044
228.8	16.5	4		0.0014	25										
276.1	7.6	15		0.0065	60	276.0	7.6		d	0.0039	80	276.5	91	6	0.00043
283.8	8.		1	0.0040	80	283.5	8.		1	0.0040	80	283.9	147^{+1}_{-0}	8	0.0064
288.1	12.6	19		0.0015	30	288.2	12.9	10		0.00194	30	288.2	146±0	17	0.0029
297.3	170.	3		0.0297	5	297.2	183.	5		0.0226	5	296.9	134±0	162	0.0103
314.3	8.2	10		0.0055	60	314.1	8.7	10		0.0082	60	314.4	138^{+0}_{-1}	9	0.0039
325.3	555.	5		0.0053	6	324.9	578.	18		0.0031	19	324.5	135±0	570	0.0031
						330.8	26.	30		0.028	33				
						330.8	168.	70		0.00021	75				
339.8	86.	6		0.00184	8	339.5	79.	14		0.00077	17				
						343.2	674.	36		0.0011	37				

Table B-1 (Continued)

PRESENT RESULTS												LIVERMORE RESULTS			
^{235}U						^{239}Pu						^{252}Cf			
E_γ (keV)	$T_{1/2}$ (nsec)	$\pm\Delta T_{1/2}$ (%)	$T_{1/2}$ Ref.	I_γ (photons/ fission)	$\pm\Delta I_\gamma$ (%)	E_γ (keV)	$T_{1/2}$ (nsec)	$\pm\Delta T_{1/2}$ (%)	$T_{1/2}$ Ref.	I_γ (photons/ fission)	$\pm\Delta I_\gamma$ (%)	E_γ (keV)	A[a]	$T_{1/2}$ (nsec)	I_γ (photons/ fission)
352.3	21.8	5		0.0326	20	352.1	22.6	5		0.0181	20	352.3	95±0	21	0.0046
381.3	57.	7		0.0012	19	381.3	57.	20		0.00095	30				
381.5	3400.		2	0.0059	22	381.1	3400.		2	0.0176	20	380.7	136	3400	0.0073
387.5	119.	10		0.0010	30	387.2	115.	3		0.0030	16	387.1	135^{+0}_{-1}	110	0.00082
400.1	7.8	10		0.0059	80	400.1	8.1	10		0.0075	80	400.2	138^{+0}_{-1}	9	0.0037
412.7	18.3	6		0.0034	25	412.1	22.4	9		0.0020	25				
415.7	24.5	6		0.0024	20	415.4	20.2	13		0.0021	20	415.6	99^{+1}_{-0}	16	0.00051
426.8	15.4	7		0.0028	30	426.4	15.7	6		0.0028	30	426.8	100±1	16	0.00086
433.0	1960.	48		0.0026	52	432.3	1450.	55		0.0038	60				
						444.7	215.	5		0.00111	15				
444.8	50.	10		0.00043	27										
444.8	520.	15		0.00099	29										
454.2	19.2	16		0.00111	25	454.2	15.5	17		0.00125	25				
461.2	161.	14		0.00062	21	461.4	90.	5		0.00075	15				
522.4	382.	11		0.00212	17										
536.3	22.7	10		0.00178	16	535.5	28.9	10		0.00161	15				
575.8	16.8	10		0.00226	30	576.2	19.8	16		0.00147	30				
589.8	68.4	6		0.00183	12	590.3	100.	50		0.0013	52				
614.2	17.3	10		0.0194	30	614.2	17.3	10		0.0179	30	614.2	100±0	20	0.0034
619.6	96.	5		0.00187	10										
648.7	165.	17		0.00146	21	648.2	104.	32		0.00076	34				
746.7	132.	37		0.00093	39										
770.4	2060.	60		0.0026	64	770.1	1050.	35		0.0025	37				
774.6	46.5	7		0.00118	12	774.8	49.9	12		0.0015	16				

Table B-1 (Continued)

PRESENT RESULTS												LIVERMORE RESULTS			
^{235}U						^{239}Pu						^{252}Cf			
E_γ (keV)	$T_{1/2}$ (nsec)	$\Delta T_{1/2}$ (%)	$T_{1/2}$ Ref.	I_γ (photons/ fission)	ΔI_γ (%)	E_γ (keV)	$T_{1/2}$ (nsec)	$\Delta T_{1/2}$ (%)	$T_{1/2}$ Ref.	I_γ (photons/ fission)	ΔI_γ (%)	E_γ (keV)	A[a]	$T_{1/2}$ (nsec)	I_γ (photons/ fission)
810.6	102.	4		0.00134	16										
815.4	15.0	10		0.00074	40										
817.5	117.	20		0.00070	35										
						840.3	129.	25		0.00084	40				
968.6	28.2	14		0.00144	17	969.5	28.8	6		0.00197	10				
974.7	120.	5		0.00239	8	975.2	69.	35		0.0020	30				
						975.2	278.	35		0.0027	30				
998.4	96.	11		0.00092	35										
1025.3	20.5	8		0.00211	20	1025.9	20.9	8		0.00146	20				
1086.5	21.6	12		0.00129	25	1087.1	19.7	10		0.00145	25				
1103.4	113.	5		0.0045	7	1103.7	111.	4		0.0062	6				
1150.7	110.	5		0.0041	5	1151.1	124.	9		0.0061	9	1151.6	134^{+0}_{-1}	90	0.0021
1180.8	612.	10		0.0054	12	1180.8	499.	13		0.0031	13	1181.0	135^{+0}_{-1}	670	0.0030
1221.5	31.	50		0.0021	60	1221.4	15.2	40		0.0042	60	1221.0	137^{+2}_{-1}	6	0.0073
1279.8	169.	3		0.0235	5	1279.8	179.	4		0.0177	5	1279.8	134±0	164	0.0126
1313.9	3400.		2	0.0095	30	1313.4	3400.		2	0.0156	35	1313.3	136	3000	0.0057

[a] Because of the large number of gamma rays at low energies, the assignment of the ^{235}U and ^{239}Pu peaks to the A values given for the ^{252}Cf peaks is not positive below ~200 keV.

[b] Part of the ^{235}U and ^{239}Pu intensity for the 85.6-keV peak could possibly be from A=133. In the ^{252}Cf measurement at LRL[1] a 85.7-keV gamma ray with a half life of 12 nsec was observed from A = 133+0,-1.

[c] Since the error bars on the ^{235}U and ^{239}Pu half lives do not overlap the value of the ^{252}Cf half life, the gamma rays in ^{235}U and ^{239}Pu may be from a different mass number.

[d] The half life was taken from the present ^{235}U data.

correlation between the multiplicity of the emitted neutrons and their energy distribution. This result can be explained on the basis of isotropic evaporation of neutrons from fully accelerated fragments. There are no similar indirect (or direct) measurements on the gamma multiplicity, namely on the correlation between the energy distribution and the number of prompt photons per fission.

The FMD is highly dependent on the multiplicity of the fission events. For example, an increase in multiplicity from 3 to 6 increases the triple coincidence rate by about a factor of 20. The gamma ray multiplicity of fission events detected in the FMD will be dependent on the gamma ray energy bias on each of the four scintillators which comprise the FMD. Measurements were made with biases at 100 keV and 750 keV. Thus, by requiring a coincidence between the FMD, to determine the dependence on the gamma multiplicity, a fission detector, to distinguish between true fission and background events, and a 3-inch x 3-inch NaI(Tℓ), as a gamma spectrometer, the prompt gamma spectrum from a small ^{252}Cf source was measured as a function of the gamma multiplicity of the fission event. All spectra were compared to the fission spectra, namely the NaI detector in coincidence with only the fission detector. Initial results showed that the spectra obtained were rather similar. Slight differences could be observed above 0.2 MeV. Larger differences appear below this energy, but it could be due in part to instrumental effects.

The results so far indicate that the multiplicity of the prompt fission gamma rays is, to a large extent, uncorrelated with their energy spectra.

C. INTEGRAL TESTS OF CROSS SECTION DATA

1. Integral Experiment to Test Carbon and Nitrogen Cross Sections (L. Harris Jr. and G. D. Trimble)

An integral experiment, designed to test gamma-ray production and neutron scattering cross sections in the MeV range, is in progress. Using the pulsed-neutron- time-of-flight method, a small sample, typically one mean free path in dimension, is located at the end of a 50-meter flight path. A single NE-213 scintillator will be used at several angles relative to the incident neutron beam to measure simultaneously the energy spectra of secondary gamma-rays and scat-

tered neutrons from the sample as a function of time, and hence incident neutron energy. These measurements will provide sensitive tests of both the gamma-ray production and neutron scattering cross sections as functions of incident neutron energy, exit energy, and exit angle.

2. Fast Reactor Spectrum Measurements (J. C. Young, V. V. Verbinski and J. M. Neill)

Spectrum measurements have been made on three fast-reactor assemblies at Gulf Radiation Technology over the past two years utilizing both the time-of-flight technique and hydrogen and methane gas proportional counters. Good agreement has been obtained with both techniques. These assemblies, STSF-7, 9 and 10 were simple two zone systems (a one region core plus a depleted uranium reflector) that had short neutron dieaways and were thus easily measurable and interpretable. STSF-7 was loaded with enriched ^{235}U and depleted uranium in a 1:7 volume ratio, while STSF-9 and 10 were loaded with enriched ^{235}U and depleted U_3O_8 in the same volume ratio. STSF-10 differed from STSF-9 through its arrangement of material plates in the cell designed so as to emphasize heterogeneity effects.

The assemblies have recently been analyzed using ENDF/B version III data to give the results shown in Figs. C-1 and C-2. Both comparisons of experiment and theory show that the calculations underpredict the flux at lower energies (< 5 KeV). This is a real effect and is not due to room return neutrons. This was verified by the agreement of the two spectral measurement techniques and by measurements with a sodium filter in the flight path which showed the same background at the 2.85 keV sodium resonance dip as appeared at very long times (i.e., at energies well below the ^{10}B filter cutoff). Calculations indicate that improvement of theory with experiment is not to be realized by any believable changes to cross sections in the range below 100 keV, instead changes to source terms are necessary. Possible candidates include the ^{238}U inelastic scattering and perhaps the fission spectrum itself. The latter is possible if the Feather representation of the fission spectrum is used instead of the current Maxwellian spectrum. If inelastic scattering from ^{238}U is the source of the spectral discrepancy, then it suggests changes to the energy distribution of secondary neutrons for incident energies greater than 800 keV. This is a consequence of kinetics limitations and cross section magnitudes. Changes to the total inelastic scattering cross sections of ^{238}U above this energy do not appear necessary.

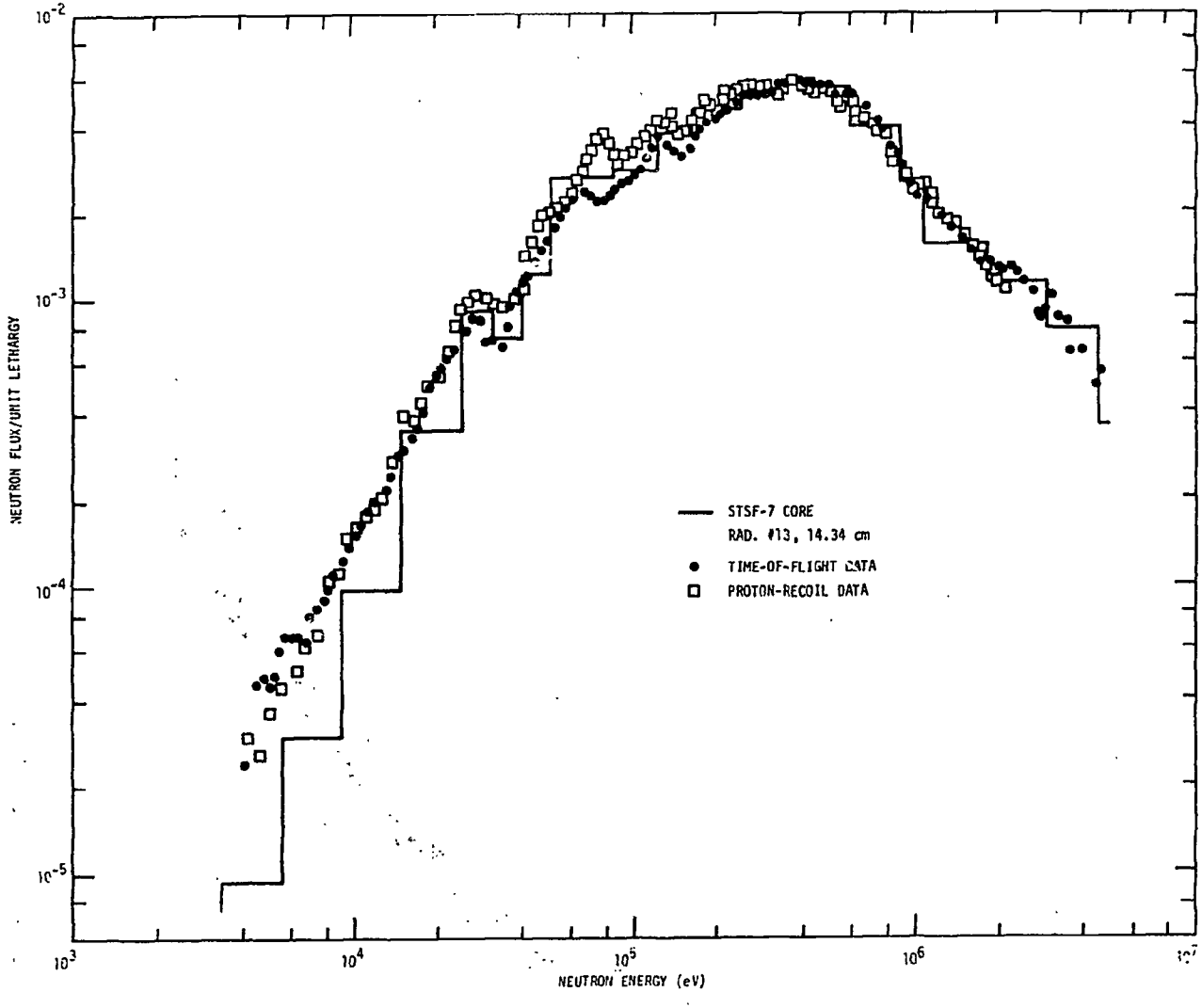

Fig. C-1. Comparison of measured and calculated fast neutron spectra in the core of STSF-7, an assembly of enriched and depleted uranium metal in 1:7 volume ratio.

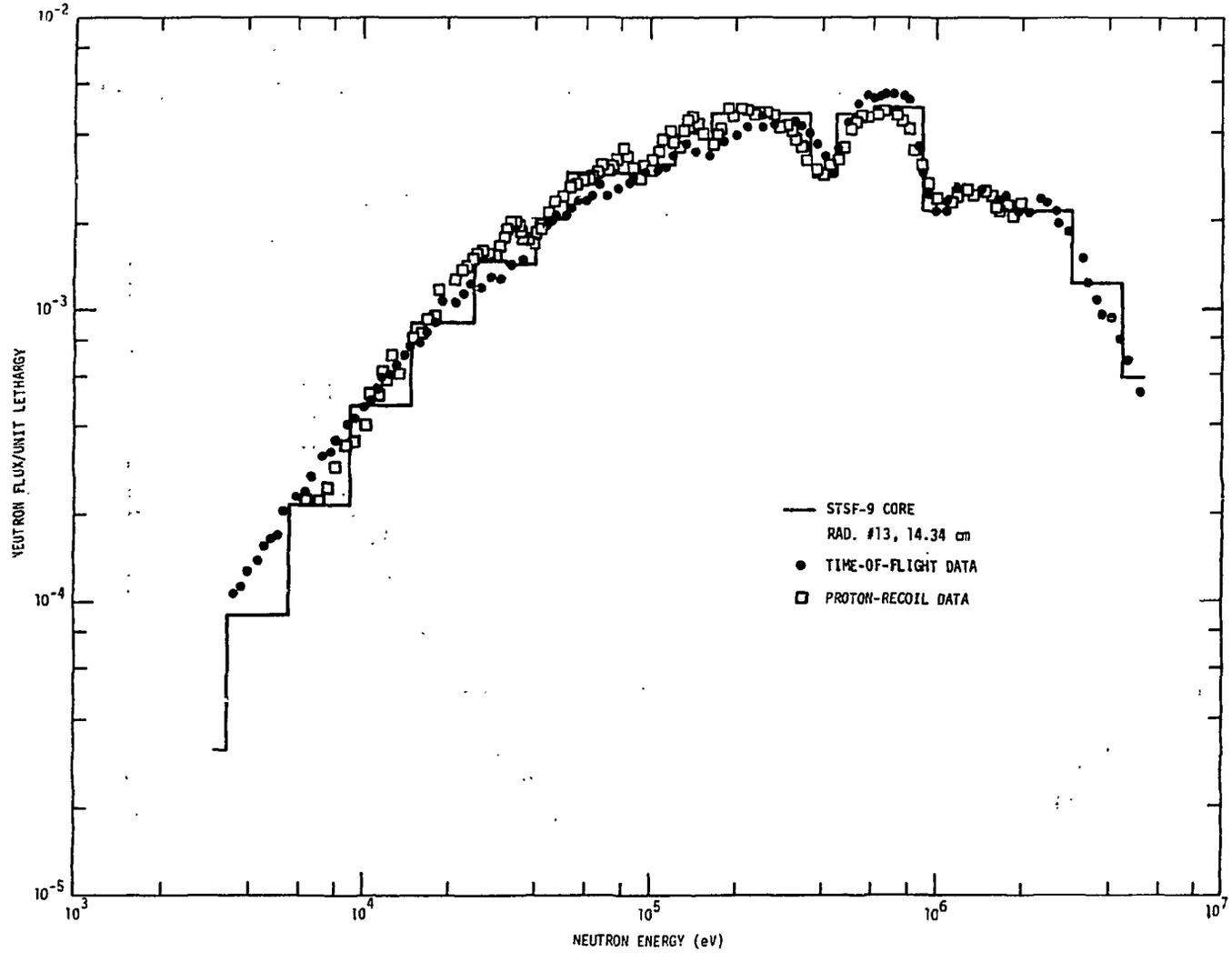

Fig. C-2. Comparison of calculated and measured fast neutron spectra in the core of STSF-9, an assembly of enriched uranium metal and depleted U_3O_8 in a 1:7 volume ratio.

D. RESEARCH IN SUPPORT OF SAFEGUARDS

1. Low Energy Bremsstrahlung Photofission (Tsahi Gozani, D. E. Rundquist, R. O. Ginaven and R. L. Bramblett)

Since 1968 some effort has been devoted to measurements of some basic integral quantities related to the low energy photofission phenomena. The interest in this domain evolves from the applications of photoinduced reactions to the nondestructive assay of fissile materials.[1] The most sensitive energy region for the various isotopes is around and below the photofission barrier (about 6 MeV). In this region slight differences in the barrier height or width will cause large differences in the photofission cross-sections. The only practical intense source of low energy photons is Bremsstrahlung beams from low energy electron accelerators. With such devices the measured quantities are yields. However, in the energy region of importance, especially below the fission barrier, the fission cross-section is a very steep function of energy and its integrated product with the Bremsstrahlung spectrum $\varphi_B(E, E_e)$ (namely the yield) rather closely resembles the fission cross-section itself with an effective resolution which broadens as the energy increases. The fission yields, namely

$$Y_f \propto \int_0^{E_e} \sigma_{\gamma, f}(E)\varphi_B(E, E_e)dE \qquad (1)$$

were measured with mica solid state track detectors.[2] Simultaneously with Y_f, the prompt (Y_p) and delayed (Y_d) neutron yields were measured in a moderated neutron detector[1] employing the gamma-cancellation technique.[3]

$$Y_p \propto \int_0^{E_e} \left[\nu(E)\sigma_{\gamma, f}(E) + \sigma_{\gamma, n}(E)\right]\varphi_B(E, E_e)dE \qquad (2)$$

---

[1] Proc. of USAEC Symp. on "Safeguards Research and Development" WASH-1147 (1969); Proc. of IAEA Symp. on "Progress in Safeguards Techniques" IAEA-SM-133 (1970).

[2] T. Gozani et al., Bull. Am. Phys. Soc. 14, 4 (1969).

[3] T. Gozani and R. O. Ginaven, Nucl. Inst. Meth. 76, 333 (1969).

$$Y_d \propto \int_0^E \beta(E)\nu(E)\sigma_{\gamma,f}(E)\varphi_B(E, E_e)dE \qquad (3)$$

where β is the fractional yield of delayed neutrons per prompt neutrons, while the other symbols are the usual ones. The fission yields for ^{235}U, ^{238}U and ^{232}Th are shown in Fig. D-1. Note the knee in the yield from ^{232}Th. This indicates the existence of a structure in the sub-threshold region of ^{232}Th and agrees well with a Russian measurement made at the same time.[4] A plausible explanation for this structure is the existence of a vibrational resonance in this region creating a shallow double hump potential barrier. The prompt and delayed neutron yields are shown in Fig. D-2. A more recent measurement of Y_p and Y_d for ^{232}Th and ^{238}U at low energies reveals a knee in the yield of ^{232}Th at the same location as is seen in Fig. D-1, namely ~ 5.8 MeV. The ratio of the prompt yield to the fission yield gives an average (over the Bremsstrahlung spectrum) "branching ratio".

$$\frac{Y_p(E_e)}{Y_f(E_e)} \propto \frac{\widehat{\nu\sigma}_{\gamma,f}(E_e) + \widehat{\sigma}_{\gamma,n}(E_e)}{\widehat{\sigma}_{\gamma,f}(E_e)} \qquad (4)$$

However, below the (γ, n) thresholds (6.34 MeV for ^{232}Th, 6.04 MeV for ^{238}U and 5.24 MeV for ^{235}U) the ratio, Eq. 4, yields directly the behavior of the average $\hat{\nu}$ as a function of energy. Such ratios are shown in Fig. D-3, which indicates the possibility of noticeable variations in $\hat{\nu}(E)$ in the sub-barrier regions. Figure D-4 shows the ratio of delayed neutron yield to Y_f, which is proportional to a Bremsstrahlung average fractional yield per fission of delayed neutrons

$$\frac{Y_d(E_e)}{Y_f(E_e)} \propto \widehat{\beta\nu}(E_e)$$

---

[4] S. P. Kapitza et al., Soviet Physics - JETP Letters 9, 73 (1969); N. S. Rabotnov et al. Report FEI-170 (1969) - LASL Translation LA-4385-TR (1970).

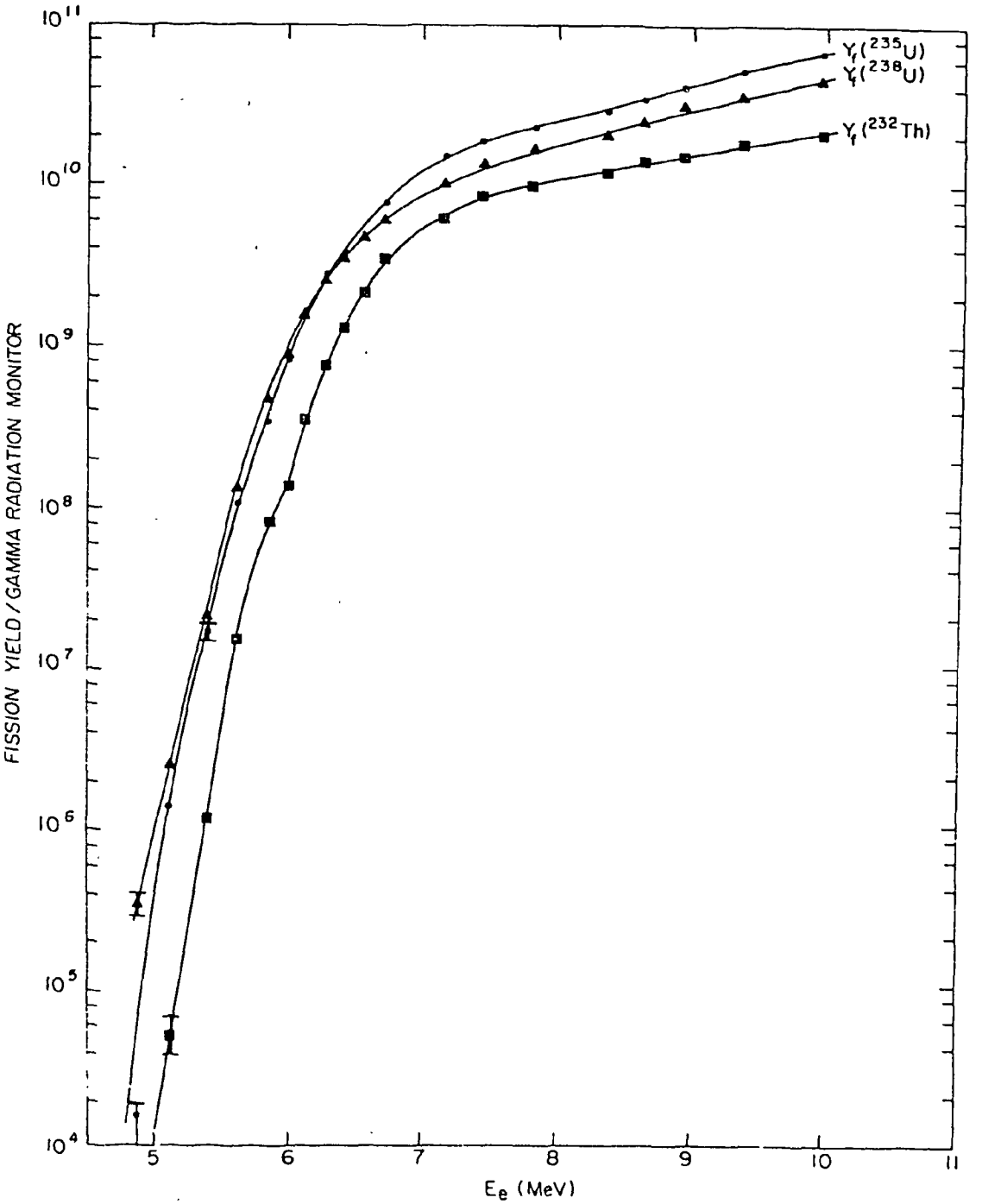

Fig. D-1. Bremsstrahlung photofission yields from ^{232}Th, ^{235}U and ^{238}U obtained using solid-state track detectors.

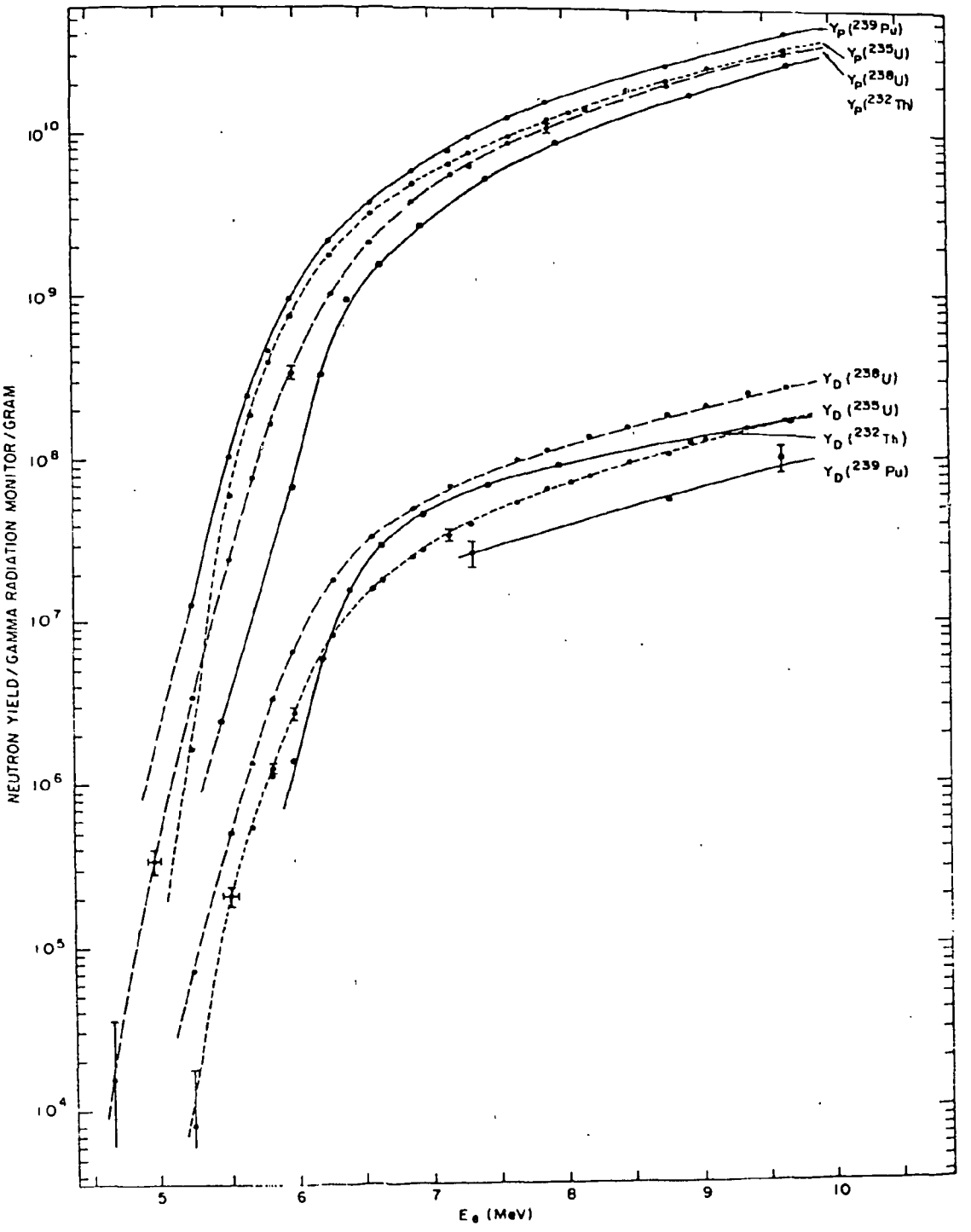

Fig. D-2. Prompt- and delayed-neutron yields by electron bremsstrahlung for ^{232}Th, ^{235}U, ^{238}U, and ^{239}Pu.

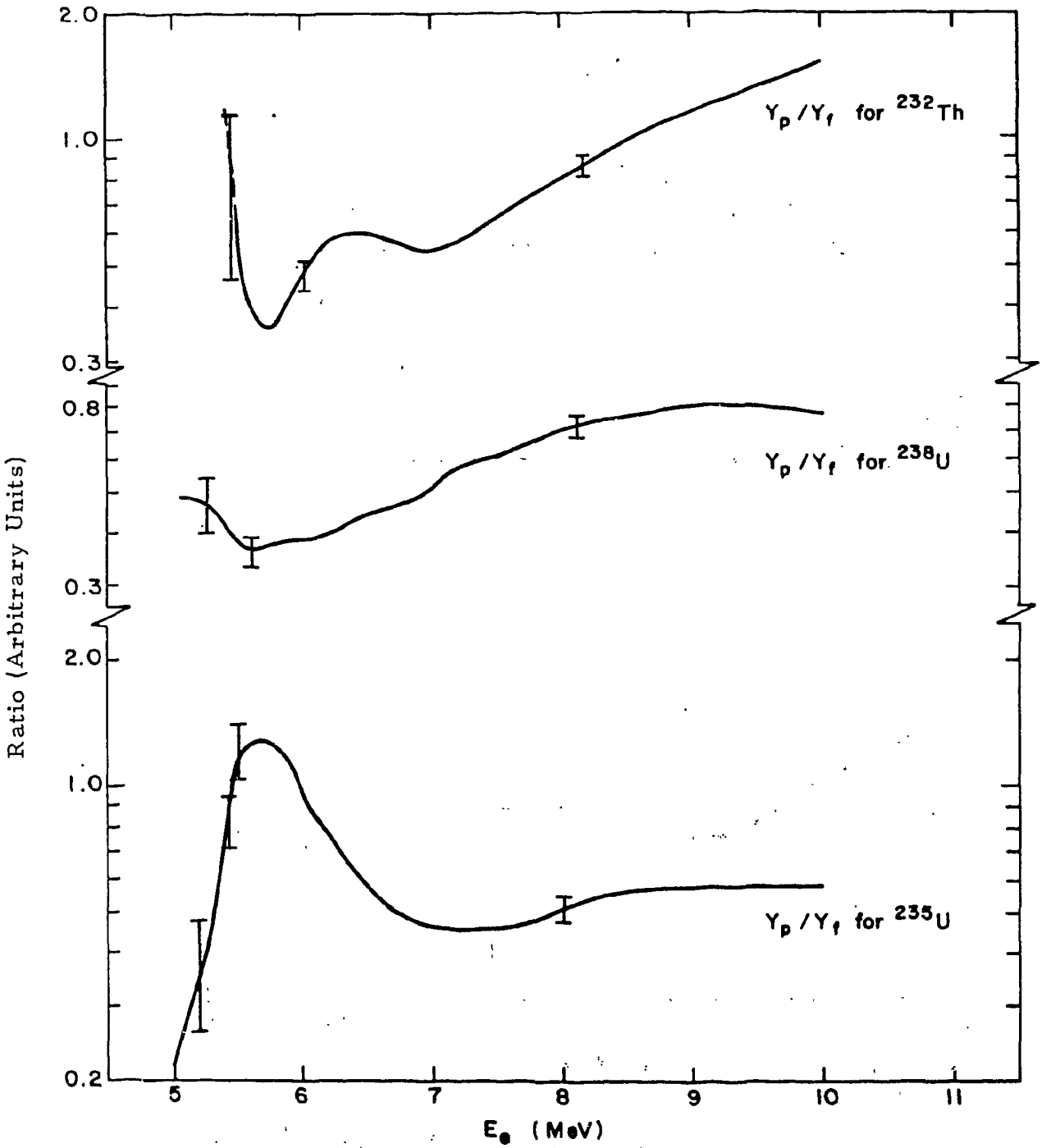

Fig. D-3. Bremsstrahlung averaged "branching ratio" for ^{232}Th, ^{235}U and ^{238}U with representative error-bars.

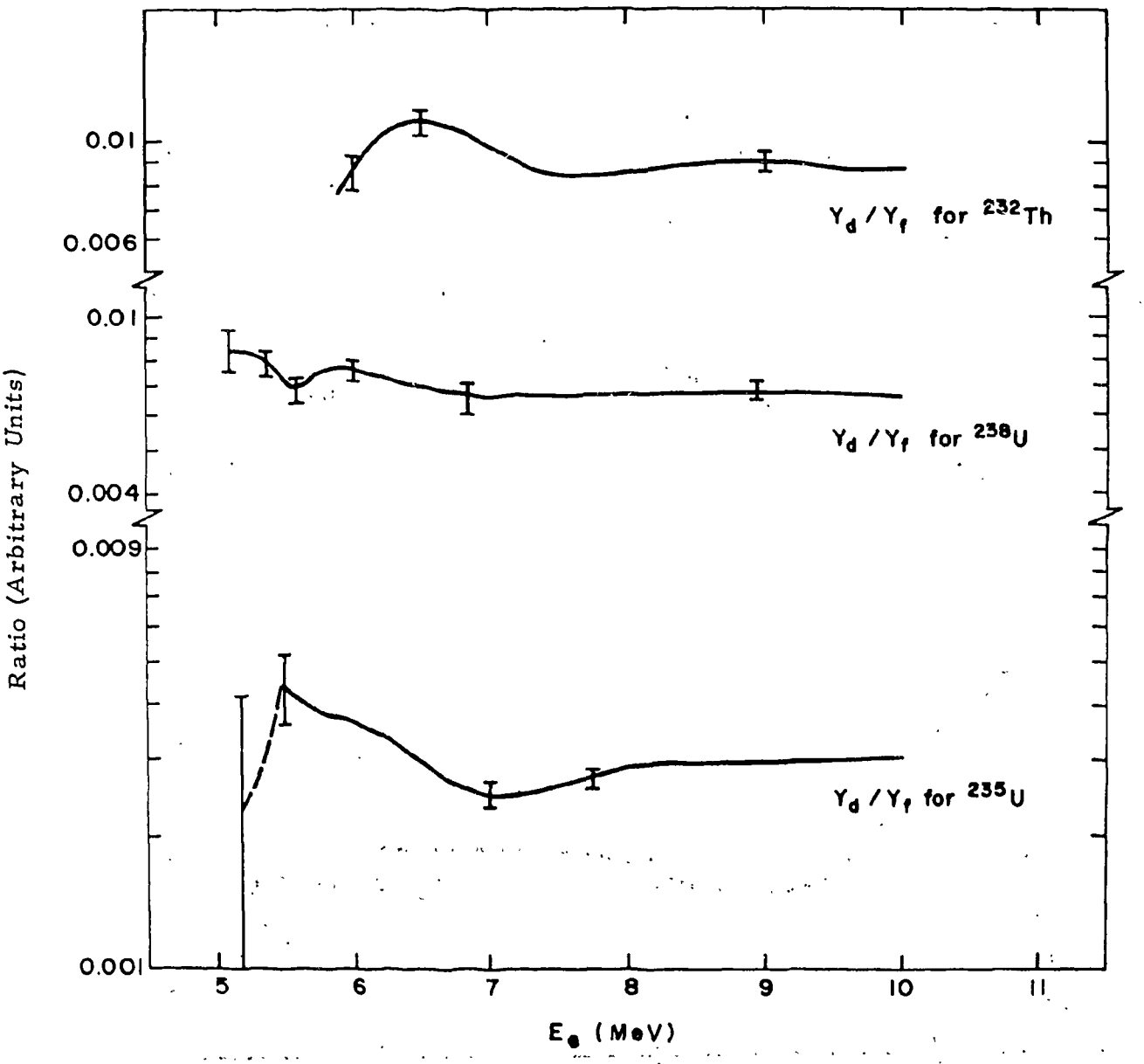

Fig. D-4. Bremsstrahlung averaged $\beta\nu$ for ^{232}Th, ^{235}U and ^{238}U with representative error bars.

Figure D-4 indicates that $\widehat{\beta\nu}(E_e)$ is rather independent of energy.

E. EXPERIMENTAL TECHNIQUES

1. High Counting Rate - Gamma Spectroscopy System (Tsahi Gozani)

A very high count-rate high resolution (over limited dynamic range) gamma spectroscopy system has been developed. It allows, for example, the detection of very weak high energy lines, with almost no loss in resolution or measuring time, in the presence of extremely high count rates from lower energy gamma rays. The system is based on current sensitive electronics and has been applied to both NaI(Tℓ) and large Ge(Li) detectors.

A test was performed with a small ^{106}Ru (1050.4 keV line) source in the presence of a 1500 times stronger source of ^{95}Zr-^{95}Nb (723.92 to 765.52 keV lines). The prevailing total count rates were 1.5×10^5 cps for the NaI(Tℓ) detector and 6×10^4 cps for the Ge(Li) detector. Without the system the 1050.4 keV line of ^{106}Ru was completely smeared out in the NaI(Tℓ) detector and partly smeared in the Ge(Li) detector. Using the system the results obtained for the peaks and the area under it were hardly effected by the presence of the Zr-Nb source.

F. EVALUATIONS

1. Evaluations of Magnesium and Copper Cross Sections for ENDF/B (M. P. Fricke, A. D. Carlson, V. J. Orphan Joseph John and C. J. Rindfleisch)

The neutron and gamma ray production cross sections for Mg and Cu are being evaluated for consideration for Version III of ENDF/B. For both of these elements complete re-evaluations of all experimental data are being performed which are supplemented with nuclear model calculations where measurements are not available. To date in this program, emphasis has been placed on the evaluation of the neutron total and gamma ray production cross sections. Recent total cross section measurements and new calculational techniques and experimental data for gamma ray production cross sections have resulted in substantial improvements of these data.

LAWRENCE LIVERMORE LABORATORY

A. NEUTRON PHYSICS

1. Capture Cross-Section Measurements (J. B. Czirr and M. L. Stelts) Relevant to Requests 155, 298, 300, 302, 306, 308, 310, 321, 336 and 422

As part of a program to accurately measure neutron-capture cross sections, we have obtained data for Ho, Au and Y in the 100 eV to 1 MeV energy range.

All capture cross sections will be reported relative to the fission cross section of ^{235}U for energies above 1 keV and to $^{6}Li(n,\alpha)$ below 1 keV. In addition, a current best estimate of $\sigma_F(^{235}U)$ will be used to convert these ratios to up-to-date capture cross sections. As measurements of $\sigma_F(^{235}U)$ improve in the future, the ratio measurements will yield improved values for σ_C. It should be noted that absolute values for the fission cross section are not needed to obtain normalized capture cross sections. All capture data will be normalized by utilizing the 3.9 eV "black resonance" of ^{165}Ho and will remain fixed in the low keV region. This resonance is particularly well suited to this purpose because of the low probability of scattering at the resonance energy ($\Gamma_n/\Gamma_\gamma = 0.026$).

The goal of this series of measurements is to obtain σ_C for Ho, Au, Y, ^{238}U, Ta, Zr, In, Tm and Lu over the above energy range and with an accuracy of better than 3% (assuming no error in the relative σ_F data). This will be the ultimate accuracy of the data after considerable improvement in the current σ_F values.

2. Investigation of γ-Ray Emission Preceding Isomeric Fission (J. C. Browne and C. D. Bowman) Relevant to Requests 405 and 483

Measurements were made to detect γ rays preceding isomeric fission in ^{236}U induced by eV-range neutrons captured in ^{235}U. These results were recently published in Physical Review Letters (PRL 28, 617 (1972)). A limit of $\leq 6 \times 10^{-5}$ was placed on the ratio of the rate of isomeric fission events with prefission γ rays to the rate for prompt fission events. This experiment provides direct evidence that the penetration of the outer barrier is much greater than that for the inner barrier for 3^- and 4^- states in ^{236}U.

Similar measurements are being performed to detect γ rays preceding isomeric fission in ^{243}Pu. In this experiment, a two dimensional

array is stored in which the fission events are recorded as a function of neutron energy in one dimension and the time relationship between the fission events and γ rays is recorded in the other dimension. Therefore it is possible to examine each subthreshold fission resonance in the $^{242}Pu(n,f)$ cross section for the existence of pre-fission γ rays which are associated with the delayed fission isomer. These data will provide a test of Lynn's theory* for weak coupling between the class I and class II states since it will be possible to relate the class II fission widths, the neutron widths** and the isomeric fission ratio (i.e. $\sigma_{iso}/\sigma_{prompt}$) for each subthreshold fission group.

3. Two-Parameter Measurement of Neutron Total Cross Sections (T. W. Phillips and B. L. Berman)

We have used the 250-m neutron-time-of-flight facility and the on-line computer and magnetic drum at the Livermore Electron-Positron Linear Accelerator Laboratory to measure the neutron total cross section for ^{207}Pb. A linear pulse-height signal from the proton-recoil scintillator detector was recorded simultaneously with the flight-time signal for each event. A schematic diagram of the data-collection apparatus is shown in Fig. A-1. Two arrays, of 24,576 2-nsec time channels x 32 pulse-height channels each, were used for the cycled sample-in and sample-out runs. The resulting two-parameter data can be used as a powerful tool to help eliminate background events, since they make it possible to discard background events having either low pulse heights at high neutron energies (short flight times) or high pulse heights at low neutron energies. Examples of both these kinds of background discrimination are illustrated by the neutron time spectra shown in Fig. A-2. Clearly, this mode of data collection enhances greatly one's ability to measure neutron and photoneutron cross sections and resonance parameters.

4. The Microscopic $^{130}Ba(n,\gamma)$ Cross Section and the Origin of ^{131}Xe on the Moon (J. C. Browne and B. L. Berman)

Berman and Kaiser*** performed a measurement of the integral $^{130}Ba(n,\gamma)$ cross section which provided evidence that this reaction explained the existence of the anomalously high concentrations of ^{131}Xe in lunar rocks. However, to obtain more quantitative information to compare with the lunar studies, a measurement of the microscopic $^{130}Ba(n,\gamma)$ cross section was performed.

---

* Theory of Neutron Resonance Reactions, J. E. Lynn, Oxford (1968), pp. 459-469

** G. F. Auchampaugh and C. D. Bowman, NCSAC-42, p. 121

***B. L. Berman and W. A. Kaiser, NCSAC-42, 17-19 Nov. 1971, p. 123

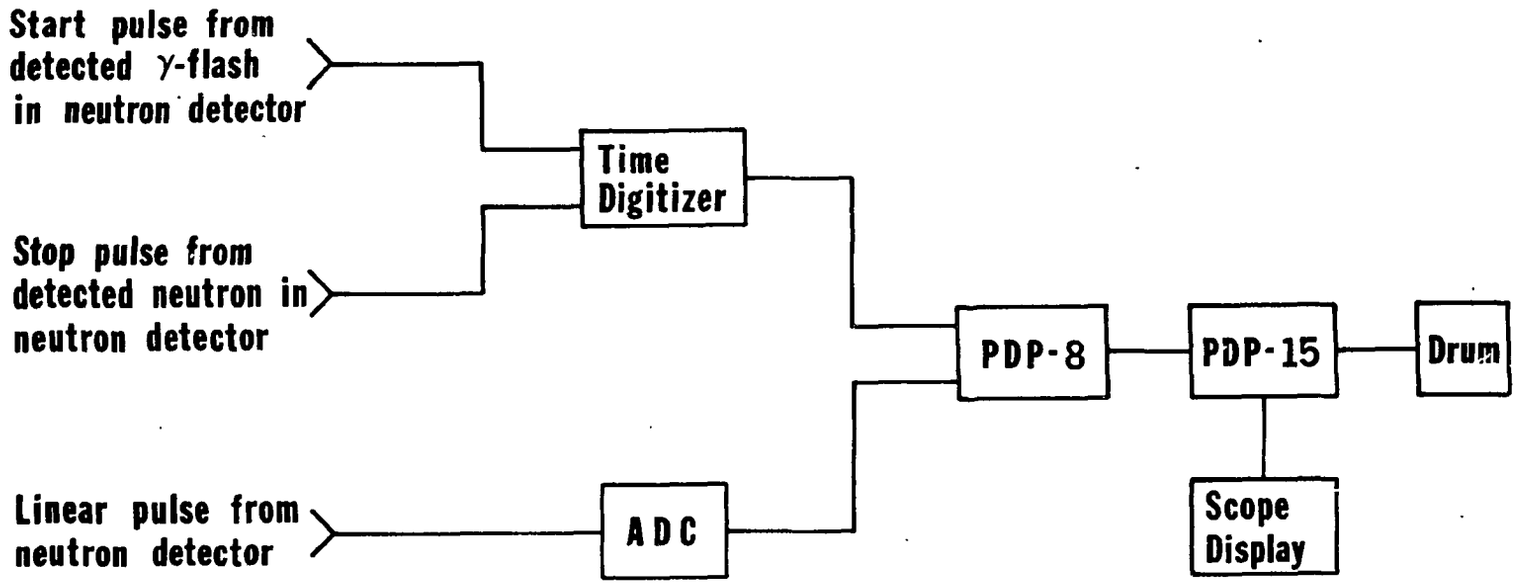

Fig. A-1. Schematic diagram of the data-collection apparatus.

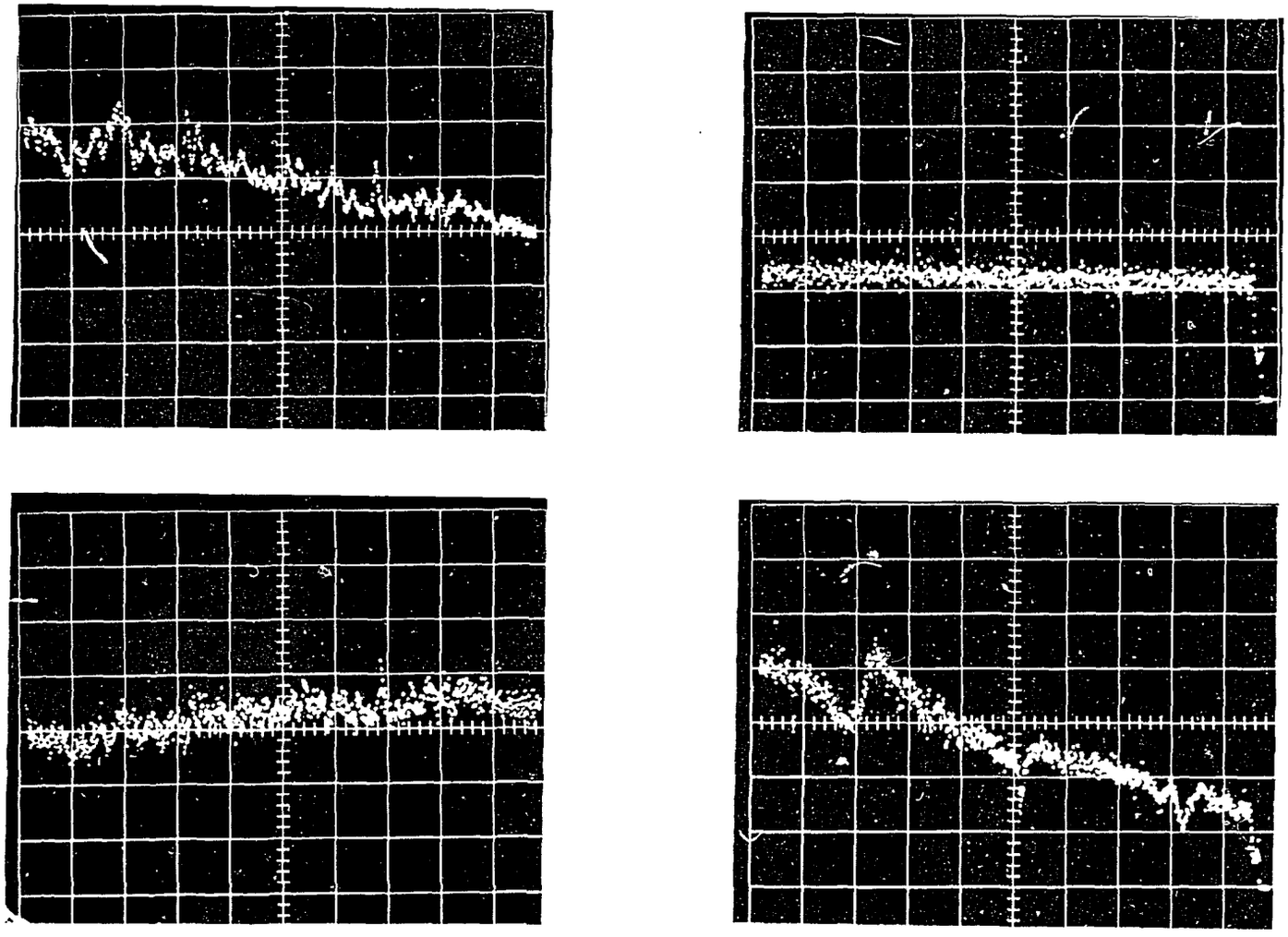

Fig. A-2. Time-of-flight spectra of neutrons transmitted through a sample of ^{207}Pb, illustrating how two-parameter data can help reduce backgrounds. Spectra shown are for (A) high pulse height, high neutron energy (mostly real events), (B) low pulse height, high neutron energy (mostly background events), (C) high pulse height, low neutron energy (mostly background events), and (D) low pulse height, low neutron energy (mostly real events). Spectrum (A) is to be compared with (B), and (C) with (D).

Enriched ^{130}Ba and natural barium samples were bombarded by neutrons from the pulsed neutron source of the Livermore 100-MeV Linac. Capture γ rays were detected by a pair of deuterated benzene scintillators. Both the time-of-flight of the capture event and the pulse height were stored in a two-dimensional array consisting of 20,000 time-of-flight channels and 64 pulse-height channels. A linear weighting function was applied to the pulse-height information to obtain the capture cross section. Figures A-3 and A-4 show the data from 20 eV to 3 keV. There are 41 resonances assigned to ^{130}Ba which are indicated by arrows, along with the resonance energies.

Schwaller et al.* estimated the resonance integral necessary to explain the excess ^{131}Xe in lunar samples by capture of epithermal neutrons in ^{130}Ba and obtained a value of 150 barns. Calculation of the resonance integral from our results yields a value of 180 barns for the $^{130}Ba(n,\gamma)$ reaction. The agreement between the two results is very good and indeed shows that the $^{130}Ba(n,\gamma)$ reaction is the most likely source of the excess ^{131}Xe in the lunar samples.

Since the flux distribution of epithermal neutrons in the lunar regolith is a function of depth, the knowledge of the $^{130}Ba(n,\gamma)$ cross section obtained here becomes a valuable quantitative tool for correlating burial depth with exposure age for lunar rocks.

5. Thermal-Neutron Cross-Sections of ^{257}Fm and ^{253}Cf (J. F. Wild and E. K. Hulet) Relevant to Requests 537 and 541

We have measured the cross section of the 100.5-d isotope ^{257}Fm for the absorption of thermalized neutrons leading to either fission of the excited compound nucleus, ^{258}Fm, or the spontaneous-fission decay of its ground state.

Our measurements were carried out in a thermal column of the Livermore Pool-Type Reactor using mica foil as the fission-fragment detector and gold foil as the flux monitor. The cadmium ratio at our irradiation position in the thermal column is greater than 500.

We obtained a weighted average value of 2950 ± 160 barns from eight individual measurements. (This value is somewhat lower than that given in the last NCSAC report.) Contributions to the number of fission tracks observed, in addition to background, were made by spontaneous-fission decay of ^{257}Fm and neutron-induced fission of its α-decay daughter, ^{253}Cf; these were corrected for. The last three measurements

*Schwaller et al., EPSL 12, 167 (1971)

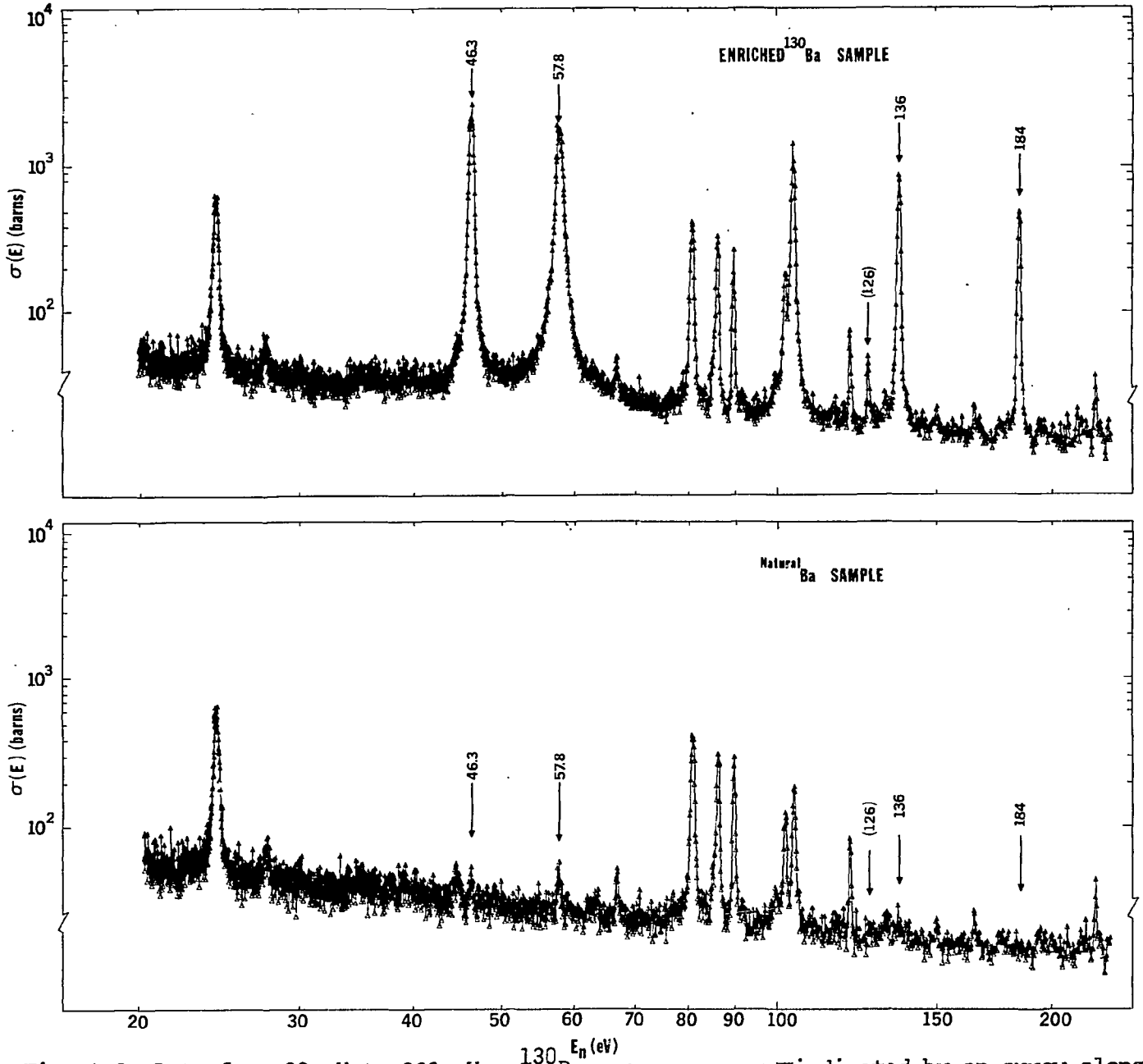

Fig. A-3 Data from 20 eV to 230 eV. ^{130}Ba resonances are indicated by an arrow along with the resonant energy. No background has been subtracted from the data. Ordinate scale refers to cross section for ^{130}Ba resonances.

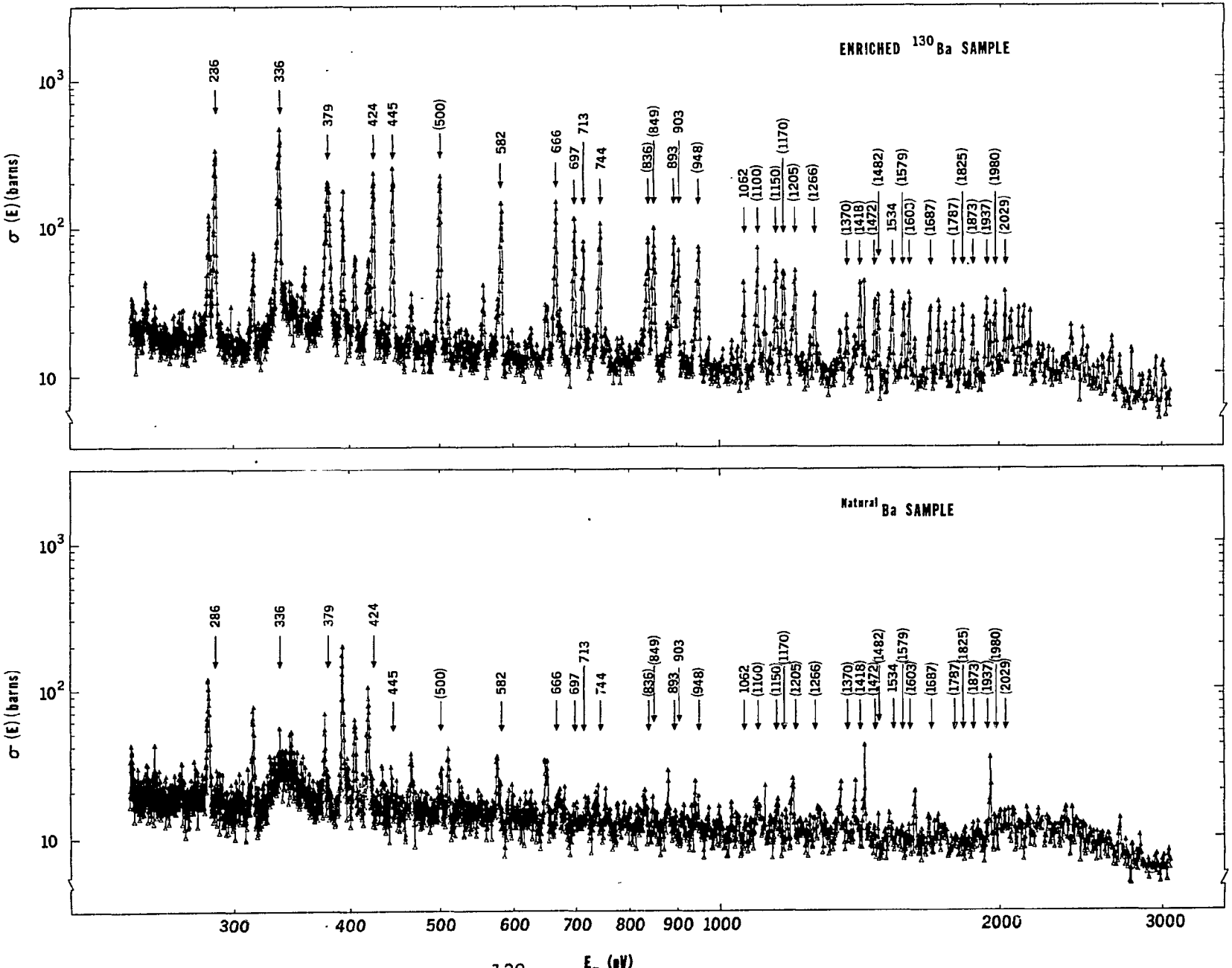

Fig. A-4 Data from 230 eV to 3 keV. ^{130}Ba resonances are indicated by an arrow along with the resonant energy. Resonances listed with parenthesis occur in either ^{130}Ba or ^{132}Ba. No background has been subtracted from the data. Ordinate scale refers to cross section for ^{130}Ba resonances.

were made with a ^{257}Fm target which had been specially purified from traces of natural uranium. The cross-section values obtained from the target were not significantly different from those from the first five experiments. It seems reasonable, therefore, to consider the level of uranium contamination in these targets insignificant insofar as the measurement of the ^{257}Fm cross section is concerned.

We have measured in a similar fashion the thermal-neutron-induced fission cross section of 17.8-d ^{253}Cf. Our target, initially $\sim 2 \times 10^7$ atoms of ^{253}Cf, was separated from about 10^8 atoms of its parent, ^{257}Fm, after a growth period of about 90 days.

Since the amount of ^{253}Cf in our target was so very minute, any natural uranium contamination in excess of about 10^9 atoms would contribute significantly to the number of fissions observed. For this reason, we performed ten irradiations over a period of seven weeks to observe the contribution of uranium fission as a constant component which would become more apparent as the ^{253}Cf contribution was reduced by decay. We fit our data to a two-component decay curve with the uranium contribution held constant with time, and thus obtained the relative fission contribution of each experiment due to ^{253}Cf.

We determined a weighted average value of 1300 ± 240 barns for the neutron-induced fission cross-section of ^{253}Cf from this series of ten experiments.

6. Intense Source of 14 MeV Neutrons (R. Booth)

The current status of the neutron source is described in a recent publication (NIM 99, 1 (1972)). The source produces 2×10^{12} neutrons/sec for a fresh target and the yield drops to half this value in about 100 hours of operation. Work is in progress to investigate the possibility of increasing the source strength and to extend target life. A larger target has been designed. An attempt to increase the output of the ion source will also be made.

The neutron source has occasionally been operated at 3×10^{12}/sec. Neutron flux densities of $1 - 1.5 \times 10^{12}/cm^2 sec$ have been observed near the target.

7. Neutron Yield from $^{9}Be(d,n)$ (K. A. Weaver*)

Deuterons of energies from 3 to 18 MeV bombarded about 1-MeV thick Be targets. Cross sections for neutron production were measured at ten angles from 3.5° to 144°. At the same angles neutron yields from the bombardment of thick targets were determined. Only neutrons of energies above 3 MeV were observed, and the data were extrapolated to zero neutron energy.

*Student guest from Univ. of Wisconsin, Madison

At 3.5° the thick-target yield varies from 3×10^8 neutrons/μC·sr at 3 MeV to 5×10^{10} neutrons/μC·sr at 18 MeV. The average neutron energy for a thin target is half the bombarding energy for deuterons above 6 MeV and approaches 3 MeV at lower bombarding energies, while for thick targets the average neutron energy is about 0.36 times the bombarding energy above 6 MeV bombarding energy.

This reaction is of applied interest both as an intermediate energy neutron source for cross-section measurements and as a neutron source for cancer therapy.

B. HEAVY IONS

1. Theory of Effective Charge and Stopping Power for Heavy Ions (S. D. Bloom and G. D. Sauter*)

A revision of the Knipp-Teller effective charge theory for the electronic stopping power of media for heavy ions is described. In the new theory the ion velocity is related to the mean ionization energy of the most loosely bound medium electrons as calculated from the Thomas-Fermi atomic model. The effective charge (γz, $0 < \gamma < 1$, where γ is the effective charge parameter) of an ion with atomic number z is related to the ionic kinetic energy ε(MeV/amu) through the equation

$$\varepsilon/z^{4/3} = 0.0277\ k\ [f_o(\gamma) + f_1(\gamma)/z]\ \text{MeV/amu},$$

where k is a constant, near unity, to be determined from the empirical data for the atomic number region of interest. Curves for f_o and f_1 as functions of γ are presented and an overall value of $k = 1.25$ is recommended. Calculated values of the effective charge parameter are compared to experimentally measured values for a wide range of ions, ionic energies, and stopping media. For $z > 10$ the agreement is very good from $\varepsilon/z^{4/3} \approx 0.001$, where exchange corrections (ignored in the Thomas-Fermi model) become important, to $\varepsilon/z^{4/3} \approx 0.1$, where a statistical theory is no longer valid.

C. COMPUTER FACILITIES

1. Magnetic Drum Storage Assembly (T. W. Phillips)

The LLL Linear Accelerator Group has recently acquired a large magnetic drum for data storage. The device we are using currently will

---

*Dept. of Applied Science, Univ. of California, Davis

hold 1.5 million 18-bit words in three word sectors on 1024 tracks recorded by 1024 separate heads. Track switching enables us to address any one of the 1024 tracks on alternate sectors. The drum is interfaced to a PDP-15 computer. A block diagram of our data acquisition facilities is shown in Figure C-1. With these facilities we have successfully concluded a number of time-of-flight, multi-dimensional experiments in which data rates of more than 1000 events per second were collected, sorted, and stored on the drum. These experiments typically required 0.5 to 1 x 10^6 channels. The drum is even very useful in conceptually simple experiments such as total cross-section measurements with plastic scintillator detectors. Time-of-flight data can be recorded as a function of pulse height and a dynamic bias set to eliminate large pulses which are backgrounds at low neutron energies and small pulses which are mainly background at high neutron energies.

At present software is nearly completed to allow these facilities to be shared by up to 4 users. We expect to receive a drum with twice the capacity of the one presently in use within the year.

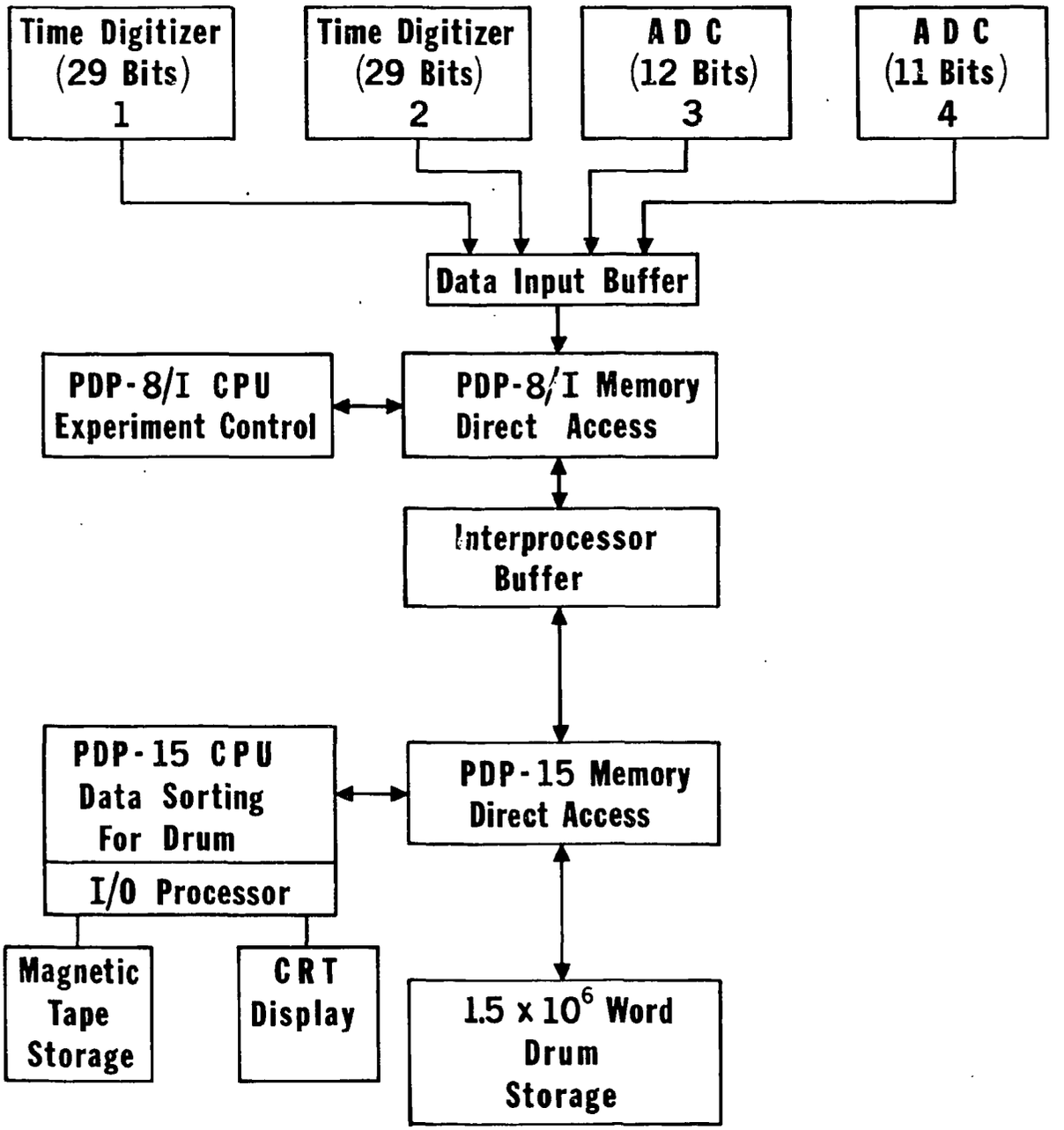

Fig. C-1. Schematic of Magnetic Drum Storage System

LOCKHEED PALO ALTO RESEARCH LABORATORY

A. NEUTRON PHYSICS

1. Gross-Fission-Product Gamma-Ray Spectroscopy (W. L. Imhof, L. F. Chase, R. A. Chalmers, F. J. Vaughn, and R. W. Nightingale)

The computer program which performs automatic peak location and analysis has been improved, especially by provision for energy calibration based on use of a selected set of prominent fission-product gamma rays, thus making each spectrum self calibrating. The entire program is being reanalysed for possible use on the ILLIAC IV computer.

2. Measurements of the ^{59}Co + n Total Cross Section using a Polarized Target (T. R. Fisher)

The ^{3}He - ^{4}He dilution refrigerator system designed for this experiment has been completed and has achieved a temperature of 0.025°K without a ^{59}Co sample attached. Two large ^{59}Co targets have been prepared from pieces cut from single-crystal rods. One target has the form of a rectangular solid 1 x 1 x 5 cm with the "C" axis parallel to the long dimension; the other has the form of a cylinder 1 cm diam. x 5 cm long with the "C" axis perpendicular to the cylinder axis. The two targets can be easily interchanged and will make it possible to study both parallel and perpendicular orientations of the target polarization axis with respect to the neutron beam direction. At 0.030°K, the nuclear polarization is 0.45 and the nuclear alignment 0.15.

Measurements of both the deformation and spin-spin effects in the ^{59}Co + n total cross section are planned covering the energy region from 0.3 to 15 MeV.

B. CHARGED-PARTICLE REACTIONS

1. The Excited States of the ^{14}O nucleus (J. G. Pronko, R. G. Hirko,* and D. C. Slater*)

Studies of the proton decay of the excited states of ^{14}O using a particle-particle angular-correlation technique[1] were performed on the Stanford Tandem accelerator. Spin assignments and natural widths of the following excited states were measured: [E_x (MeV), J, Γ(keV)]; 5.91, 0 or 1, <70; 6.29, 2 or 3, 103±6; 6.59, 2 or 3, <70; and 7.78, 2 or 3, 76±10.

---

*Stanford University, Stanford, California.

[1] J. G. Pronko and R. A. Lindgren, Nuc. Inst. and Meth. 98 (1972) 445.

2. A Study of Some ^{20}F Excited States (J. G. Pronko)

Excited states which decay through the 823-keV state were studied in order to establish the level scheme of the predicted ground-state rotational band of ^{20}F. Doppler-shift lifetime measurements and angular-correlation experiments established the 823- and 1824-keV states as the $J^{\pi} = 4^{+}$ and 5^{+} members of this band. Additional information concerning negative parity states was also obtained.

3. The Excited States of ^{28}Mg (T. T. Bardin, T. R. Fisher, A. R. Poletti, J. G. Pronko, and R. E. McDonald)

The properties of the excited states of the ^{28}Mg nucleus are being studied using the ^{26}Mg (t, pγ)^{28}Mg reaction. Attenuated-Doppler-shift measurements as well as γ-ray angular-correlation studies have been performed. The analysis of this data is presently underway and is expected to yield information on level spins, lifetimes of excited states, and branching and mixing ratios of the electro-magnetic de-excitation modes.

4. Properties of the ^{33}P Excited States (A. R. Poletti, J. G. Pronko, and R. E. McDonald)

The higher lying excited states of ^{33}P were examined with the ^{31}P(t, pγ) ^{33}P reaction using 5-crystal NaI(Tl) spectrometer. Angular-correlation measurements were made which yielded new spin information on a number of these excited states. Further studies are in progress.

5. Lifetime Measurements using Electronic Timing (A. R. Poletti, J. G. Pronko, E. K. Warburton,* and R. E. McDonald)

Long-lived excited states in the ^{39}Cl and ^{43}K nuclei are being studied using the respective (t, pγ) reactions. The method of electronic timing is being used to obtain lifetime information on the 0.98- and 1.3-MeV states of ^{43}K and ^{39}Cl, respectively. These studies are still in progress and hopefully will eventually lead to an understanding of the $f_{7/2}$ structure of these nuclei.

---

*Brookhaven National Laboratory, Upton, New York.

6. The Level Structure of ^{48}Ti for $E_x < 3.5$ MeV (T. T. Bardin, J. A. Becker, and T. R. Fisher)

A number of reactions using the Stanford Tandem accelerator have been employed to measure excitation energies, lifetimes, and γ-decay branching ratios for ^{48}Ti levels. Reduced electro-magnetic transition-matrix elements have been derived from the data, and for the 3.224-MeV state a $J^\pi = 3^+$ assignment is preferred to the previously accepted 4^+ assignment. The present results are in reasonable agreement with the predictions of an $f_{7/2}$ model calculation.

7. A Study of ^{52}Ti using the ^{50}Ti (t,pγ)^{52}Ti Reaction (J. G. Pronko, T. T. Bardin, A. R. Poletti, and R. E. McDonald)

The angular correlations of cascading γ rays observed in a collinear geometry with a 5-crystal array of NaI(Tℓ) detectors were measured. These studies provided information on the previously unobserved level scheme of ^{52}Ti including spin assignments and decay modes of the excited states. The analysis of this data is presently still in progress.

8. A Study of ^{56}Cr using the ^{54}Cr(t,pγ)^{56}Cr Reaction (T. T. Bardin, J. G. Pronko, A. R. Poletti, and R. E. McDonald)

The decay modes of the excited states of ^{56}Cr were studied using the technique of angular-correlation measurements obtained in a collinear geometry. An array of 5 NaI(Tℓ) crystals was used in the collection of the correlation data. The analysis of the data is presently being continued and is expected to yield information on spin assignments as well as branching and mixing ratios of the electro-magnetic de-excitations.

9. Elastic Scattering of Protons and Alpha Particles by Aligned ^{165}Ho (T. R. Fisher, B. A. Watson, D. Parks,* S. L. Tabor,* B. B. Triplett,* and H. King*)

Proton and α beams produced by the Stanford University Tandem accelerator have been scattered from a target of ^{165}Ho having a nuclear alignment B_2/B_2 (max) = -0.30. The difference between the aligned and unaligned cross sections has been measured for proton energies between 6 and 16 MeV and for α energies between 14 and 24 MeV. Some preliminary results have already been published.[1]

---

* Stanford University, Stanford, California.

[1] T. R. Fisher, S. L. Tabor, and B. A. Watson, Phys. Rev. Lett. 27, 1078 (1971).

10. Polarized β Emitters (R. E. McDonald, A. R. Poletti, L. F. Chase, J. A. Becker, T. R. Fisher, T. T. Bardin, and R. W. Nightingale)

The production of polarized β emitters by polarization transfer is being investigated with the Stanford University Tandem accelerator and a polarized ion source. Residual nuclei from deuteron- or proton-induced reactions are imbedded in suitable hosts in a strong magnetic field along the polarization direction. By observing the β-decay anisotropies, it is hoped that the technique can be applied to measurements of ground-state magnetic moments of short-lived β emitters.

11. Radiation-Damage Effects on Superconducting Microwave Cavities (T. R. Fisher and I. Ben Zvi*)

An X-band niobium cavity having a Q of 2.0×10^9 and a a breakdown field $H_{max} > 300$ Oe was irradiated by approximately 5×10^{16} deuterons of 2.5 MeV energy. The irradiation was confined to a spot size approximately 1.5 mm in diameter. No significant change in the Q of the cavity was observed, but a drastic reduction in the breakdown field ($H_{max} \approx 30$ Oe) occurred. Further measurements are in progress to study annealing and recovery rates. It appears desirable to increase the beam spot size in future measurements.

---

*Stanford University, Stanford, California .

LOS ALAMOS SCIENTIFIC LABORATORY

A. NEUTRON CROSS SECTIONS BY TIME-OF-FLIGHT

1. Parameters of the Subthreshold Fission Structure in ^{242}Pu. (G. F. Auchampaugh and C. D. Bowman)

A paper on the parameters of the subthreshold fission structures in ^{242}Pu has been prepared for publication. This paper combines the results of a recent high-resolution total cross-section measurement (NCSAC-42, p. 12) with the results from the Physics-8 fission cross-section measurement (Nucl. Phys. A171, p. 31) to provide information on six Class II resonances seen in these data below 4 keV. The results strongly suggest that the coupling between the primary and secondary minima in a double-humped fission barrier is very weak and that the widths being much less than the average spacing between levels in the primary well. The distribution of the fission widths of the levels in the primary well about their expected values is found to be consistent with a Porter-Thomas distribution. However, the distribution of the square of the coupling matrix element appears to require more than one degree of freedom. The Wigner distribution is shown to adequately describe the spacings between levels in the intermediate well.

2. Neutron Leakage Spectrum from Bare, Subcritical Spheres. (L. R. Veeser, R. R. Fullwood, E. R. Shunk, and A. A. Robba)

The purpose of this experiment is to measure the neutron spectra emitted by subcritical multiplying assemblies. This provides a very useful check on the cross sections for the individual neutron-induced reactions in the assemblies because the leakage spectra can be calculated by a transport code if the cross sections are accurately known.

Photoneutrons were produced in the center of the multiplying spheres by bombarding a tungsten target with 25 MeV electrons from the Electron Prototype Accelerator (EPA) to make bremsstrahlung. Beam bursts 50-nsec long were used because the multiplication time of the sphere is about 50 nsec. The neutrons were observed after a flight path of 27 m by either of two detectors. The first detector is a 2 by 2-inch NE-213 liquid scintillator which gave useful results in the neutron energy range from several hundred keV up to a few MeV. The other detector, a 5-inch-diam by 1/2-inch-thick Ne-908 lithium glass, gave results from about 1 MeV down to 10 keV or lower. However, since the amount of neutron scattering from the surroundings has not yet been calculated at low energies, it is not known whether the data below 40 keV are meaningful.

Measurements were made for spheres of ^{238}U, ^{235}U, and ^{239}Pu. Similar experiments had been done at General Atomic for uranium assemblies; they were redone in this case to provide a checkout of our detectors as well as to ascertain that the handling procedures for the target were safe enough to permit the plutonium measurements. The plutonium is a 10-kg sphere with a 1.3-cm-diam hole through which the beam can pass. The sphere can be disassembled into three pieces. When assembled the multiplication factor is about 7.5.

After the EPA runs, the detectors were calibrated using monoenergetic neutrons from the Group P-9 8-MeV Van de Graaff accelerator. Analysis of the detector calibrations has been begun but is not yet far enough along to give any results. The spectrum of ^{239}Pu as determined relative to the ^{235}U measurements appears to be quite reasonable. It is similar to that of uranium but is somewhat harder. Further data analysis is continuing.

3. Fission Neutrons from ^{257}Fm.
(L. R. Veeser, A. Hemmendinger, E. R. Shunk, J. A. Farrell, P. A. Seeger, J. P. Balagna, D. C. Hoffman, G. P. Ford, J. D. Knight and E. G. Hantel)

It is planned to measure $\bar{\nu}$, the number of neutrons per fission, as a function of the mass division of the two fission products of ^{257}Fm. In addition, an attempt will be made to learn the number of neutrons emitted from each fission product as a function of its mass.

The ^{257}Fm source has been obtained from Oak Ridge National Laboratory. It is a 90-day half-life, spontaneously fissioning source with a strength of at most 10 decays per minute. It exhibits a preference for symmetric fissions which is not ordinarily found in spontaneously fissioning nuclides. (Perhaps because Z = 100, it tends to divide into products with Z = 50 because of the shell closure.) Furthermore, there is some evidence that $\bar{\nu}$ may be lower for symmetric fission than for asymmetric fission in ^{257}Fm.

The masses of the two fission products will be deduced from a measurement of their energies using solid state detectors and a coincidence system. This apparatus will be placed inside a 75-cm-diam scintillator tank to measure the number of neutrons emitted. Since the neutrons are preferentially emitted in the direction of the fission product from which they evaporate, it may be possible to tell how many neutrons originate from each fission product. The neutron detector is divided into quadrants, and the solid state detectors will be oriented to aim the detected fission products toward opposite sections of the neutron tank.

The fermium source is presently being purified and prepared. The neutron detector is being interfaced to the PDP-8/L computer which will record the data and the software is being written. The detector is being checked out with a pulse height analyzer. A serious problem with the tank is that its energy resolution is not very high, making it difficult to set a discriminator level above the background from ^{40}K gamma rays in the surroundings without losing neutron efficiency. (Neutrons are detected after thermalization by observing the gamma rays from their capture in gadolinum in the scintillant.) The experiment will be done in a shielded counting room to minimize backgrounds. In addition it may be necessary to use additional lead shielding.

4. p-^{4}He and n-^{3}He Total Cross Sections.
(J. D. Seagrave, P. Stoler and P. Yergin (RPI))

Preparations are near completion for a collaborative effort to measure the total cross sections for the helium isotopes up to about 30 MeV with the Rensselaer continuum source technique. Gas handling will be entirely cryopumping, and two recovery cells checked out for liquid helium temperatures have been sent to RP I. The ^{4}He experiment will be conducted as a dry run for the ^{3}He experiment which involves 71 liters of ^{3}He. The procedure will be carefully evaluated with ^{4}He before introducing the ^{3}He. No pressure changes will be required during the experiment. The ^{4}He cross section has never been known adequately for use in phase shift and polarization analysis, and the ^{3}He cross section is quite poorly known above 8 MeV. The 1959 LASL measurements up to 21 MeV were made with a rather high transmission in a meter-long cell, and had statistical errors of about 10%. The recent measurements of Drosg et al., of the elastic integral between 8 and 24 MeV suggest that the old total cross section data may be as much as 10% high above 20 MeV. Improved measurements will be of value in removing some absolute scale uncertainties in the elastic data. Existing data for $\sigma_T(^{4}He)$ is also unsatisfactory for phase shift and polarization determinations, and a substantial improvement is expected from the current effort.

B. FAST NEUTRON STUDIES

1. Absolute Fission Cross Section for ^{235}U.
(G. E. Hansen, D. M. Barton, G. A. Jarvis and R. K. Smith)
Relevant to NCSAC-35, Requests 388, 389, 390, 391.

Data have been taken from 1 to 6 MeV with a total of $\sim$ 40 different energies. A preliminary study of the data would appear to indicate that we will have a three percent absolute measurement when completed.

The foil assay on both fission and polyethylene is incomplete and after complete analysis of the present data, plans are to take a few more check points under improved conditions to recheck the absolute values.

2. $T(p,^3He)n$ Neutron Source Reaction.
(N. Jarmie, J. H. Jett and John Martin)

A measurement has been made of the $T(p,^3He)n$ cross sections at 13.600 MeV. This was done after a very detailed examination of all aspects of the earlier experiment and its analysis did not resolve the scale discrepancy between our existing $T(p,^3He)n$ data and the $T(p,n)^3He$ data of Team 4. The scale difference is on the order of 15%. During the same run, some T(p,p)T and T(p,d)D cross sections were also measured with the same target gas.

As an additional check, two p-p elastic cross sections were measured. The resulting p-p cross section values were in agreement with our measurements of two years ago to within 0.5% and with cross sections calculated with the Yale phase shift set to within 0.1%. The standard deviations are 0.8% and 0.5%, respectively, for each comparison.

The T(p,p)T and T(p,d)D remeasurements are in agreement with the old measurements to within $\sim$ 3.0%. We believe that the difference is real and that it can be attributed to improper evaluation of the tritium purity for the old data. The purity of the tritium and its behavior with time and beam current is now much better understood. The purity for the recent data is known to ± 0.4%. The data compare well with those of Drosg et al., (see below) and our numbers have provided a consistent base for the absolute normalization (and hence prediction of absolute fluxes) of the time-of-flight data.

3. $^3T(p,n)^3He$.
(M. Drosg (U. of Vienna), D. K. McDaniels (U. of Oregon), J. C. Hopkins, J. T. Martin and J. D. Seagrave)

A draft of this paper has been completed, and least-squares Legendre polynomial fitting of the distributions is in process. Preliminary cross section results are given in Table B1. New data by Jarmie et al., for the reaction $^3T(p,^3He)n$ at 13.6 MeV have been used to normalize the absolute cross section scale.

4. $^3H(d,n)^4He$.
(M. Drosg (U. of Vienna), D. K. McDaniels (U. of Oregon), J. C. Hopkins, J. T. Martin and J. D. Seagrave)

The final efficiency curve as derived from Jarmie's results for $D(t,^4He)n$ has been used to establish the absolute cross section scale.

TABLE B1

Laboratory angular distributions for the reaction $^{3}T(p,n)^{3}He$ for proton energies E_p between 6 and 16 MeV. Relative cross sections, $R(\theta)$, are tabulated in terms of the cross section at the laboratory angle θ relative to the value measured at 0°, together with the absolute cross section $\sigma(0°)$ and its probable error. Errors in the relative angular distributions are ± 3% for θ = 0-110° and ± 6% for θ = 120-140°. Absolute forward yields were normalized to $^{3}T(p,^{3}He)n$ data at 13.6 MeV.

	E_p (MeV)								
θ(deg)	6.00	7.00	10.00	11.00	12.00	13.00	14.00	15.00	16.00
0	1.000	1.000	1.000	1.000	1.000	1.000	1.000	1.000	1.000
10	0.990	0.967	0.934	0.920	0.890	0.891	0.871	0.876	0.857
20	0.890	0.874	0.794	0.708	0.688	0.650	0.644	0.640	0.625
30	0.766	0.794	0.715	0.588	0.530	0.486	0.433	0.416	0.396
40	0.626	0.645	0.703	0.569	0.479	0.425	0.365	0.322	0.309
50	0.473	0.615	0.706	0.597	0.507	0.427	0.366	0.316	0.280
60	0.342	0.484	0.677	0.577	0.507	0.435	0.376	0.334	0.303
70	0.267	0.362	0.556	0.497	0.439	0.384	0.339	0.302	0.262
80	0.222	0.299	0.425	0.377	0.334	0.304	0.265	0.236	0.206
90	0.313	0.324	0.340	0.272	0.239	0.204	0.169	0.162	0.133
100	0.408	0.415	0.312	0.235	0.195	0.158	0.130	0.099	0.088
110	0.525	0.548	0.366	0.268	0.204	0.160	0.120	0.093	0.076
120	0.588	0.647	0.482	0.343	0.254	0.209	0.138	0.123	0.122
130	0.657	0.769	0.610	0.438	0.331	0.267	0.191	0.176	0.196
140	0.751	0.887	0.718	0.510	0.402	0.346	0.255	0.216	0.236
σ(0°)	50.3	38.1	30.1	32.5	36.3	38.3	42.5	44.4	45.2
mb	±1.4	1.1	0.9	0.9	1.0	1.1	1.2	1.3	1.4

A draft has also been completed for this paper, and Legendre polynomial fitting of the distributions is in progress. Preliminary cross sections are given in Table B2.

5. $^{2}H(d,n)^{3}He$.
(M. Drosg (U. of Vienna) and D. K. Drake)

Angular distributions at 6, 7, 8, 10, 11, 12.305, 13, 14, 15, and 16 MeV have been measured. Whereas below 13 MeV the quality of the data seems to be very good, there may be problems at higher energies, especially with the background subtraction. This work has low priority and will be finished by M. Drosg in Vienna.

6. Intercomparison of the Cross Sections of Neutron Producing Reactions.
(M. Drosg (U. of Vienna))

The release of Jarmie's $^{2}H(d,^{3}He)n$ differential cross sections at 12.305 MeV together with his $^{2}H(t,^{4}He)n$ cross sections at 20.0 MeV made it possible to check the efficiency curve of the detector from 4 MeV through 29 MeV.

Using the newly established efficiency curve, the following results were obtained.

a. Comparison of scale between d-D and t-D cross sections: The scale of the d-D cross sections is lower by 2.1%. The error in this number should be close to 1%, since there is a common energy range on the efficiency curve where the results overlap.

b. Comparison of scale between (new) p-T and t-D data: Two independent measurements show that the p-T data are high by 3.65%. (Individual results: 3.5% and 3.8%.) The uncertainty in this number is about 2.5%. Therefore it can be assumed that the scale of Jarmie's (new) data is correct within the errors given by him. The disagreement with counter-telescope measurements which are low by more than 10% has not been resolved.

7. n-^{3}He Angular Distribution.
(M. Drosg (U. of Vienna), D. K. McDaniels (U. of Oregon), J. C. Hopkins, J. D. Seagrave, J. T. Martin and E. D. Kerr)

Drosg has returned to Vienna with a preliminary draft of the paper. Further multiple-scattering correction calculations remain to be done, but preliminary results without such corrections are shown in Fig. B1.

TABLE B2

Laboratory angular distributions for the reaction $^{3}T(d,n)^{4}He$ for proton energies E_p between 5 and 15.7 MeV. Relative cross sections, $R(\theta)$, are tabulated in terms of the cross section at the laboratory angle θ relative to the value measured at 0°, together with the absolute cross section $\sigma(0°)$ and its probable error. Errors in the relative angular distributions are ± 2.8% for θ = 0-110° and ± 8% for θ = 120-140°. Absolute forward yields are normalized to $D(t,^{4}He)n$ data.

	E_d(MeV)									
θ(deg)	5.00	6.00	7.00	10.00	11.00	12.00	13.00	14.00	15.00	15.70
0	1.000	1.000	1.000	1.000	1.000	1.000	1.000	1.000	1.000	1.000
10	0.897	0.876	0.861	0.761	0.766	0.750	0.723	0.708	0.711	0.762
20	0.710	0.645	0.574	0.398	0.360	0.328	0.292	0.268	0.258	0.250
30	0.532	0.436	0.344	0.178	0.158	0.135	0.118	0.110	0.102	0.100
40	0.421	0.351	0.278	0.194	0.186	0.189	0.184	0.184	0.185	0.195
50	0.354	0.316	0.287	0.258	0.264	0.257	0.254	0.257	0.263	0.261
60	0.294	0.281	0.284	0.254	0.244	0.234	0.222	0.218	0.197	0.197
70	0.236	0.237	0.225	0.188	0.167	0.149	0.142	0.122	0.111	0.104
80	0.190	0.178	0.166	0.115	0.102	0.085	0.068	0.060	0.052	0.053
90	0.165	0.147	0.135	0.086	0.074	0.066	0.058	0.052	0.052	0.048
100	0.174	0.149	0.126	0.090	0.084	0.079	0.072	0.071	0.073	0.069
110	0.193	0.165	0.142	0.108	0.104	0.097	0.089	0.086	0.085	0.082
120	0.235	0.215	0.166	0.127	0.143	0.108	0.099	0.088	0.090	0.083
130	0.283	0.218	0.195	0.138	0.159	0.110	0.102	0.084	0.083	0.072
140	0.288	0.224	0.199	0.173	0.183	0.136	0.117	0.099	0.083	0.087
σ(0°)	25.2	27.4	27.6	25.7	24.5	24.9	24.7	24.7	24.3	24.8
mb	±0.8	0.8	0.8	0.8	0.7	0.7	0.7	0.7	0.7	0.7

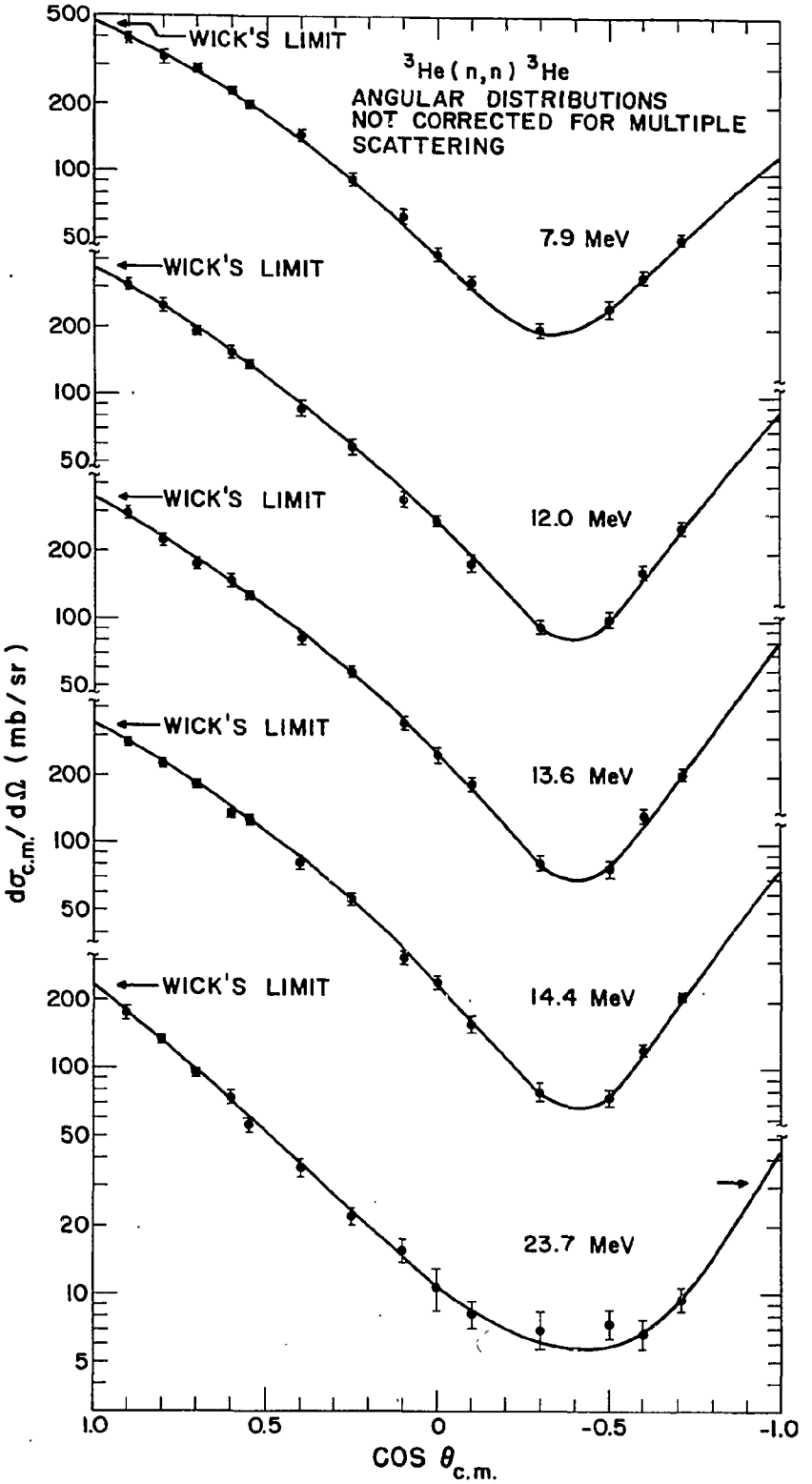
WICK'S LIMIT
^{3}He (n,n) ^{3}He
ANGULAR DISTRIBUTIONS
NOT CORRECTED FOR MULTIPLE
SCATTERING
7.9 MeV
WICK'S LIMIT
12.0 MeV
WICK'S LIMIT
13.6 MeV
WICK'S LIMIT
14.4 MeV
WICK'S LIMIT
23.7 MeV
500
200
100
50
20
10
5
1.0
0.5
0
-0.5
-1.0
$d\sigma_{c.m.}/d\Omega$ (mb / sr)
COS $\theta_{c.m.}$

Fig. B1

8. Fast Neutron Breakup of Deuterium.
(J. D. Seagrave)

This project has been shelved and the equipment of the late Elizabeth Graves' experiment has been dismantled. On a recent visit, Prof. Ivo Slaus noted that the work at UCLA on the D(p,2p)n reaction confirms our projection made from the Graves D(n,p)2n integral cross section at 14.46 MeV and the differences $\sigma_{ne} = \sigma_T - \sigma_e$ obtained from the new n-D elastic integrals, and he expressed interest in a future extension of the D(n,p)2n measurements to higher energies.

C. FISSION ISOMER STUDIES
(H. C. Britt, O. R. Nix and J. L. Norton)

Most of the effort on fission isomers has concentrated on trying to fit fission isomer excitation functions using an improved statistical model. Single particle level spectra were recalculated for each nucleus of interest at the ground state minimum and at the first maximum in the fission barrier. These levels were used in a new fit to fission isomer excitation functions from 2n and 3n evaporation reactions and in calculations of excitation functions for populating nuclei at the ground state deformation from 3n evaporation reactions. In these fits the value for the height of the first peak in the fission barrier is taken from the theoretical calculations and the only adjustable parameters are the height of the secondary minimum and the second peak above the ground state. In addition the effect of pre-equilibrium emission is taken into account using calculations of neutron spectra supplied by Marshall Blann at the University of Rochester. The addition of a pre-equilibrium component does a good job of accounting for the shape of the high energy tail in the isomer excitation functions.

The results of the fits with the new model show that we can reproduce the cross sections for ground state population to an accuracy of better than a factor of 2 with no adjustable parameters. Except for the $^{235}U(\alpha,3n)^{236}Pu$ reaction which we measured, most of the experimental results are only accurate to about a factor of 2. For the ^{236}Pu data we reproduce the threshold to within the experimental error and the magnitude of the cross section to within 20%. This indicates that the model and the Nix calculations are really much better than we had originally hoped, at least for decays from the first well. The values obtained for the height of the second minimum and the second maximum also agree quite well with the Nix calculations for the Pu isotopes but there appear to be some systematic differences in the heavy Am isotopes and in the Cm isotopes. This effect is currently being investigated.

D. THERMAL NEUTRON CAPTURE GAMMA-RAY STUDIES

1. Studies of the $^{150}Nd(n,\gamma)^{151}Nd$ Prompt γ-spectrum.

(H. A. Smith, J. W. Starner and M. E. Bunker)

Our analysis of the high- and low-energy ^{150}Nd capture γ-ray spectra has revealed more than 100 γ rays attributed to transitions in ^{151}Nd. Using the data from these spectra and the previous (d,p) data (C. L. Nealy and R. K. Sheline, Phys. Rev. 164, 1503 (1967)), we have constructed a level scheme for ^{151}Nd which involves approximately 70 levels below 2.5 MeV. The above data, together with Coriolis calculations involving the odd-neutron Nilsson orbitals expected to be lowest lying, have led to the conclusion that the ground state of ^{151}Nd is 3/2, $3/2^+(651)$, in disagreement with the assignment proposed by Nealy and Sheline.

2. Capture Gamma-ray Study of ^{188}Re.

(E. B. Shera)

Some interesting physics regarding the $0^+ \rightarrow 0^+$ β transition between the ^{188}W ground state and the $I^\pi = 0^+$, $9/2^-(514\uparrow) - 9/2^-(505\downarrow)$ state at 207.8 keV in ^{188}Re has recently come to light. Such $0^+ \rightarrow 0^+$ beta transitions are caused solely by the Fermi matrix element. However, Fermi matrix elements can act only between isobaric pairs for which $\Delta T = 0$. In light nuclei transitions of this type are commonly observed with log ft values of 3.5 (superallowed). However, in heavy nuclei the Fermi strength is concentrated in an isobaric analog state which lies high in the spectrum where it is unavailable to beta decay. Only through mixing of the isobaric analogue states into the low-lying 0^+ state can the decay proceed. The observed log ft of 9.9 for the ^{188}W decay gives a measure of this mixing. Mixings of this order have, in fact, been theoretically predicted for the rare earth and actinide nuclei.

3. Photon Production Cross Sections.

(E. T. Jurney)

In order to make measurements of photon production cross sections as a function of energy in the neutron capture processes, it is necessary to determine the system response for photons over the energy range of interest. This response function has been determined for a 6" long by 2" diameter NaI crystal operated as a pair spectrometer. In the energy range $2 < E_\gamma < 11$ MeV the response to a single gamma ray can be characterized by a gaussian function with a simple exponential tail extending to the low energy side. The ratio of area under the gaussian component to that under the tail is approximately 5:1.

Some preliminary spectra have been taken with a 300 mg/cm^2 foil of highly depleted ^{238}U. These data are currently being unfolded.

4. $^{240}Pu(n,\gamma)^{241}Pu$.
(E. T. Jurney)

High- and low-energy GE(Li) and pair spectrometer NaI spectra have been obtained from a 24-mg target to ^{240}Pu. The high resolution spectrum at high energies exhibits a few intense, well resolved lines and a considerable continuum of unresolved radiation. The low energy spectrum is dominated by an extremely intense 162 keV transition, presumably the ground state transition from the $1/2^+(631)$ band head observed at 163 keV in charged-particle experiments. The cluster of intense gammas observed between 650-750 keV in ^{235}U is also present in ^{241}Pu.

E. EVALUATION

1. Total Neutron Cross Section of ^7Li.
(M. E. Battat and D. G. Foster, Jr.)

A partial re-evaluation of the total neutron cross section of ^7Li has been completed, making use primarily of new data which are in good agreement. It follows the results of Meadows and Whalen[1] below 1 MeV. From 1 to 25 MeV it follows mainly the results of Goulding et al.[2], modified slightly between 5 and 20 MeV to improve the agreement with Fister and Glasgow[3] and with Peterson et al.[4]. Above 0.5 MeV the evaluation is probably accurate to within 1 or 2 percent. A thorough study has not been made below 0.5 MeV, and the uncertainty may be somewhat greater below the first resonance.

---

1. J. W. Meadows and J. F. Whalen, "Total Neutron Cross Section of Lithium-7 and Carbon from 100 to 1500 keV," Nucl. Sci. Eng., 41, 351 (1970).
2. C. A. Goulding, P. Stoler, and J. M. Clement, "Total Neutron Cross Sections on ^7Li from 1.0 to 25 MeV," Rensselear Polytechnic Institute Report C00-3058-1 (1971).
3. D. Graham Foster, Jr. and Dale W. Glasgow, "Neutron Total Cross Sections, 2.5-15 MeV. I. Experimental," Phys. Rev. C3, 576 (1971).
4. J. M. Peterson, A. Bratenahl, and J. P. Stoering, "Neutron Total Cross Sections in the 17- to 29-MeV Range," Phys. Rev. 120, 521 (1960).

2. Evaluation of the $^9Be(d,n)^{10}B$ Cross Section from 0 to 2.8 MeV.
(J. J. Devaney and G. M. Hale)

The $^9Be(d,n)$ reaction is of interest as a neutron source and because it is a source of background neutrons from beryllium backstops. The cross section for this reaction has been evaluated by augmenting measured values at deuteron energies at and above 1.1 MeV by a theoretical expression based on penetration and spin statistical considerations. These results were

extended to lower energies using the energy dependence of the Coulomb penetration factor as well as a relative measurement of the cross section. The method and results are described in LA-4851, to be published.

3. Total Cross-Section Evaluation for Wolfram and Its Isotopes. (J. J. Devaney and D. G. Foster, Jr.)

A new evaluation of the total cross section for wolfram and its isotopes between 0.02 and 22 MeV has been completed. Except for ^{183}W below 0.6 MeV, the total cross sections of the isotopes do not differ significantly from that of natural wolfram in this energy range, so a separate curve is given for the low-energy portion of ^{183}W and a single curve for the others. Gaps in the measurements were filled with the aid of Peterson's theory of the nuclear Ramsauer effect. Although some evidence for fluctuations exists, much of it is inconclusive. Accordingly, the fluctuations have been smoothed out in the evaluation. As smooth cross sections, the evaluated curves are expected to be correct within 6% below 2.5 MeV and 2% above. A report is in preparation (LA-4928).

NATIONAL BUREAU OF STANDARDS

A. NEUTRON PHYSICS

1. MeV Neutron Total Cross Sections (R. B. Schwartz, R. A. Schrack, H. T. Heaton II, and H. S. Camarda)

We have just finished measuring the total cross sections of ^{235}U, ^{238}U, and ^{239}Pu in the energy range 0.5 to 15 MeV, using samples provided by Los Alamos. The data are still being analyzed.

2. keV Cross Sections (J. Menke, H. T. Heaton II, R. A. Schrack, R. B. Schwartz, and H. S. Camarda)

A paper entitled "Use of a Li Glass Scintillator in a Neutron T-O-F Spectrometer" was presented at the 1972 Washington Meeting of the American Physical Society. The abstract follows:

"The properties of a Li glass scintillator for use with the T-O-F facility at the NBS Linear Accelerator to cover the energy range 4 keV to 2 MeV have been investigated. The two main criteria were to develop a system capable of taking data close in time to the gamma flash (produced when the electron beam strikes the neutron producing target) and having a low background counting rate. This system allows data to be taken within 1.5 μsec (~ 2 MeV) of the gamma flash. The primary neutron source is out of the line of sight of the detector and neutrons are scattered down the 38 meter flight path. To keep the background to a minimum as much hydrogenous material as possible has been kept out of the neutron beam line. Using black resonance techniques the background measured at 35 keV in less than 1%. As an application of this system preliminary data on the total cross section of carbon will be presented."

In addition to the Li glass scintillator, a ^{10}B-NaI detector has also been developed. This detector uses ~ 1 kg of ^{10}B metal powder, viewed by four 3" × 3" NaI scintillators. This device has several useful attributes: it is relatively immune to gamma-flash problems, has a reasonably high efficiency, and has no machine-dependent background.

Preliminary measurements of the carbon total cross section have been made with both detectors over the energy range 4 keV to 2 MeV. The measurements with the two detectors agree with each other, and with recent evaluations, to within < 2%.

3. ^{252}Cf Source (V. Spiegel)

Calibration of the low-mass 1 mg ^{252}Cf spontaneous fission source to be used as a standard reference field and in fission cross-section validation studies has required extension of the NBS $MnSO_4$ bath facility to handle sources of about 100 times the neutron emission rate of those handled previously.

The neutron emission rate of our 1 mg ^{252}Cf spontaneous fission source has been calibrated to be $2.154 \times 10^9 \pm 1.6\%$ as of December 1971. The source was calibrated by comparing its strength indirectly to that of the NBS primary Ra-Be photoneutron standard source in a manganous sulfate bath by continuously counting the induced, saturated manganese-56 activity with two scintillation counters.

One scintillation counter sampled the activity at the center of the remotely located actuated manganese volume. The second counter viewed a fraction of the same volume through a collimator. The first counter operated at about 100 cps for the standard source of about 10^6 neutrons per second and was partially paralyzed for the ^{252}Cf source. The second counter operated at about 800 cps for the ^{252}Cf source but close to background for the standard source. Relative counter efficiencies were obtained with an intermediate source of 10^8 neutrons/s, allowing the source comparison involving scaling of 2000 in neutron emission rate to be carried out.

4. Emission of Long Range Alpha Particles from Fission. (I. G. Schröder)

Abstract of paper presented at the Washington American Physical Society Meeting, April 1972:

Extreme-Angle Emission of Long-Range Alpha Particles in the Thermal Neutron Fission of ^{235}U. I. G. Schröder, NBS.--An experiment has been performed in order to seek a correlation between the kinetic energy of long-range alpha particles emitted at extreme angles ($0^\circ \leq \theta \leq 30^\circ$, $180^\circ \leq \theta \leq 150^\circ$) with respect to the line of emission of the light fission fragments and the kinetic energy of the fission fragments. An annular surface barrier detector (alpha detector) subtended an angle of $\pm 30^\circ$ at the target (^{235}U) with respect to a fission fragment detector placed behind the annular detector. An annular aluminum foil was introduced between the alpha detector and the source. This let through alpha particles $\geq$ 6 MeV but stopped all fission fragments. A coincidence circuit (15 nsec resolving time) demanded coincidence between the two detectors. The output from these was displayed on a 2-dimensional PHA. The results obtained show that extreme-angle alpha particles have higher than average kinetic energies (> 20 MeV) and rate of emission. Further-

more, these alpha particles are associated with fission fragments in the region of minimum kinetic energy between the light and heavy fission fragments.

5. Search for Two-Photon Neutron Capture in Hydrogen. (R. G. Arnold and B. T. Chertok, American University; I. G. Schröder, NBS; J. L. Alberi, Harvard)

Abstract of paper presented at the Washington American Physical Society Meeting, April 1972:

A Search for Doubly Radiative np Capture.* R. G. Arnold and B. T. Chertok, American U., I. G. Schröder, NBS, and James L. Alberi, Harvard U.--It has been suggested[1] that the long-standing discrepancy of 24 mb between the measured and the calculated thermal np capture cross sections might be ascribed to captures leading to emission of two photons. An experiment has been performed. Gated prompt- and delayed-coincidence γ spectra were obtained with two 2"X2" NaI(Tl) detectors using a H_2O target and a D_2O target for background exposed to a beam of thermal neutrons from the NBS reactor. The result is that no two photon captures are observed at the 1 mb level, so the long-standing discrepancy still remains. Analysis of data is in progress to reduce this upper limit in order to test for the presence of an orthogonality breaking $^3S \rightarrow {}^3S + \gamma$ transition. A calculation[2] predicts an upper limit of 42 μb for $^3S \rightarrow {}^3S + 2\gamma$.

*Supported in part by the National Science Foundation.

[1] R. J. Adler, B. T. Chertok, and H. C. Miller, Phys. Rev. C2, 69 (1970).

[2] R. J. Adler (in press).

6. Forced Reflection Neutron Collimators. (L. V. Spencer)

An approach to neutron collimator design has been suggested by L. V. Spencer and S. Woolf in which wall-emergent background neutrons are forced to reflect from each of a number of (tapered) segments beyond the point of first emergence. Simple Monte Carlo and approximate analytic studies have been made using an isotropic scattering model. In these studies several designs with two and three segments were intercompared in the context of a proposed neutron-neutron scattering experiment. A talk at the fall meeting of the American Nuclear Society has been given on this subject and a paper is just out: L. V. Spencer and S. Woolf, "Forced-Reflection" Collimators and the n-n Scattering Experiment, Nuclear Instruments and Methods 97, 567-576 (1971).

B. DATA COMPILATION

1. Photonuclear Data Center. (E. G. Fuller, H. Gerstenberg)

The Center is continuing work on its library of digitized photonuclear cross section information. For cases where digital data have not been received directly from those performing the work, printouts of the library record are being sent to the authors of the papers in which the data are published. The authors are being requested to check the printouts against their original data for accuracy as well as to indicate where corrections are necessary due to later revisions of the published results. The library now contains data for over 350 cross section curves measured for more than 70 different nuclides covering 43 elements.

In the course of this work considerable experience has been obtained using the Center's sonic delay-line digitizer. Based on measurements made on a precision grid, the uncertainty in the determination of the coordinates of a point is ± 0.01 inch (based on the standard deviation of a large number of measurements of coordinate points.

The plans to evaluate the data in the Center's files and publish a comprehensive, annotated compilation of the best available information on the photonuclear interaction have received a big boost with the award of a NAS-NRC, Nuclear Information Research Associate postdoc appointment to H. Vander Molen. He will work with the group for a two-year period starting in September 1972. The objective of the proposed "atlas" will be to present, in a uniform format, all of the information relevant to the interaction of photons with nuclei in such a way that it is readily available and useful not only for theoretical and experimental physicists working in the field but also for various applied users of such data in areas of activation analysis, radiation shielding, medical physics, etc. It is planned to use nuclides and elements suggested by the Cross Section Evaluation Working Group (AEC) as test cases to develop both evaluation procedures as well as formats for the presentation of the evaluated data.

2. Photon Cross Sections (J. H. Hubbell, G. L. Simmons)

As an NSRDS-NBS "X-ray Attenuation Coefficient Information Center" we are continuing to extract from the literature and systematize measured and theoretical photon cross section data over the energy range 10 eV to 100 GeV for all photon interaction processes except photonuclear absorption which is in the province of the NSRDS-NBS Photonuclear Data Center (E. G. Fuller).

The photon attenuation coefficient data index described in the previous USNDC (NCSAC) report has now been published[1], also a briefer

survey article[2].

Work continues on the DNA-sponsored intercomparison and evaluation of existing quasi-independent photon cross section compilations (NBS, LLL, LASL, Sandia, Kaman, and Gulf General Atomic), results of which are being made available as a series of NBS reports[3].

Through participation in the Shielding Subcommittee of CSEWG (Cross Section Evaluation Working Group, AEC) we are continuing to examine, update and expand the ENDF/B photon cross section library tape. As part of this program, an evaluated set of coherent and incoherent scattering factors is in preparation, in collaboration with workers at LLL, LASL, EG&G, and Kaman, for presentation at the 4th International Conference on Reactor Shielding, Paris, October 1972, and for publication in the new Journal of Physics and Chemistry Reference Data.

---

[1] J. Hubbell, Survey of Photon Attenuation Coefficient Measurements 10 eV to 100 GeV, Atomic Data 3, 241-297 (1971).

[2] J. Hubbell, Photon Cross Section Compilation Activity in the U.S. in the Range 1 keV to 100 GeV, J. Physique 32 (Colloq. C4), 14-20 (1971).

[3] G. L. Simmons and J. H. Hubbell, Comparison of Photon Interaction Cross Section Data Sets. I. Storm-Israel and ENDF/B, NBS 10668 (unpublished); II. Biggs-Lighthill and ENDF/B, NBS 10818 (unpublished).

C. FACILITIES

1. Linac Above-Ground Neutron Facility (S. Penner)

Construction of the above-ground neutron facility for the NBS linac is proceeding. The vertical shaft connecting the existing magnet room with the above-ground neutron source area is in place, and completion of the building construction is expected in August. New beam transport apparatus has been completely designed and construction is nearing completion. Major sections of the magnet system are being preassembled at present in order to minimize installation and alignment time when the building becomes available. We expect that the facility will be ready for use by October of this year.

2. 3-MeV Van de Graaff Facility (M. Meier)

Installation of the 3 MeV positive ion Van de Graaff formerly utilized in the neutron physics program at Argonne National Laboratory has been completed. The first d.c. proton beam was extracted in November 1971. New beam handling and monitoring hardware (magnetic dipoles, profile monitors and beamstops) have been installed along with

their associated electronics and the beam transport system has been aligned. The pulser has been recently operated for the first time at a terminal voltage of 2 MV. Five nanosecond bursts (FWHM) and average analyzed beam of 3 μA (3.3 MhZ repetition rate) were obtained. Design and construction of components for absolute flux measurements has begun.

NAVAL RESEARCH LABORATORY

A. NEUTRON PHYSICS

1. Resonance Spin Determinations in Os^{189} (A. I. Namenson, A. Stolovy, T. F. Godlove and G. L. Smith)

Using neutrons from the U. S. Naval Research Laboratory Linac we applied the low-energy γ-ray technique to measure the spins of resonances in Os^{189}. In addition to the ratio of the intensity of the 360 keV line to that of the 187 keV line (used by Wetzel and Thomas[1]), we also used the intensity of the 569 keV line and the coincidence method of Coceva et al[2]. Since the latter two experiments are still in progress this report is mainly on the ratio of the intensities of the 360 and 187 keV lines.

By an extension of a calculation described in a forthcoming publication[3] we determined spin assignments and probabilities of correctness for 38 resonances up to 187 eV. Fig. 1 shows a typical time-of-flight spectrum. In Fig. 2 we show the ratios used to determine the spins. The Porter-Thomas fluctuations are negligible compared to the experimental errors on the points. Table I shows our results. There are no disagreements with the results of Wetzel and Thomas. However our preliminary results from the other experiments indicate that at 43.5 eV our final determination will be a spin of 1 with confidence limits of about 90 percent. Wetzel and Thomas report a spin of 2 with doubt brackets for this resonance.

Our calculation enables us to obtain probabilities of correctness for the spin assignments, best fits to the Porter-Thomas fluctuations and the average ratio of the intensity of the 360 keV line to that of the 187 keV line for each spin. An extension of this calculation also gives best fits to the relative density of levels for each spin and the uncertainty in this number. We can also compute, on the basis of our data, the probability that some new unmeasured s-wave resonance will have one spin or the other. This probability is given by

$$P_J = \sum_{i=1}^{M} P_{i,J} / M$$

---

[1] K. V. Wetzel and G. E. Thomas, Phys. Rev. C1, 1501 (1970)
[2] C. Coceva, F. Corri, P. Giacobbe and G. Cavvaro, Nucl. Phys. A117, 586 (1968)
[3] A. Stolovy, A. I. Namenson, J. C. Ritter, T. F. Godlove and G. Smith, To appear in Phys. Rev. 1972

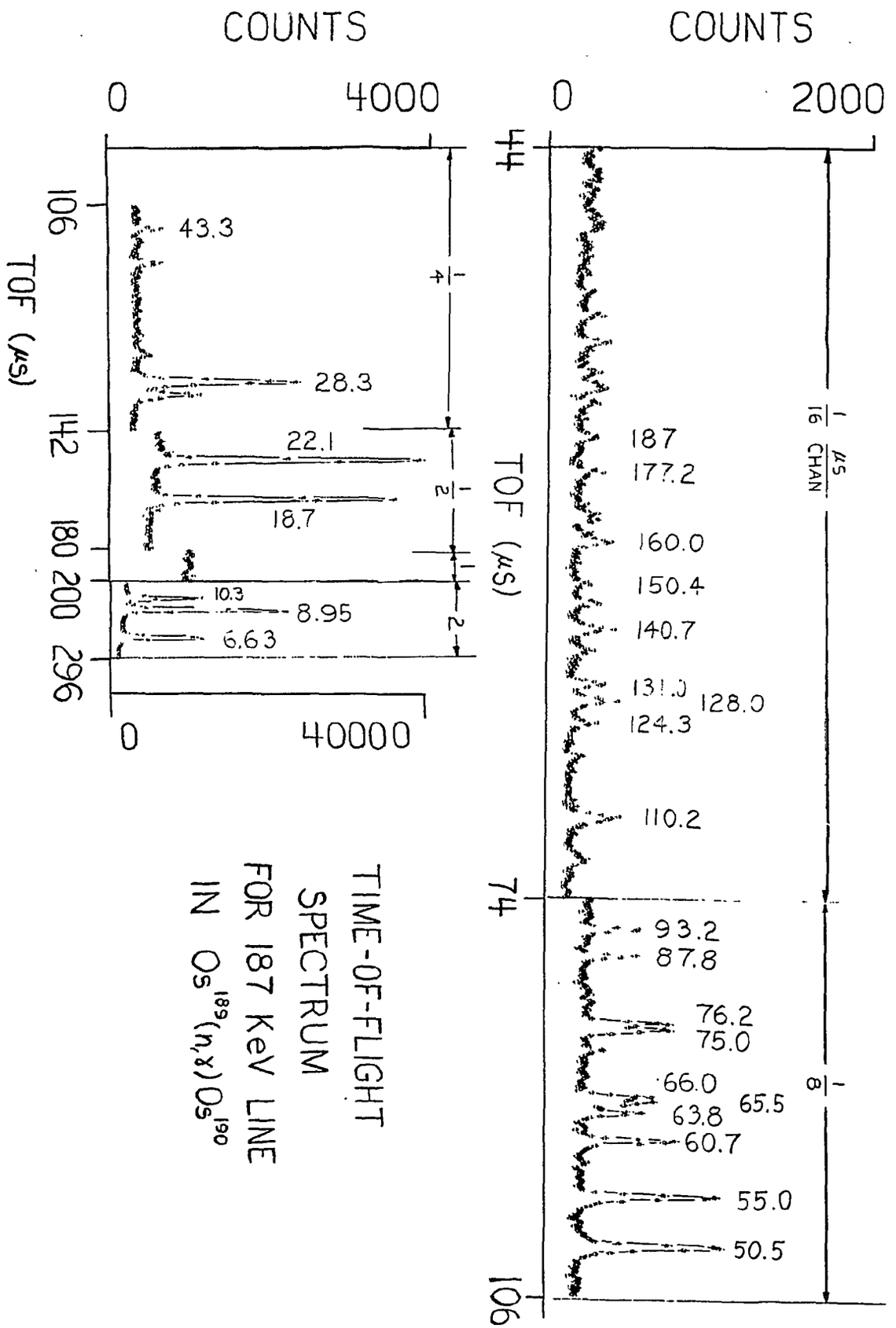

TIME-OF-FLIGHT SPECTRUM FOR 187 KeV LINE IN $Os^{189}(n,\gamma)Os^{190}$

Figure A1

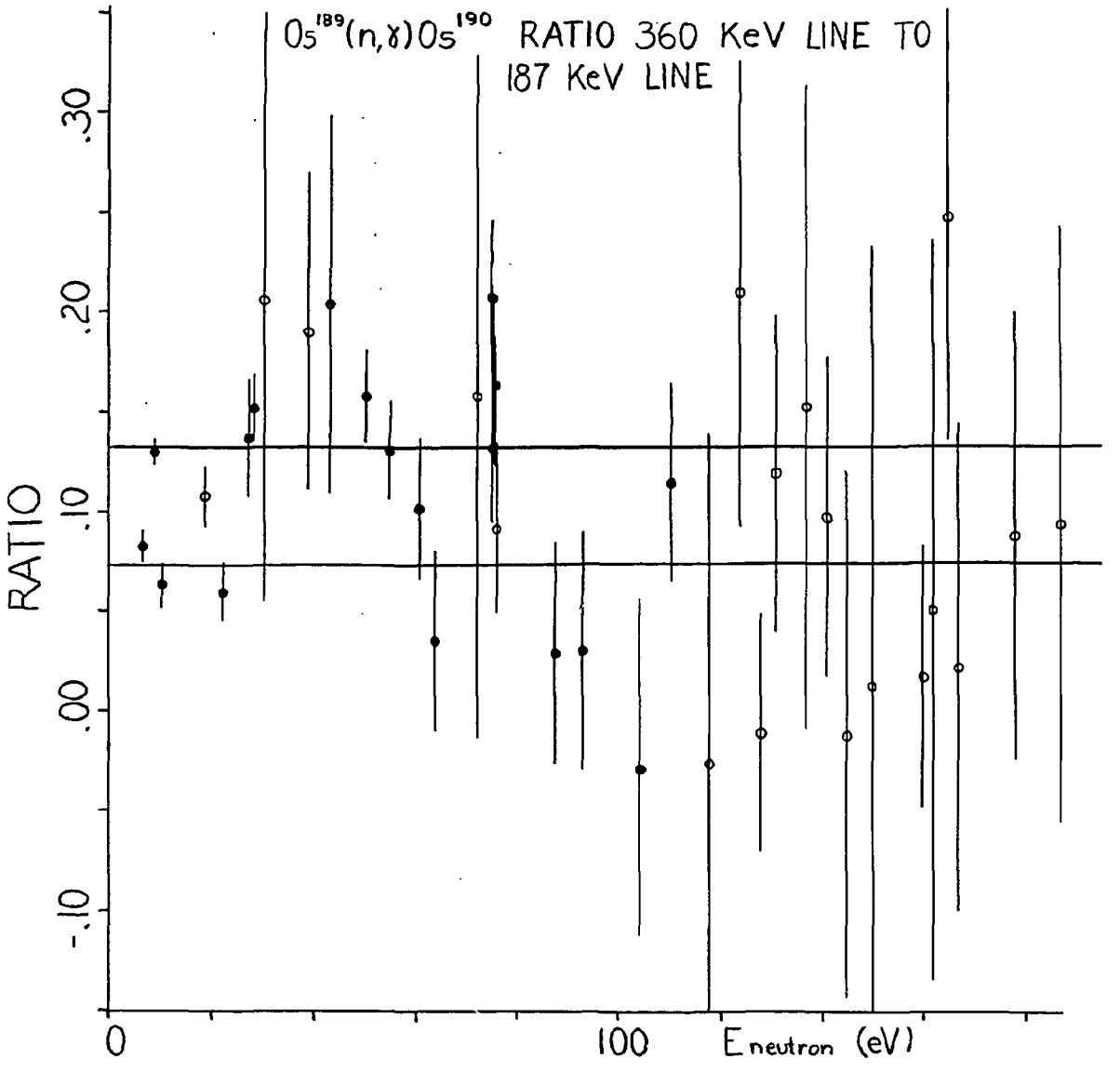
$Os^{189}(n,\gamma)Os^{190}$ RATIO 360 KeV LINE TO 187 KeV LINE
RATIO
.30
.20
.10
.00
-.10
0
100
E neutron (eV)

Figure A-2

TABLE A-1

Spins of Resonances in Os^{189}

E_o (eV)	J	Prob (%)	E_o (eV)	J	Prob (%)
6.63	1	100	87.8	(1)	76
8.95	2	100	93.1	(1)	72
10.3	1	100	104.3	(1)	70
18.7	2	81	109.0	((2))	56
22.1	1	100	110.3	((2))	63
27.4	2	93	118.0	((1))	51
28.3	2	100	124	((2))	67
30.5	((2))	62	128	(1)	83
39.1	(2)	74	131	((2))	60
43.3	(2)	71	137	((2))	59
50.3	2	99.8	141	((2))	55
54.9	2	95	145	((1))	54
60.7	((2))	55	110	((2))	53
63.9	(1)	84	160	(1)	71
65.4	(2)	81	162	((2))	54
66.0	2	92	165	(2)	71
72.2	((2))	58	167	((1))	52
75.3	2	98	178	((2))	54
76.2	((1))	53	187	((2))	55

where p_J is the probability that an unknown resonance will have spin J, $P_{i,J}$ is the probability that the i'th measured resonance has spin J, and M is the number of observed resonances. The uncertainty in p_J is

$$\sigma_p = p_{I+\frac{1}{2}}\, p_{I-\frac{1}{2}} \Big/ \sqrt{\left(P_{i,\, I+\frac{1}{2}} - p_{I+\frac{1}{2}}\right)^2}$$

For the ratio of the density of levels in the two spin groups we have

$$r = p_{I+\frac{1}{2}} \Big/ p_{I-\frac{1}{2}}$$

with an uncertainty of

$$\sigma_r = r \Big/ \sqrt{\left(P_{i,\, I+\frac{1}{2}} - p_{I+\frac{1}{2}}\right)^2}$$

where I is the spin of the target nucleus.

From our experiment we have $p_{J=2} = .563 \pm .141$ and we have $p_{J=1} = .437 \pm .141$. For the relative densities of the two spin groups we have $r = 1.29 \pm .74$ which is consistent with the value of 1.67 which one would expect from a 2J+1 law. (Preliminary data on our other experiments indicated that agreement with the 2J+1 law might not be so good once we have analyzed all the data.)

The average ratio of the intensity of the 360 keV line to that of the 187 keV line is $80 \pm 14\%$ higher for spin 2 resonances than for spin 1 resonances. This is in agreement with the data of Wetzel and Thomas which gives 74% and with our Monte Carlo calculation which gives $80 \pm 15\%$.

2. Monte Carlo Simulation of Gamma Cascades (A. I. Namenson)

A Monte Carlo simulation of the gamma decay of neutron resonances was performed in order to evaluate the spin measurements described in part 1. This calculation is similar to an earlier one[4] but it includes estimates for the spin effect in the low-energy γ-ray technique. Using Weisskopf estimates for the gamma rays, we obtained remarkable agreement with experimental results for neutron capture by Nd^{143}, Nd^{145} and Os^{189}. Using various other estimates for the gamma intensities (such as extrapolations from the tail of the giant resonance) does not significantly affect the calculation for the coincidence experiments[2] but does have a strong effect on the predicted relative population of low lying levels. On the particular nuclei for which we have both experimental and calculated results, the Weisskopf estimates give the best answers.

[4] A.I. Namenson, Bull. Am. Phys. Soc. 16, 15 (1971)

OAK RIDGE NATIONAL LABORATORY

A. NEUTRON PHYSICS

1. Total Cross Sections

a. R-Matrix Analysis with a Diffuse-Edge Potential for ^{16}O + n Data*,**

(C. H. Johnson, J. L. Fowler, and R. M. Feezel†)

An R-matrix analysis of the $^{16}O(n,n)$ and $^{16}O(n,\alpha)$ cross sections below 5.8 MeV shows that the off-resonance cross sections are described by scattering in a potential, that the boundary radius must be inside the tail of this potential, that the total spectroscopic factors for five observed $d_{3/2}$ fragments is unity, and that the spectroscopic factors for other partial waves are about as expected from the shell model. Table I tabulates the parameters which have been determined from the analysis of the measurements which are shown in Figure (A.1.a).

Table I. Parameters for the $3/2^+$ States

E_λ (keV)	E_{res}(lab) (keV)	E_{ex} (keV)	γ^2 (keV)	$\gamma^2/(\hbar^2/\mu r^2)$ (%)
709	1000	5083	2035	69.0
1838	1833	5867	28	1.0
3536	3248	7198	500	16.9
4311	4167	8062	252	8.5
5156	5054	8897	123	4.2
			Total	99.6

*To be presented at Conference on Nuclear Structure Study with Neutrons, Budapest, Hungary, July 31 - August 5, 1972.

†Undergraduate student from Auburn University.

**Relevant to Request NCSAC-35 No. 43.

b. A Definitive Measurement of the J-Value for the 5696-keV Level in ^{17}O*,**

(L. Galloway†, J. L. Fowler, J. A. Harvey, and C. H. Johnson)

Using time-of-flight techniques with a 5 nsec burst from the Oak Ridge Electron Linear Accelerator, ORELA, and with a 200 meter flight path we have observed the narrow 1651-keV resonance in total cross section for neutrons on ^{16}O. We find $E_r = 1651 \pm 1$ keV. Lane et al.[1] found from differential scattering measurements that this is an f-wave resonance and they assigned $J^\pi = 7/2^-$ rather than $5/2^-$. A definitive selection of the J-value on the basis of a high resolution measurement of the total cross section has not been made previously. Now we have observed a peak

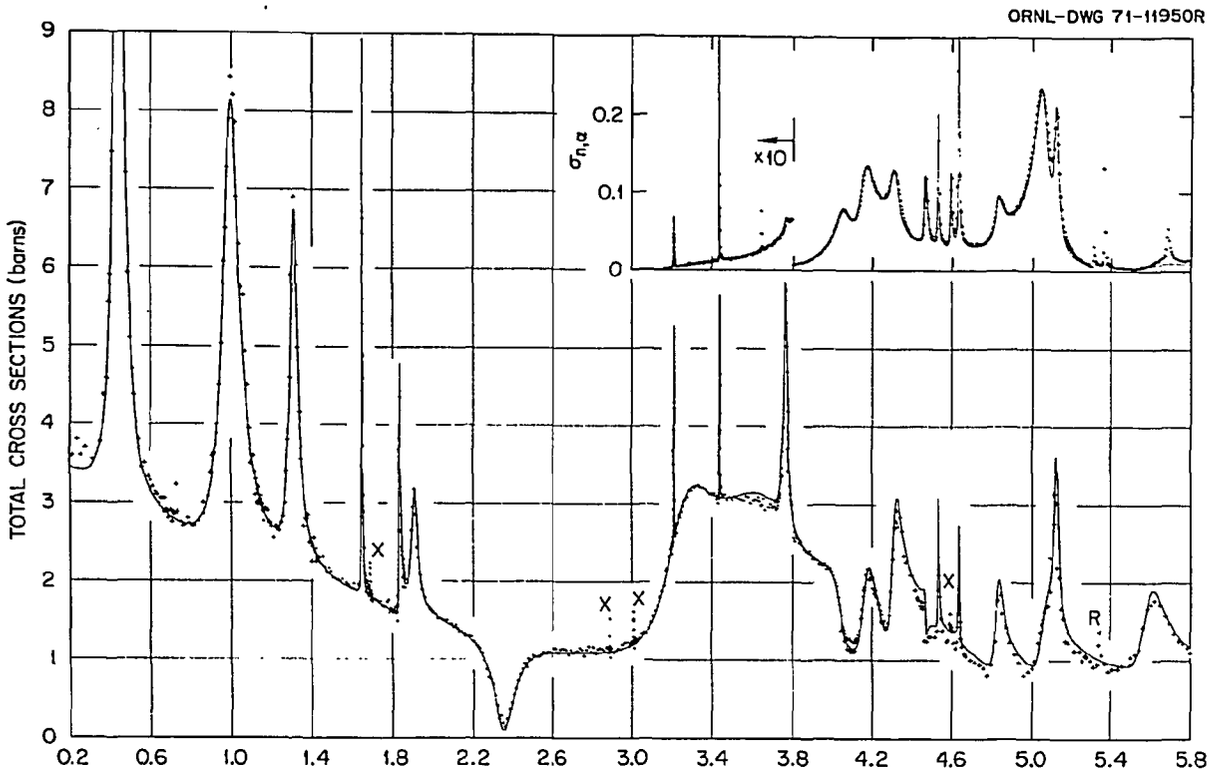

Figure (A.1.a) Total Neutron Cross-Section of O^{16} as a Function of Neutron Energy

cross section 0.5 barn above the maximum allowed for $J = 5/2$. Thus J^{π} must be $7/2^-$ rather than $5/2^-$. The width, corrected for the 2.4 keV resolution, is $\Gamma = 3.7$ keV and corresponds to about 10% of the single-particle strength. The ^{16}O total cross section was measured from 0.6 to 4 MeV and will be discussed.

---

*To be presented at Washington, D.C., APS Meeting, April 24-27, 1972.
†Present address: Centenary College.
[1]R. O. Lane, A. S. Langsdorf, J. E. Monahan and A. J. Elwyn, Ann. Phys. 12, 135 (1961).
***Relevant to Request NCSAC-35 No. 43.

2. Radiative Capture Cross Sections and Spectra

a. Cross Section Measurements of $^{92}Mo + n^*$,*** (O. A. Wasson**, B. J. Allen†, R. R. Winters‡, R. L. Macklin, and J. A. Harvey)

Resonance parameters for the interaction of neutrons with ^{92}Mo were deduced from a combination of total capture and transmission experiments performed at the Oak Ridge Electron Linear Accelerator with a 5 nsec pulse width. The capture measurements used the total energy detector[1] at the 40 m flight station while the transmission experiments utilized the 80 m flight path. The measurements, which extended to 1 MeV neutron energy, resolved resonances up to 100 keV. Comparisons with previous experiments will be given. The implications of these results for the radiative neutron capture reaction mechanism will also be presented.

---

*To be presented at Washington, D.C., APS Meeting, April 24-27, 1972.
**Guest assignee from Brookhaven National Laboratory.
†Present address: Australian Atomic Energy Commission, Lucas Heights.
‡Guest assignee from Denison University.
[1]R. L. Macklin and B. J. Allen, Nucl. Instr. and Meth. 91, 565 (1971).
***Relevant to Request NCSAC-35 No. 222.

b. Neutron Capture Cross Section Measurements in $^{111}Cd(n,\gamma)^{112}Cd^*$ (O. A. Wasson†, B. J. Allen‡, and R. L. Macklin)

The resonant capture areas of an enriched ^{111}Cd sample were measured for 270 eV $< E_n <$ 10 keV using the total energy γ-ray detector at the 40 m flight path at ORELA. Capture yields were measured in the γ ray energy interval from 7.3 MeV to the neutron binding energy at 9.3 MeV as well as below 7.3 MeV in order to determine resonance spins and parities. Since the states in the product nucleus ^{112}Cd below 2 MeV which are populated by the highest energy γ ray group are positive parity and since the average E1 γ ray width is ~ 5 x the M1 width, the relative strength of the high energy γ ray group depends on the spins and parities of the resonances. These results as well as the resonance parameters are presented.

---

*Presented at San Francisco APS Meeting, January 31, 1972 - February 3, 1972.

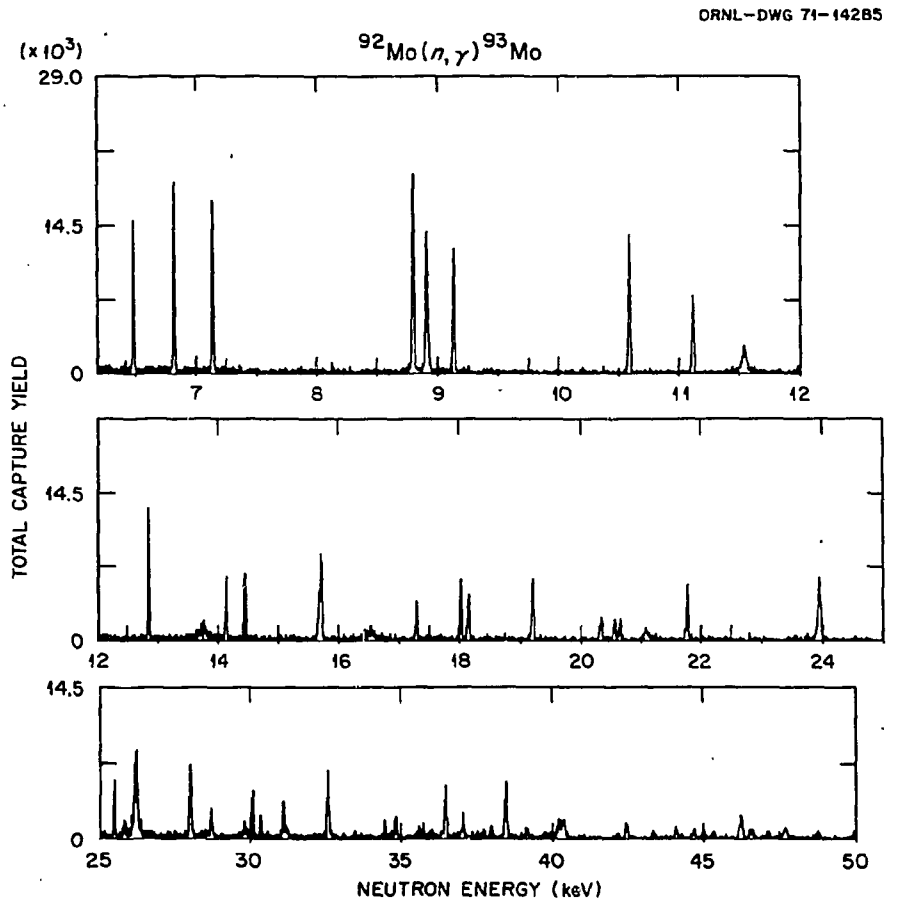

Figure (A.2.a) Gamma Ray Yield from Neutron Radiative Capture by ^{92}Mo as a Function of Neutron Energy

†Guest assignee from Brookhaven National Laboratory.
‡Present address: Australian Atomic Energy Commission, Lucas Heights.

c. Neutron Capture Cross Sections of the Lead Isotopes*,**
(B. J. Allen†, R. L. Macklin, C. Y. Fu, and R. R. Winters‡)

The neutron capture cross sections of ^{204}Pb, ^{206}Pb, ^{207}Pb, ^{208}Pb have been measured from 3 keV to over 500 keV with total energy detectors at ORELA. Measurements were made at 40 meters with 5 ns pulses on < 0.5 mole samples of separated isotopes. Detector efficiency was determined by the saturated resonance method using the 4.9 eV resonance in gold. The neutron flux was measured via the $^{6}Li(n,\alpha)$ reaction in a 0.5 mm thick glass, with appropriate corrections being made for scattering in the glass. Capture areas and resonance parameters are obtained for all resolved resonances. Maxwellian averaged capture cross sections are calculated as a function of energy. The correlation between these averaged cross sections and the solar system isotopic abundances are discussed in terms of stellar nucleosynthesis by slow neutron capture. See Figure A.2.c.

---

*Presented at San Francisco APS Meeting, January 31 - February 3, 1972.
†Present address: Australian Atomic Energy Commission, Lucas Heights.
‡Guest assignee from Denison University.
**Relevant to Request NCSAC-35 Nos. 342, 343.

d. A Test of the Valency Model of Neutron Capture in $^{92}Mo(n,\gamma)$ ^{93}Mo*,**
(G. G. Slaughter, O. A. Wasson†, R. E. Chrien‡, S. F. Mughabghab‡, and G. Cole‡)

As a continuing test of the single particle model of radiative neutron capture near the 3P peak in the neutron strength function, the γ ray spectra from neutron capture in an enirhced ^{92}Mo sample were measured with a Ge(Li) detector at the 10 m flight path at ORELA. Captures were recorded for neutron energies from 10 eV to 100 keV. From a total of 17 resonances which were resolved for $E_n < 16$ keV, about half are assigned to P 3/2 capture on the basis of the γ ray spectra. The nature of the capture apparently changes above 25 keV since the transition to the d 5/2 ground state is dominant in the neutron energy region (25 keV < E_n < 100 keV) while the transition to the S 1/2 first excited state dominates the decays of the resonances below 25 keV. A detailed comparison of the data with the predictions of the single particle model of radiative neutron capture will be presented.

---

*Presented at San Francisco APS Meeting, January 31 - February 3, 1972.
†Guest assignee from Brookhaven National Laboratory.
‡Brookhaven National Laboratory.
**Relevant to Request NCSAC-35 No. 223.

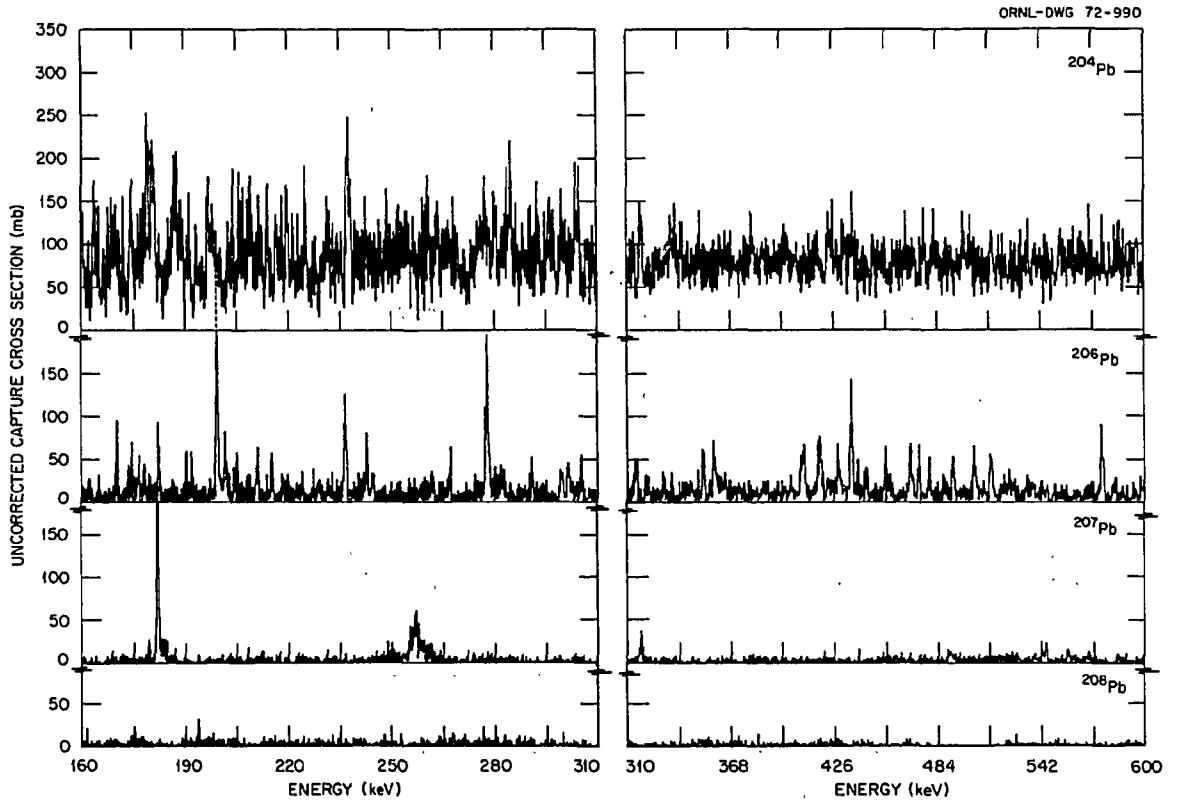

Figure (A.2.c-1) Neutron Radiative Capture Cross Sections of Isotopes of Lead as a Function of Neutron Energy

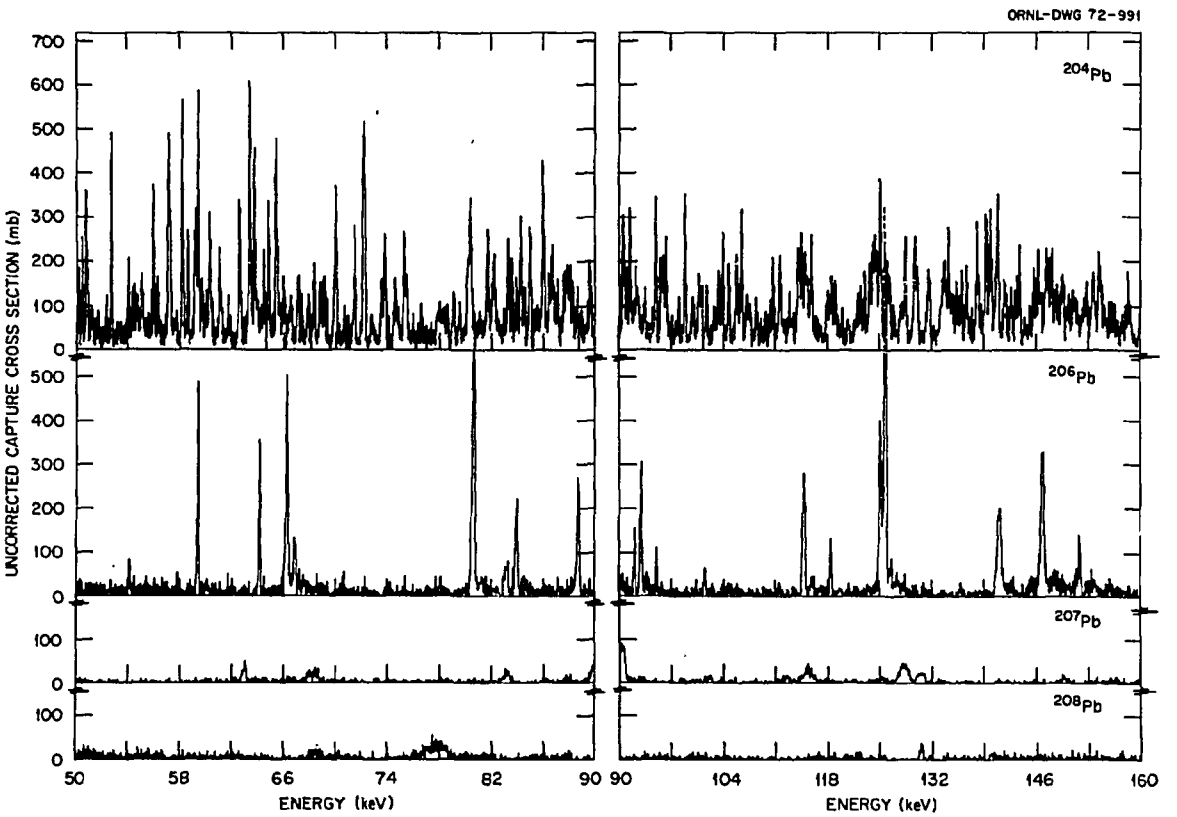

Figure (A.2.c-2) Neutron Radiative Capture Cross Sections of Isotopes of Lead as a Function of Neutron Energy

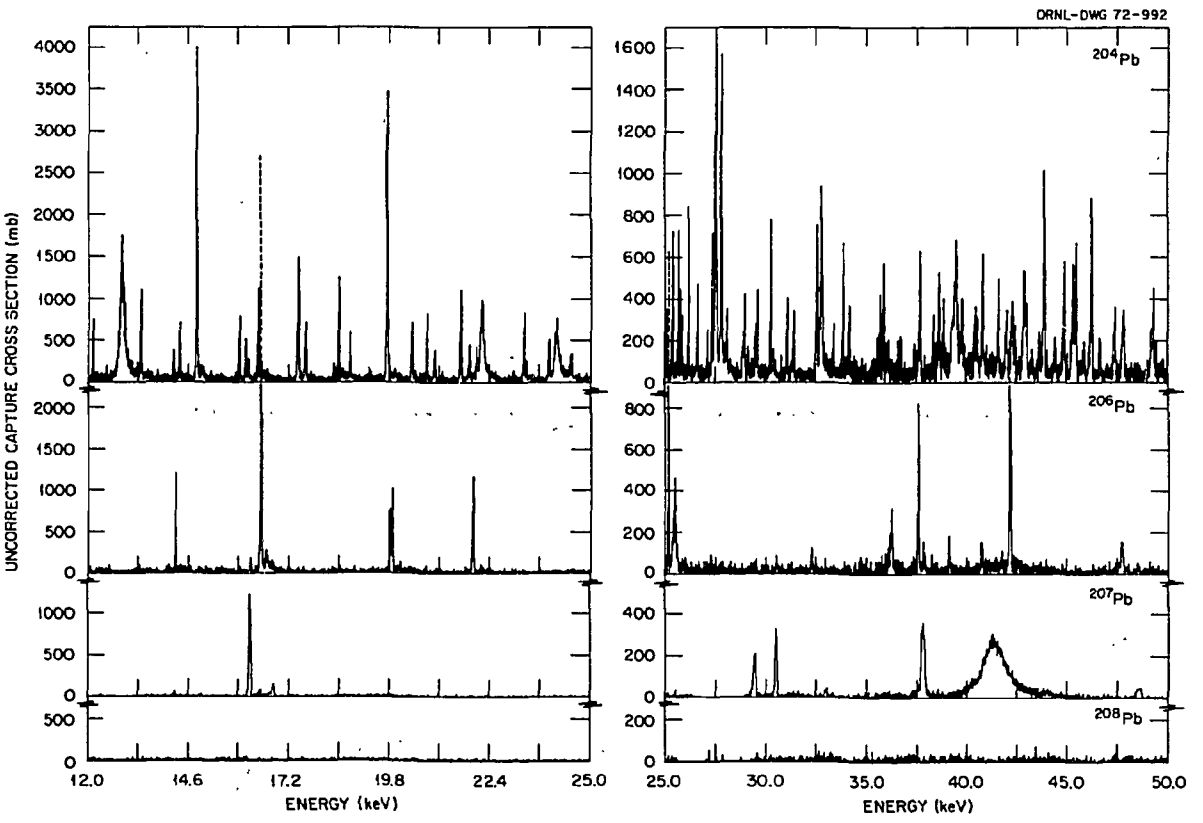

Figure (A.2.c-3) Neutron Radiative Capture Cross Sections of Isotopes of Lead as a Function of Neutron Energy

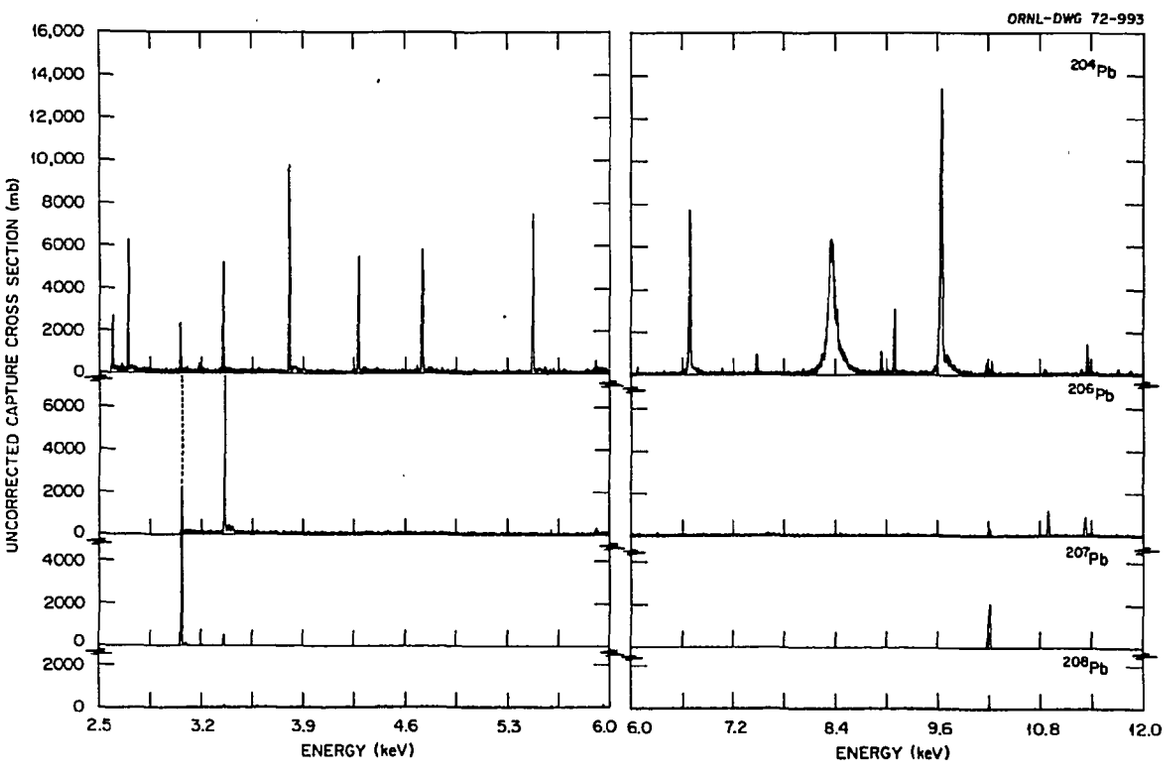

Figure (A.2.c-4) Neutron Radiative Capture Cross Sections of Isotopes of Lead as a Function of Neutron Energy

e. Spin Assignments of Neutron Resonances of Zr^{91}*,**
(S. F. Mughabghab†, G. W. Cole†, R. E. Chrien†, M. R. Bhat†, O. A. Wasson‡, and G. G. Slaughter)

The method of assigning spins of s-wave and p-wave neutron resonances with the aid of low energy γ rays proved to be a powerful tool.[1] This technique, when applied in combination with primary γ rays, gives unambiguous spin assignments. As a byproduct of the investigations reported above in a separate abstract, we have studied with a 50 cc Ge-Li detector the low energy and high energy γ rays due to neutron capture in Zr^{91} resonances. By considering the γ-ray intensity ratios of the 558 keV ($4^+ \rightarrow 2^+$) and 934 keV ($2^+ \rightarrow 0^+$) transitions we are able to make the following spin assignments: J=3 for the resonances at 182, 681, and 890 eV and J=2 for the 240, 293, 445, and 1540 eV resonances. In addition the present data indicate that the 240, 445, and 890 resonances are formed by p-wave interaction of neutrons with Zr^{91}.

---

*Presented at San Francisco APS Meeting, January 31 - February 3, 1972.
†Brookhaven National Laboratory.
‡Guest assignee from Brookhaven National Laboratory.
[1]S. F. Mughabghab, O. A. Wasson, G. W. Cole, and R. E. Chrien, Proceedings of 3rd Neutron Cross Sections and Technology, p. 804, March 1971.
**Relevant to Request NCSAC-35 Nos. 180, 181.

f. $Dy^{163}(n,\gamma)Dy^{164}$ Reaction Revisited*
(G. G. Slaughter, O. A. Wasson†, S. F. Mughabghab‡, R. E. Chrien‡, G. W. Cole‡, and M. R. Bhat‡)

In an effort to study the nonstatistical aspects of the reaction mechanism in neutron capture[1] in Dy^{163} at higher neutron energies, measurements of γ ray spectra were carried out with a 30 cc Ge-Li detector at the ORELA facility. The spin of neutron resonances are determined by examining the ratio of intensities of γ rays at energies of 168.8 and 215.1 keV. The resonances at energies of 35.7, 58.8, 75.2, 78.7, 106.7, 143, 146, 189, 204 are found to have spin 2 while those at 16.2, 19.6, 50.0, 55.7, 66.0, 71.3, 85.9, 93.9, 105.9, 120, 127, 135, 163.3, 177, 185, 207, 215, 225, 235 and 253 have spin 3. The implications of these results for the search for a correlation between partial radiative widths and reduced neutron widths will be discussed.

---

*To be presented at Washington, D.C., APS Meeting, April 24-27, 1972.
†Guest assignee from Brookhaven National Laboratory.
‡Brookhaven National Laboratory.
[1]S. F. Mughabghab, R. E. Chrien, and O. A. Wasson, Phys. Rev. Letters 25, 1670 (1970).

g. The Valence Neutron Model in the 3p Giant Resonance*
(S. F. Mughabghab†, G. W. Cole†, R. E. Chrien†, M. R. Bhat†, O. A. Wasson‡, and G. G. Slaughter)

The valence neutron model[1] was remarkable in accounting for the magnitude of the $Mo^{92,98}$ partial radiative widths of strong p-wave resonances. This model would be expected to be valid in the 3p giant resonance and in particular for the 302 eV resonance of Zr^{96}. The angular distribution of γ rays due to neutron capture in this resonance was studied at the BNL fast chopper facility of HFBR and measurements of absolute intensities were made at ORELA. The present angular distribution measurements supported by thermal absorption cross section and absorption resonance integral data indicate that this resonance is $p_{1/2}$. The absolute intensities of γ rays ($\Gamma_{\gamma ij}$) populating the g.s. ($s_{1/2}$) and first excited state ($d_{3/2}$) of Zr^{97} are 860 (219 meV) and 140(36 meV) photons/1000n. With $\gamma_{sp}^2 = 3\hbar^2/2ma^2$, the model predicts 219 and 73 meV for the $p_{1/2} \rightarrow s_{1/2}$ and $p_{1/2} \rightarrow d_{3/2}$ transitions respectively. This is another example where transitions of the type p → s retain their strength while p → d lose it to the G.D.R.

---

*Presented at San Francisco APS Meeting, January 31 - February 3, 1972.
†Brookhaven National Laboratory.
‡Guest assignee from Brookhaven National Laboratory.
[1]S. F. Mughabghab et al., Phys. Rev. Letters 26, 1118 (1971).

3. Elastic and Inelastic Scattering Cross Sections

a. Neutron Elastic- and Inelastic-Scattering Cross Sections for Oxygen in the Energy Range 4.34 to 8.56 MeV*,**
(W. E. Kinney and F. G. Perey)

We have measured neutron elastic- and inelastic-scattering cross sections for oxygen in roughly 0.5 MeV intervals between 4.34 and 8.56 MeV. The data were obtained with conventional time-of-flight techniques utilizing pulsed (2MHz), bunched (~ 1 nsec full width at half maximum, FWHM) deuterons accelerated by the ORNL Van de Graaff and interactions with deuterium in a gas cell to produce neutrons by the $D(d,n)^3He$ reaction. Our data are presented graphically, Figure A.3.a, in company, for comparison purposes, with the results of others and with ENDF/B-1013 and 4134.

---

*Relevant to Request No. 43.
**Extracted from ORNL-TM-4780.

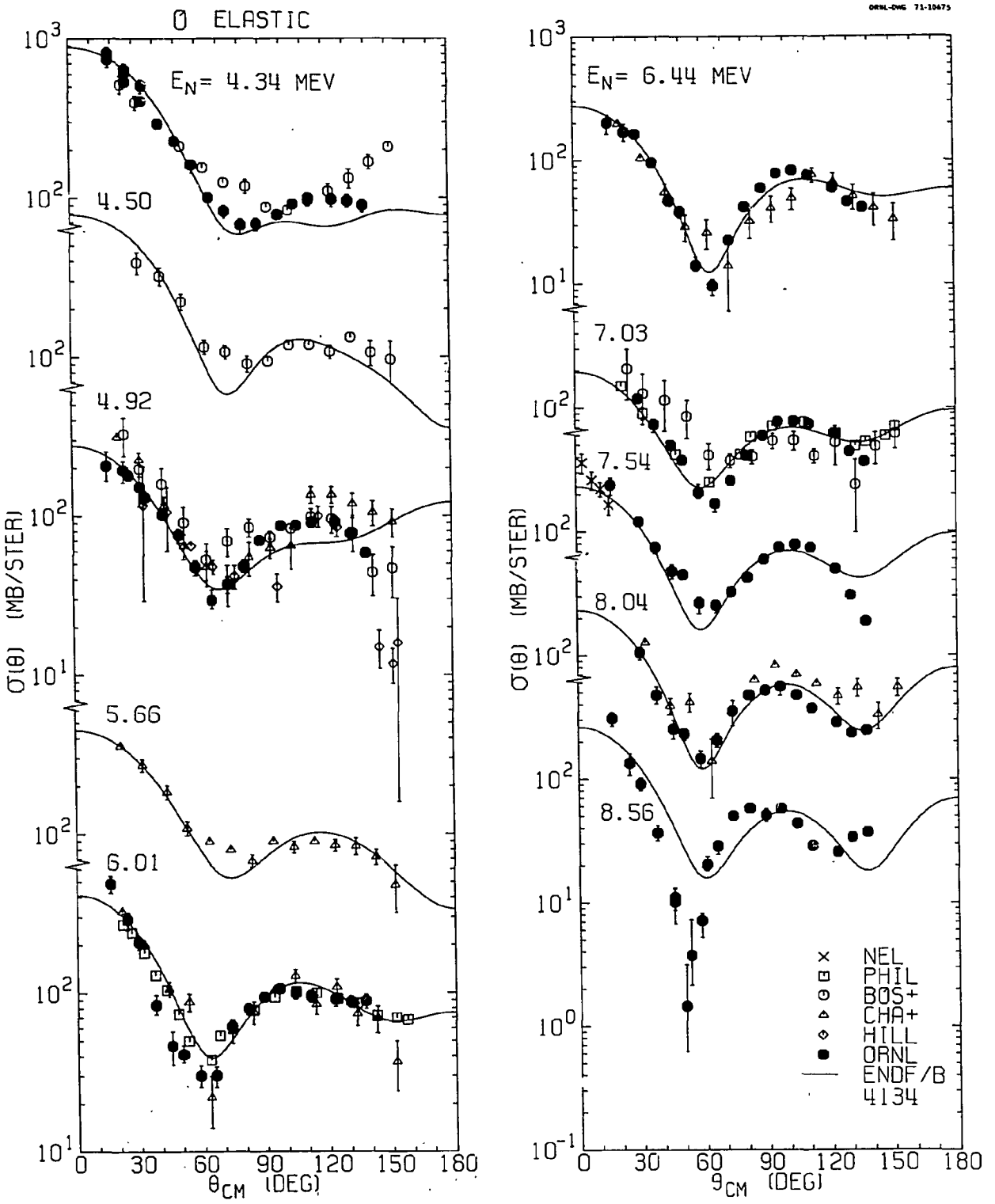

Figure (A.3.a) Experimental Neutron Differential Elastic Scattering Cross Sections from O

4. Neutron Reaction and Gamma Ray Production Cross Sections

a. Gamma-Ray-Production Cross Sections of Tantalum and Carbon for Incident Neutron Energies Between 0.007 and 20.0 MeV*,** (G. L. Morgan, T. A. Love, J. K. Dickens, and F. G. Perey)

Cross sections for neutron induced gamma radiation from tantalum have been measured as a function of both neutron and gamma-ray energy. Neutron energies ranged from 0.007 to 20.0 MeV while gamma-ray energies from 1.0 to 10.5 MeV were measured. Data were taken at angles of 90° and 125° with respect to the incident neutrons. Similar measurements were made for natural carbon and these results demonstrate the efficacy of the data acquisition and reduction systems.

*Relevant to Request NCSAC-35 Nos. 35, 322.
**ORNL-TM-3702.

b. The $^{23}Na(n,x\gamma)$ Reaction for $4.85 \leq E_n \leq 7.5$ MeV*,** (J. K. Dickens)

Interactions of neutrons with sodium have been studied by measuring gamma-ray-production cross sections. Spectra were obtained for incident mean neutron energies E_n = 4.85, 5.4, 5.9, 6.45, 7.0 and 7.5 MeV. Data were obtained at angles of 125° and 55° using Ge(Li) detectors. Time-of-flight was used to discriminate against pulses due to neutrons and background radiation. Absolute cross sections for production of gamma rays were obtained for the incident neutron energies quoted above. The data have been compared with previous inelastic neutron scattering results and with evaluated cross sections with good agreement. The spectra were studied for gamma rays which could be associated with deexcitation of nuclear levels having unknown decay modes. Gamma rays were found having energies appropriate for decay of levels at excitation energies E_x = 5762, 5934, 5967, 6115, 6576 and 6866 keV.

*Relevant to Request No. 57.
**ORNL-TM-3737.

c. Level Structure of ^{54}Mn*,** (J. K. Dickens)

Properties of levels in ^{54}Mn have been studied using the $^{54}Fe(\underline{n},p\gamma)$ ^{54}Mn reaction. These data alone were not sufficient to determine spin and parity assignments, but when correlated with data from prior experimental investigations of the ^{54}Mn nucleus, a set of unique J^π assignments for the lowest five excited states was determined. These assignments are consistent with nearly all presently available experimental data and are in good agreement with shell-model calculations. The level excitation energies and J^π values obtained are: ground-state, 3^+; 54.3 keV, 2^+; 156.9 keV, 4^+;

367.6 keV, 5^+; 407.5 keV, 3^+; and 839.0 keV, 4^+. Transitions from higher lying states were observed and possible J^π values were obtained.

---

*Relevant to Request Nos. 95, 96.
**ORNL-TM-3674.

5. Fission

a. Simultaneous Measurements of the Neutron Fission and Capture Cross Sections for ^{235}U for Neutron Energies from 8 eV to 10 keV*,**
(R. B. Perez, G. de Saussure, E. G. Silver, R. W. Ingle, and H. Weaver)

Simultaneous measurements of the neutron fission and capture cross sections of ^{235}U have been performed at the Oak Ridge Electron Linear Accelerator (ORELA) for neutrons with energies between 8 eV and 10 keV. These cross sections were measured relative to the standard $^{10}B(n,\alpha)$ reaction cross section. The comparison of the present ^{235}U capture cross section with the other available sources shows that below 200 eV there is a general agreement within an error band of ± 5%. In the keV energy region, the average difference observed rises to ± 12%. The fission cross section results presented here agree with a world-wide compilation of fission data typically within a 3% error in the entire range of neutron energies investigated in this work. The values of alpha, capture-to-fission ratio, exhibit a remarkable amount of structure superimposed on the featureless behavior predicted by Bohr's fission channel theory. Results are shown in Figure A.5.a-1 and Figure A.5.a-2.

*ORNL-TM-3696.
**Relevant to Request NCSAC-35 No. 388, 390, 391, 393.

b. Multilevel Analyses of the ^{235}U Fission and Capture Cross Sections*
(G. de Saussure, R. B. Perez, and W. Kolar†)

The neutron capture and fission cross sections of ^{235}U were analyzed up to 60 eV with the multilevel formalism of Reich and Moore. The statistical distribution of the R-matrix parameters obtained in this analysis has been investigated in detail. After corrections for the "missed levels", the observed statistical distributions of the parameters and level spacings agree well with the expected Porter-Thomas distributions and Wigner law, respectively. The average values of the resonance parameters do not agree for the same cross sections with the values obtained by other authors on the basis of the single-level formalism. The set of resonance parameters obtained in this work has been used to compute the fission cross section at liquid nitrogen temperature, for comparison with existing measurements, and to "mock-up" the cross sections

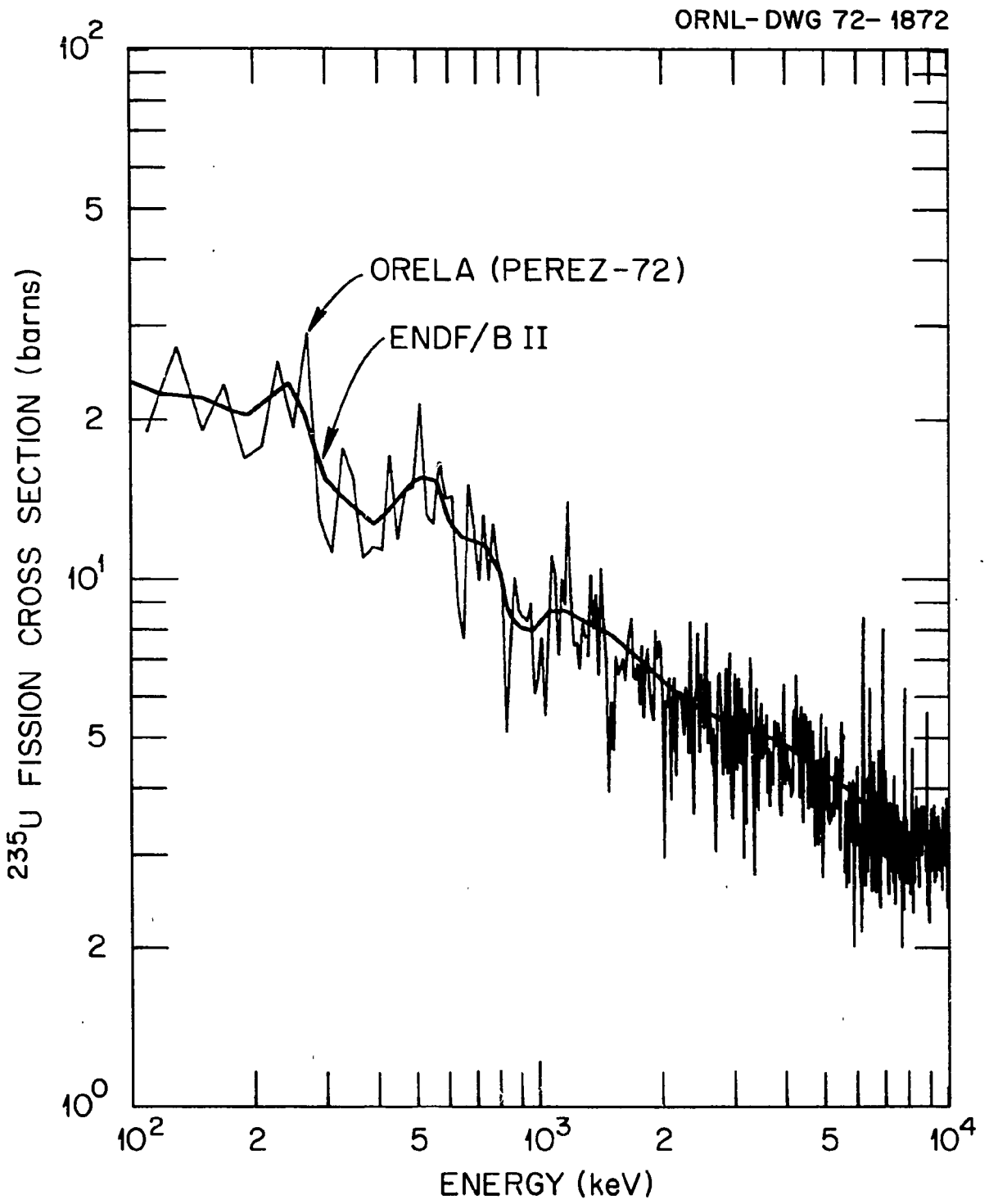

Figure (A.5.a-1) Comparison of the ORELA ^{235}U Fission Cross Section with the ENDF/B-II Evaluation

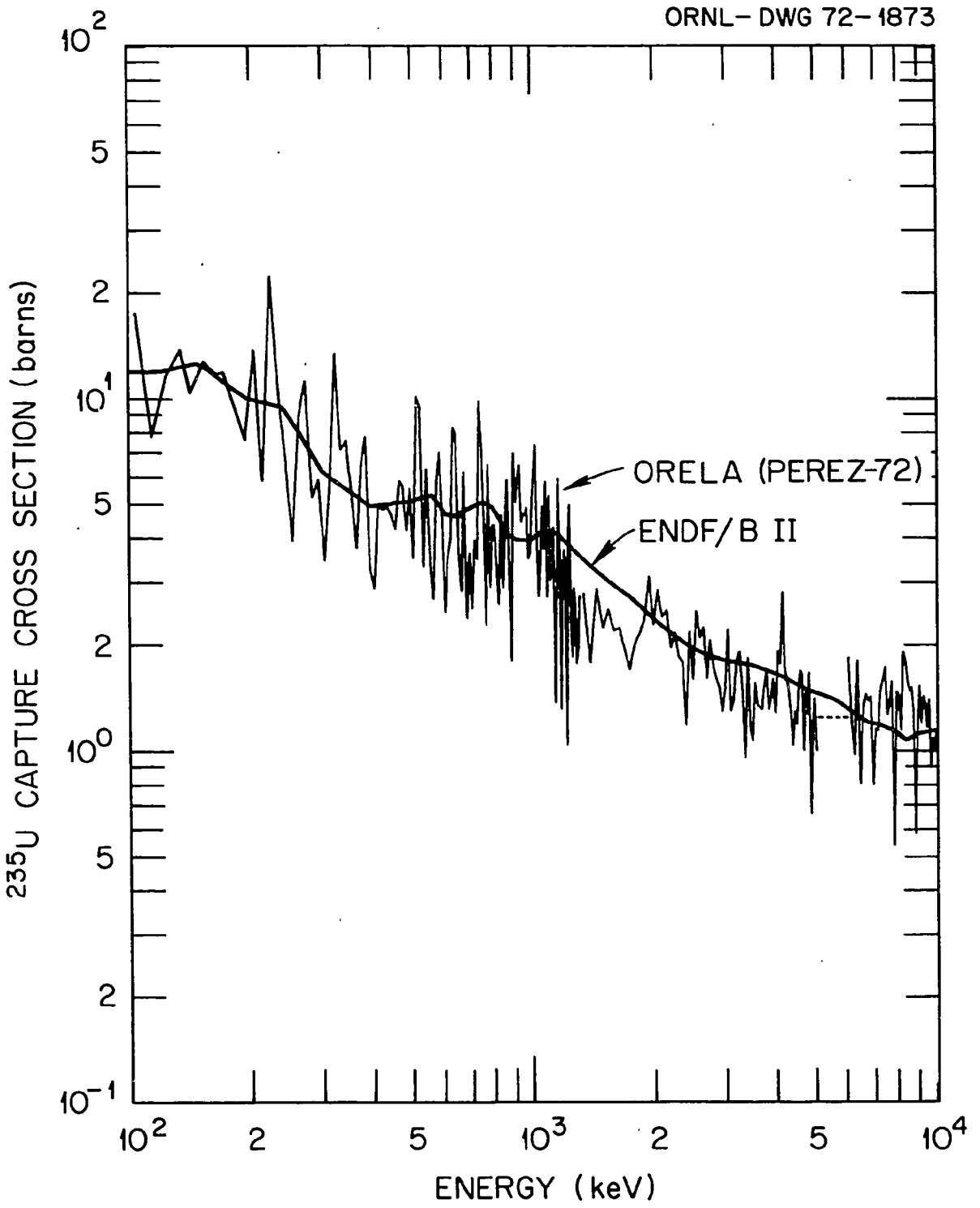

Figure (A.5.a-2) Comparison of the ORELA ^{235}U Capture Cross Section with the ENDF/B-II Evaluation

in the unresolved resonance region near 1 keV, where S-wave processes still dominate. See Figure A.5.b-1 and Figure A.5.b-2.

---

*ORNL-TM-3707.
†Central Bureau for Nuclear Measurements, Euratom, Geel, Belgium.

c. High Resolution Cross Section Measurement for $^{236}U(n,f)$*,** (Helmut Rosler, Franz Plasil, and H. W. Schmitt)

The cross section for neutron-induced fission of ^{236}U has been measured with high resolution in the neutron energy range $0.5 \lesssim E_n \lesssim 8$ MeV. This study was carried out with several objectives in view: (1) to investigate the widths of the known peak at 1.4 MeV and the apparent structure at ~ 1.0 MeV[1], (2) to search for other, similar structure peaks in the neighborhood of the fission threshold, which might be interpretable as collective levels in the second well of the double barrier for fission[2], (3) to determine whether Class II levels as described by Lynn[3] which were apparently observed in $^{239}Pu(d,pf)$[4], are observable in $^{236}U(n,f)$, and (4) to extend the energy range of cross section data for $^{236}U(n,f)$. In this paper we present the experimental results in the vicinity of the fission threshold ($E_n \leq 2.6$ MeV) and point out some of the features observed. Results at higher energies, and interpretation of the data will be published later. The experiment was carried out with the Oak Ridge Electron Linear Accelerator (ORELA) used as a pulsed neutron source. The neutron flux was monitored independently with an ionization chamber similar to the ^{236}U chamber but containing ^{235}U, and also by a 5/8" diam, 1/4" high Naton 136 plastic scintillator. The results as determined from the two monitors are shown in Figure A.5.c. Our results thus far confirm the existence of structure in the ^{236}U cross section superimposed on a smooth barrier-penetrability function. In addition to the structure previously observed[1] at 0.95 and 1.4 MeV, we find maxima at 0.75 and 1.15 MeV. The peak at 1.4 MeV appears to be at least a doublet (peaks at approximately 13. and 1.4 MeV). Further data for $^{236}U(n,f)$, together with analysis and interpretation, will be published in a more complete paper later.

---

*Extracted from Physics Letters (January 4, 1972).
**Presented at San Francisco APS Meeting, January 31 - February 3, 1972.
[1]R. W. Lamphere, Phys. and Chem. of Fission (Proc. Symp. Salzburg, 1965), Vol. I, IAEA, Vienna (1965), p. 63.
[2]See, e.g., V. M. Strutinsky, H. C. Pauli, Proc. Second Symp. on the Physics and Chem. of Fission, IAEA, Vienna (1969), p. 155.
[3]J. E. Lynn, Proc. Second Symp. on the Physics and Chemistry of Fission, IAEA, Vienna (1969), p. 249.
[4]H. J. Specht, J. S. Fraser, J. C. D. Milton, W. G. Davies, Proc. Second Symp. on the Physics and Chemistry of Fission, IAEA, Vienna (1969), p. 363.

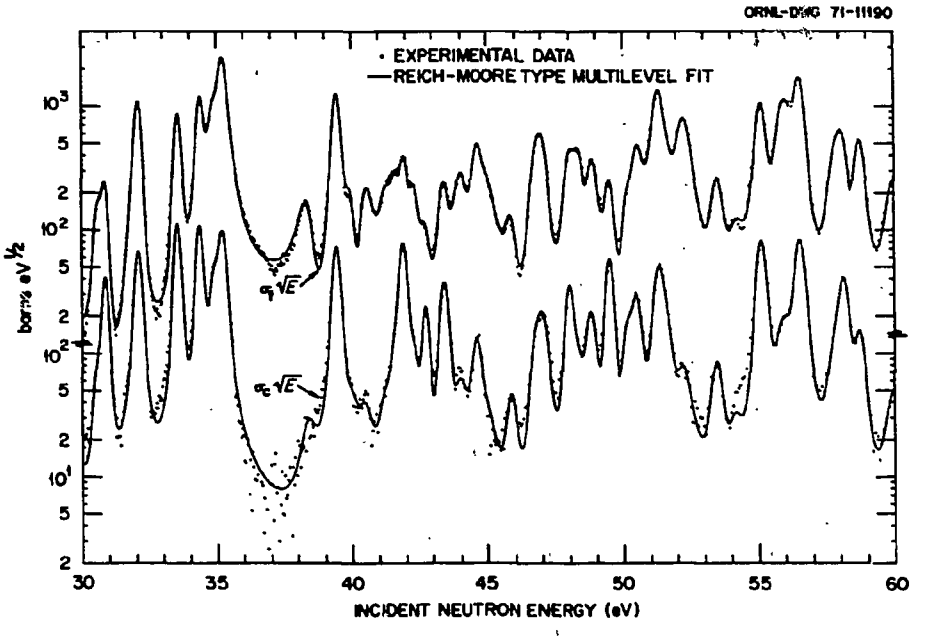

Figure (A.5.b-1) Fission and Capture Cross Sections of ^{235}U from 30 to 60 eV. The dots are the experimental data from the ORNL-RPI measurement (Ref. 14). The solid lines are the resolution broadened cross sections computed with the parameters of Table 1.

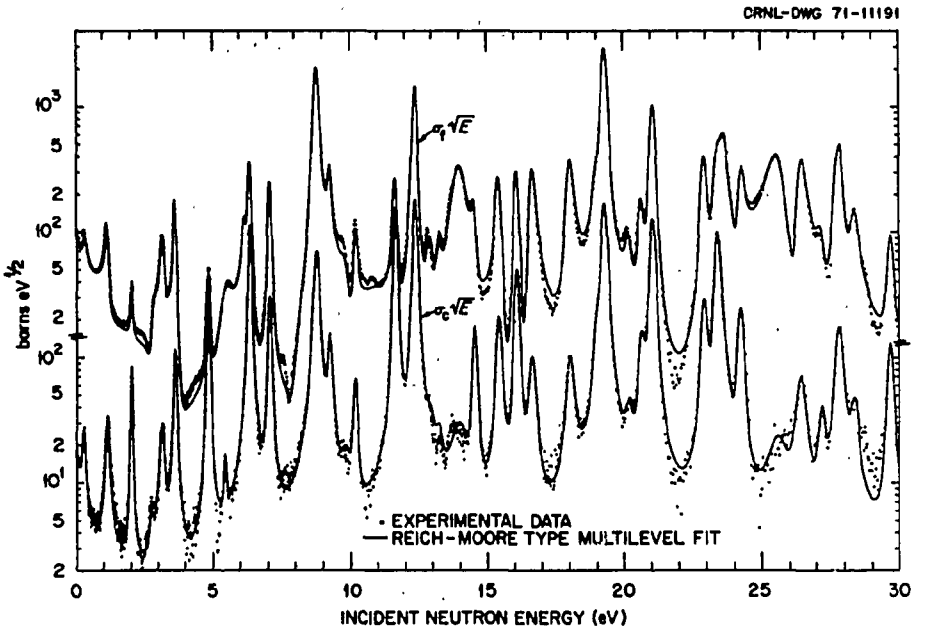

Figure (A.5.b.-2) Fission and Capture Cross Sections of ^{235}U from 0 to 30 eV. The dots are the experimental data from the ORNL-RPI measurement (Ref. 14). The solid lines are the resolution broadened cross sections.

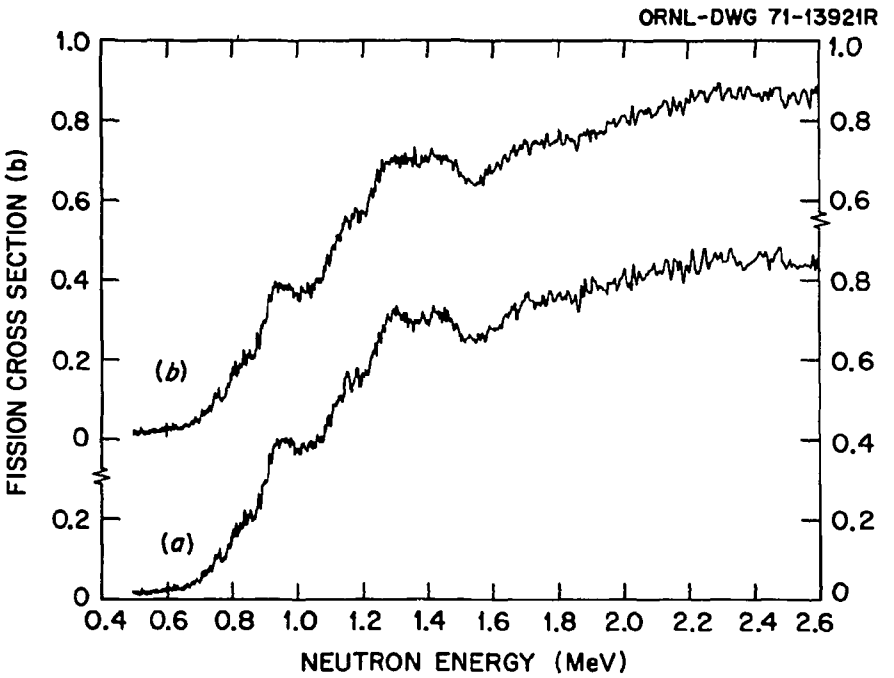

Figure (A.5.c) $^{236}U(n,f)$ Cross Section based on (a) the Scintillator Monitor, (b) the ^{235}U Monitor. Both ^{236}U cross sections were arbitrarily normalized to 0.805 barns at 2 MeV.

d. Prompt Gamma Rays Emitted in the Thermal Neutron Induced Fission of ^{235}U*
(Frances Pleasonton, R. L. Ferguson, and H. W. Schmitt)

The average number and average energy of gamma rays emitted within ~ 5 nsec after fission have been determined as functions of fragment mass and as functions of fragment mass and total kinetic energy in two-dimensional representations. In a four-parameter experiment, energies of coincident pairs of fission fragments were measured with surface barrier detectors and gamma-ray energies were measured with a large NaI(Tl) detector, which was located 89 m from a thin ^{235}U target and positioned coaxially with the fragment detectors. The time difference between detection of a fission fragment and a gamma ray was measured to allow time-of-flight discrimination against fission neutrons. The gamma-ray data were analyzed with a "weighting method" proposed by Maier-Leibnitz to deduce average numbers and energies of gamma rays from measured pulse heights. The Doppler shift in the laboratory angular distribution of gamma emission was utilized to obtain the number and energy of gammas as functions of single-fragment mass. The results, for both average number and average energy as functions of single fragment mass, are characterized by a sawtooth behavior similar to that which is well known for neutron emission. The overall average number and energy of gamma rays emitted per fission were found to be 6.51 ± 0.3 and 6.43 ± 0.3 MeV, respectively, giving an average photon energy of 0.99 ± 0.7 MeV. These results are shown graphically in Figure A.5.d.

---

*Submitted to Phys. Rev. for publication.

e. Fission Barriers for Light Elements (A = 180-212)*
(U. Mosel† and H. W. Schmitt)

Fission barriers for elements in the mass range A = 180-212 have been calculated in the Two Center Shell Model using the Strutinsky prescription. The theoretical predictions agree well with recent experimental results.

---

*Submitted for publication in Physics Letters.
†University of Washington, Seattle.

f. Asymmetry in Nuclear Fission*
(M. G. Mustafa†, H. W. Schmitt, and U. Mosel‡)

The two-center model has been generalized to asymmetric deformations. Our earlier calculations of potential energy surfaces for symmetric fission[1], in which two degrees of freedom were used, have been extended to a four-dimensional calculation, where the two additional degrees of freedom now describe asymmetric shapes. Results will be shown for ^{236}U, ^{252}Fm, and ^{264}Fm. Mass asymmetry is found to be favored for both ^{236}U and ^{252}Fm, whereas mass symmetry is favored for ^{264}Fm. The results indicate strong fragment shell effects; in ^{264}Fm the preference for mass

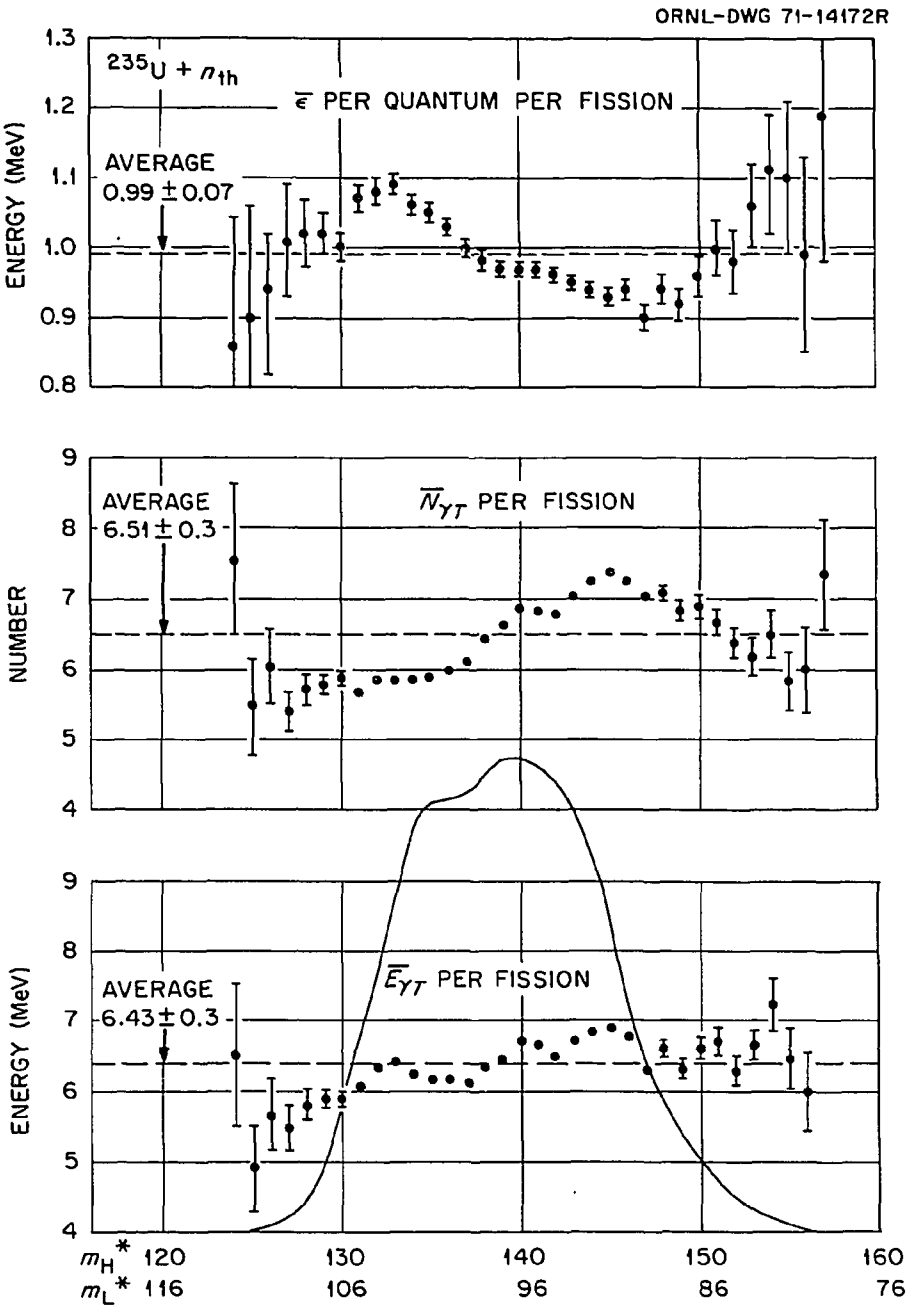

Figure (A.5.d) The average total energy $\bar{E}_{\gamma T}$ and average total number $\bar{N}_{\gamma T}$ of gamma rays emitted per fission as functions of complementary mass pairs. The top part of the figure shows the average photon energy $\bar{\epsilon} = \bar{E}_{\gamma T}/\bar{N}_{\gamma T}$. Error bars, including statistical undertainties.

symmetry may be due to the formation at symmetry of two-doubly magic ^{132}Sn nuclei.

---

*To be presented at Washington, D.C. APS Meeting, April 24-27, 1972.
†Visitor from the Pakistan Atomic Energy Commission.
‡University of Washington, Seattle.
[1]U. Mosel and H. W. Schmitt, Phys. Rev. C4, 2185 (1971).

g. Fission Properties of Heavy and Superheavy Nuclei*
(H. W. Schmitt and U. Mosel†)

Calculations have been carried out to estimate the total fragment kinetic energies E_K, total fragment excitation energies E_X, and approximate total number of neutrons ν emitted in the binary fission of heavy and superheavy nuclei. The kinetic energy calculations are based on a static scission model reported earlier for fissioning nuclei in the actinide region. The total energy release Q is calculated from a recent mass formula of Seeger, and the total excitation energy is obtained from the difference, $E_X = Q - E_K$. The results show a strong peak in $E_K(A)$ [A = compound nucleus mass number] and a corresponding minimum in $E_X(A)$, at $A \cong 264$, corresponding to fission into two nearly double-magic ($Z \sim 50$, $N \sim 82$) fragments. Our predictions of E_K, E_X, and ν disagree sharply with the liquid drop predictions in the range $255 \lesssim A \lesssim 290$. It appears from these results that kinetic energy measurements do not provide an unambiguous test for superheavy nuclei, while measurements of ν, if $\nu \gtrsim 5$, seem to provide such a test.

---

*Submitted for publication to Nuclear Physics.
†University of Washington, Seattle.

h. Asymmetric Fission in the Two-Center Model*
(M. G. Mustafa†, U. Mosel‡, and H. W. Schmitt)

Four dimensional potential energy surfaces have been calculated in the asymmetric two-center model for ^{252}Fm, ^{258}Fm, ^{264}Fm, and ^{236}U. Symmetric fission is found to be preferred in ^{258}Fm, consistent with a recent observation; symmetric mass division is strongly preferred in ^{264}Fm. Asymmetric fission is preferred in ^{252}Fm, and in ^{236}U for which the fission path is investigated in more detail. The development of asymmetry in the fission of ^{236}U is described.

---

*Submitted for publication to Phys. Rev. Letters.
†Visiting scientist from Pakistan Atomic Energy Commission.
‡University of Washington, Seattle.

i. Neutron Emission in Proton-Induced Fission of ^{209}Bi at 36.1 MeV*
(F. Plasil, R. L. Ferguson, Frances Pleasonton, and H. W. Schmitt)

The fission fragment mass distribution for 36.1-MeV proton-induced fission of ^{209}Bi, obtained from our earlier correlated fragment kinetic energy measurements, differs from radiochemical results: our distribution shows no asymmetric peaks in the wings and is much broader than the radiochemical one. Recently, we have calculated the average number of neutrons emitted as a function of fragment mass. An iterative procedure was used: N(m), the pre-neutron-emission mass yield (dispersion-corrected), was calculated from the provisional mass yield and a $\nu(m)$ function; this N(m) was subsequently used together with the radiochemical mass distribution in a cumulative yield calculation to obtain a new $\nu(m)$; and so forth to convergence. The neutron emission function rises from about 1 neutron at fragment mass 85 to 6 neutrons at mass 125 -- consistent with measurements for $^{209}Bi(\alpha,f)$. The difference in width between our mass distribution and radiochemical results is thus explained by neutron emission, but the discrepancy regarding the asymmetric fission component remains.

*Presented at San Francisco APS Meeting, January 31 - February 3, 1972.

j. Mass and Energy Distributions from 77.3 MeV-^{4}He-Induced Fission of ^{181}Ta, ^{209}Bi, and ^{233}U; A Test of Liquid Drop Model Predictions*
(F. Plasil and H. W. Schmitt)

Thin targets of ^{181}Ta, ^{209}Bi and ^{233}U have been bombarded with 77.3 MeV ^{4}He ions at the Oak Ridge Isochronous Cyclotron. Correlated measurements of kinetic energies of fission fragment pairs have been made and mass and total kinetic energy distributions were obtained. The widths of the distributions were compared to predictions of the liquid drop model for fission. The trends predicted by theory were observed, but the absolute magnitude of the distribution widths were not in agreement with liquid drop model predictions. It is concluded that the liquid drop model describes fission of relatively light nuclei in general terms, but that it must be used with caution when quantitative predictions are required.

*Submitted for publication to Physical Review.

6. Standards and Other Aspects of Neutron Interactions

a. Experimental Upper Limit for the Electric Dipole Moment of the Neutron*

(P. D. Miller, W. B. Dress, and N. F. Ramsey†)

We have modified our previous magnetic resonance experiment[1] to eliminate the systematic effect of v/c x E, and consequently obtain an improvement of about a factor of 5 in sensitivity to a neutron electric dipole moment.

*To be presented at Washington, D.C., APS Meeting, April 24-27, 1972.
†Harvard University.
[1]J. K. Baird, P. D. Miller, W. B. Dress and N. F. Ramsey, Phys. Rev. 179, 1285 (1969).

7. Instruments and Techniques

a. Neutron Multiplicity Counter*

(R. L. Macklin, F. M. Glass, J. Halperin, R. T. Roseberry, H. W. Schmitt, R. W. Stoughton, and M. Tobias)

A neutron multiplicity counter assembly has been constructed to enable a search for superheavy elements in natural samples and in accelerator targets. The detector consists of twenty ^{3}He counters placed in a paraffin moderator. These counters surround a central sample cavity with a capacity of about 20 liters, capable of accommodating samples up to 100 kg in weight, depending on the density. A particular feature of this counter is its relative insensitivity to gamma rays. The efficiency for detecting a single neutron is $\sim 30\%$. An estimate of $\bar{\nu}$, the number of neutrons emitted per fission in a sample, may be obtained from the observed multiplicity distribution P(n), where n is the number of neutron counts in an event. More accurate values of $\bar{\nu}$ may be obtained for small, isolated samples of spontaneously fissioning isotopes, where the neutron counters may be gated by a fission fragment detector. The design of the counter and an analysis of its properties are presented.

*Submitted for publication to Nucl. Instr. and Meth.

b. A Proton-Recoil Neutron Detector for Neutrons of a Few keV Energy*

(N. W. Hill, J. A. Harvey, G. G. Slaughter, A. St. James†)

In the process of testing plastic detectors for MeV neutron total cross section measurements, it was discovered that a new plastic scintillator, NE 110, when suitably mounted on a selected RCA 4522 5" phototube with a special base was capable of detecting neutrons whose energies were only 1 keV. The voltage divider used in this base was essentially the RCA type C recommended by RCA for high peak current applications. The grid

adjustment is made for optimum pulse height resolution for the ~3 inch diameter scintillators with a gamma source remote from the scintillators. The dynode 14 to anode potential is adjusted to give maximum gain at the anode consistent with the photomultiplier tube noise level with some dynode 14 saturation. The scintillators, machined with a concave spherical curvature, were coupled directly to the phototube with Dow Corning optical coupling compound. Three different pieces of NE 110 from the same ingot were used on separate photomultipliers and further tests of a different batch are planned. The efficiency of this new detector as a function of neutron energy was determined using many groups of essentially monoenergetic neutrons due to the neutron "windows" in Fe from 24.5 to 954 keV and with a sample of copper 1" thick which has many large resonances from ~1 to 50 keV. These 2 measurements were made with several NE 110 detectors mounted on different RCA 4522 phototubes, 2 Naton 136 detectors and a ^{6}Li-glass scintillation detector. The efficiencies of these plastic detectors were normalized to that of the ^{6}Li glass detector, correcting for their differences in areas; and some of the results are shown in Figure A.7.b. It is obvious that this NE 110 scintillator is superior in efficiency to ^{6}Li glass above a few keV neutron energy by as much as an order of magnitude. The efficiency of the NE 110 scintillator for low energy neutrons is very sensitive to the photomultiplier gain and discriminator bias. We expect that the efficiencies of these plastic detectors can be further improved using photomultipliers selected for high-quantum efficiencies and optimizing the electronics. The NE 110 scintillator is not sensitive to low-energy neutrons, is very fast (3.3 nsec decay constant), and the tail produced by the gamma rays from neutron capture by hydrogen from the moderated neutrons is small (< 0.1% for 10-keV energy neutrons).

---

*USNDC Report.
†Student participant in Great Lakes Colleges Association Program, fall 1971, from Denison University.

c. Some Tests Related to the Use of Proton Recoil Proportional Counters for Neutron-Flux Measurements*
(E. A. Straker†, T. A. Love, C. E. Burgart‡, R. M. Freestone, Jr., and G. L. Morgan)

Several tests have been made in order to check the accuracy of neutron-flux measurements obtained with a spherical proton-recoil counter. The results indicate such measurements are valid for neutron energies as low as 10 keV.

---

*ORNL-TM-3631
†Present address: Science Applications, Inc., Huntsville, Alabama.
‡Present address: Science Applications, Inc., Albuquerque, New Mexico.

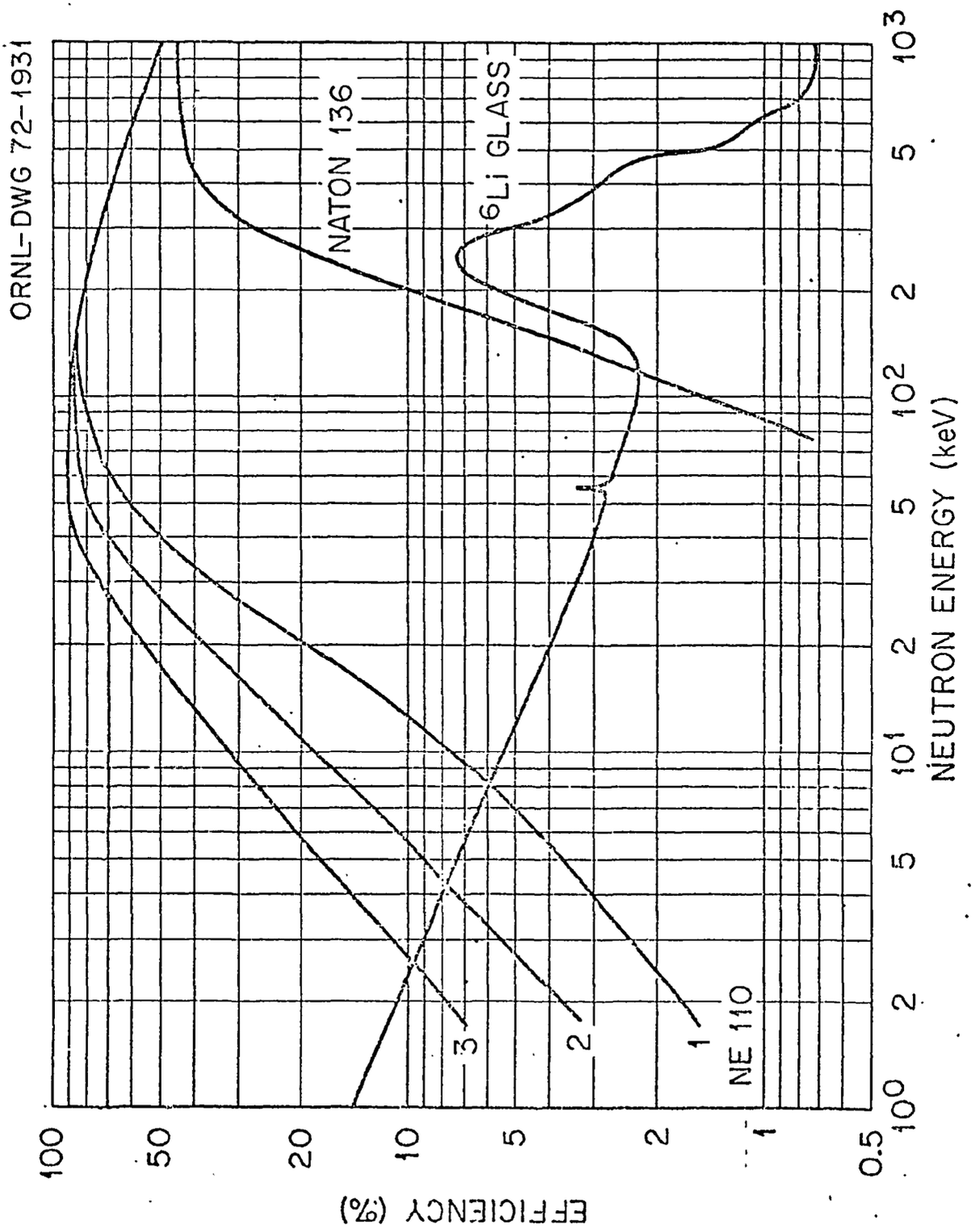
ORNL-DWG 72-1931
NATON 136
^{6}Li GLASS
NE 110
1
2
3
EFFICIENCY (%)
NEUTRON ENERGY (keV)
100
50
20
10
5
2
1
0.5
10^0
10^1
10^2
10^3

Figure (A. 7.-b.)

8. Evaluation

a. An Evaluation of Neutron and Gamma-Ray-Production Cross Sections for Lead*
(C. Y. Fu† and F. G. Perey)

A survey was made of the available information on neutron and gamma-ray-production cross section measurements of lead. Evaluated nuclear data sets in the ENDF/B format were prepared for lead covering the energy range from 0.00001 eV to 20.0 MeV. The cross section sets were based on experimental results available to June 1971 and on nuclear model calculations.

*MAT. No. 4136 in the DNA Library and 1136 for CSEWG.
†University of Tennessee, Knoxville.

B. CHARGED PARTICLES

1. Heavy Ion Neutron Yields*
(W. B. Dress, J. K. Bair, C. H. Johnson, and P. H. Stelson)

Absolute total neutron yields have been measured for the reactions (^{16}O,xn) and (^{18}O,xn) using targets of ^{16,18}O, ^{63,65}Cu, ^{58,60,61,62,64}Ni and ^{64,66}Zn. The energy region covered was from below the coulomb barrier to 55 MeV in the laboratory system. Target thicknesses ranged from 140 to 750 kev at 40 MeV. The ^{12}C(^{16}O,xn) yield, measured with a target 200 kev thick at 20 MeV shows evidence of structure, in contrast to the (^{18}O,xn) yield from the same target. The yield of the latter reaction is a factor of almost seven times that of the former. The ^{16,18}O(^{16,18}O,xn) yields measured using a target 200 kev thick at 40 MeV shows no evidence of structure. The relative yields of the reactions ^{16}O(^{16}O,xn):^{18}O(^{16}O,xn): ^{18}O(^{18}O,xn) are 1:5.5:11. The relative yields for ^{16}O on ^{58}Ni, ^{60}Ni, ^{61}Ni, ^{62}Ni, and ^{64}Ni are 1:3.2:5.2:6.5:10.7 at a bombarding energy of 50 MeV. The corresponding numbers for ^{18}O bombardment are 1:17.:-:2.4:3.8. The yield for ^{64}Ni(^{18}O,xn) is 50% greater than that for ^{64}Ni(^{16}O,xn).

*To be presented at Washington, D.C., APS Meeting, April 24-27, 1972.

2. Level Structure of ^{54}Mn*
(J. K. Dickens)

Properties of levels in ^{54}Mn have been studied using the ^{54}Fe(p,nγ) ^{54}Mn reaction. These data alone were not sufficient to determine spin and parity assignments, but when correlated with data from prior experimental investigations of the ^{54}Mn nucleus, a set of unique J^{π} assignments for the lowest five excited states was determined. These assignments are consistent with nearly all presently available experimental data and are in good agreement with shell-model calculations. The level excitation energies and J^{π} values obtained are: ground-state, 3^+; 54.3 keV, 2^+; 156.9 keV, 4^+;

367.6 keV, 5^+; 407.5 keV, 3^+; and 839.0 keV, 4^+. Transitions from higher lying states were observed and possible J^π values were obtained.

---

*ORNL-TM-3674.

3. Investigation of Collective Properties of ^{208}Pb by the $^{208}Pb(p,p')$ Reaction at E = 55 MeV*
(F. E. Bertrand, M. B. Lewis, and C. B. Fulmer)

We have investigated the collective states in ^{208}Pb with the proton inelastic scattering reaction. The spectra covered the entire bound-state region for scattering angles between 9° and 58°. A 55-MeV proton beam from ORIC was used, and scattering particles were detected with nuclear emulsions in a broad-range spectrograph. Energy resolution was $\approx$ 35-40 keV. The experimental angular distributions obtained for 24 peaks were compared to those predicted by DWBA calculations utilizing a collective-model form factor. The location of the low spin members of a sequence of positive parity states has been confirmed; however, we find that the 10^+ state suggested from earlier work is, in fact, L = 3. Likely candidates for $J > 8$ states were found, as well as several collective fragments of the 2.615-MeV 3^- state and the 4.323-MeV 4^+ state. No fragments of the 4.086-MeV 2^+ state were found and the observed quadrupole strength was only $\approx$ 7% of the E2 sum rule strength.

---

*To be presented at Washington, D.C., APS Meeting, April 24-27, 1972.

4. Elastic Scattering of 40-MeV Protons from ^{48}Ti, ^{nat}Cr, and ^{64}Zn: Tabulated Differential Cross Sections*
(J. K. Dickens, E. E. Gross, F. G. Perey, A. Van der Woude, and A. Zucker†)

Numerical values of differential cross sections for elastic scattering of 40-MeV protons from targets of ^{48}Ti, ^{nat}Cr, and ^{64}Zn for scattering angles between 10 and 145 degrees are reported in tabular form.

---

*ORNL-TM-3691.
†National Academy of Sciences, Washington, D.C.

5. Evidence from Inelastic Proton Scattering for the Excitation of Strong Vibrations in the Nuclear Continuum*
(M. B. Lewis and F. E. Bertrand)

In a recent series of reports[1] on 30-60 MeV inelastic proton scattering from several elements, cross sections for the reaction products were reported for a large secondary energy range ($\sim$ 60 MeV). We noted an enhancement in the low excitation (high exit energy) region of the proton continuum for all targets. In order to complement this data which was

taken with a GeLi detector system, we have made some similar measurements with a spectrograph. All the data are consistent with an enhanced region of the continuum at an excitation energy of ≈ 10-20 MeV. The excitation energy centroid is a function of target mass, but not of target angle. We interpret this to suggest that the enhancement is a manifestation of strong collective vibrations in the nuclear continuum. The possibility that the enhancement is a confirmation of the E2 sum rule will be discussed.

---

*To be presented at Washington, D.C., APS Meeting, April 24-27, 1972.
[1]F. E. Bertrand and R. W. Peelle, ORNL Reports 4455, 4469, 4456, 4450, 4698, 4471, 4460, 4638.

6. Cross Sections for ^{58,60}Ni(^{16}O,X) Reactions*
(R. L. Robinson, H. J. Kim, and J. L. C. Ford, Jr.)

The absolute cross sections for different exit channels have been determined for reactions induced by bombardment of enriched 1-2 mg/cm^2 targets of ^{58,60}Ni with 38, 42 and 46 MeV ^{16}O ions. They were obtained from yields of gamma rays from the residual radioisotopes, and from the targets when in-beam. Identification of the products was based on gamma-ray energies and intensities, and for the radioactivities, on the half-life of the parent. Because of the proximity of the Coulomb barrier (E ≈ 42 MeV), all of the cross sections increase rapidly with energy. Cross sections in mb for 46 MeV ^{16}O projectiles are (x represents the particles emitted:

x	^{58}Ni	^{60}Ni	x	^{58}Ni	^{60}Ni
1(n/p)	1.0	2.3	α	0.8	-
2n	} 50	17	αn	} 53	8
np		140	αp		60
2p	190	130	2α	1	-
3(n/p)	58	44	^{12}C	10	-

---

*To be presented at Washington, D.C., APS Meeting, April 24-27, 1972.

Addendum to Report to the U.S. Nuclear Data Committee
W. M. Good

TOF Measurement of σ_f for ^{249}Cf wrt ^{235}U at ORELA

C. E. Bemis, Jr.,† J. W. T. Dabbs, N. W. Hill,‡ M. S. Moore,* A. N. Ellis*

A technique applicable to very small samples has been developed in which a large area diffused-junction detector[1] is placed directly in the neutron beam from ORELA and nearly in contact with the fissioning sample. The detector is only 5 mils thick and gave a gamma-flash pulse approximately equal in size to a fission fragment pulse.

A 128 μg sample of ultra-pure ^{249}Cf was compared with a masked ^{235}U sample of 406 μg/cm^2 over the energy range 0.32 eV - 1.5 MeV. A specially developed ultra-fast current pulse amplifier (10 ns rise, 30 ns fall time) was used to reduce α particle pileup from the ^{249}Cf ($\sim 10^7$ α/sec). Radiation damage effects required replacement of the detectors after 10-15 hrs. of use. Three detectors were used in this series of measurements. Measurements were made at 9.73 m in flight path 2 at ORELA at an average power level of 25 kW.

A prominent feature of the results is a very large resonance found at 0.71 eV which accounted for approximately 60% of all ^{249}Cf fissions observed in the experiment. The initial estimate of the peak cross section is $\sigma_{of} \sim 8000$ barns with a FWHM of 150 meV. Our data overlap with and extend to lower energies the unpublished results of Silbert measured on the Physics-8 underground explosion.

---

†Chemistry Division.
‡Instrumentation and Controls Division.
*Los Alamos Scientific Laboratory.
[1]Solid State Radiations, Inc., Type 600-PIN-125.

OHIO UNIVERSITY ACCELERATOR LABORATORY

A. TANDEM ACCELERATOR PROGRAM

1. Neutron Scattering

a. Fast Neutron Time-of-Flight Facility (C. E. Nelson, S. L. Hausladen, and R. O. Lane)

A time-of-flight facility has been designed and constructed to measure angular distributions of fast neutrons. This system presently utilizes the $^{7}Li(p,n)^{7}Be$ reaction and the 'wobble target' design of Mooring[1] as a source of fast neutrons. The system consists of two main detectors, each a 6"-diameter liquid scintillator and employing pulse shape discrimination to eliminate gamma radiation. These detectors are encased in large water tanks and have polyethylene collimators to reduce background, in addition to copper shadow bars which shadow the entrance to the collimators from the direct neutrons of the source reaction. A small detector, located at zero degrees, has a separate time-of-flight system and serves as a monitor of the neutron flux. This facility has been used to measure approximately 84 elastic angular distributions from ^{10}B and ^{11}B in the energy interval 1.5-5.0 MeV. (see below).

---

[1] F. P. Mooring, Argonne National Laboratory, 1958

b. Fast Neutron Elastic Differential Scattering Cross Sections for ^{11}B (C. E. Nelson, S. L. Hausladen and R. O. Lane)

A total of 68 differential scattering cross sections have been determined at 7 angles between 20-160 degrees for ^{11}B, using the new time-of-flight facility above. Measurements were made between 2.2 MeV and 5.0 MeV at intervals of 15 keV to 30 keV. The experimental results, when corrected for finite geometry and detector efficiency, will be compared to theoretical calculations based on the R-Matrix formalism of Lane and Thomas[1] with the hope of determining the spins and parities of levels in the compound nucleus ^{12}B.

---

[1] A. M. Lane and R. G. Thomas, Rev. Mod. Phys. 30, 257(1958).

c. Fast Neutron Elastic Differential Scattering Cross Sections for ^{10}B(S. L. Hausladen, C. E. Nelson, and R. O. Lane)

The time-of-flight facility described above has been used to measure 60 differential scattering cross sections for ^{10}B. Measurements were made between 1.4 MeV and 4.8 MeV at intervals of approximately 50 keV. Detector efficiency, finite geometry, and multiple-scattering corrections are presently being made to the data. Comparisons with the level structure of ^{11}B will be made with a 2 level-4 channel R-matrix analysis as described in a previous paper.[1] Preliminary results show strong d-wave formation at energies below 3.5 MeV. At higher energies the effects of direct interaction contributions will be investigated.

---

[1] Lane, Hausladen, Monahan, Elwyn, Mooring and Langsdorf, Jr., Phys. Rev. C4, 380(1971).

2. Nuclear Theory

a. R-matrix Calculations of Compound States in ^{17}O (G. D. Westin and J. L. Adams)

We are analyzing published data for the four reactions $^{16}O(n,n)^{16}O$, $^{16}O(n,\alpha)^{13}C$, $^{13}C(\alpha,n)^{16}O$, and $^{13}C(\alpha,\alpha)^{13}C$. The R-matrix theory of nuclear reactions is used, and a single set of parameters is used to fit data from all four reactions. The effect of varying each of the R-matrix parameters is also being investigated.

---

b. A Study of the Neutron Plus ^{12}C System Using the Unified Reaction Formalism, I. Elastic Scattering(T. Leung and R. D. Koshel)

In this paper a consistent application of Feshbach's unified reaction formalism is applied to the neutron plus ^{12}C system. A collective model is used for the ^{13}C system. Calculations of the differential cross sections, polarization, and level structure are presented.

This is an abstract of a paper which has been accepted by Annals of Physics.

B. COCKROFT-WALTON NEUTRON PROGRAM

1. Neutron Scattering

a. Differential Cross Section and Polarization for Neutrons Scattered from ^{10}B at 2.63 MeV (J. Cox, H. Knox, R. Lane, and R. Finlay)

The differential cross section and polarization for 2.63 MeV neutrons scattered from ^{10}B have been measured at eight angles from 18° to 123° c.m. The neutrons were produced by the $D(d,n)^3He$ reaction using a pure Al drive-in target with a 120-keV deuteron beam. Neutron pulse shape discrimination and associated particle time-of-flight techniques were employed. A spin-precession magnet was used in the measurement of the asymmetry. A companion experiment with ^{12}C produced the value of the source polarization and detector absolute efficiency. Multiple scattering and finite geometry corrections have been made. The data obtained in this experiment are presented in the table below. The present results are predominantly influenced by the broad resonance at 2.8 MeV (E_x = 14.0 MeV). Attempts to fit the region of E_x = 11 MeV to 15 MeV with R-matrix parameters for states in ^{11}B have been made. Based on this analysis, the level at 14.0 MeV appears to have positive parity (ℓ=2) and a spin of 11/2 or 9/2.

C.M. Angle (degrees)	Cross Section (barns)	Polarization (%)
18.69	0.3865±0.0149	9.2±5.9
32.89	0.3036±0.0116	36.7±10.6
49.08	0.1839±0.0066	32.0±10.6
65.00	0.0905±0.0031	34.9±14.0
80.58	0.0376±0.0013	36.5±23.4
95.78	0.0348±0.0012	-0.3±21.0
110.58	0.0668±0.0023	15.5±16.1
123.10	0.1231±0.0043	30.9±14.5

b. Differential Cross Section and Polarization of 2.63 MeV Neutrons Scattered from ^{12}C(H. Knox, J. Cox, R. Finlay, and R. Lane)

Neutrons emitted at 50° in the laboratory system from the D(d,n)^{3}He reaction were elastically scattered from ^{12}C and the differential cross section, asymmetry and total cross section were measured. Associated particle time-of-flight and a spin precession solenoid were used in these measurements. The total cross section, asymmetry and differential cross section were simultaneously least squares fitted using an iterative search. A consistent set of scattering phase shifts and source polarization were obtained from this search. These phase shifts along with the predictions of Wills,[1] Meier[2] and Reynolds[3] for this incident energy are given in Table 1. The predictions of both Wills and Reynolds differ from the results of this work mainly in the $d_{5/2}$ phase shift. Presently a two level R-matrix description of the scattering is being used to fit the results of the present experiment and others in the neutron energy range of zero to 5 MeV.

---

[1] Wills, Bair, Cohn and Willard, Phys. Rev. 109, 891(1958).

[2] Meier, Scherrer and Trumpy, Helv. Phys. Acta 27, 577(1954).

[3] Reynolds, Slavik, Lubitz and Francis, Phys. Rev. 176, 1213(1968).

	$\delta_{s_{1/2}}$	$\delta_{p_{1/2}}$	$\delta_{p_{3/2}}$	$\delta_{d_{3/2}}$	$\delta_{d_{5/2}}$
Present Work	-99.7±5.1	-9.9±9.4	-4.0±7.8	24.4±2.5	-10.6±2.5
Meier et al.	-72.0	-9.5	-1.0	32.0	-2.0
Wills et al.	-101.0	-7.0	-3.5	27.0	-1.5
Reynolds et al.	-96.1	-13.9	-9.3	19.2	-4.7

RENSSELAER POLYTECHNIC INSTITUTE

A. CROSS SECTION MEASUREMENTS

1. KeV Neutron Elastic Scattering Cross Section in Iron*
(R. Zuhr, Z. Bell and K. Min)

The differential elastic scattering cross section of natural iron was measured at six angles from 45 to 60 degrees with an energy resolution of 10% (FWHM) in the region from 10 to 600 keV. The cross sections were measured relative to lead, using time-of-flight methods over a 27-meter flight path, and the scattered neutrons were detected by a 5" D x 1/2" thick ^{6}Li glass scintillator. Background was found using the method of black resonances, and the cross sections used for the standard lead sample were those of Lane, Langsdorf, Elwyn and Monahan.[1]

The results have been corrected for multiple scattering using a combined Monte Carlo analytical method based on the work of Lane and Miller.[2] It includes energy dependent scattering through fourth order and is adequate for all energies except in the neighborhood of the 28 keV resonance, where the sample thickness is such that even more extensive corrections are necessary.

Differential scattering cross sections as a function of the scattering angle in laboratory coordinates are shown in Figs. A1, A2, and A3. The solid lines represent the least square fits of second order Legendre polynomial expansions. The interference between s- and p-waves begins to show appreciably at about 160 keV; and by 180 keV, the p-wave scattering makes an appreciable contribution. At several higher energies, comparison is made with the 1969 results of Elwyn and Monahan,[3] indicated by the open circles. Their energy resolution is a constant 20 kilovolts.

* Req. No. 97

2. The Total Neutron Cross Sections of ^{238}U From 0.5 to 30 MeV
(S. H. Hayes, P. Stoler, J. M. Clement and C. A. Goulding)

A measurement of the total neutron cross section of ^{238}U was made, using the RPI electron LINAC. The operating electron energy was about 60 MeV, and the beam burst width was 20 ns, the flight path was 250 meters. The neutron energies were determined using the time-of-flight technique with a resolution of .08 ns/m.

The ^{238}U cross section is presented from 0.7 to 30.0 MeV in figures A4 to A7. Figure A4 is a plot of the cross section on a log energy scale. The cross sections displayed have been energy averaged. There is good agreement between the data reported here and the data

---

1. Lane, Langsdorf, Elwyn and Monahan, Annals of Physics, 12, 135, (1961).
2. Lane and Miller, Nucl. Instr. and Methods, 16, 1 (1962).
3. Elwyn and Monahan, Nucl. Phys., A123, 33 (1969).

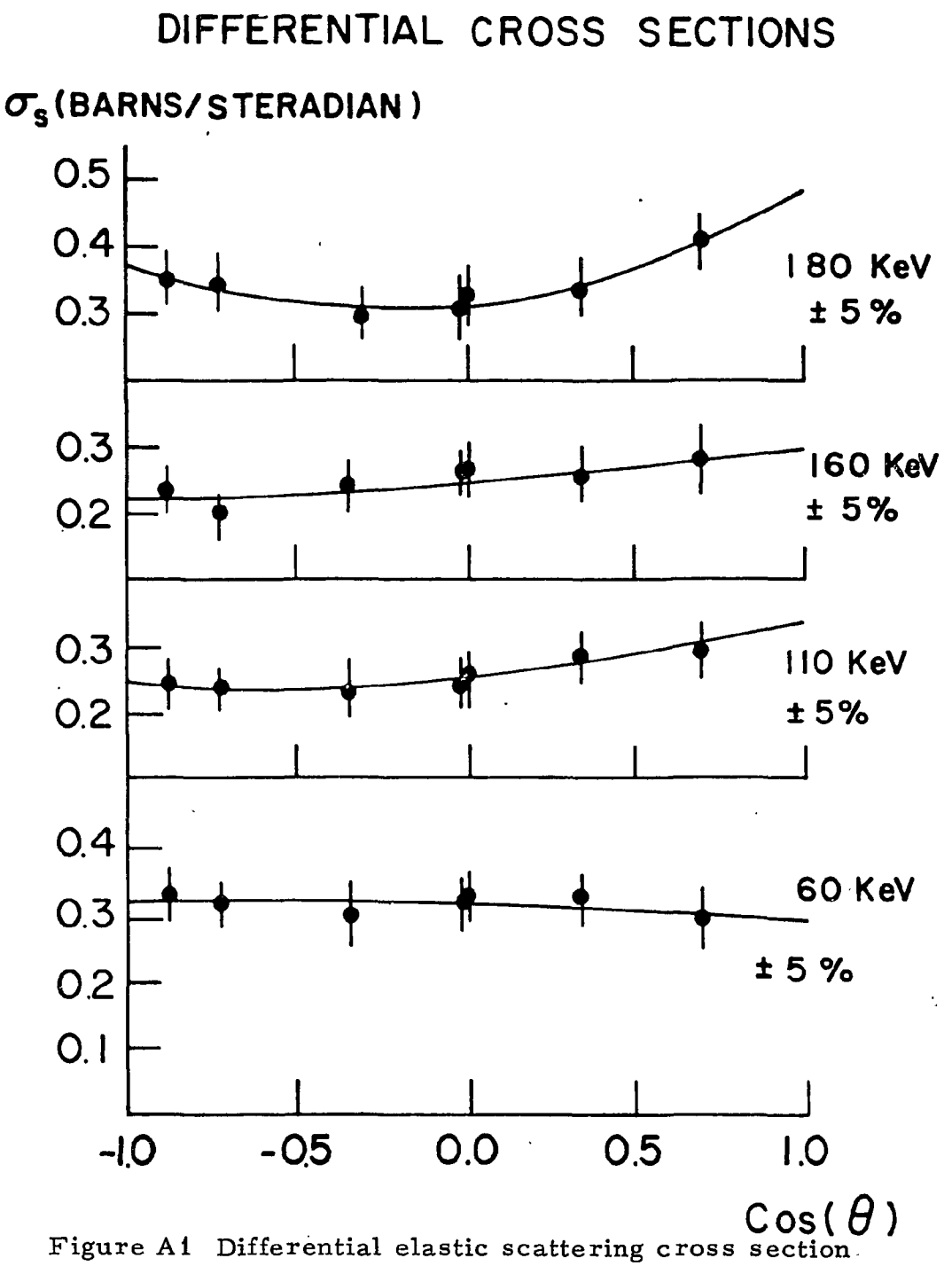

Figure A1 Differential elastic scattering cross section of Fe as a function of laboratory scattering angle.

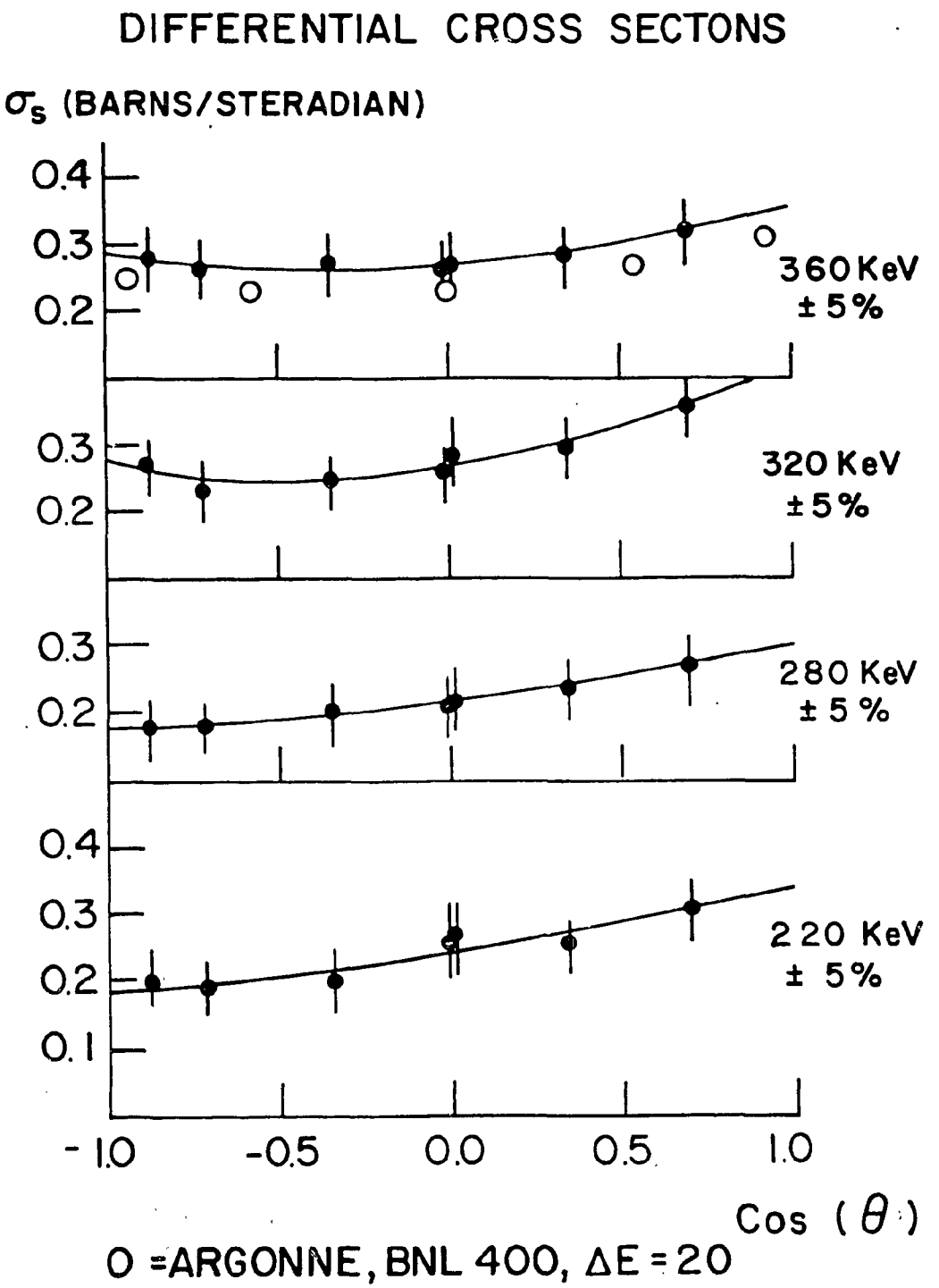

Figure A2 Total scattering cross section of Fe with an energy resolution of 10%.

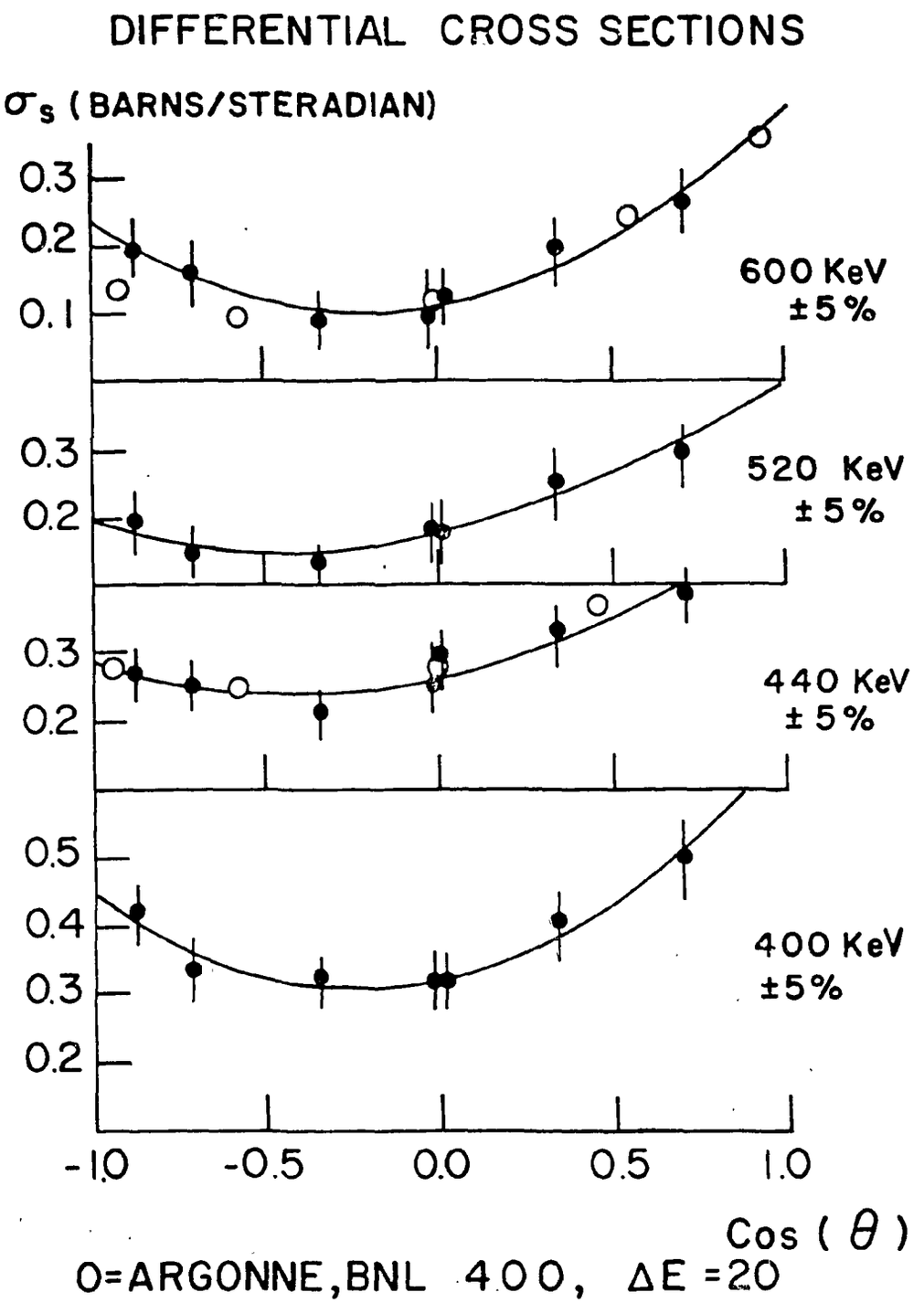

Figure A3 Total scattering cross section of Fe with an energy resolution of 100 keV.

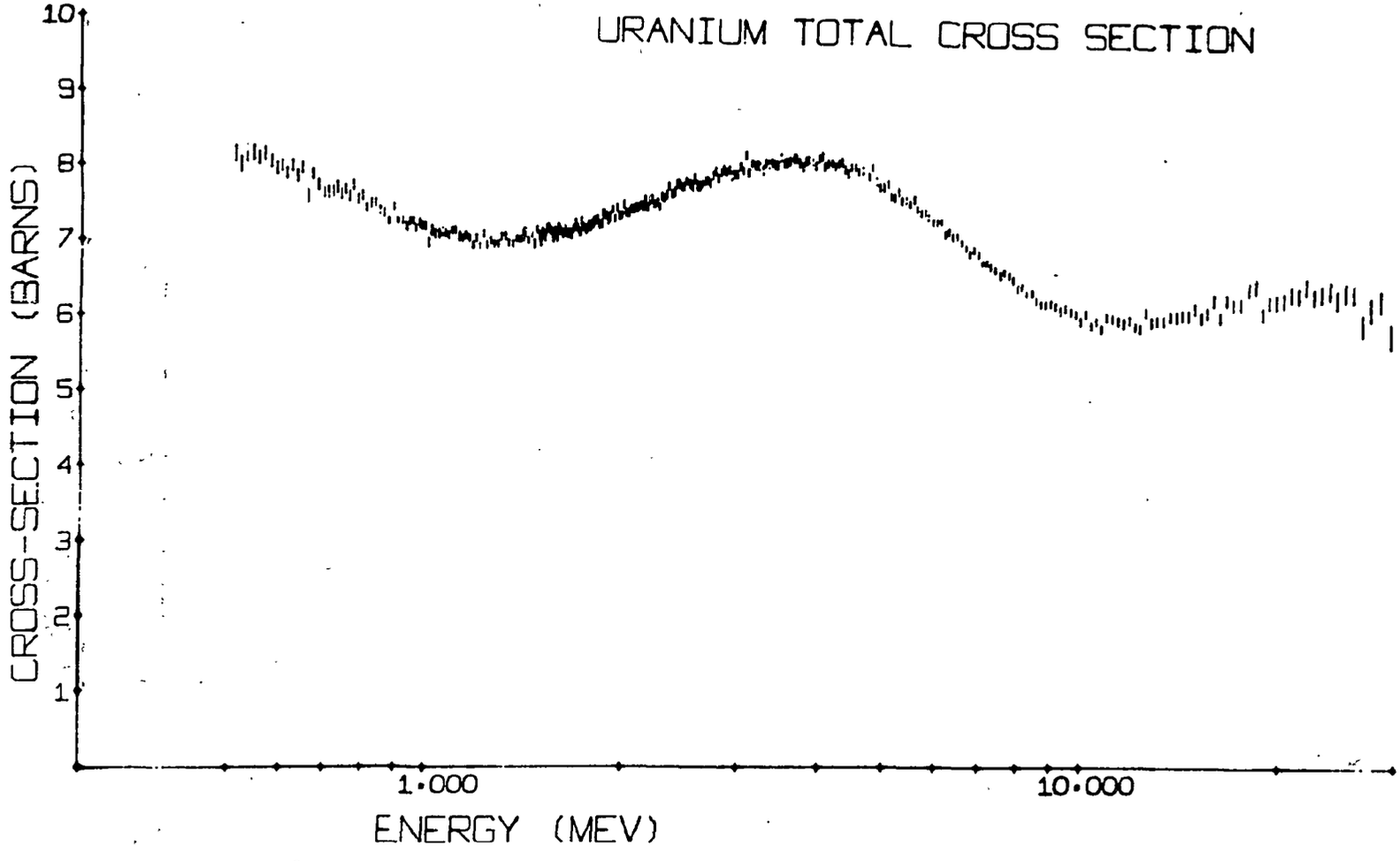

Figure A4 The ^{238}U total neutron cross section from 1 to 30 Mev. The data have been pre-averaged to improve the statistical precision. Thus, the number of points shown are less than the total number of data channels.

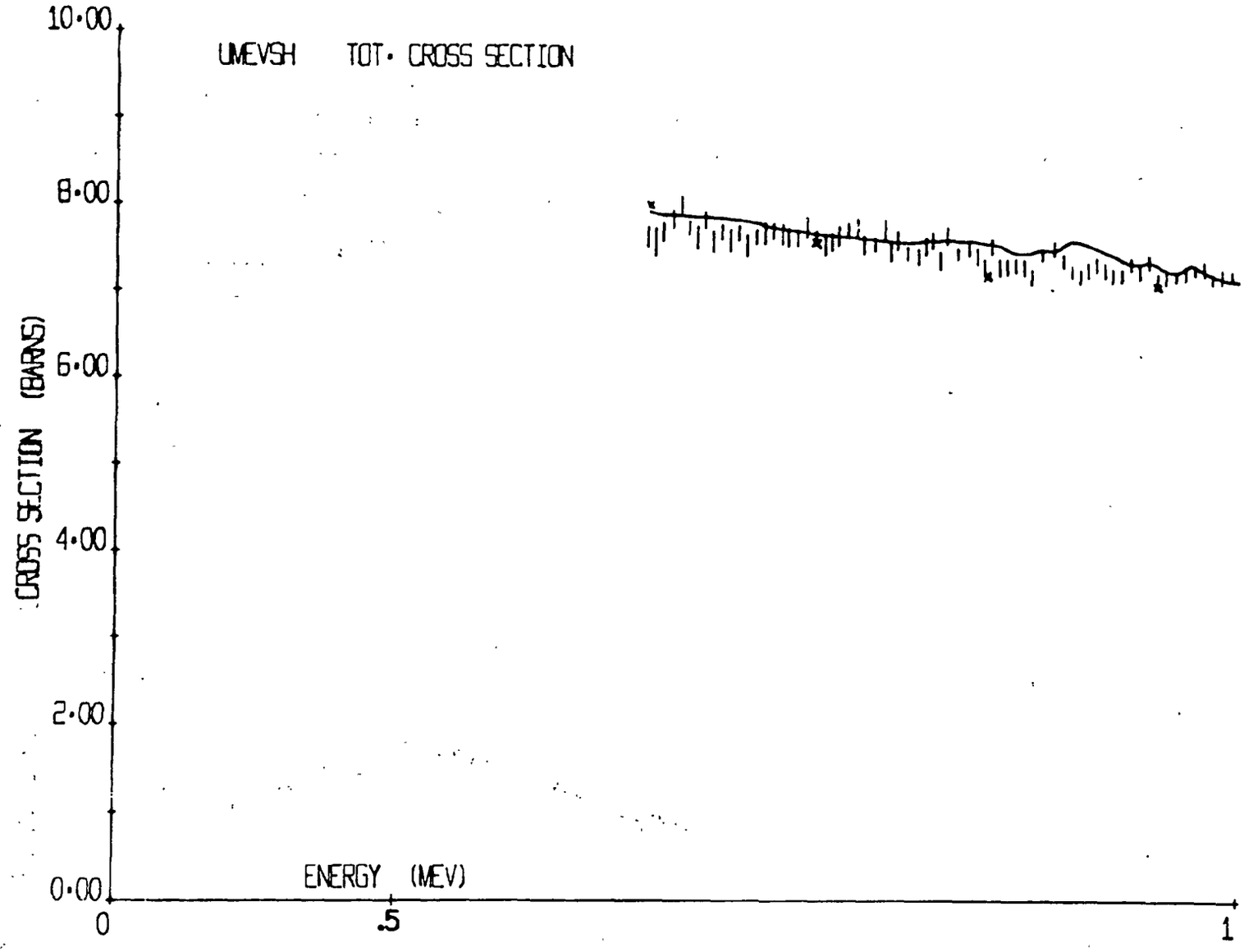

Figure A5 The ^{238}U total neutron cross section from 0.7—1.0 MeV. The solid curve is an "eyeball" fit through the data of Smith and Whalen.[1]

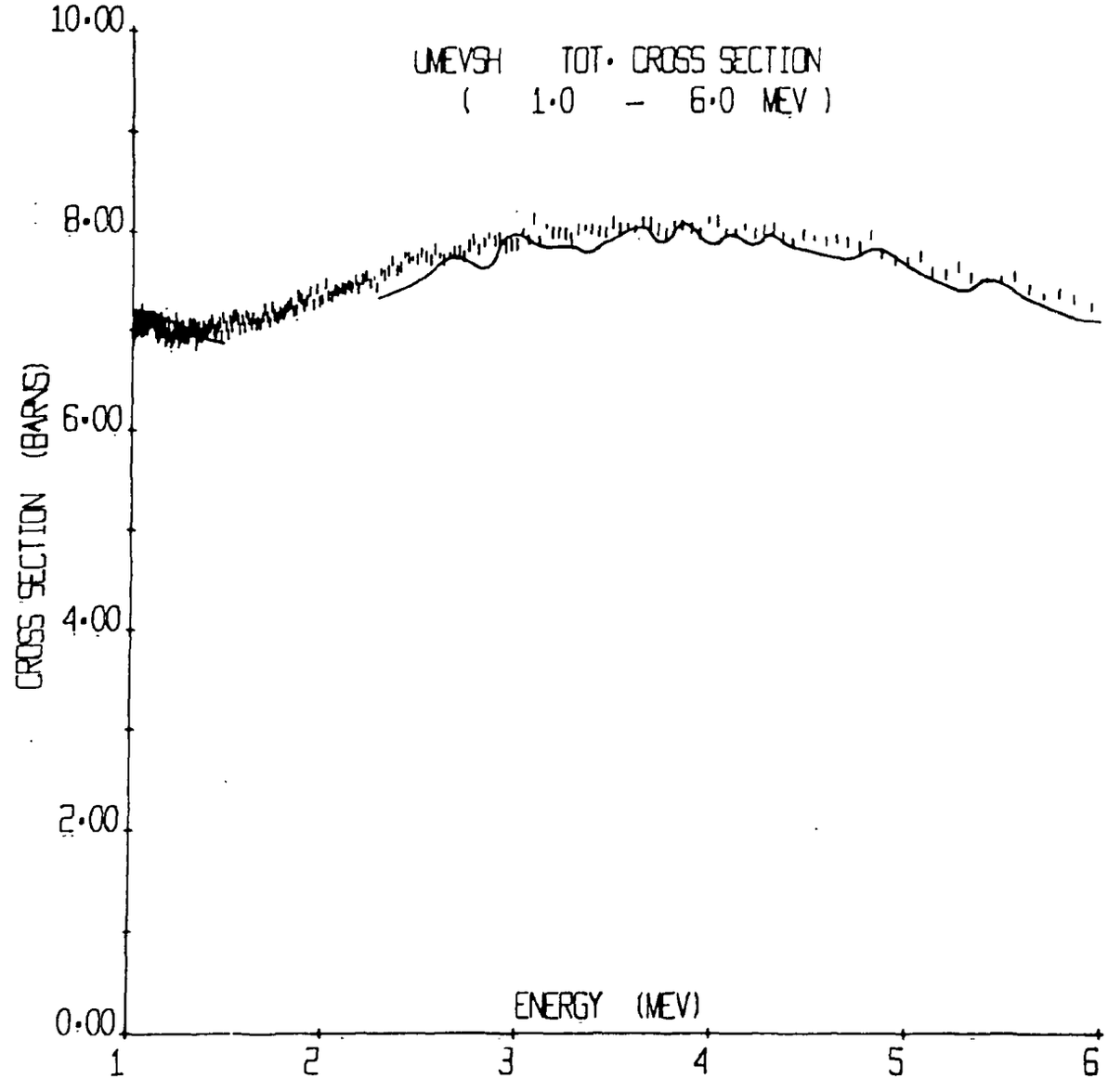

Figure A6 ^{238}U total neutron cross section from 1—6 MeV. The solid curve on the left is a fit to the data of Smith and Whalen.[1] The solid curve from 2.5—6 MeV is an "eyeball" fit to the data of Foster and Glasgow.[2]

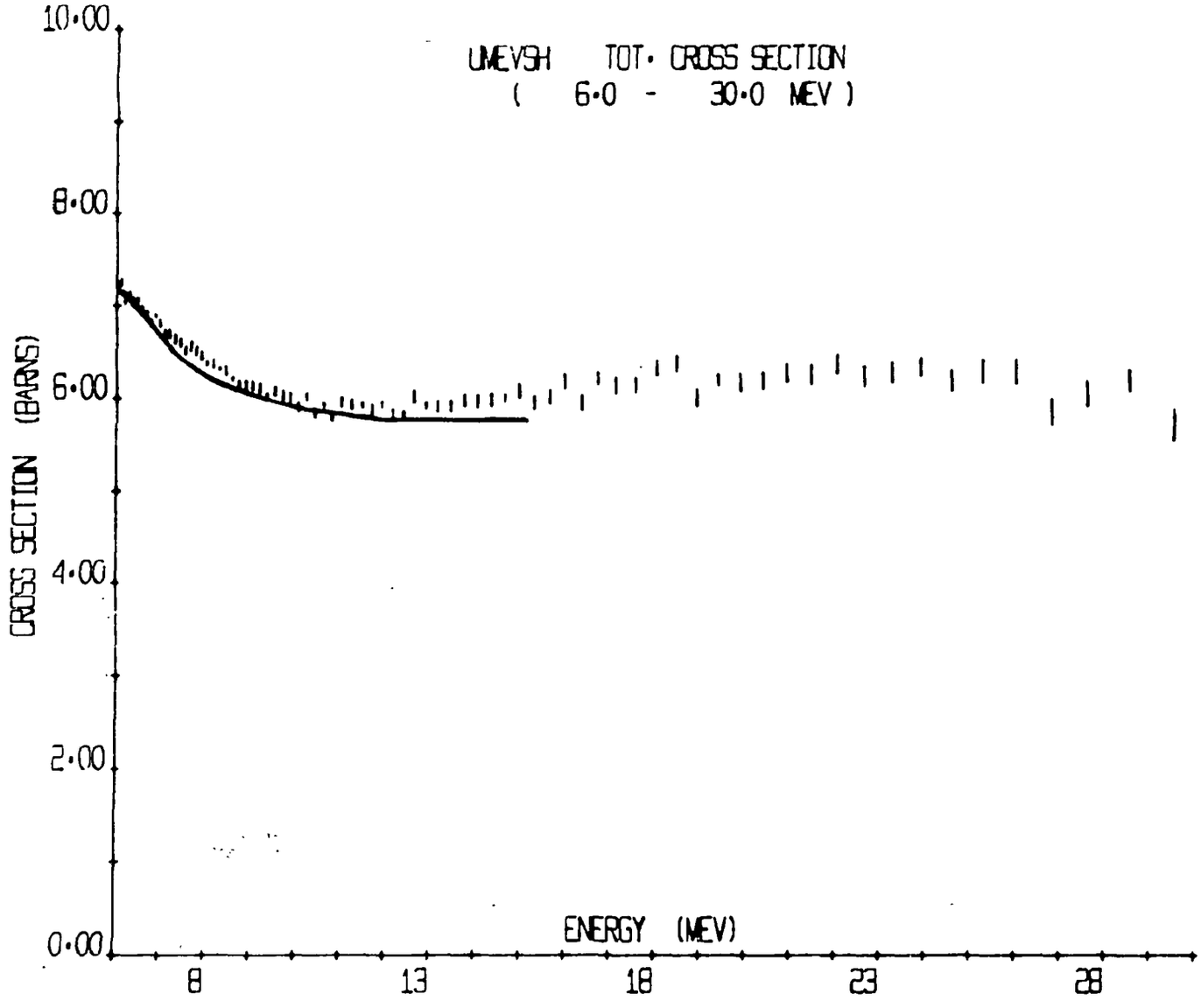

Figure A7 ^{238}U total neutron cross section from 6—30 MeV. The solid curve is a fit to the data of Foster and Glasgow.[2]

taken by other experimenters. The Brookhaven library furnished current date on ^{238}U. One set was taken by Smith and Whalen[1] and covered the energy range from 0.5 to 1.5 MeV. The other set was taken by Foster and Glasgow[2] and covered the energy range from 2.5 to15 MeV. Our data were about 1% lower than the Smith and Whalen data and about 1% higher than the Foster and Glasgow data. Detailed comparisons are shown in Figs. A5 to A7.

3. Total Neutron Cross Sections on ^{6}Li and ^{4}He From 0.7 to 30 MeV: Preliminary Report *
(C. A. Goulding, J. M. Clement and P. Stoler)

Total cross-section measurements of neutrons on ^{6}Li have recently been completed with a resolution of 0.13 ns/m. The sample consisted of enriched ^{6}Li (95.7%) encapsulated in Al cans. The sample thickness was 0.351 atoms/barn. The correction for sample impurity was achieved by subtracting off the ^{7}Li contributions using our previously measured ^{7}Li cross section.

Preliminary work has been done on obtaining the ^{4}He total neutron cross section. The sample consisted of one of the stainless tubes used in earlier experiments filled to a pressure of 1809 psi. This gave a sample thickness of .301 atoms/barn.

* Req. No. 97

4. Neutron Capture Measurements on ^{54}Fe, ^{58}Fe, ^{61}Ni and ^{64}Ni *
(R. W. Hockenbury, N. N. Kaushal, B. Ward and R. C. Block)

Capture measurements were made on ^{61}Ni, ^{64}Ni and ^{54}Fe using a new data acquisition program with automated sample cycling. A capture gamma pulse-height vs. time-of-flight measurement was made on ^{54}Fe to determine the detector efficiency for this voltage. A capture yield has been obtained for ^{54}Fe in the 8-30 keV region.

* Req. No. 102, 106, 107, 111, 120, 126

5. KeV Sub-Threshold Fission in ^{240}Pu *
(R. W. Hockenbury and R. C. Block)

At least 21 fission groups are observed in the sub-threshold fission cross section of ^{240}Pu from 750 eV to 30 keV. The average level spacing D_{II} of these fission groups is 710 $\pm$ 60 eV compared to a spacing D_{I} of 13.7 $\pm$ 0.5 eV for levels in the first minimum. This level spacing D_{II} corresponds to an excitation energy of 3.1 MeV, implying that the second minimum proposed by Strutinsky[1] is about 2.3 MeV above the first

* Req. No. 464, 471

---

1. A. B. Smith and D. W. Whalen, private communication to Brookhaven National Laboratory.
2. D. G. Foster and D. W. Glasgow, Phys. Rev., 3, 576 (1971).
3. J. M. Clement, P. Stoler, C. A. Goulding and R. W. Fairchild, Nucl. Phys. (in press).

minimum in ^{241}Pu. Fission widths are obtained for the Class I resonances below 2.5 keV (where the resolution is good). Fission widths for the Class II resonances have been obtained up to 10 keV by integrating over the Class I resonances in each fission group. The distribution of fission widths over the Class I resonances indicates very weak coupling between Class I and Class II states.

6. Iron-Filtered Neutron Beams - A New Approach to Precision Time-Of-Flight Cross-Section Measurements *
(R. C. Block, N. N. Kaushal and R. W. Hockenbury)

Iron filters varying in thickness from 2 to 20 inches were placed in the 25-meter spectrometer of the RPI LINAC; for filters 6 inches and thicker, over ten distinct neutron energy bands were observed below 1 MeV. In particular, the band at 24.3 keV is ~2 keV wide and is separated by more than 45 keV from the next nearest energy band. In the upper half of Fig. A8 are plotted the relative neutron intensities near 24 keV for neutrons filtered by 2, 8, 14 and 20 inches of 'pure' Armco iron. A ^{10}B-NaI detector was used for this measurement. For the thicker filters the peak counting rate is about 500 times greater than background (as measured in the wings), and this small background can readily be determined, permitting high accuracy cross-section measurements near 24 keV. Measurements using this technique have been made for the total cross section of iron near the resonance-interference minima (see next contribution).

For capture cross-section measurements, 8 inches of iron was used for the filter, and the 1.25-meter liquid scintillator was used to detect neutron captures. These results are plotted in the lower half of Fig. A8 for two relatively short runs on the LINAC with samples of depleted U and Ta. The high peak-to-background ratios of 46:1 for Ta, and 9:1 for U provide an ideal low-background environment for precision capture measurements with a minimum of time-dependent background effects (caused by neutrons scattered into the scintillator).

A preliminary filtered-beam capture measurement was carried out for the following samples: 0.020" Au, 0.020" In, 0.020" Ta and 0.030" depleted U (99.8% ^{238}U and 0.2% ^{235}U). The capture detection efficiency was obtained by measuring the capture pulse-height spectra and by extrapolating to zero bias. The ratios of the measured capture cross sections near 24 keV were determined to be

$\sigma_\gamma(U)$: $\sigma_\gamma(Au)$: $\sigma_\gamma(In)$: $\sigma_\gamma(Ta)$=(0.54): (0.68): (0.96): (1:00).

These ratios have not yet been corrected for multiple scattering, resonance self-shielding or gamma ray escape; an overall uncertainty of about ± 8% is estimated for each number.

* Req. No. 321, 336, 421, 422

1. W. M. Strutinsky, Nucl. Phys., A95, 420 (1967).

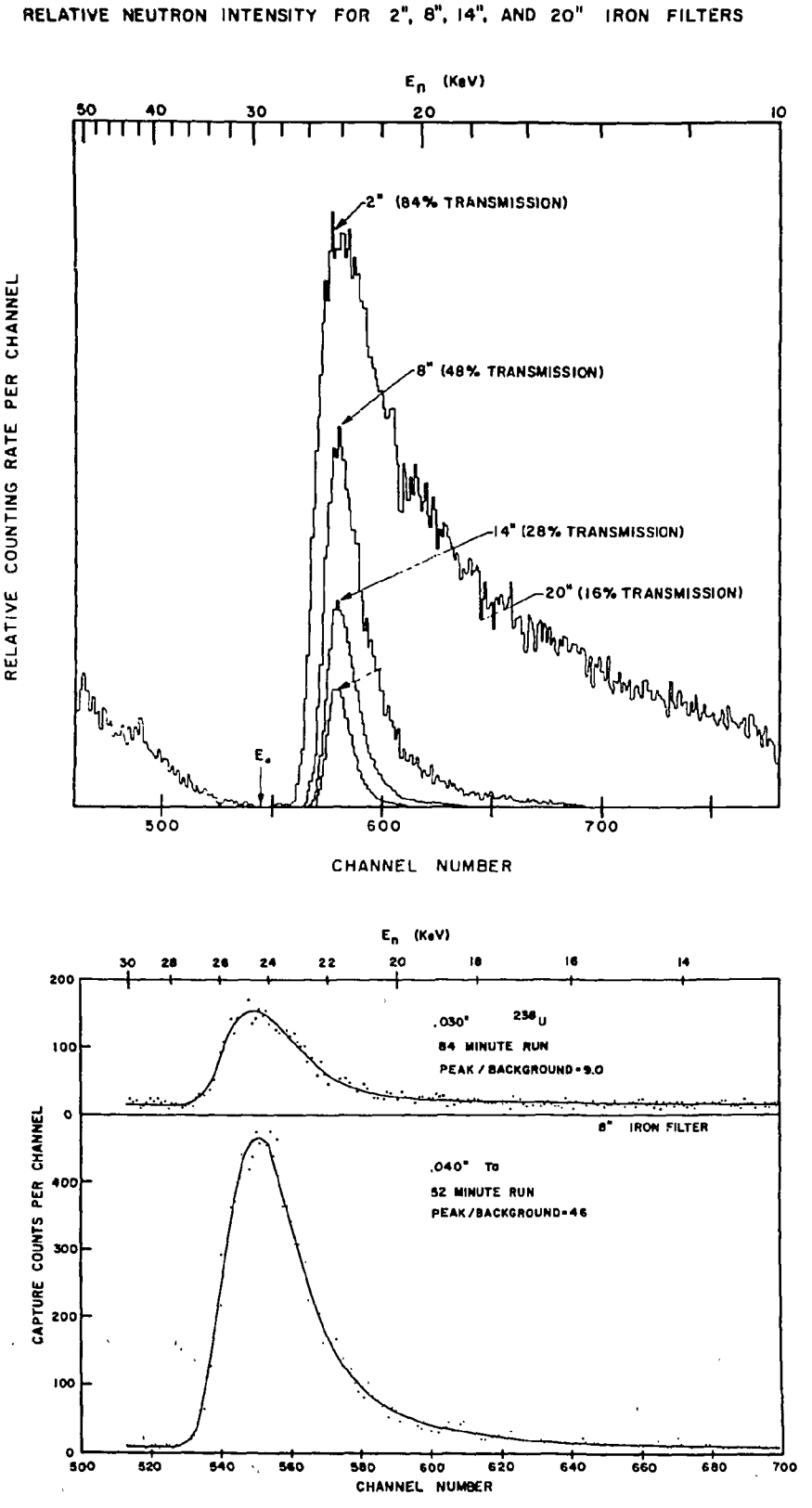
RELATIVE NEUTRON INTENSITY FOR 2", 8", 14", AND 20" IRON FILTERS
E_n (KeV)
50
40
30
20
10
2" (84% TRANSMISSION)
8" (48% TRANSMISSION)
14" (28% TRANSMISSION)
20" (16% TRANSMISSION)
E_o
RELATIVE COUNTING RATE PER CHANNEL
500
600
700
CHANNEL NUMBER
E_n (KeV)
30
28
26
24
22
20
18
16
14
.030" ^{238}U
84 MINUTE RUN
PEAK / BACKGROUND = 9.0
8" IRON FILTER
.040" Ta
52 MINUTE RUN
PEAK/BACKGROUND=46
CAPTURE COUNTS PER CHANNEL
200
100
0
400
300
200
100
0
500
520
540
560
580
600
620
640
660
680
700
CHANNEL NUMBER

Figure A8

7. The Iron Minimum At 24.3 KeV
(R. C. Block, K. Alfieri and P. J. Turinsky)

A measurement of the total cross section of type C1018 steel (nominal purity: 99.05%) was reported earlier. The total cross section of this steel is plotted in the upper portion of Fig. A9, and a minimum cross section of 0.50 ± 0.03 barn was reported for this material. Perey[1] pointed out that the bump at about 23.7 keV was probably due to the ~0.7% Mn content of the steel, and an additional low energy transmission measurement was carried out to determine the exact Mn content. This measurement was completed in December, and by comparing the observed area of the Mn resonance at 330 eV with the known Mn resonance parameters, we obtained a Mn content by weight of (0.82 ± 0.05)% in this batch of C1018 steel. This value is 15% greater than the nominal 0.71% previously assumed for this steel, but is within the range of Mn contents reported by manufacturers for this type steel.

A new transmission measurement was more recently carried out in which very pure (>99.9%) Armco iron was used both as the 14-inch filter and as the 5.95-inch transmission sample. In addition, a measurement with a pure Mn sample was interspersed with the iron measurement to determine both our resolution-broadened Mn cross section and the relative location of the iron minima and the Mn peak.

The total cross section for the Armco iron is plotted in Fig. A10, and we now observe both a deeper minimum of 0.41 ± 0.03 barn and a wider minimum. We have also corrected the steel C1018 cross section for the 0.82% Mn content (determined by us) and the 0.17% C, 0.031% Cr, 0.02% S, and 0.01% P content (reported by the manufacturer). This corrected iron cross section is plotted in the lower portion of Fig. A9. The shaded region essentially represents the range of uncertainty in the amount of Mn and C in the C1018 steel. This corrected iron cross section has a minimum of 0.40 ± 0.03 barn, and it is in excellent agreement both in shape and in magnitude with the pure Armco iron cross section of Fig. A10.

The effect of the 0.82% Mn in this batch of C1018 steel is seen to be quite dramatic in the upper curve of Fig. A9. Not only does the Mn increase the minimum cross section by about 20% from about 0.40 to 0.50 barn, but it also fills in part of the width of this valley in the iron cross section. This combination of raising the minimum and decreasing the width of the iron window has a great effect upon the transport of neutrons in iron assemblies. This explains the correct interpretation by the Fast Spectra group that for their C1018 steel assembly

---

1. F. Perey (private communication).
2. B. K. Malaviya et al., accepted for publication in Nucl. Sci. Eng. (1972).

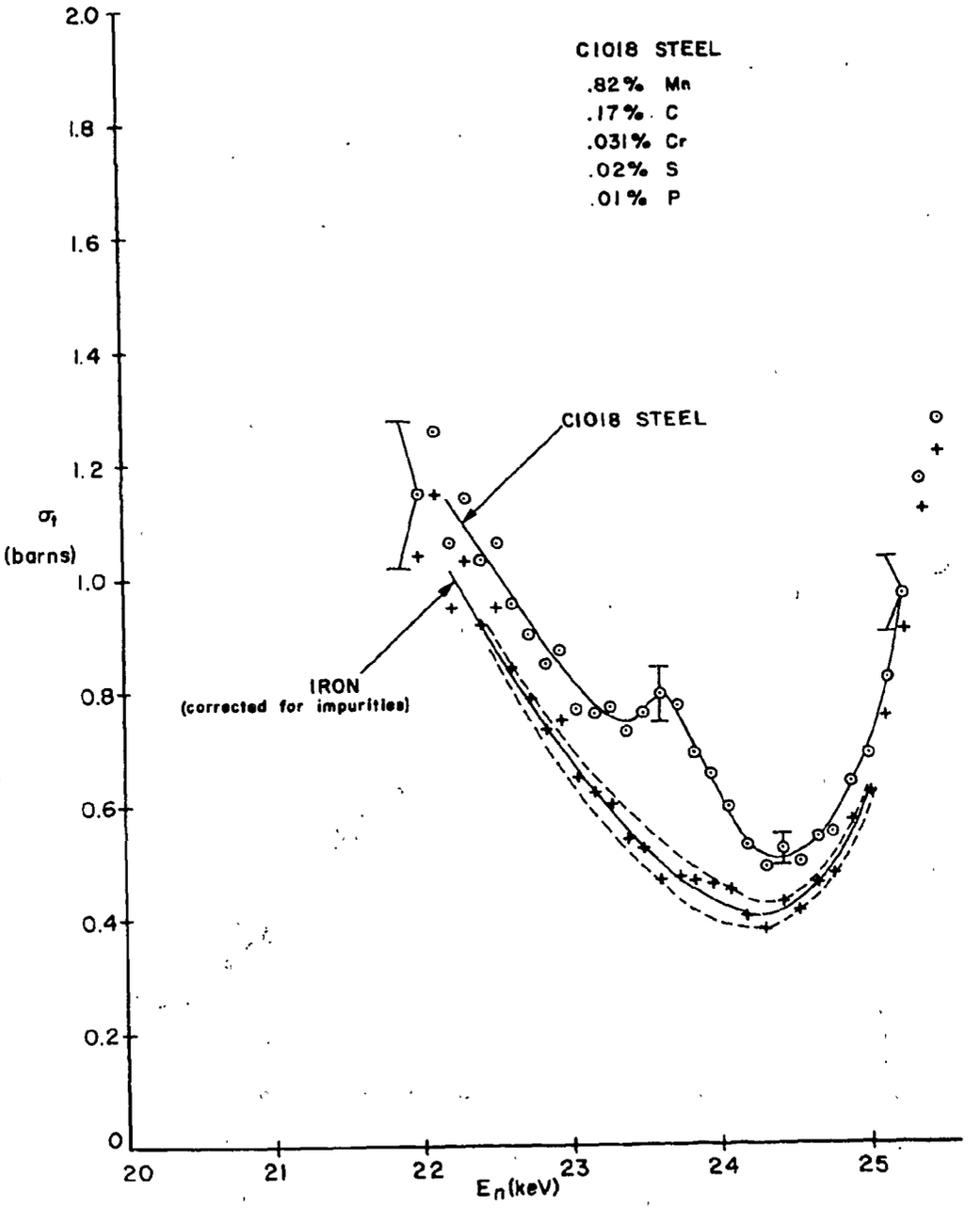

Figure A9 The upper set of points is the total neutron cross section near 24.3 keV of the C1018 steel used for the fast spectrum measurements.[2] The lower set of points has been corrected for impurities and represents the pure iron cross section. The shaded area surrounding the lower curve represents the range of uncertainty in the impurity corrections. The curves through the points are eyeball fits and the error bars represent standard deviations due to counting statistics.

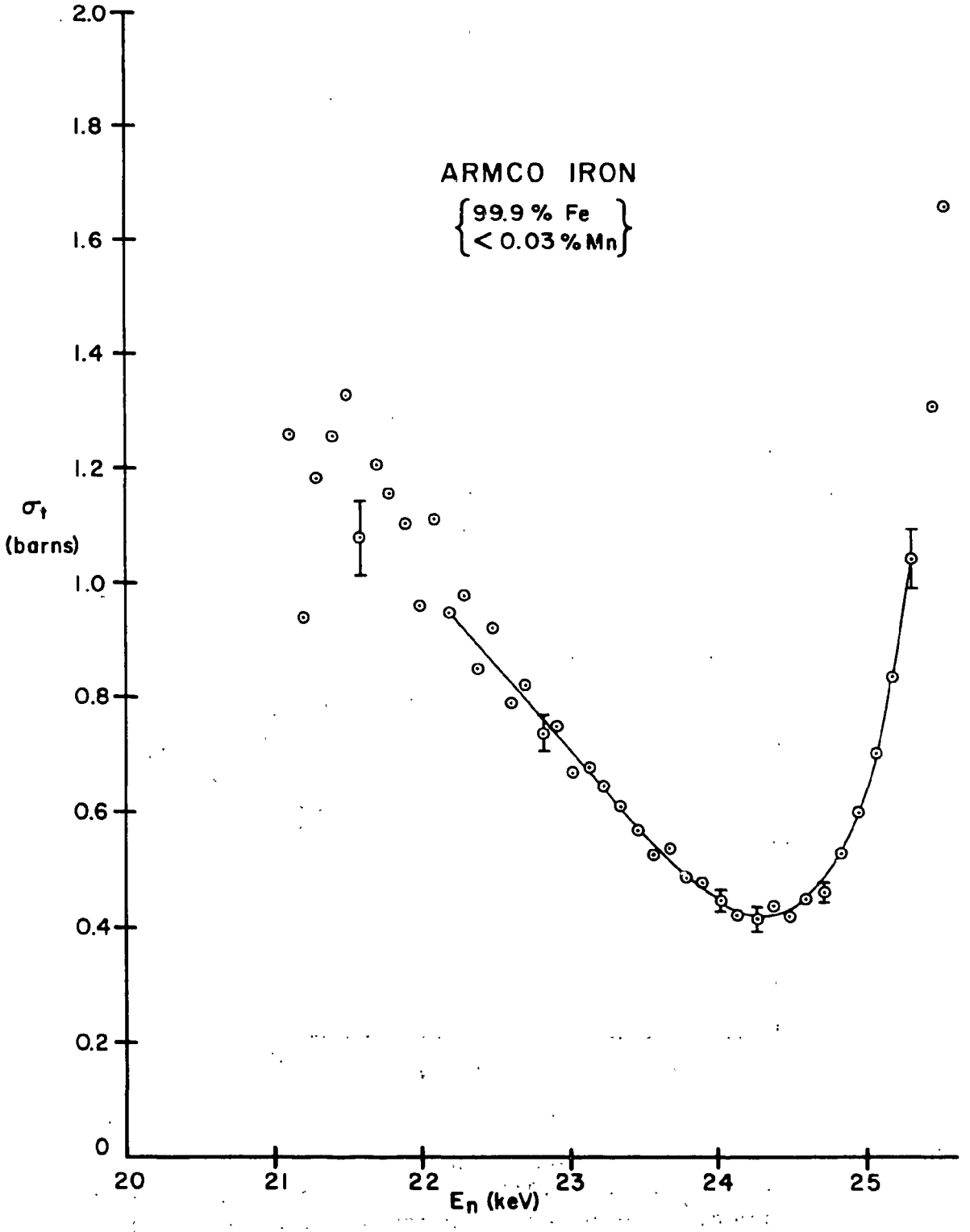

Fig. A10 The total neutron cross section of Armco iron (> 99.9% iron) near the 24.3 keV minimum. The curve through the points is an eyeball fit and the error bars represent standard deviations due to counting statistics.

they need a minimum cross section slightly in excess of 0.50 barn to fit their data.

The experimental results are summarized as follows:

Minimum Fe Cross Section:	0.41 ± 0.03 barn
Energy of Fe Minimum:	24.3 ± 0.1 keV
Energy of Mn Resonance Peak:	23.65 ± 0.05 keV
Difference in Energy Between FE Minimum and Mn Resonance Peak:	0.65 ± 0.11 keV

8. Differential and Area Analysis of Iron Total Cross Section Minima

(K. Alfieri and P. J. Turinsky)

Recent neutron spectrum measurements[1] have emphasized the importance of the minima in the total neutron cross section of iron. The RPI Linac has been employed to measure these minima from 20 to 1300 keV by thick sample (14" and 20") time-of-flight (TOF) transmission experiments on high purity Armco iron (>99.9% Fe, <0.03% Mn). Results for the 24.3 keV minimum are presented in the previous report. For cross section minima at higher energies, point values of cross section cannot be presented without resolution corrections. However, meaningful comparisons of experimental data and tabulated files can be made for integral properties of the cross section minima. Let $C(d,E)$ be the counts recorded for a sample of thickness d in TOF channel associated with energy E. Further, let E_L and E_U be energies bracketing a maxima in the $C(d,E)$ versus E curve, i.e. minima in the total cross-section. The ratios of areas under the $C(d,E)$ curve between E_L and E_U for two sample thicknesses is then approximately independent of resolution corrections and given by

$$R = \frac{\int_{E_L}^{E_U} C(d_1,E)\,dE}{\int_{E_L}^{E_U} C(d_2,E)\,dE} \cong \frac{\int_{E_L}^{E_U} e^{-\Sigma_t(E)d_1}\,dE}{\int_{E_L}^{E_U} e^{-\Sigma_t(E)d_2}\,dE} \quad . \quad (1)$$

We have compared the values of R obtained directly from our experiment, denoted R_{RPI}, to those calculated from the RHS of Eq. (1) employing total iron cross sections from files of Penny and Kinney[2] and Version 19,[3] denoted R_T.

In Table A1 are presented results in terms of relative percentage errors, defined by

$$\varepsilon = \frac{R_{RPI} - R_T}{R_{RPI}} \times 100\% \quad (2)$$

for various energy regions spanning minima. As stated (for d_1 = 14"

and d_2 = 20"), $\varepsilon > 0$ indicates that the data files generally underestimate the experimentally measured minima cross section; whereas, $\varepsilon < 0$ implies overestimation. From Table A1 we conclude that the Version 19 file is superior to the ENDF/B-III file in correctly representing the minima in Fe for most of the 20-400 keV energy range analyzed.

	PENNY AND KINNEY[2]		VERSION 19[3]	
ENERGY RANGE (KeV)	RELATIVE ERROR (ε)	COMPARISON WITH RPI'S CROSS SECTION	RELATIVE ERROR (ε)	COMPARISON WITH RPI'S CROSS SECTION
20.2-27.0	13 ± 1%	Under	-6 ± 1%	Over
67.9-71.8	12 ± 12%	-	-116 ± 32%	Over
76.8-83.0	-200 ± 1%	Over	-18 ± 1%	Over
114.8-130.5	-148 ± 4%	Over	-16 ± 2%	Over
132.0-139.6	-57 ± 1%	Over	-44 ± 1%	Over
155.2-169.2	-133 ± 2%	Over	-19 ± 1%	Over
171.3-187.6	26 ± 1%	Under	-13 ± 2%	Over
203.4-224.6	-202 ± 4%	Over	-19 ± 1%	Over
231.2-278.1	-112 ± 4%	Over	-8 ± 1%	Over
282.7-317.8	-103 ± 2%	Over	21 ± 1%	Under
323.3-387.9	-7 ± 1%	Over	4 ± 1%	-
419.2-505.2	-33 ± 4%	Over	-	-
527.9-740.2	-4 ± 2%	-	-	-
802.3-1413.2	-6 ± 5%	-	-	-

TABLE A1. Comparison of Experimental and Evaluated Total Iron Cross Sections Through Minima by Area Analysis.

9. Temperature-Dependent Transmission and Self-Indication Measurements Upon Depleted U in the Unresolved Region+ *
(T. Y. Byoun, R. C. Block and T. Semler#)

Neutron transmission and self-indication ratio measurements have been made at the RPI LINAC on depleted U (99.8% ^{238}U and 0.2% ^{235}U) up to 100 keV in order to investigate the temperature dependence of reson-

1. B. Malaviya et al., accepted for publication in Nucl. Sci. Eng. (1972)
2. S. K. Penny and W. E. Kinney, Trans. Am. Nucl. Soc. 14, 410 (1971).
3. C. Lubitz, Private Communication (1971).

ance self-shielding. These measurements were carried out at 77°K, 295°K, and 973°K. The experimental results are plotted in Fig. A11. The linear thermal expansion of the U samples was measured to be (1.7 ± 0.1)% between 295°K and 973°K, and -(0.20 ± 0.02)% between 295°K and 77°K.

The average cross section and strength functions for s- and p-wave neutrons in the energy range 1 keV to 70 keV and the limited range 5.0 to 5.6 keV have been determined from the room-temperature transmission data by using the least squares method. A stochastic sampling method using the computer code DAISY[1,2] was used to analyze the temperature-dependent transmission data in the energy range 5.0 keV to 5.6 keV. The results and the parameters used are listed in Table A2.

* Req. No. 421, 422, 427

10. Measurement of Nubar for ^{233}U and ^{235}U
(R. L. Reed and R. C. Block)

Instrumentation improvements have been completed and tested. Data are now being taken for ^{235}U in the neutron resonance energy region. Some data have also been obtained in the keV region using the filtered beam method. The ^{233}U measurements in the resonance region will be started shortly with the ORNL multiplate fission chamber.

11. Neutron Capture Gamma Ray Experiments Using the PDP-9/L Data Acquisition System *
(P. H. Brown, J. R. Tatarczuk and W. R. Moyer)

The two-parameter hardware and corresponding software developed for use on the PDP-9/L computer (with disk) is now complete. This will allow study of neutron capture gamma rays at the 12.65-meter flight station with up to 81 regions of neutron time of flight. Each region will have 2048 channels of ADC pulse height (gamma ray energy)information.

The hardware to be used consists of several versatile devices. The RPI Time Digitizer will be used to measure the neutron time-of-flight with 62.5 nsec channel widths. A high speed hardware sorter determines what region of time-of-flight the clock data word represents. The ADC data is also hardware sorted into one of 32 core data buffers depending on its bit configuration. These hardware sort processes allow the data

---

+Supported by NASA Grant NGR 33-018-134.

#NASA Lewis Research Center, Cleveland, Ohio 44135

1. T. Y. Byoun, R. C. Block and T. Semler, Conf.-710301, Vol.2, 3rd Neutron Cross Sections and Technology Conference (1970).
2. T. Semler, The DAISY Program, NASA TND-5827.

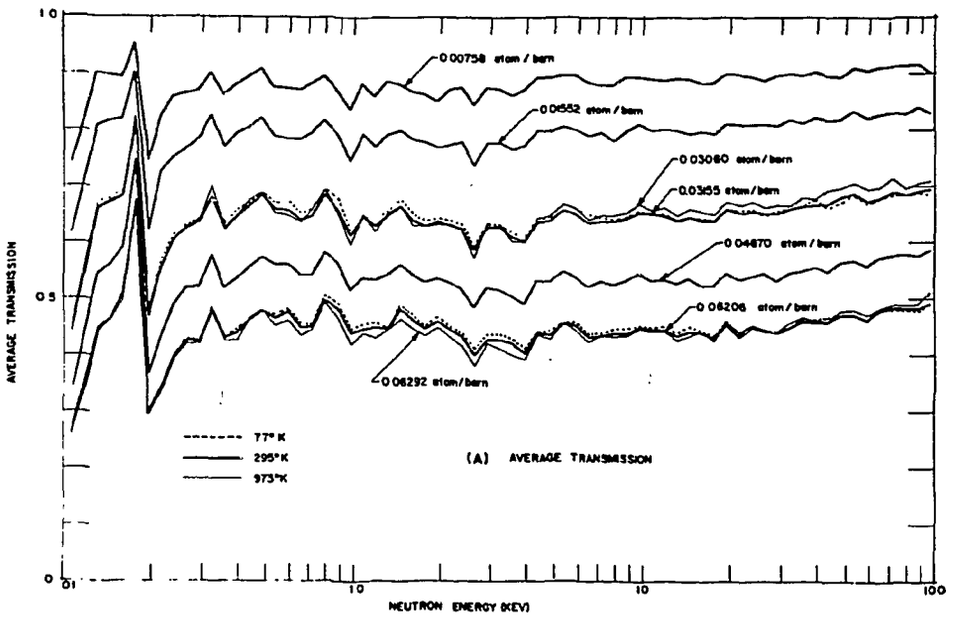
1.0
0.5
0
AVERAGE TRANSMISSION
0.00758 atom / barn
0.01552 atom / barn
0.03080 atom / barn
0.03955 atom / barn
0.04670 atom / barn
0.06206 atom / barn
0.06292 atom/barn
77°K
295°K
973°K
(A) AVERAGE TRANSMISSION
0.1
1.0
10
100
NEUTRON ENERGY (KEV)

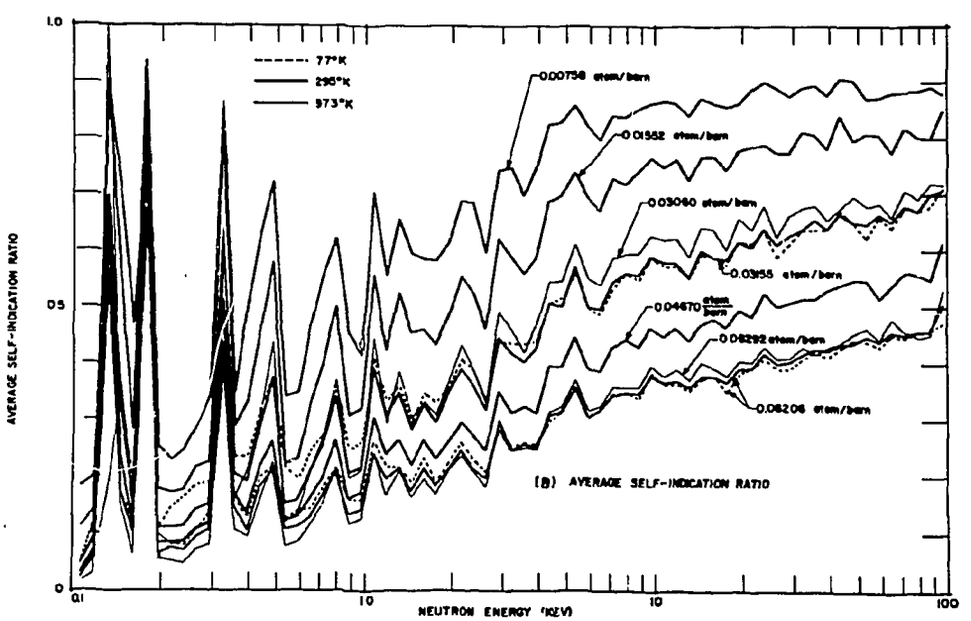
1.0
0.5
0
AVERAGE SELF-INDICATION RATIO
77°K
295°K
973°K
0.00758 atom/barn
0.01552 atom/barn
0.03080 atom/barn
0.03955 atom/barn
0.04670 atom/barn
0.06292 atom/barn
0.06206 atom/barn
(B) AVERAGE SELF-INDICATION RATIO
0.1
1.0
10
100
NEUTRON ENERGY (KEV)

Figure A11

TABLE A2, TRANSMISSION DATA ANALYSIS

Sample Thickness (a) (atom/barn)	Sample Temp. (°K)	Energy Range 5.0 to 5.6 keV				Energy Range 1 to 70 keV
		Effective Ave. Cross Section (barns)				
		Experimental	Analytical (e) Calculation	DAISY Code (c) Calculation	Parameters used in the DAISY Code	Strength Functions (d),(e) determined from Analytical Calculation
0.03155	77	12.8 ± 0.3		12.70	S_o (b) = 0.35 x 10^{-4}	$S_o = (0.91 \pm 0.12) \times 10^{-4}$
0.03155	295	13.3 ± 0.2	13.33	12.91	$\bar{D}_s$ = 17.8 eV	
0.03060	973	12.8 ± 0.3		13.11	σ_p = 10.0 barn	$S_1 = (2.3 \pm 0.6) \times 10^{-4}$
0.06206	77	12.6 ± 0.3		12.39	$\bar{\Gamma}_\gamma$ = 0.023 eV	
0.06206	295	12.7 ± 0.1	12.71	12.62	Debye Temp.=200°K	
0.06292	973	12.6 ± 0.1		12.88		

(a) Measured at 295°K

(b) Local value of S_o in the energy range 5.0 keV to 5.6 keV

(c) Doppler broadening of p-wave resonance has not been considered

(d) For a given potential cross section of 10.8 barn and the formula used is:

$$\langle\sigma_t\rangle = 2\pi^2 \lambda\lambda_1 \sum_{\ell=0}^{1} (2\ell+1) S_{\ell} \cos 2\xi_\ell + \sigma_p$$

(e) Least squares fit by using the following approximate formula:

$$\langle T\rangle = e^{-n_i\langle\sigma_t\rangle}\left\{1 + \frac{1}{2} n_i^2 \langle(\sigma_t - \langle\sigma_t\rangle)^2\rangle - \frac{1}{6} n^3{}_i \langle(\sigma_t - \langle\sigma_t\rangle)^3\rangle\right\}$$

to be stored rapidly on-line on the PDP-9/L disk. The system is capable of storing a few hundred cts/sec of TOF X PHA data. In addition, a single parameter program (up to 8192 channels of TOF or ADC) allows count rates up to 1500 cts/sec to be stored on-line on the disk.

*Req. No. 361, 367, 395, 400

B. NUCLEAR THEORY

1. Correlation Between Neutron and Radiative Widths

(M. Lubert, N. C. Francis, and R. C. Block)

The $^{57}Fe(\gamma,n)$ and $^{53}Cr(\gamma,n)$ reactions have been recently measured. No correlations between the neutron and radiative widths were observed for ^{53}Cr. The experimental results at RPI[3] for Cr do exhibit strong correlations. In order to understand this paradox, the $^{57}Fe(\gamma,n)$ cross section was computed using both the channel direct and the compound nucleus reaction amplitudes. The channel contribution was obtained for final S-wave continum states using R-matrix phase shifts. The channel partial radiative widths for transitions to the ground state were obtained from area analyses of the (γ,n) data. The results of this investigation are interesting from several points of view. The theoretical calculation predicts a level at 80 keV with Γ_γ=0.14eV. This level is not observed in the experiments. The theoretical line shapes are asymmetric. It is expected that levels with large channel components would exhibit a marked asymmetry. The shapes computed for single levels show constructive interference on the low energy side of the resonance and destructive interference above the resonance. The level-level interference introduced by the R-matrix further distorts this line shape. The experimental cross sections do not in general look markedly asymmetric nor does the cross section appear to go through a minimum above the resonance as predicted by the theory. This can be attributed to resolution broadening and the compound nucleus resonance amplitude contribution. The interference between the channel and compound nucleus amplitudes affects the line shape. Further, it is possible that a level would not appear in the experimental results if the amplitudes cancelled.

There are no correlations between Γ_n and $\Gamma_{\gamma o}$ for the four levels where the experiments agree. Similar results for these relatively isolated levels were obtained from the theoretical results. However, inclusion of the eleven levels for which interference was significant yielded a rank and product-moment coefficients for ^{56}Fe of 0.97 and 0.25 respectively. The conclusions thus far are that analysis of experiments must include level-level effects and that compound nucleus and channel interference can be of considerable importance when the channel contribution is large.

---

1. R. J. Baglan, UCRL-50902, August 1970.

2. H. E. Jackson, E. N. Strait, PR C 4, 1314, 1971.

3. R. G. Stieglitz, R. C. Block, R. W. Hockenbury, RPI-328-218, January 1 - March 31, 1971.

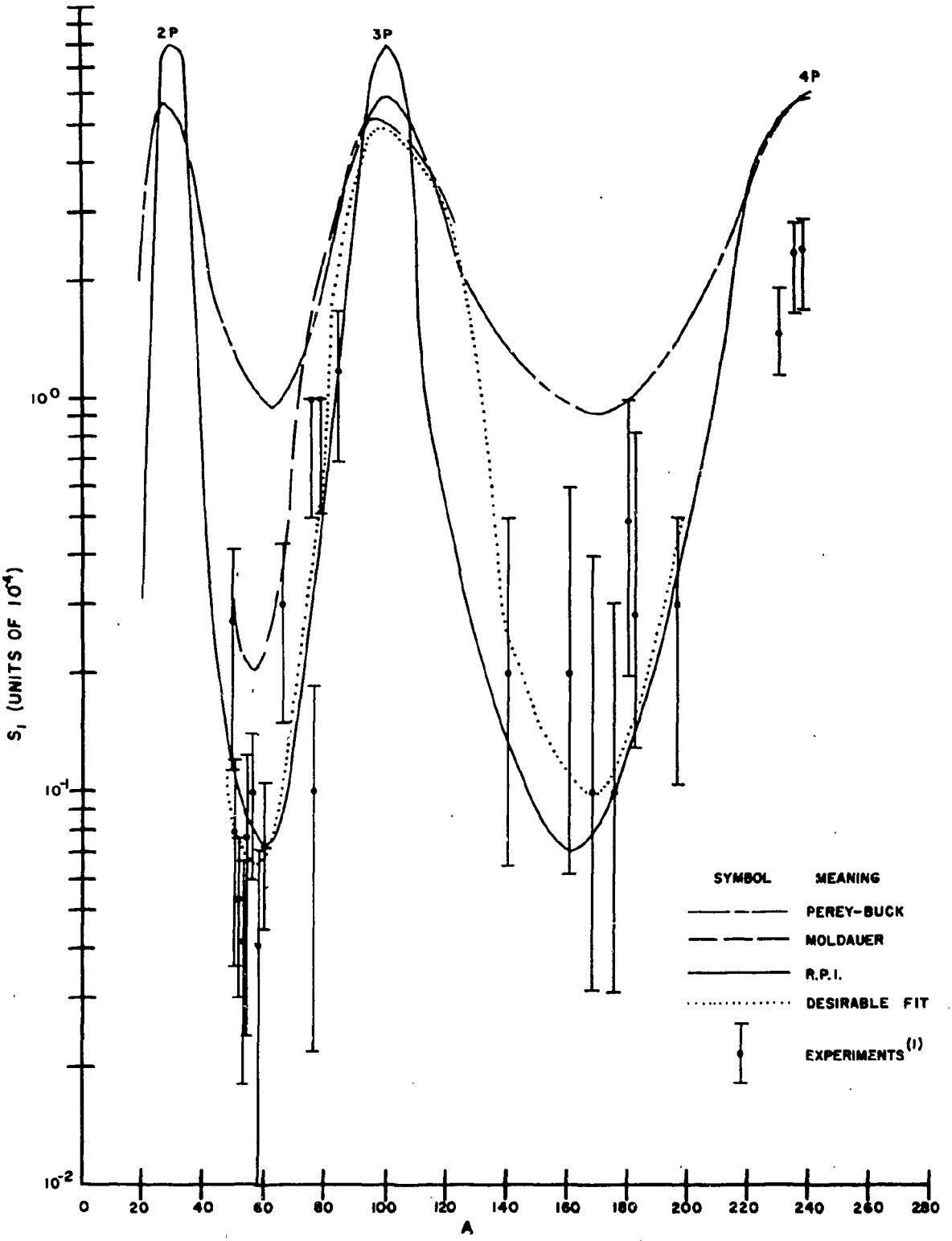

Figure B1

Neutron p-wave strength function.

2. The P-Wave Neutron Strength Function Near Mass Number 55 and 160

(P. J. Turinsky and R. C. Block)

Recent capture measurements at RPI[1,2,3] have revealed deep minima in the p-wave neutron strength function, S_1, in the mass number 55 and 160 range. Figure B1 presents RPI and other laboratories data in these mass ranges, with the curve labeled "Desirable Fit" representing a smooth fit through the vast peak S_1 data. Employing the code JUPITOR, spherical optical model calculations using the potential

$$V(r) = -Vg(r,a_v) - 4iWa_w p(r,a_w) - V_{so}(\vec{\sigma}\cdot\vec{l})\lambda_\pi^2 \frac{1}{r} p(r, a_{V_s}),$$

where $g(r,a) = [1 + \exp\{(r-R)/a\}]^{-1}$

$p(r,a) = dg(r,a)/dr$

$r = r_o A^{1/3}$

was employed to obtain global optical parameters to fit S_1. Our calculational results are shown on Figure B1 for the parameters

V=52 MeV, W=4 MeV, V_{so} = 6 MeV, a_v = o.40 fm,

a_w = 0.25 fm, a_V = 0.65 fm, and r_0 = 1.27 fm.

The S_1 minima are fit quite satisfactory, but S_1 peaks are observed to narrow. For these same parameters, the s-wave strength function, S_o, exhibited too narrow maxima peaks and approximately, 2.5 deeper minima than observed. The potential scattering radii, R', oscillated considerable with respect to A. We summarize that S_o, S_1 and R' cannot be fit simultaneously for the present well potential. Concluding, we observed that the parameter a_v and W are required to be decreased to fit S_1, in contrast to S_o and R', for global fits.[4,5,6]

---

1. Hockenbury, Bartolome, Tatarczuk, Moyer and Block, Phys. Rev. 178, 1746 (1968).
2. Bartolome, Hockenbury, Moyer, Tatarczuk and Block, Nucl. Sci. & Eng. 37, 137 (1969).
2. Stieglitz, Hockenbury and Block, Nucl. Phys. A163, 592 (1971).
4. Buck and Perey, Phys, Rev. Letters 8, 444 (1962).
5. P. Moldauer, Nucl. Phys. 47, 65 (1963).
6. A. P. Jain, Nucl. Phys. 50, 157 (1964).

C. INTEGRAL CHECKS ON CROSS SECTION DATA

Fast Neutron Spectra in Bulk Media

(E. R. Gaerttner, N. N. Kaushal, B. K. Malaviya, A. N. Mallen and M. Becker).

Measurements and analysis of fast neutron spectra in homogeneous assemblies of materials pertinent to LMFBR, are continuing. These spectra are compared with transport calculations with a view to evaluate cross section data in various data files. Results of such studies on iron and depleted uranium have been reported in journal publications.[1,2] Analysis of data from an aluminum assembly is continuing. Currently, measurements are being made on a large assembly of metallic sodium.

---

1. B. K. Malaviya, N. N. Kaushal, M. Becker, E. T. Burns, A. Ginsburg and E. R. Gaerttner, Nucl. Sci. Eng., 47, 329 (1972).
2. N. N. Kaushal, B. K. Malaviya, M. Becker, E. T. Burns and E. R. Gaerttner, Nucl. Sci. Eng. (1972) to be published.

TRIANGLE UNIVERSITIES NUCLEAR LABORATORY

A. NEUTRON AND FISSION PHYSICS

1. Resonance Cross Section Measurements with Continuous Beam (J. G. Malan,* W. F. E. Pineo, E. G. Bilpuch, H. W. Newson)

An improved version of our multilevel R-Matrix code is used to analyze natural Sr(82% Sr^{88}) total cross section data. The analysis is now complete and the previously reported difficulty in differentiating p- and d-wave resonances up to 850 keV has been eliminated. All strong resonances are due to s- and p-waves. A detailed paper comprising the experimental s- and p-wave reduced widths with the already published[1] theoretical doorway predictions is in preparation.

2. Resolved Neutron Total Cross Sections and Intermediate Structure (B.-H. Choi, W. F. E. Pineo, M. Divadeenam,** H. W. Newson)

R-Matrix analysis has been extended up to 4 MeV for the natural Si(92% Si^{28}) total cross section data measured at NBS.[2] For the purpose of analysis the effect of the inelastic channel ($\sim$ 1.9 MeV) is ignored. This procedure is adequate for the detection of doorway state effects. Actually strong doorway effects are observed only below the neutron inelastic threshold.

As observed earlier there is no ambiguity between p- and d-waves, but similar shapes for d- and f-wave neutrons complicate the analysis. However shell and optical model arguments favor the f-wave rather than d-wave, and R-Matrix shape analysis suggests that there are two strong f-wave resonances. A short paper[3] giving the details of R-Matrix shape fits to Si data (in the energy range 1.5 - 2.0 MeV) has been submitted to the Budapest Conference as a contributed paper. Fig. A-1 presents R-Matrix fits to the cross section data.

---

* Now at the Atomic Energy Board of the Republic of South Africa

** North Carolina Central University, Durham, N. C.

1 M. Divadeenam, W. P. Beres, H. W. Newson, Ann. of Phys. 69, 428 (1972)

2 R. B. Schwartz, R. A. Schrack, and H. T. Heaton, II, Bull. Am. Phys. Soc. 16, 495 (1971)

3 B.-H. Choi, M. Divadeenam, W.F.E. Pineo and H. W. Newson, submitted to the Budapest Conference on Nuclear Structure Studies with Neutrons, July 31-August 5, 1972

Natural S neutron cross section data measured at Duke are being analyzed to extract resonance parameters beyond 700 keV. Analysis of Bi^{209}, Li^{6} and Li^{7} cross section data is planned.

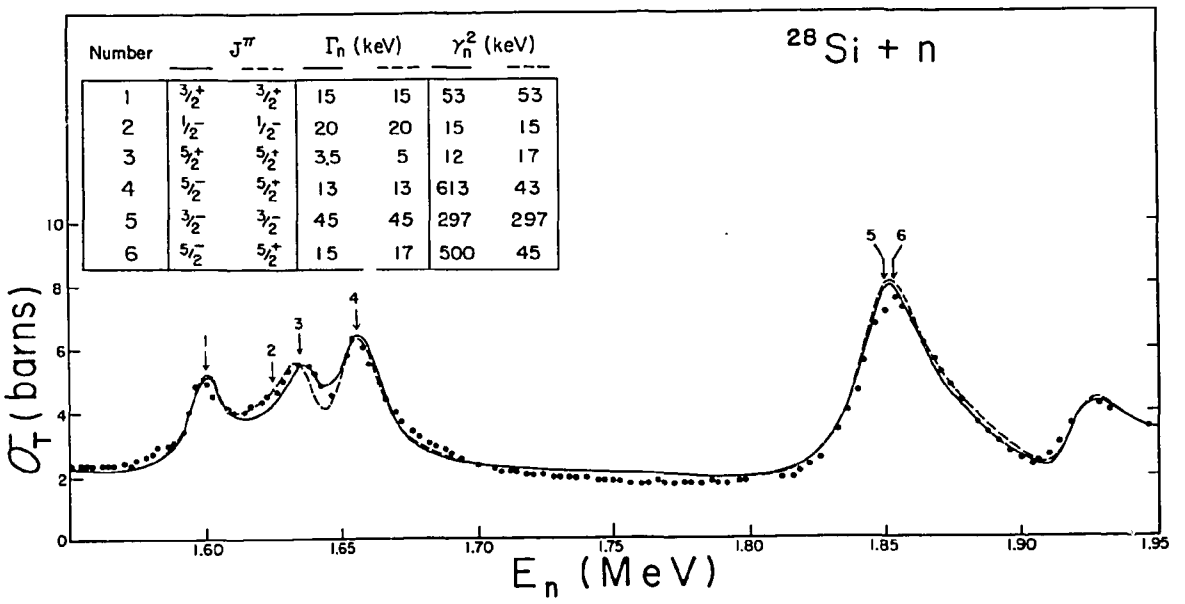

3. Averaged Cross Sections, Strength Functions, and Intermediate Structure (W. F. E. Pineo, M. Divadeenam, E. G. Bilpuch, H. W. Newson)

Preparation of papers on this topic based on the theses of M. Divadeenam and W. F. E. Pineo and later work has been inactive since the last report but will be resumed when classes are over.

4. Shell Model and Particle-Vibration Model Calculation of Neutron Resonances and Intermediate Structure (M. Divadeenam, W. P. Beres,* H. W. Newson)

In the s-d shell region, the neutron s-, p-, d- and f-wave doorway state energies and escape widths for $Si^{29}(Si^{28}+n)$ have been calculated. Unusually

* Wayne State University, Detroit, Michigan.

strong mixing of the basic states is required to account for doorways in the low neutron energy region. To predict p-wave reduced widths comparable to those observed, a small value (42-45 MeV) of the real Woods-Saxon depth (Vo) is required to generate the continuum neutron wave functions. However for the s-wave case, the predicted doorway reduced widths are insensitive to the choice of Vo. The observed strong Si^{29} s-wave, p-wave and f-wave doorway effects will be compared to 2p-1h predictions. In addition, Optical Model calculations indicate that the trend of the integral plot of $\Sigma g_J \gamma_n^2$ can be reproduced only with a small imaginary potential ($W < 1$ MeV). Sr^{89} behaves similarly.

Mo^{93} and Mo^{99} $1/2^+$ 2p-1h doorway escape widths are calculated and an extension to the p-wave case is in progress. The particle-vibration model will also be applied to these compound nuclei.

Since the last report no progress has been made for the Ca^{40}+n, Ni^{56}+n, and Ni^{60}+n cases. The combined experimental Ca^{40} results of Duke[1] and Karlshrue[2] will be utilized to compare with the 2p-1h calculations which are still in progress. S^{33} doorway calculations are also in progress. They will be compared to the results of R-Matrix fits to the experimental data. See above.

Based on the Particle-Vibration model the predicted $1/2^+$ Pb^{207} and Pb^{209} doorway spreading widths $\Gamma_d^{\downarrow}$ are found to agree well with the corresponding experimental values. In particular the Pb^{207} $1/2^+$ doorway spreading width is 10 times as large as that of Pb^{209}. These results were presented at the 1972 Washington APS meeting.[3] A short paper based on these results will be submitted for publication. An extension of the $\Gamma_d^{\downarrow}$ prediction for the other Pb doorways is planned.

An application of the Particle-Vibration model to the γ-channel (in the Pb region) was undertaken. Even though the unperturbed $(4^+ \otimes g_{9/2})_{1/2^+}$ doorway has the right escape and damping widths small impurities of certain configurations in the doorway state wave function are required for the prediction of γ-ray widths ($Pb^{207}(\gamma,n)$). A paper giving the details of these results will be submitted to Physical Review Letters.

---

[1] C. D. Bowman, E. G. Bilpuch and H. W. Newson, Ann. of Phys. 17, 319 (1962)

[2] J. Nebe and G. J. Kirouac, Nucl. Phys. A185, 113 (1971)

[3] W. P. Beres, M. Divadeenam, Bull. Am. Phys. Soc. 17, 579 (1972)

5. Charged Particle Fission (F. O. Purser, J. R. Boyce, D. E. Epperson, T. D. Hayward, E. G. Bilpuch, H. W. Newson, H. W. Schmitt*, R. Bass* *)

a. Cross Section Measurements

The cross section measurements for proton induced fission of the Uranium isotopes are complete and are being prepared for publication. Analysis of the data is continuing with a major effort being devoted to development of a general computer analysis program based on the statistical model. The formalism chosen uses single particle level densities for the neutron evaporation channels but modified level densities for the fission saddle point states. Either a single or double peaked fission barrier can be chosen. Using total reaction cross sections calculated via the optical model and neutron-fission branching ratios developed in the new program, contributions to the total fission cross section from first, second, third and fourth chance fission may be calculated. By iterative comparison with one measured fission yield, a self consistent set of neutron emission to fission branching ratios and appropriate fission barrier parameters for the Neptunium isotopes ^{233}Np-^{239}Np can be obtained. Various level density formalisms can be tested against the data and provision has been made to include pre-compound and direct reaction contributions.

b. Angular Distributions

These have been analyzed to obtain $\overline{K}_o^2$ and effective nuclear temperatures at the fission saddle points and will be reported with the cross section data.

c. Mass and Kinetic Energy Distributions

This work has been relatively inactive for the past report period, but will occupy more of our experimental time in the coming period with the completion of the analysis program referred to above which is essential for unfolding the mass and kinetic energy systematics for fission individual compound nuclei at the higher excitation energies.

---

* Oak Ridge National Laboratory, Oak Ridge, Tennessee

** University of Frankfurt, Frankfurt, Germany

6. A Fermi Gas Model for Thermal Neutron and Spontaneous Fission (H. W. Newson)

Either a liquid drop (LDM) or Fermi gas (FGM) model for highly excited nuclei leads to practically the same prediction (See Bethe 1936) without shell corrections. They are much easier for FGM, but more difficult corrections to LDM should lead to the same result. The FGM alone predicts sawtooth neutron emission, asymmetric yields, and slightly distorted fragments, but FGM statistics predict yields more like (p,f) than (n_{th},f). This discrepancy is ascribed to sensitivity to shell closure in the liquid phase very close to threshold where changes $\simeq$ 1/10 MeV are so important that selection rules may be expected. One finds that the most favored masses are those where all possible shells at 28, 50 and 82 can be filled in both fragments with the available nucleon numbers. For other masses, yields are reduced $\simeq$ 1/10 for each missing filled shell. This selection rule is in accord with the rapid change of peak to valley ratio with energy, lack of asymmetric fission of stable targets, and of the sudden appearance of three (or more) humped spontaneous fission in Fm. The selection rules are explained by the high surface tension of nuclei near closed shells, and their durability, by the properties of doorway states of doubly magic clusters and other kinematic effects.

7. Analysis of Nucleon-^{4}He Scattering Below 20 MeV (Th. Stammbach,* R. L. Walter)

Available cross-section and polarization data for p-^{4}He and n-^{4}He have been fit in the R-matrix formulation. Best available phase shifts for n-^{4}He are tabulated. This work appeared in Nuclear Physics A180 (1972) 225.

8. Polarization in (^{3}He,n) Reactions on ^{9}Be, ^{11}B and ^{13}C Below 4 MeV (R. S. Thomason,** L. A. Schaller,+ Th. Stammbach, R. L. Walter)

The experimental and DWBA results for the ^{9}Be(^{3}He,n) reactions have appeared in Nuclear Physics A176 (1971) 535. Interpretation of the ^{11}B(^{3}He,n) and ^{13}C(^{3}He,n) will depend on the findings of the higher energy work discussed below.

---

* Now at Schweiz. Inst. f. Nuklearphysik, Zurich, Switzerland

** Now at G. E. Co., Miss. Test Facility, Bay St. Louis, Mississippi

\+ Now at Yale University, New Haven, Connecticut

9. Polarization in (^{3}He,n) Reactions from ^{12}C and ^{13}C from 8 to 22 MeV (T. C. Rhea, R. A. Hardekopf,* P. W. Lisowski, J. M. Joyce, R. Bass, R. L. Walter)

Data has now been obtained for the ^{12}C(^{3}He,n) reaction in 2 MeV steps from 8 to 22 MeV and ^{13}C(^{3}He,n) at 12, 16 and 20 MeV. The data indicates that a direct reaction analysis should be meaningful above 16 MeV for ^{12}C and at all energies for ^{13}C. Initial DWBA calculations appear to give good agreement for ^{12}C but the same optical model parameters (obtained from ^{12}C(^{3}He, ^{3}He)^{12}C scattering) do not work for the ^{13}C(^{3}He,n) polarization. More analyses will follow (^{3}He,^{3}He) and (^{3}He,n) cross-section measurements for ^{13}C targets.

10. Neutron Polarization from (d,n) Reactions on ^{24}Mg, ^{28}Si, and ^{40}Ca (J. Taylor,** Th. Stammbach, R. L. Walter)

This work (for $E_d < 4$ MeV) has been accepted for publication in Nuclear Physics.

11. Polarization of Neutrons from ^{10}B, ^{11}B and ^{13}C(d,n) Reactions for $E_d < 4$ MeV (M. M. Meier,+ R. L. Walter)

This work has been accepted by Nuclear Physics.

12. The j-dependence in the ^{11}B(d,n$_0$) and ^{11}B(d,n$_1$) Reactions (J. Taylor, G. Spalek,++ Th. Stammbach, R. A. Hardekopf, R. L. Walter)

This work was conducted from 7 to 12 MeV. A final manuscript is still nearly completed. (See Madison Polarization Symposium Report.)

13. The ^{9}Be(d,$\vec{n}$) Reaction from 3 to 4 MeV (G. Spalek, J. Taylor, R. A. Hardekopf, Th. Stammbach, R. L. Walter

This work was covered in one portion of the thesis of G. Spalek. A copy of his Ph.D. thesis abstract follows:

---

* Now at Los Alamos Scientific Laboratory, Los Alamos, New Mexico

** Now at Armed Forces Institute of Pathology, Washington, D. C.

\+ Now at National Bureau of Standards, Gaithersburg, Md.

++ Now at the University of Wisconsin, Madison, Wisconsin

"Accurate neutron polarization angular distributions the $D(d,n)^3He$ reaction were measured at 6, 8, 10, 12 and 14 MeV. The results show large polarizations near 45° c.m. increasing from a value of .13 at 6 MeV to .44 at 14 MeV. A shift of the peak polarization from 45° c.m. towards 40°c.m. as the energy increases is also seen. Comparison of the obtained polarization distributions with those from the D(d,p)T reaction shows that the neutron polarizations are consistently smaller up to 12 MeV. The implications of this with respect to the concept of charge symmetry of nuclear forces are discussed. In addition the usefulness of the $D(d,n)^3He$ reaction as a source of polarized 8 to 15 MeV neutrons is also discussed.

Polarization angular distributions were measured for the five most energetic neutron groups from the $^9Be(d,n)^{10}B$ reaction at 3 and 3.5 MeV bombarding energies. All these transitions involve the transfer of an $\ell_p = 1$ proton. A decrease in structure of the polarization distributions with increasing excitation of the residual nucleus was observed at both energies. At angles less than 50°c.m. the n_0 group polarization becomes more negative with increasing energy and there is evidence that the $j_p = 1/2$ transfer component of the n_1 group polarization is positive.

Cross sections for $^9Be(d,d)$ elastic scattering were obtained and optical model parameters extracted. Agreement between DWBA calculations using these parameters and $^9Be(d,n)$ polarization and cross section data was minimal. In particular, the j dependence of the neutron polarization was not reproduced. Reasons for the above are discussed."

The $^9B(d,d)$ data with an optical model analysis and the $^9Be(d,n)$ polarization data with DWBA comparisons will be written up for publication.

14. Polarization of Neutrons from the D(d,n) Reaction from 6 to 22 MeV
(G. Spalek, R. A. Hardekopf, P. W. Lisowski, T. C. Rhea, Th. Stammbach, J. M. Joyce, R. L. Walter)

A portion of this data was described in the Ph.D. thesis abstract of G. Spalek. The higher energy data obtained with the pulsed Cyclo-Graaff beam is included in the thesis of R. A. Hardekopf. The abstract follows:

"The neutron polarization from the $D(d,n)^3He$ reaction has been measured at 45 degrees c.m. for incident deuteron energies between 16 and 22 MeV. In addition, a polarization angular distribution was measured at 18 MeV. The results show that the 45 degree c.m. polarization remains above 0.35 in this energy range, but the peak polarization has shifted to near 40 degrees c.m. The usefulness of $D(d,n)^3He$ as a source of 16 to 22 MeV polarized neutrons is discussed.

Accurate angular distributions of the analyzing power in the T(p,d)D reaction were measured at eight energies from 6.7 to 14.7 MeV. By reciprocity, these distributions are the same as the proton polarizations of the D(d,p)T reaction from 2.0 to 14.0 MeV. Comparisons are made with the polarizations from the mirror reaction $D(d,n)^3He$, and good agreement is found when the reactions are compared at the same exit channel energies. The implications of this are discussed in the light of other recent comparisons which suggest that differences in these mirror reactions may be a violation of charge independence of nuclear forces.

Very accurate polarizations in T(p,p)T elastic scattering were obtained in conjunction with the T(p,d)D measurements. Single energy complex phase shift parameterizations were made at five energies from 9.4 to 14.7 MeV. No resonance structure was seen for any of the phase shifts in this energy range."

This neutron polarization data and the analyses have been submitted to Nuclear Physics.

15. Neutron Scattering Studies Utilizing Polarized Neutrons Produced With Polarized Deuteron Beams (P. W. Lisowski, T. C. Rhea, R. L. Walter, T. B. Clegg)

Polarized neutrons with $\simeq 0.5$ have been obtained through the use of the $D(\vec{d},\vec{n})^3He$ transfer reaction at 0°. (Simmons et al. at Los Alamos showed that neutrons with a high polarization could be produced in this fashion.) The scatterer was ^3He gas contained in a high pressure scintillation cell at 50 atm. The neutron background was greatly reduced using the 0° neutrons over previous methods where polarized neutrons produced in reactions induced with unpolarized incident charged

particles have been employed. $^3He(\vec{n},n)$ data were obtained at 8 and 12 MeV for comparison to earlier ^3He data as well as the $T(\vec{p},p)$ data reported below. Our new results show that the earlier $^3He(n,n)$ data had systematic discrepancies and that the differences in $^3He(\vec{n},n)$ and the $T(\vec{p},p)$ are indeed small over the angular range from 50° to 140° lab. This experiment marks the beginning of a new era in neutron polarization (scattering) studies but until our polarized-ion source works more reliably in the 20 na region, it may be unwise to devote more accelerator time to these studies.

16. Survey of Neutron Polarization Studies (R. L. Walter)

A review paper surveying all neutron polarization work from the past ten years has been prepared for Nuclear Spectroscopy II (J. Cerny, editor). Another paper of a similar nature for Reports on Progress in Physics is underway.

B. CHARGED PARTICLE REACTIONS

1. Fine Structure of Isobaric Analogue States - Charged Particle Scattering (E. G. Bilpuch, T. Dittrich, J. D. Moses, D. Outlaw, N. H. Prochnow,* W. M. Wilson, G. E. Mitchell, H. W. Newson)

a. The Chromium Isotopes

A paper covering measurements on the isotopes $^{50,52,54}Cr$ entitled "Fine Structure of Analogue States in ^{51}Mn, ^{53}Mn, and ^{55}Mn" has been published--Nuclear Physics A175, 556 (1971).

b. The Iron Isotopes

A paper entitled "Fine Structure of an Analogue State in ^{59}Co" has been accepted for publication in Nuclear Physics. The following is the abstract of that paper:

> "Differential cross sections were measured at four angles for proton elastic scattering from ^{58}Fe at energies from 2.65-3.11 MeV. Using the TUNL 3 MV Van de Graaff accelerator and high resolution analyzer-homogenizer system, a total resolution of 300-350 eV was achieved for thin solid targets

* Now at Wisconsin State University, River Falls, Wisconsin

of enriched iron ^{58}Fe. The analogue of the $3/2^-$ third excited state of ^{59}Fe shows a fine structure pattern. The spectroscopic factor and Coulomb energy difference were extracted for this analogue state. Spins, parities and widths were determined for approximately 125 resonances."

c. The Titanium Isotopes

A paper on ^{48}Ti has been submitted for publication. The following is the abstract of that paper:

"Differential cross sections were measured for $^{48}Ti(p,p)$ and $^{48}Ti(p,p_1)$ at four angles between E_p = 1.8 and 3.1 MeV. The overall energy resolution was 250-350 eV. Spins, parities, total widths and partial widths were extracted for 301 resonances. Two analogue states were observed, and spectroscopic factors and Coulomb energies determined for these analogue states. A large, positive correlation was observed between the elastic and inelastic widths for one analogue; no correlation was observed away from the analogue. The spacing distributions of the $s_{1/2}$ and $p_{1/2}$ resonances (after correction for the energy dependence of the average spacing) are in reasonable agreement with the Wigner distribution. $s_{1/2}$, $p_{1/2}$ and $p_{3/2}$ proton strength functions were determined."

A paper on ^{46}Ti is being prepared for publication. This summer it is planned to study ^{50}Ti plus proton reaction. The previous data on ^{50}Ti were obtained over a narrow energy range in the vicinity of one analogue state. The data on the Ti isotopes have proven so interesting that we shall try to study a wide energy range on ^{50}Ti. Subtraction may be necessary to eliminate the effects of ^{48}Ti resonances. However, the procedure for performing this type of subtraction has been established and proven quite successful in the analysis of our ^{46}Ti data.

d. The Calcium Isotopes

After appreciable difficulty in obtaining good data for ^{44}Ca (ascribed mainly to contaminants in the carbon backings), we have succeeded in obtaining very good elastic and inelastic scattering data for ^{44}Ca. Differential cross sections were measured at four angles (160°, 135°, 105°, and 90°) for the $^{44}Ca(p,p)^{44}Ca$ reaction over the proton energy range 1.5-3.0 MeV. The $^{44}Ca(p,p')^{44}Ca$ reaction was also studied; the inelastic yields (on resonance) were appreciable above 2.6 MeV. Thin (1-2 $\mu g/cm^2$) solid targets of enriched ^{44}Ca were

used and a total energy resolution of 300-350 eV was achieved. Approximately 350 resonances were observed. The data have been analyzed from 1.5-2.6 MeV and spins, parities and widths (single channel case, so the proton partial width is essentially equal to the total width) have been determined for 223 resonances, including 85 $p_{1/2}$ levels, 60 $s_{1/2}$, 45 $p_{3/2}$ and 33 d levels (3/2 or 5/2). The following analogue states were identified: the $p_{3/2}$ analogue of the 6th excited state in ^{45}Sc at E = 1.646 MeV with Γ_p = 650 eV, the $p_{1/2}$ analogue of the 8th excited state at E_p = 2.024 MeV with Γ_p = 1.259 keV. The $s_{1/2}$ state at 2.232 MeV is tentatively identified as the analogue of the 10th excited state.

The remaining 400 keV of data will be analyzed in the near future. A similar experiment is planned for ^{42}Ca.

A talk has been presented on this work at the Washington American Physical Society meeting: Bull. Am. Phys. Soc. 17, 535 (1972).

e. Analysis of Fine Structure Distributions of Analogue States

This work has been delayed--we hope to finish the analysis of all of our fine structure distributions this summer.

f. Sulfur and Silicon Isotopes

Elastic scattering experiments are being considered on the Silicon and Sulfur isotopes. At present we are learning to make suitable thin targets for elastic scattering measurements.

2. Fine Structure of Analogue States--The Capture Reaction (G. E. Mitchell, R. O. Nelson, W. C. Peters, J. F. Wimpey, E. G. Bilpuch)

The capture program has (experimentally) moved past the exploration stage. Topics of interest include analogue to anti-analogue transitions, channel correlations, comparison of M1 matrix elements with Gamow-Teller beta decay strengths and a search for intermediate structure. This work may also prove of value in our statistical studies, since we observe many more levels than observed in our high resolution elastic scattering. As a byproduct we obtained very good data on the gamma rays following inelastic scattering, even for cases where no inelastic scattering was observed with charged particle detectors.

a. Calibration of Ge(Li) Detector

The primary calibration was made with the $^{27}Al(p,\gamma)$ reaction,

using the 992, 1831, and 1388 keV resonances. We also used ^{56}Co and ^{66}Ga sources which we made on the tandem using the (p,n) reaction. An absolute measurement was performed using ^{22}Na and a Ge(Li) -Ge(Li) coincidence technique. NaI(Tl) - Ge(Li) coincidences were performed on the decay of the 992 keV resonance in Al. We have an overall absolute efficiency curve for the 80 cc Ge(Li) from .5 MeV to greater than 10 MeV.

Absolute energy calibrations have also been performed for ^{54}Fe, ^{54}Cr and ^{58}Fe using the standard 992 keV resonance in ^{27}Al.

b. ^{54}Fe

Decay of the $p_{3/2}$ analog at E_p = 2.242 MeV has been studied. This state is not fragmented since the level spacing of this isotope is quite large. Analysis is in progress.

c. ^{54}Cr

The very interesting decay of the fragmented $p_{3/2}$ analogue at E_p = 2.010 MeV (analogue of the ground state of ^{55}Cr) has been completely remeasured under improved experimental conditions and with the detector at 55°. Analysis is in progress. A preliminary study of this analogue has been published: "Channel Correlation Effects for Fragmented Analogue States", Statistical Properties of Nuclei (Plenum Press, New York, 1972) p. 299.

d. ^{58}Fe

The $p_{3/2}$ fragmented analogue at $E_p \simeq$ 2.24-2.30 MeV has been thoroughly studied. Analysis is in progress.

e. ^{62}Ni

The $p_{3/2}$ fragmented analogue at $E_p \simeq$ 2.4 - 2.5 MeV has been studied. In addition the gamma decay of a large number of $s_{1/2}$ resonances has been studied to consider the apparent anomaly in s-wave strength near 2.44 MeV. Analysis is in progress.

3. Statistical Properties of Nuclei from Proton Resonance Reactions (E.G. Bilpuch, G. E. Mitchell, J. D. Moses, H. W. Newson)

a. General

Statistical aspects of the high resolution proton resonance data measured at this laboratory over the past several years are being investigated. The primary interest in these data when they were obtained was the study of analogue states. The study of statistical properties was delayed until a sizeable body of data was accumulated. A report[1] on some preliminary results was presented at the International Conference on Statistical Properties of Nuclei in Albany, N. Y. A brief overview of the data is given below, followed by discussion of specific topics.

The data consist of proton elastic scattering excitation functions measured on most of the stable even-even isotopes in the mass region A = 40 to A = 64. Most of the data were measured over the proton energy range 2 to 3 MeV, with overall energy resolution 300 to 400 eV. Proton inelastic scattering and (p,n) excitation functions were measured simultaneously with the elastic scattering whenever the partial widths in these channels became appreciable.

The complexity of the measured excitation functions varies greatly; the number of analyzed resonances ranges approximately from 15 to 300 per MeV. A systematic increase in level density with increasing neutron number in a given isotopic series is noted; this is expected from the increase in proton separation energy with increasing neutron excess in the compound nucleus.

A multi-level, multi-channel analysis of these data has yielded resonance parameters for > 2000 levels. Resonance energies, partial and total widths and reduced widths, orbital angular momenta, and in most cases total angular momenta have been assigned by this analysis. All but a very few of the observed resonances have $\ell_p = 0$, 1, or 2. Most of the resonances of uncertain J have $\ell_p = 2$.

The detailed analysis of this large body of data is clearly a major undertaking. At the present only first steps have been taken in this analysis; most of the preliminary conclusions are tentative.

b. Proton Strength Functions

Preliminary results on $1/2^+$, $1/2^-$, and $(3/2^+ + 5/2^+)$ proton

[1] E. G. Bilpuch, Statistical Properties of Nuclei. J.B. Garg (Plenum Press, New York, 1972) p. 99.

strength functions were presented at the recent Washington meeting of the American Physical Society. The $1/2^-$ strength functions show systematic variations with isospin and with A, exceeding those predicted by optical model calculations using standard parameters based on higher energy data. Local strength functions in some cases show systematic variation with excitation energy in a particular compound nucleus, although this effect is sometimes masked by statistical fluctuations. Fluctuations larger than expected from Porter-Thomas statistics are observed in some cases, notably in the ^{46}Ti(p,p) $1/2^-$ strength function.

c. Distribution of Proton Reduced Widths

A computer code has been written to analyze the distribution of proton reduced widths, based on a method due to Garrison.[1] It is assumed that all levels whose reduced width lies below some minimum value will be missed. The remaining reduced widths are assumed to follow a chi-squared distribution of ν degrees of freedom, truncated at the minimum reduced width and renormalized. The value of ν and a correction factor for the average reduced width are then determined by the method of maximum likelihood. Preliminary results indicate that the distribution of most of the $1/2^+$ levels is consistent with a Porter-Thomas distribution. For favorable cases, the technique should yield estimates of the number of missed levels.

d. Nuclear Level Densities

Level densities can be determined directly from the data in cases where essentially all of the levels are observed, for example in the vicinity of a strong analogue state. Estimates of the number of missed levels from an analysis of the reduced width distribution should yield estimates of level densities when up to $\sim$ 50% of the resonances are missed. A program of using (p,γ) data to supplement the elastic scattering data for level density determinations is under consideration.

4. Studies of The Gamma Decay of Excited Levels of ^{51}Ti (G. P. Lamaze*, C. R. Gould, N. R. Roberson, D. R. Tilley)

Preparation of a paper on this subject, based on the Ph.D. dissertation of G. P. Lamaze, is in progress. The following is the abstract of the dissertation:

---

* Now at the National Bureau of Standards, Washington, D. C.

[1] J. D. Garrison, Annals of Physics 30 (1964) 269

"The excited states of ^{51}Ti populated with the reaction ^{50}Ti(d,pγ)^{51}Ti have been studied with the angular-correlation method which utilizes a geometry of axial symmetry. The observed protons were detected in an annular semiconductor counter positioned at 180° relative to the beam direction. From the analysis of the experimental angular correlations, and in conjunction with known ℓ_n values for ^{51}Ti, a spin and parity assignment of $9/2^+$ was established for the level at 3774 keV. Correlations for other levels did not yield unique spin assignments. Branching ratios were measured for the levels at 1167, 2144, 2198, 2907, 3174, 4162, 4592, 4747, 4810, 4882, 5139, 5214, and 5440 keV. New levels were observed at 2346 keV and 5440 keV.

The reaction ^{48}Ca(a,nγ)^{51}Ti was also used to populate many levels of ^{51}Ti. The resultant decays were studied with n-γ coincidence techniques using a 30 cm^3 Ge(Li) detector, and with γ-γ coincidence techniques using 30 cm^3 and 80 cm^3 Ge(Li) detectors. Five previously unreported levels were observed at 2733, 2755, 2922, 3235, and 3636 keV. Additionally, tentative assignment of two previously unreported levels was made. These levels are at 3473 and 3619 keV excitation."

5. Mean Lifetimes in ^{27}Si (E. C. Hagen, C. R. Gould, N. R. Roberson, D. R. Tilley)

These results have been published in Particles and Nuclei 3, 92 (1972).

6. Gamma Decay of Excited Levels of ^{38}Ca (E. C. Hagen, C. R. Gould, N. R. Roberson, D. R. Tilley)

The reaction ^{36}Ar(τ,nγ)^{38}Ca is being used to populate some of the low-lying states of ^{36}Ca. Preliminary n-γ coincidence measurements have been completed at a beam energy of 9 MeV.

The target was prepared by ion implantation with ^{36}Ar beams of 500 keV to 2500 keV obtained from the 4 MeV Van de Graaff accelerator. A Ta foil was the host material.

7. Lifetime Measurements in ^{42}Sc (C. R. Gould, J. D. Hutton, N. R. Roberson, D. R. Tilley)

This work has been submitted for publication in The Physical Review.

8. Electromagnetic Transition Studies in ^{57}Ni (C. R. Gould, N. R. Roberson, G. E. Mitchell, D. R. Tilley)

This work has been published in Phys. Rev. C5, 281 (1972).

9. High Resolution Search for the $J^\pi = 0^+$, $T = 1$ Level in ^{26}Al Near 3.7 MeV (G. A. Bissinger, C. R. Gould)

This work has been published in Particles and Nuclei 3, 105 (1972).

10. Lifetimes of Levels in ^{26}Al (C. R. Gould, D. R. Tilley, J. D. Hutton, N. R. Roberson)

The lifetimes of 21 levels below 4 MeV have been studied in ^{26}Al with the Doppler shift attenuation method and the reaction $^{24}Mg(^3He,p)^{26}Al$. Results for levels below 3 MeV are generally in agreement with previous work. New results for levels above 3 MeV include 27 ± 11 fs for the 0^+, T= 1 analogue state at 3754 keV. The M1, $\Delta T = 1$ transitions range in strengths from $\sim 10^{-2}$ W.u. up to 1.5 W.u. and are stronger than any of the known $\Delta T = 0$, M1 transitions in ^{26}Al. The results have been presented at the Washington meeting of the American Physical Society (BAPS 17, 533 (1972)).

11. A Study of Low Lying Levels in ^{59}Ni (J. D. Hutton, N. R. Roberson, C. R. Gould, D. R. Tilley)

The properties of excited states of ^{59}Ni up to 2 MeV excitation energy have been studied using the $^{56}Fe(\alpha,n)^{59}Ni$ reaction. Angular correlation and Doppler shift attenuation techniques were used to assign spins, mixing and branching ratios, and lifetimes. The excited states at 878, 1189, 1302, 1680, 1735 and 1948 keV were found to have lifetimes of 0.62, 0.44, 0.18, 0.5, 0.18, and 0.2 picoseconds, respectively. The level at 1189 keV was assigned a spin of $5/2^-$. This work was reported at the Washington Meeting of the American Physical Society, 24-27 April 1972 (Bull. Am. Phys. Soc., Vol. 2, No. 4, Abs. No. KE9).

12. The Decay Properties of Low Lying Levels of ^{53}Fe (R. O. Nelson, N. R. Roberson, C. R. Gould, D. R. Tilley)

The low lying levels of ^{53}Fe have been studied using the $^{50}Cr(\alpha,n\gamma)^{53}Fe$ reaction. Gamma ray angular distributions were measured for the 1328-, 1423- and 1696-keV levels in order to measure their spin and decay properties. The levels were populated with α-particle beams with energies ~600 keV above threshold, and the gamma rays were detected in singles at nine angles between 0° and 90° to the beam with a 30 cc Ge(Li) detector. The doppler shift attenuation method was used to study the lifetimes of these levels at bombarding energies of 8.7- and 10.5-MeV. Gamma rays were detected in coincidence with neutrons detected at 0° in a 4" x 5" NE213 liquid scintillator. Preliminary results are summarized in Table B-1.

Table B-1

Transition Properties for Levels of ^{53}Fe

E_x (keV)	E_γ (keV)	J_i^π	J_f^π	τ (fsec)	δ
741	741	$3/2^-$	$7/2^-$	92 ± 2 ns[a]	0.0[b]
1328	1328	$9/2^-$	$7/2^-$	25 ± 10	0.15 ± 0.03
1423	682	$5/2^\pm$	$3/2^-$	$1_{ps} < \tau < 3ns$	-0.34 ± 0.03
					or < -10.
		$3/2^\pm$	$3/2^-$		-3.50 ± 1.70
1696	955	$7/2^-$	$3/2^-$	1750 ± 850	0.09 ± 0.04
		$(7/2^+)$	$3/2^-$		
2339	1011	$11/2^-$	$9/2^-$	76 ± 17	0.4 ± 0.4[d]
2697	2226	$1/2^+$	$3/2^-$	112 ± 22	

[a] S. Cochavi et al.

[b] Assumed to be zero.

[c] Calculation assumed $\delta = 0.0$.

[d] Z. P. Sawa et al.

13. Study of The γ-decay of ^{23}Mg Excited by The ^{12}C(^{12}C,n)^{23}Mg Reaction (R. O. Nelson, J. D. Hutton, N. R. Roberson, C. R. Gould, D. R. Tilley)

The ^{12}C(^{12}C,n)^{23}Mg reaction has been used to investigate some of the low-lying levels of ^{23}Mg at a bombarding energy of 22 MeV. Gamma rays detected in singles indicated states in the ground state rotational band were populated with moderate strength. Transitions in other bands were not observed. Analysis of gamma-rays detected in coincidence with neutrons has produced preliminary F(τ) values for members of the ground state band.

14. Gamma Ray Studies (S. M. Shafroth, P. H. Nettles, T. White*)

a. The 9" x 9" NaI crystal and anti-coincidence shield have been tested. For proton bombarding energies above 14 MeV the γ-ray spectra are badly distorted by contributions from neutrons. Efforts are being made to improve the system.

15. X-Ray Studies (A. B. Baskin, G. A. Bissinger, C. E. Busch, J. M. Howard, P. H. Nettles, D. M. Peterson, W. R. Scates, S. M. Shafroth, A. W. Waltner)

a. Ag K and L, and Au L x-rays Produced by 12 to 50 MeV ^{16}O Bombardment

This work has been presented at the International Conference on Inner Shell Ionization Phenomena, Atlanta April 17-21, 1972 and will be published in the Conference Proceedings.

b. Yields of K and L x-rays Produced by 2-30 MeV Proton Bombardment of Ag

This work has been presented at the International Conference on Inner Shell Ionization Phenomena, Atlanta April 17-21, 1972 and will be published in the Conference Proceedings.

It is also scheduled for publication in Phys. Rev. A, May 1, 1972

---

* Furman University, Greenville, S. C.

c. Relativistic Effects in Au L x-ray Production by 0.5-3.0 MeV Protons

This work has been presented at the International Conference on Inner Shell Ionization Phenomena, Atlanta April 17-21, 1972. It is also accepted for publication in Physical Review A.

d. Yields of Au L x-rays from 2-30 MeV and K and M x-rays from 2-14 MeV Proton Bombardment

This work has been presented at the International Conference on Inner Shell Ionization Phenomena, Atlanta April 17-21, 1972. It is being prepared for journal publication as well.

e. Angular Distributions

Ag K, and Au L x-ray angular distribution data at E_p = 2.2 MeV were found to be isotropic to within 3%.

f. M x-rays

Pb M x-ray yields have been measured from E_p = 2-14 MeV. The M x-ray cross sections are $\sim 10^3$ barns. The trend of the data vs. E_p agrees well with PWBA calculations of Choi. At the same time new data were taken on Au and Pb L x-rays with a higher resolution detector (290 eV at $E\gamma$ = 6 keV) than was previously available. This permitted the $L\gamma$ peak to be resolved into three components whose behavior vs. E_p is being analyzed.

g. $K\alpha/K\beta$ Ratio Measurements

This ratio has been measured for Cl, Ca, Cr, Mn and Ni. Final results await detector efficiency calibration.

h. Argon Beam Experiments

A yield curve for Ar K x-rays from 0.48-2.5 MeV has been run using the 4 MeV Van de Graaff. However this data must be repeated.

The 0.48 MeV Ar^+ beam on Cu targets shows Si, Cl and S as well as Ar K x-rays. All but the Ar x-rays are probably due to beam deposit.

We have observed a broad 1 keV peak when 20-40 $\mu g/cm^2$ car-

bon foils (thin to 0.48 MeV Ar^{+}) are bombarded with 0.48 MeV Ar^{+} ions. This suggests that the explanation by Saris et al. in Phys. Rev. Letters 28, 717 (1972) of observation of molecular x-rays due to Ar^{-1} + Ar is incorrect.

A new Al target chamber has been built for this work which permits the Si(Li) detector to be in the accelerator vacuum.

16. ^{3}He Scattering and Polarization Studies (E. J. Ludwig, T. Clegg, R. L. Walter)

A publication reporting the polarization of ^{3}He particles scattered from ^{9}Be, ^{12}C and ^{16}O has recently appeared in Nuclear Physics.

Data have more recently been obtained corresponding to the scattering of ^{3}He particles from targets of Al and Si at a ^{3}He-beam energy of 21 MeV. The polarization angular distributions are quite similar except for a large polarization measured at $\theta_{LAB} = 55°$ for Al. The data were taken to see if differences existed in the polarizations which might be attributed to the target spin of Al. The results are still preliminary.

17. (d,t) and (d,^{3}He) Cross-Section and Polarization Studies at 15 MeV (E. J. Ludwig, T. B. Clegg, S. Datta, C. E. Busch)

a. ^{10}B(d,t) and ^{10}B(d,^{3}He) Reactions

The cross section angular distributions have been obtained at $\theta_{LAB} \leq 130°$ for the (d,t) and (d,^{3}He) reactions leading to the ground states and excited states of ^{9}B and ^{9}Be respectively. The angular distributions to the ground state and 2.43 MeV state of ^{9}B indicate an $\ell = 1$ neutron transfer as do the distributions pertaining to the mirror states in ^{9}Be. The similarity in the angular distributions of the mirror states has been tested by computing the function $\sigma_t - \sigma_{^3He} / \sigma_t + \sigma_{^3He}$ which can be compared to theoretical predictions of this ratio to show the extent to which charge symmetry breaks down in nuclear reactions.

Polarization asymmetries have been measured for $\theta_{LAB} < 90°$ for the two reactions. The (d,t) and (d,^{3}He) asymmetries to mirror states are almost identical while the (d,t)(and (d,^{3}He)) corresponding to different low-lying states of the final nucleus vary slightly.

The $\ell = 1$ transferred particles are in either a $J^{\pi} = 3/2^{-}$ or $1/2^{-}$ state and asymmetry measurements can be used to determine the j-value or mixture of j-values for the transferred particles.

The shape of the polarization asymmetry distribution indicates that the spin and parity transferred in populating the states mentioned above is $3/2^-$. This is expected from the shell model.

b. $^{14}N(d,t)$ and $^{14}N(d,^3He)$ Reactions

The cross section and asymmetry angular distributions have also been measured for (d,t) and $(d,^3He)$ reactions leading to the ground state of ^{13}N and ^{13}C respectively. The transferred particle for these reactions can be in a $J^\pi = 1/2^-$ or $3/2^-$ state. Asymmetry measurements show that the spin transfer is predominantly $J^\pi = 1/2^-$ although the magnitude of the measured asymmetries is somewhat below the values predicted by distorted wave calculations. This may indicate a small $J^\pi = 3/2^-$ admixture. These data are being prepared for publication.

c. $^{32}S(d,t)$ and $^{32}S(d,^3He)$ Reactions

The cross section and polarization asymmetries have been measured for (d,t) and $(d,^3He)$ reactions populating the low-lying states of ^{31}S and ^{31}P. The cross-section yield for the (d,t) reaction is much lower at forward angles than for the $(d,^3He)$ reaction since the ground state Q-value for the (d,t) reaction is quite large (-8.83 MeV).

The asymmetry measurements for these reactions leading to the ground states of the final nuclei are especially interesting since they involve $\ell = 0$ transfers and spin-dependent distortions are primarily responsible for the measured asymmetries. The asymmetry measurements out to $\theta_{LAB} = 90°$ show a strong similarity to the measurements for elastic deuteron scattering. Estimates of the extent to which this behavior is explained by a Weakly-Bound Projectile Model are being made.

18. A Comparison of the Polarization in the Mirror Reactions $D(d,\vec{p})$ and $D(d,\vec{n})$ (R. A. Hardekopf,* T. B. Clegg, R. L. Walter)

A report comparing the polarization in the $D(d,\vec{n})$ reaction to the $D(d,\vec{p})$ charge symmetric reaction has appeared in Phys. Rev. Letters 28 (1972) 760. Here it was shown that the charge effects in these reactions are indeed small if one compares the polarization data at equal energies in the outgoing channel.

---

* Now at Los Alamos Scientific Laboratory, Los Alamos, New Mexico

19. The Analyzing Power for $T(\vec{p},p)T$ (R. A. Hardekopf, P. W. Lisowski, T. C. Rhea, T. B. Clegg, R. L. Walter)

The data obtained from 8 to 15 MeV have been reported in the Ph.D. thesis of Hardekopf. (Additional data are now needed at 16 MeV for comparison to the $^3He(\vec{n},n)$ measurements underway at our laboratory.) The data and a twelve parameter phase shift analysis were submitted to Nuclear Physics.

20. Measurement of The Analyzing Power in The $T(\vec{p},d)D$ Reaction (R. A. Hardekopf, P. W. Lisowski, T. C. Rhea, R. L. Walter, T. B. Clegg)

Data on the $T(\vec{p},d)D$ reaction were obtained for studying the polarization in the inverse reaction $D(d,\vec{p})T$ for further comparison to the $D(d,\vec{n})$ case. A full report of this work has been given in the thesis of Hardekopf and has been submitted to Nuclear Physics.

21. $^{28}Si(^3He,\alpha)^{27}Si$ Reaction at 21 MeV (J. M. Joyce, E. J. Ludwig)

The angular distributions corresponding to the lowest 12 states of ^{27}Si have been extracted and analyzed.

Spectroscopic factors for these states have been obtained when unique ℓ-value assignments could be made to the levels. Coupled-channel calculations, which included coupling to the first-excited state of ^{28}Si, have been made for several of the states expected to be weakly populated by a direct pickup mechanism. The angular distributions of certain states which show an $\ell = 4$ pickup character are also well described by a two-step process according to calculations made with Code JUPITOR. These results are being prepared for publication.

22. Elastic Deuteron Scattering at 15 MeV (C. E. Busch, T. B. Clegg, S. Datta, E. J. Ludwig)

Cross section angular distributions and asymmetry distributions have been obtained for the elastic scattering of deuterons from ^{10}B, ^{14}N and ^{32}S. The cross section data extend to backward angles ($\simeq 150°$) while the asymmetry data is generally confined to the forward angular range. These data have been analyzed with the optical model code SNOOPY and optical model parameters have been obtained which have been useful in distorted-wave calculations.

23. The $^{54}Fe(p,t)^{52}Fe$ Reaction (R. O. Nelson, N. R. Roberson, C. R. Gould)

This work is being prepared for publication.

24. Inelastic Effects in The Study of ^{23}Na and ^{23}Mg (R. O. Nelson, N. R. Roberson)

Fourteen states of ^{23}Na with excitation energies <5.6 MeV and their mirror states in ^{23}Mg have been studied using the $^{24}Mg(d,^3He)^{23}Na$ and $^{24}Mg(d,t)^{23}Mg$ reactions at the bombarding energy of 21.1 MeV. A DWBA analysis of the angular distributions could not reproduce the pronounced differences observed between known $\ell = \alpha$ distributions. However, agreement with the data was obtained by including inelastic effects in the incident channel as treated in the Coupled-Channel Born Approximation. From calculations with the computer code MARS[1] it was possible to identify mirror states of the nuclei and to establish spin and parity assignments of $9/2^+$, $3/2^+$, $(5/2^+)$, $(5/2^-)$, $(7/2^+)$, $(5/2^+)$ and $(11/2^+)$ for levels in ^{23}Mg at 2.71, 2.90, 3.86, 3.97, 4.68, 5.29 and 5.45 MeV, respectively.

25. Inelastic Deuteron Scattering from ^{24}Mg, ^{28}Si, $^{208,206}Pb$ (R. A. Hilko, R. O. Nelson, T. G. Dzubay, N. R. Roberson)

Inelastic scattering data at 21.1 MeV have recently been taken on ^{28}Si from 20° to 155° in the laboratory using the high resolution 90-90 analyzing system for the Cyclo-Graaff beam. Energy resolution for the solid-state ΔE-E telescope was about 38 keV. Deformation parameters assuming a rotational model are being calculated using DWBA and Coupled-Channel method.

26. The (d,X) Reaction from ^{12}C, ^{16}O, ^{24}Mg, and ^{28}Si (R. A. Hilko, R. O. Nelson, T. G. Dzubay, N. R. Roberson)

By using one detector and also measuring the time of flight we were able to mass identify groups 1, 2, 4, 6, 10, and 12. Spectra from 11° to 50° in the laboratory were taken with 21.1 MeV deuterons from the TUNL Cyclo-Graaff on ^{12}C, ^{16}O, ^{24}Mg, and ^{28}Si. The $(d,^6Li)$ reaction has only been analyzed so far. DWBA calculations are being made for this alpha particle pick-up.

---

[1] T. Tamura, private communication.

27. The Lowest T = 3/2 State in ^{41}Sc (T. A. Trainor, T. B. Clegg, E. J. Ludwig, W. J. Thompson)

An attempt has been made to identify the lowest T = 3/2 state in ^{41}Sc via the reaction $^{40}Ca(p,p)^{40}Ca$. Excitation functions at Lab angles of 45°, 56°, 121°, 125° and 136° have been measured over an energy range of 4.880 MeV to 4.940 MeV. The data is in good agreement with that of Brown (unpublished Ph.D. thesis, Rice, 1963). Preliminary fits to this data using the computer code ANSPEC have been made. Difficulties have been encountered in isolating the T = 3/2 level from two other close lying levels in this energy region.

28. $^{208}Pb(p,p')$, $^{208}Pb(p,d)$ and $^{208}Pb(p,t)$ Reactions from 18.8 to 27.3 MeV (P. Nettles, E. J. Ludwig, C. E. Busch, E. Klema,* J. M. Joyce)

Excitation curve data have been taken for ^{208}Pb + p from 18.8 MeV to 27.3 MeV in 100 keV steps using the TUNL Cyclo-Graaff. Particle identification techniques were used to separate and store the particle groups obtained using E and ΔE telescopes set at 90° and 150°. The excitation curves for tritons and deuterons showed little structure over the energy range while the inelastically scattered protons exhibited resonance-type structures at energies where the excited core + single particle resonances were expected to occur. These measurements will be extended to energies between 17 and 18.8 MeV and some of the present data repeated using the high-resolution magnet system.

29. Channeling Studies (R. A. Haglund, E. J. Ludwig, T. B. Clegg)

A goniometer has been purchased and apparatus is being assembled to begin a program of channeling studies using the 4 MeV Van de Graaff. The first experiments will involve tests of the quality of some 2000 Å thick single crystal nickel foils which have been produced by epitaxial growth in the laboratory of E. N. Mitchell at the University of North Carolina in Chapel Hill.

30. (p,n) Experiments with Chopped Beam (S. M. Shafroth, A. A. Jaffe,** G. A. Bissinger, T. G. Dzubay, F. Everling, D. W. Miller, D. A. Outlaw, E. J. Ludwig, P. Nettles)

The $^{36}Ar(p,n)^{36}K \rightarrow \beta^+ + {}^{36}Ar^*/\gamma)$ reaction work has been submitted for publication to Physical Review Letters.

---

* Tufts University, Medford, Massachusetts

** Now at Hebrew University, Jerusalem, Israel

C. DEVELOPMENT

1. Accelerator Improvements (F. O. Purser, T. D. Hayward, J. R. Boyce, Jr., H. W. Newson, M. T. Smith, E. G. Bilpuch, R. L. Rummel, J. D. Moses, G. E. Mitchell)

a. Tandem Accelerator

The tandem has generally run satisfactorily for this report period. A new charging belt made by HVEC using a new type of rubber has been installed. The new belt seems to provide superior voltage holding and dust characteristics but produces a more non-uniform charge distribution at the terminal screen with a resulting increase in terminal ripple.

The direct extraction negative ion source has been completely assembled on the test bench and is undergoing tests prior to installation. This source with its improved energy spread, intensity and transmission characteristics is now scheduled for installation on the tandem in June.

A ^{3}He recovery system for use with the regular tandem source is in the design stages and the major components are on hand. Installation in early summer will greatly reduce the cost of ^{3}He operation.

b. Injector Cyclotron

A second set of harmonic coils has been installed in the cyclotron at a mean radius of 4.5" as an aid in orbit centering and to minimize the radial betatron oscillations. The coils appear to perform their designed function well, however, improved extraction efficiency has not yet been obtained due to other problems.

Following installation of the new coils and a major realignment of the dees, 100 μA of H^- beam were obtained at 8" radius. At this beam current a vertical blow-up of the beam between 8" and 11" radius was observed. Further tests are in progress to determine the cause of the additional vertical oscillation.

The singlet quadrupole installed between the cyclotron and its analyzing magnet has improved overall transmission of the beam from extraction to the high energy faraday cup of the tandem from 30% to 70% when using the high resolution beam.

c. Improved Beam Energy Resolution for The Tandem Accelerator

A paper on this work has been accepted for publication in Nuclear Instruments and Methods. This paper describes the system in some detail and presents sample results at both low energies ($E_p \simeq 3.229$ MeV resonance on ^{54}Fe) and high energies ($E_p = 14.23$ MeV resonance on ^{12}C).

A direct extraction ion source is being constructed and should be put into operation this summer. This new source should provide increased beam intensities and make the high resolution experiments practical on a production basis.

2. Pulsed Beams (F. O. Purser, T. D. Hayward, D. E. Elliott, H. W. Newson, R. O. Nelson, R. A. Hilko, T. G. Dzubay, N. R. Roberson, P. Nettles, E. J. Ludwig, S. M. Shafroth)

a. Mass Identification of Charged Particles by Time of Flight

By using the pulsed deuteron beam from the TUNL Cyclo-Graaff, we were able to identify by kinematics of angular distribution mass groups 1, 2, 4, 6, 10, and 12 from targets of ^{28}Si, ^{24}Mg, ^{16}O, and ^{12}C. A computer on-line analysis program forms the product of pulse height from detector (E) and square of time-of-flight (T^2) which is found to be roughly proportional to mass. Time resolution of 550 picoseconds has been measured. Incorporated in the on-line computer program is a time monitor which checks for drifts in the beam burst relative to the rf frequency. The data is corrected for drifts during a run and the time structure of a selected energy peak is displayed. Data can also be stored on magnetic tape for subsequent reanalysis.

3. Polarized Source Improvements (T. B. Clegg, C. E. Busch, P. W. Lisowski, T. C. Rhea, T. A. Trainor)

The Lamb-shift polarized source has in the last six months undergone a one-month period of major maintenance and modification which has resulted in much improved operation. The major topics of interest are summarized below:

1. The troublesome oil and deionized water closed circuit cooling systems which had been constructed with government surplus parts have now been replaced with new efficient heat exchangers and a neatly designed pumping system. Since installation, only one minor problem has remained. The circulation pumps for both these systems require small leakage of water or oil around the shaft for lubrication. This requires that the oil system be refilled quite often. Parts are

now available to modify the pumps to eliminate this problem.

2. The coils which establish the uniform 575G field for the "spin filter" and for the argon charge exchange canal are enclosed in steel containers which are sealed vacuum tight with "O" rings. These coils are cooled with oil. Oil leaks around these "O" ring seals appeared and caused several problems. The vacuum in the ion source in the "spin filter" region became too bad to allow proper selection of the m = 0 magnetic substate when polarized deuteron beams are needed. The oil deposited on surfaces near the beam axis also formed insulating layers which charged up quenching the desired polarized metastable beam. To eliminate these problems, the coils were removed from the ion source and leaky "O" ring seals were replaced. This part of the ion source has now operated for three months with no further problems on maintenance.

3. Insulating layers have also been a problem in the region of the extraction electrode for the duoplasmatron. Much of this problem was eliminated by the installation of a new freon baffle on the diffusion pump in the duoplasmatron region and a new, larger freon compressor.

4. The extraction electrode and probe for the duoplasmatron have been modified so they are moveable while the polarized source is in operation. This helps align these components to obtain optimum beam.

5. A new all copper cesium oven and charge exchange canal has been installed in the source. The cesium density is now controlled by regulating the temperature of the oven with the current through the oven heaters.

All of these modifications have resulted in more intense, relatively stable, and reproduceable beams from the polarized source since about 1 February. Data have been taken rather routinely with currents on target of between 10 and 25 nA. Only deuteron beams have been run during this period.

4. Rotating Scattering Chamber (A. Lovette, P. W. Lisowski, T. B. Clegg, E. J. Ludwig, F. O. Purser)

The totating chamber discussed in the last TUNL report has now been completed. The scattering chamber previously installed on the 52° beam leg after the first analyzing magnet was removed from its support table, modified, and reinstalled with bearings at the front and rear of the chamber to allow it to be rotated around the beam axis. The beam polarization monitor apparatus at the back of the chamber is attached to the chamber and rotates with it. Precise alignment of the chamber and monitor have been completed and the chamber is now being used

again as it was before the modification. Tests will begin within the next few weeks to determine how best to use the chamber rotation in collecting tensor and vector polarization data for deuterium elastic scattering and deuterium induced reactions. A motor drive is being installed which, at present will allow control of the chamber rotation locally, but later may be computer controlled.

5. High-Intensity Duoplasmatron for Polarized Ion Source (T. A. Trainor, T. B. Clegg)

A new duoplasmatron has been constructed and is now being tested. This high-powered source is designed to operate with arc currents up to 35A. The plasma from the source expands into an expansion cup and a beam is extracted from a multiaperture plate over the end of this cup. The extraction electrode and deceleration electrode are also multiapertured plates. They are constructed carefully so the holes in these three multiaperture plates are aligned during operation. A magnetic lens follows the duoplasmatron, and the test bench allows additional momentum analysis of the beam from the source with a 20° deflection magnet.

The ion source has been turned on for the first time within the last few weeks. On the first attempt, without using the magnetic lens, a current of 18 μA of 1100 eV positive ions was obtained in a 2.5 cm diameter Faraday cup 1.6 m away. The source gas for this test was deuterium. Visual observation of the extracted beam showed that it was expanding immediately following the extraction region in a manner which could be attributed to the space charge of the beam.

Momentum analysis of the beam shows that approximately 66% of the positive ion current is D^+ with the remaining being D_2^+ when the ion source is operated with a 17A arc current.

6. Polarization Monitors (C. E. Busch, P. W. Lisowski, and T. B. Clegg)

A new monitor has been constructed which utilizes the $^3He(\vec{d},p)^4He$ reaction to measure the tensor polarization of the deuteron beam from the Lamb-shift source when they are being used in the 52° scattering chamber. The detectors for the old vector polarization monitor which utilizes p-^{4}He and d-^{4}He elastic scattering have shown signs of severe radiation damage. The possibility of using proportional counters as detectors in these devices is being investigated.

An additional $^3He(d,p)^4He$ monitor has been designed for use first in the 59° leg after the first analyzing magnet.

7. A Two-Crystal NaI Polarimeter for Gamma Rays (J. R. Williams, C.R. Gould, R. Bass, D. R. Tilley, N. R. Roberson)

A Compton polarimeter for the meusurement of γ-ray linear polarization has been constructed according to a design similar to that described by Bass et al.[1] The device consists of two 1-3/4" (diam.) x 2" (thick) NaI cylindrical crystals with axes parallel mounted on separate phototubes such that the pair can be rotated about an axis through the target. Gamma rays entering one crystal and Compton scattered into the other are identified by the requirement of a coincidence between the two detectors with the sum of the two pulses corresponding to the full energy of the gamma ray.

Calibration measurements are underway.

8. New 24" Scattering Chamber (E. J. Ludwig, F. Purser)

The new 24" scattering chamber is now installed in the "high resolution" target area and has been successfully used in several experiments.

D. THEORY

1. ^{9}Be(p,p)^{9}Be Optical-Model Potentials (H. J. Votava, W. J. Thompson)

Analyses of TUNL cross section and polarization data for 13- to 30-MeV protons has been completed and an abstract submitted to the Washington American Physical Society meeting.

2. Excited-State-Threshold Resonance Effects in ^{9}Be(p,p$_0$)^{9}Be and ^{9}Be(p,n)^{9}B (J. H. Votava, W. J. Thompson)

A resonant-type anomaly near 7-MeV proton energy has been shown to be strongly influenced by the excited-state threshold ^{9}Be(p,n$_4$)^{9}B. This is the first reported observation of excited-state-threshold resonance effects. A detailed description including an R-matrix analysis has been submitted to Physical Review Letters.

---

[1] R. Bass, S. Brinkmann, C. Charzewski and Hanle (To be published in Nuclear Instruments and Methods)

3. Rapid Energy Dependence of The Optical-Model Potential from Proton Bombardment Below the Coulomb Barrier (J. S. Eck ((Kansas State University)) W. J. Thompson)

Continuing analysis of this data suggests that the traditional optical-model potential energy dependence is too slow at energies near the Coulomb barrier. A surface-peaked real potential has been shown to improve the fits, especially to polarization data, while still giving a rapid energy dependence. All calculations have been made using the DDP-224 interactive program OPTICS.

4. Inelastic Effects in Direct Nuclear Reactions (W. J. Thompson)

The formalism used to treat inelastic effects in direct nuclear reactions has been re-examined in relation to the s-d shell transfer-reaction studies made at TUNL by R. O. Nelson and N. R. Roberson. The relations between Born approximation treatments by Distorted Waves, by Coupled Channels, by Core Excitation and by the Source Term method have been clarified. A paper on this has been submitted to Physical Review.

5. Nuclear Theory Computer Programs (S. K. Datta, R. J. Eastgate, W. J. Thompson)

Continued development of computer programs for the theoretical analysis of nuclear data, with special emphasis on the use of the DDP-224 display facilities, has been made.

OPTICS--This optical-model-analysis program for shape- and compound-elastic scattering for use at TUNL is now completed and a description has been accepted for publication in Computer Physics Communications.

BSEF--Energy eigenvalues or well depths and wave functions of bound states in a Woods-Saxon or harmonic-oscillator well can be generated and displayed on the oscilloscope of the DDP-224 computer at TUNL. Alternatively an energy-level spectrum can be generated and displayed. Documentation is nearly complete.

P.E.A.--Algorithms for prime-exponent arithmetic (P.E.A.) with rational numbers have been programmed in PL/1 and in FORTRAN to allow exact evaluation of 3n-j angular momentum coupling coefficients. A description of these algorithms has been submitted to Computer Physics Communications.

6. Calculation of Relativistic L-Subshell Ionization Cross Sections by Heavy Charged Particle Impact (B.-H. Choi)

L subshell ionization cross section by an incident heavy but slow charged particle were evaluated. Incident particles are described in the plane wave Born approximation and relativistic wave functions are used for the bound and free atomic electrons. Numerical results are presented for proton impact on holmium and gold. Relative ratios of each L subshell ionization cross sections are compared with other calculations. A paper on this work has been submitted to Physical Review A and to the conference on Inner Shell Ionization.

7. Computer Program for Strength Functions And Single Particle Reduced Widths (B.-H. Choi, M. Divadeenam)

Optical Model code SNOOPT2 has been modified to evaluate s-, p-, and d-wave neutron strength functions as a function of both mass number and neutron energy. In particular, for a given A the calculated strength function has a resonance shape as a function of energy for a suitable optical model potential. The program is designed to compute the integral $\int_0^{E_n} \langle\gamma^2\rangle / D \, dE$ as a function of neutron energy. In addition the single particle resonance reduced widths can be predicted with proper choice of potential parameters for any nucleus. The computed results are being used to analyze the neutron reduced widths observed in terms of the spreading of the s.p. resonance into more complicated states.

UNIVERSITY OF COLORADO

A. STUDY OF THE (p,n) REACTION

1. Neutron Time-of-Flight Instrumentation

(R. F. Bentley, J. D. Carlson, D. A. Lind, C. D. Zafiratos)

The neutron time-of-flight spectrometer used for all the experimental data obtained thus far has now been replaced by a beam swinger and multiple detector system. Data accumulation was completed with the old system in July, 1971. The old system used the Colorado cyclotron to deliver up to 1 μa average proton current at 23 MeV to the target with 3 of 4 R.F. beam bursts suppressed. The cyclotron was operated in the single turn extraction mode for which the beam width is 0.3 ns with an interval between bursts of 224 ns.

Neutron detectors were 2.5 cm thick by 15.2 cm diameter consisting of lucite cells filled with NE 224. Pulse shape discrimination permitted excellent separation of neutrons from background gamma rays. Two such detectors plus a smaller monitor detector were used for data acquisition over flight paths of 6 to 11 meters and at two selected angles over 27 meters. The overall observed resolution of the system was 0.8 to 0.9 ns. For the angular distribution studies cross sections were measured from 10° to 160° in about 7° steps for some 33 targets. A detailed description of this system is in preparation for publication.

A new system has been built and tested in the last nine months. This consists of an energy loss configuration for charged particle studies with a beam swinger to change direction of the incoming particle beam relative to the direction at which the reaction products are observed. The primary beam is deflected by 45° and then by 135° in the reverse direction so that it intersects the initial beam direction at 90°. Upon rotation of the system about the primary beam direction, the direction of the incoming beam relative to the direction of observation of the reaction products can be varied from +140° to -160°. The system can be tuned for isochronism to preserve the pulse length quality of the cyclotron beam.

Three observation stations for neutrons located at a 9 meter flight path separated by 8° in angle are provided. Additional stations at 28 meters and 80 meters are also available. For the 9 meter stations 21 cm diameter detectors will be used employing extensive shielding and n-γ discrimination. The first test neutron spectrum obtained with the new system showed an overall time resolution of 1.1 ns, while the detector alone had a timing spread of about 0.6 ns. Since some parts of the charged particle analysis system will not be available until September, 1972, the system will be used exclusively for (p,n) and (^{3}He,n) studies in the next

four months.

2. Macroscopic DWBA Analysis of Isobaric Analogue Transitions
(J. D. Carlson, D. A. Lind, and C. D. Zafiratos)

Angular distributions of (p,n) reactions leading to isobaric analogue states at E_p=23 MeV have been measured for 29 nuclei.[1] The targets studied were ^{9}Be, $^{25,26}Mg$, ^{27}Al, ^{31}P, ^{40}Ar, ^{49}Ti, ^{50}Cr, $^{54,56,58}Fe$, $^{58,61,62,64}Ni$, ^{64}Zn, ^{90}Zr, ^{93}Nb, ^{96}Zr, ^{96}Mo, $^{96,104}Ru$, ^{115}Sn, $^{117,118,119,120}Sn$, ^{165}Ho, and ^{208}Pb. Ground state (quasi-elastic) analogue transitions were observed on all of these targets. Excited 2^+ analogue transitions were also observed on all of the even mass targets with A ≤ 96 except for ^{90}Zr. See Table A-1 for data.

A macroscopic DWBA analysis has so far been attempted for all of the nuclei with A ≥ 50 by using the code DWUCK.[2] The proton and neutron optical parameters were taken from the compilation of Becchetti- and Greenlees.[3] The analytic expressions used were their "best fit" expressions having the radius of the spin-orbit interaction equal to the real radius.

The Becchetti-Greenlees expression contains a complex isospin dependent term (real volume and imaginary surface) from which it is possible to write down a self-consistent isospin form factor.

According to Lane[4] the nucleon-nucleus interaction may be written as

$$U(r) = U_o(v) + 4U_1(r)\,\frac{\vec{t}\cdot\vec{T}}{A}$$

The diagonal matrix elements of this expression give the proton and neutron potentials for elastic scattering

$$\langle t_3 = \pm 1/2, T_3 = 1/2(N-Z) \,|\, U \,|\, t_3 = \pm 1/2, T_3 = 1/2(N-Z)\rangle = U_o \pm U_1\epsilon$$

where ϵ=N-Z/A is the asymmetry factor. One of the off-diagonal matrix elements gives the form factor for (p,n) reactions leading to isobaric analogue states.

$$\langle t_3 = +1/2,\ T=1/2(N-Z)-1 \,|\, U \,|\, t_3 = -1/2, T_3 = 1/2(N-Z)\rangle = 2U_1(\epsilon/A)^{1/2}$$

Thus the form factor is given by

$$\text{Form factor} = \frac{2}{\sqrt{N-Z}}\,U_1\epsilon = 2\frac{(N-Z)^{\frac{1}{2}}}{A}\left[V_1 f_R(r) + i4W_1 a_I \frac{df_I(r)}{dr}\right]$$

Becchetti-Greenlees potentials were also used for computing the distorted waves and an iteration procedure used to successively correct the potentials by the resultant form factor. Best fit cross sections to the quasielastic transitions are compared to the data in

Fig. A-1. For these fits $W_1/V_1=1/2$, $r_R=1.17$ fm, $a_r=0.75$ fm. The values of r_I, a_I and the strength of V_1 were varied separately to achieve these optimum fits.

An attempt to determine a global set of parameters to be used for any nucleus was carried out yielding a complete specification of U_1 for 23 MeV protons. The results of these fits is shown in Fig. A-2. A detailed discussion is available[5] and a paper has been prepared for publication[6] which presents the complete analysis.

An analysis of excited 2+ analogue states has been attempted as well as coupled channel calculations of the analogue ground state. The best conclusion reached thus far is that the effect of the 2+ states is slight so far as the conclusions regarding the potential is concerned.

Perhaps two-step processes of the form (p,d)(d,n) will be important; the calculations are not definitive as yet.

3. Exploitation of the Lane Model to Predict Neutron Elastic Scattering (J. D. Carlson, D. A. Lind, and C. D. Zafiratos)

According to the Lane model for nucleon optical potentials the isospin interaction determines the difference between proton and neutron optical potentials. A self-consistent neutron optical potential can be written as

$$U_n(E_n,A,\epsilon)=U_p(E_n,A,\epsilon)-\Delta V_c+ 2\epsilon[V_1,f_{R1}(r)+i4W_1a_{I1}\frac{df_{I1}(r)}{dr}]$$

where $\epsilon=N-Z/A$. The subscript 1 refers to the isospin dependent term determined from the (p,n) studies. The proton potential can be represented by any suitable set of parameters which reproduces the elastic scattering data. The term $\Delta V_c=0.4Z/A^{1/3}$ cancels a corresponding term which is explicitly included in the proton potential U_p to correct for the different kinetic energy of a proton and neutron inside the nucleus.

For comparison, measured angular distributions of neutrons scattered from selected targets, Fe, Ni, Zn, In, and Sn, at energies near the corresponding outgoing neutron energy in the (p,n) reaction studied here were calculated. Thus from elastic proton scattering and (p,n) reaction data neutron scattering cross sections were predicted.

---

1 Bentley, Carlson, Lind, Perkins, Zafiratos, Phys. Rev. Lett. 27, 1081 (1971).

2 P. D. Kunz, Univ. of Colorado, Boulder, private communication.

3 F. D. Becchetti, Jr., and G. W. Greenlees, Phys. Rev. 182, 1190 (1969).

4 A. M. Lane, Nucl. Physics 35, 676 (1962).

5 J. D. Carlson, Ph.D. Thesis, Univ. of Colorado (1972).

6 J. D. Carlson, D. A. Lind, C. D. Zafiratos. Submitted to Nucl. Phys.

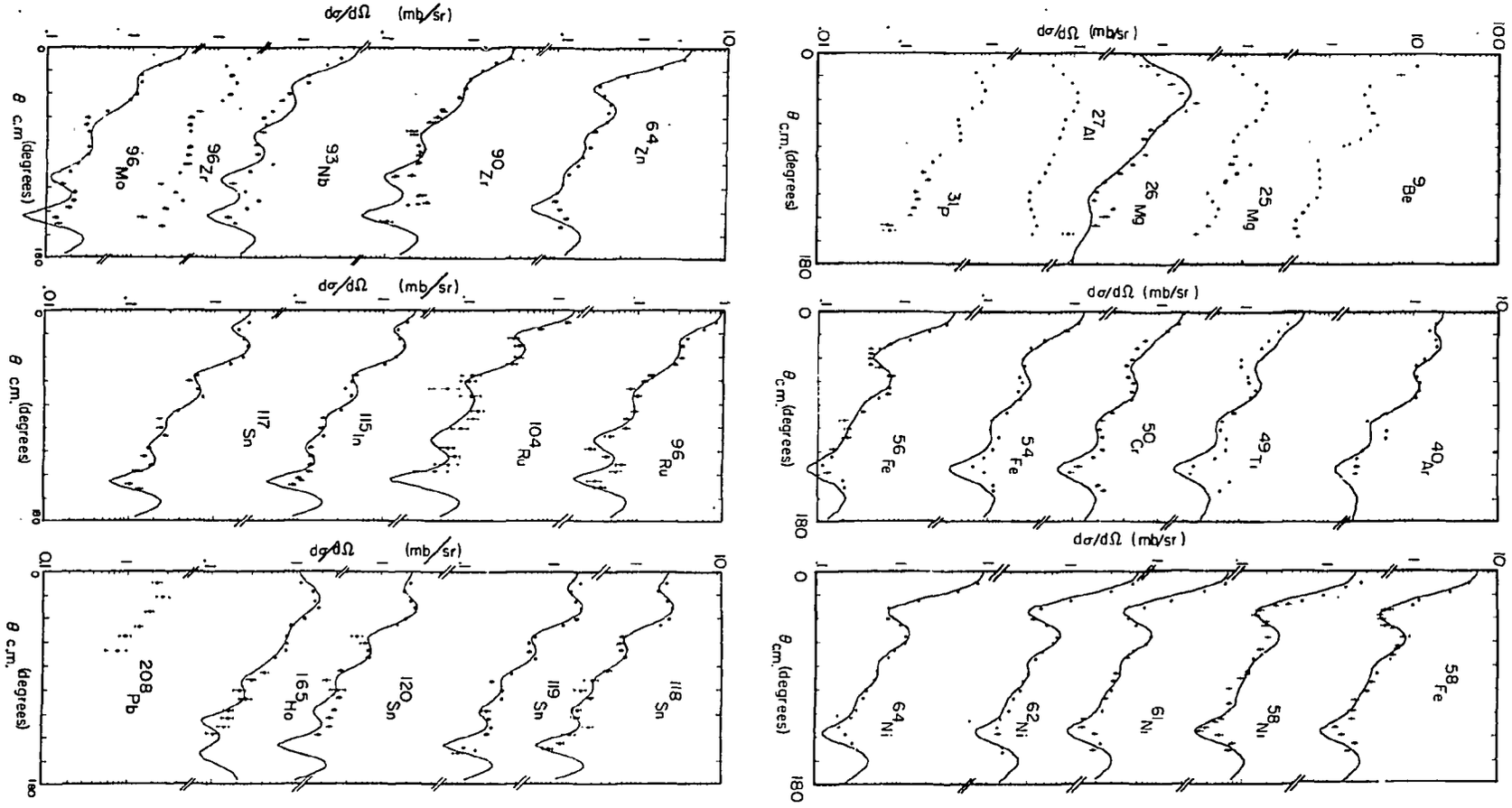

Figure A-1. Best fit cross sections for quasielastic (p,n) transitions compared with experimental data. Except for the isospin dependent term, Becchetti-Greenlees potentials were used. Each case was treated separately to determine best fit parameters of the isospin dependent potential U_1.

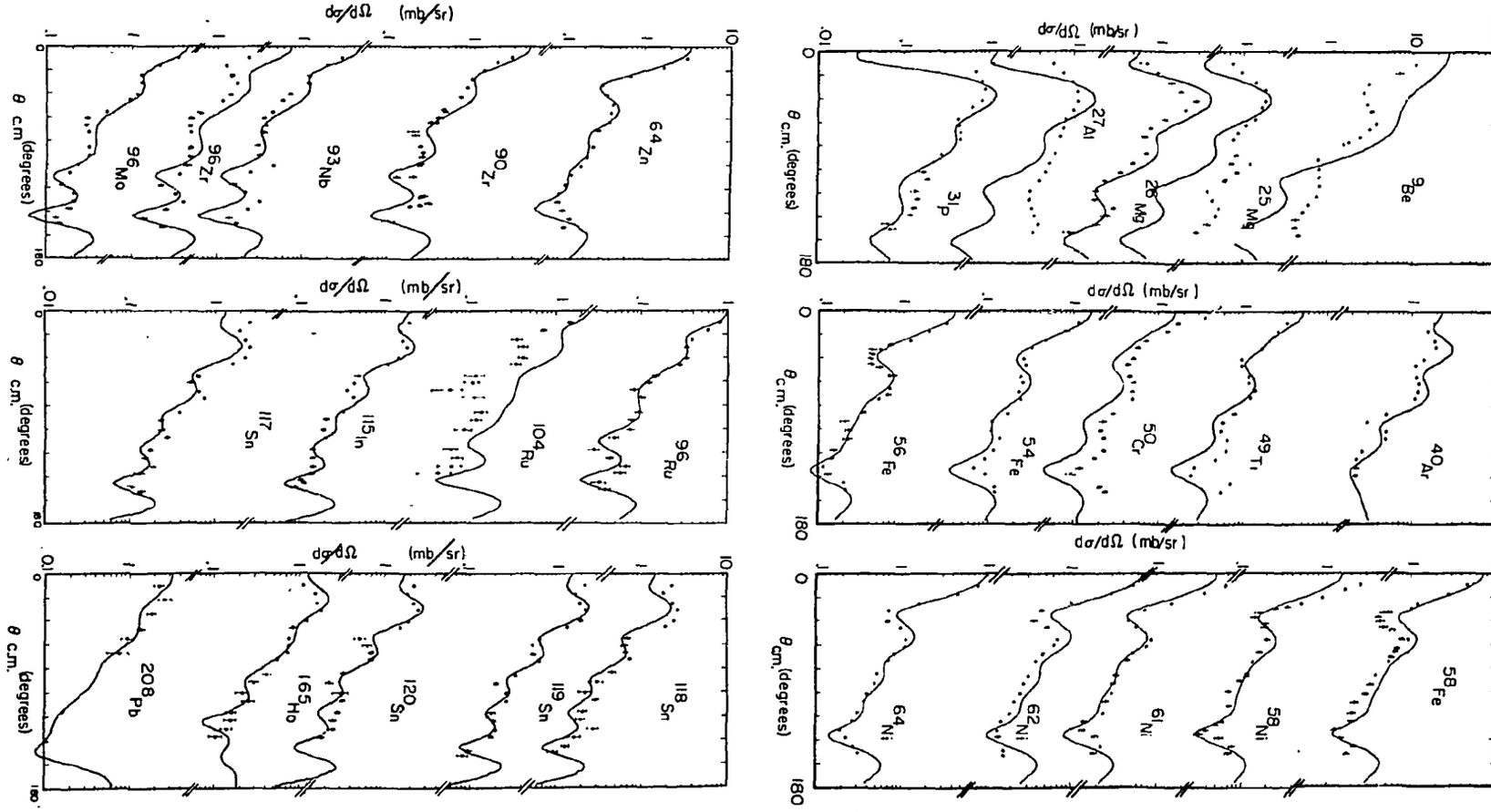

Figure A-2. Predicted (p,n) quasielastic angular distributions given by parameterized values for the isospin dependent potential U_1.

The comparison with measured data is shown in Fig. A-3. The neutron reaction cross sections predicted are also in good agreement with measured values. A brief letter describing these results has been submitted to Physics Letters.[1] The consequence of these observations is that it may be possible to construct adequate neutron optical model potentials by using only the (p,p) and (p,n) experimental data. However, further tests of these ideas must be made.

---

[1] J. D. Carlson, D. A. Lind, and C. D. Zafiratos. Submitted to Physics Letters, 1972.

4. Microscopic Analysis of Analogue and Non-Analogue Transitions (R. F. Bentley and C. D. Zafiratos)

DWBA and coupled channels calculations have been carried out with a macroscopic model. Bound state wave functions obtained from the single particle shell model are connected by the effective nucleon-nucleon potential represented by the expression

$$\vec{\tau}_o \cdot \vec{\tau}_i [V_T + V_\sigma (\vec{\sigma}_o \cdot \vec{\sigma}_i) + V_{TEN} (\vec{\sigma}_o \cdot \vec{r}_o)(\vec{\sigma}_i \cdot \vec{r}_i)]$$

The subscript o refers to the projectile and i refers to the target nucleon. The calculations are insensitive to small changes in the optical potentials and the bound state wave functions. An effort has been made to determine the strengths of the three terms in the effective nucleon-nucleon interaction which can give rise to the (p,n) reaction.

Due to poor agreement of calculated and observed shapes of the angular distributions, the normalization of the calculations to determine potential strengths is quite uncertain. Inclusion of an imaginary component to the interaction by a method suggested by Satchler[1] afforded no consistent improvement to the shapes. It now appears that the inclusion of the two-step process (p,d)(d,n) as calculated through a coupled channels formalism may be an important factor.

---

[1] G. R. Satchler, Phys. Letters 35B, 279 (1971).

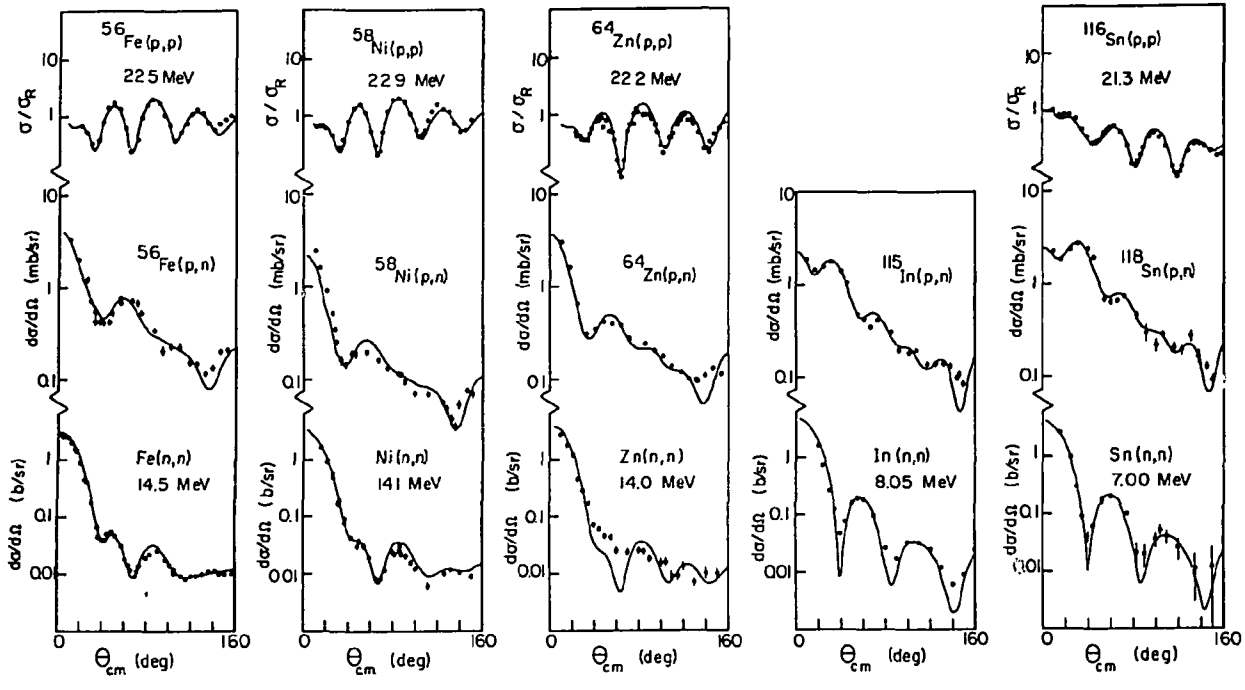

Figure A-3. Comparison of experimental cross section data with predictions derived from proton elastic scattering and quasielastic (p,n) scattering. Becchetti-Greenlees best-fit proton optical model parameters are used with the best fit values from the quasielastic data to predict, using the Lane model, neutron scattering cross sections.

US ARMY ABERDEEN RESEARCH AND DEVELOPMENT CENTER
RADIATION DIVISION
BALLISTIC RESEARCH LABORATORIES

A. SMALL-ANGLE ELASTIC SCATTERING OF FAST NEUTRONS.
(W. P. Bucher, C. E. Hollandsworth, D. McNatt, and A. Niiler)

Measurements of the forward-angle scattering of 7.40, 8.00, 8.55, and 9.00 MeV neutrons from C, N, and O have been completed. Tables A-1 through A-3 summarize the results. These tables also include slightly revised cross sections for incident neutron energies of 7.55 and 9.5 MeV. The difference between the values given in these tables and those reported previously are slight. The new values result from a renormalization of the absolute cross section scale as discussed below.

The scattering measurements for C, N, and O with the special-purpose collimator were made, as a matter of convenience, relative to the scattering from a Pb sample. The differential scattering cross section for Pb was then determined by auxiliary measurements carried out in ring geometry. The Pb data for neutron energies of 8.00, 8.55, and 9.00 MeV, reported previously (NCSAC-42) have been analyzed. These data, in conjunction with data for neutron energies of 7.55 and 9.50 MeV, have been compared with the prediction of the Perey-Buck[1] optical model using the equivalent energy-dependent parameters given by Wilmore and Hodgson.[2] There are slight differences between the shape of the experimental curve and the optical-model prediction; however, the differences do not appear to be energy dependent at least in the region from 7.55 to 9.50 MeV. Thus all of our Pb data at a given angle have been used to compute the average difference between theory and experiment. This difference is then applied as a correction to the model calculation. The corrected calculation then provides the normalization for our small-angle collimator data and should provide a slightly better value for the Pb cross section than the original experimental value.

The C, N, and O results are pertinent to the following requests listed in NCSAC-35: 31, 33, 38, 39, and 43.

Measurements of the forward-angle scattering of 7.55 MeV neutrons from Be, C, Al, Fe, Cu, Sn, and W have been made for six angles between 25° and 15°. Analysis of these data is nearly completed.

These data are pertinent to the following requests documented in NCSAC-35: 22, 31, 33, 60, and 98.

---

[1] F.G. Perey and B. Buck, Nucl. Phys. 32, 352 (1963).

[2] D. Wilmore and P.E. Hodgson, Nucl. Phys. 55, 673 (1964).

TABLE A-1

CARBON

θ_L	θ_{cm}	7.40 ± 0.13 σ_{cm}(mb)	% error	θ_L	θ_{cm}	7.55 ± 0.06 σ_{cm}(mb)	% error
2.7°	2.9°	697	7	2.6°	2.8°	718	8
6.8°	7.4°	644	5	6.6°	7.2°	609	5
10.4°	11.3°	584	4	10.4°	11.3°	596	5
14.2°	15.4°	518	4	14.2°	15.4°	534	4
		8.00 ± 0.12 σ_{cm}(mb)	% error			8.55 ± 0.07 σ_{cm}(mb)	% error
2.7°	2.9°	1039	8	2.7°	2.9°	375	8
6.8°	7.4°	885	5	6.8°	7.4°	400	5
10.8°	11.7°	820	5	10.5°	11.4°	320	5
14.1°	15.3°	755	4	14.2°	15.4°	304	4
		9.00 ± 0.10 σ_{cm}(mb)	% error			9.50 ± 0.05 σ_{cm}(mb)	% error
2.7°	2.9°	349	7	2.6°	2.8°	475	7
6.8°	7.4°	332	5	6.6°	7.2°	452	5
10.5°	11.4°	310	5	10.4°	11.3°	411	4
14.2°	15.4°	269	4	14.2°	15.4°	353	4

TABLE A-2

NITROGEN

θ_L	θ_{cm}	7.40 ± 0.13 σ_{cm}(mb)	% error	θ_L	θ_{cm}	7.55 ± 0.06 σ_{cm}(mb)	% error
2.7°	2.9°	594	13	2.6°	2.8°	625	14
6.8°	7.3°	530	9	6.6°	7.1°	537	11
10.4°	11.1°	482	6	10.4°	11.1°	537	8
14.2°	15.2°	434	8	14.2°	15.2°	403	7
		8.00 ± 0.12 σ_{cm}(mb)	% error			8.55 ± 0.07 σ_{cm}(mb)	% error
2.7°	2.9°	656	12	2.7°	2.9°	480	13
6.8°	7.3°	533	9	6.8°	7.3°	400	10
10.8°	11.6°	437	8	10.5°	11.2°	360	8
14.1°	15.1°	389	8	14.2°	15.2°	318	9
		9.00 ± 0.10 σ_{cm}(mb)	% error			9.50 ± 0.05 σ_{cm}(mb)	% error
2.7°	2.9°	453	13	2.6°	2.8°	517	10
6.8°	7.3°	410	10	6.6°	7.1°	415	10
10.5°	11.2°	334	8	10.4°	11.1°	412	7
14.2°	15.2°	263	9	14.2°	15.2°	379	8

TABLE A-3

OXYGEN

θ_L	θ_{cm}	7.40 ± 0.13 σ_{cm}(mb)	% error	θ_L	θ_{cm}	7.55 ± 0.06 σ_{cm}(mb)	% error
2.7°	2.8°	301	22	2.6°	2.8°	365	16
6.8°	7.2°	301	14	6.6°	7.0°	281	14
10.4°	11.1°	298	11	10.4°	11.1°	248	14
14.2°	15.1°	249	11	14.2°	15.1°	165	14
		8.00 ± 0.12				8.55 ± 0.07	
		σ_{cm}(mb)	% error			σ_{cm}(mb)	% error
2.7°	2.8°	356	18	2.7°	2.8°	281	21
6.8°	7.2°	257	15	6.8°	7.2°	325	12
10.8°	11.4°	238	13	10.5°	11.2°	232	12
14.1°	14.9°	164	15	14.2°	15.1°	246	10
		9.00 ± 0.10				9.50 ± 0.05	
		σ_{cm}(mb)	% error			σ_{cm}(mb)	% error
2.7°	2.8°	383	15	2.6°	2.8°	411	13
6.8°	7.2°	338	11	6.6°	7.0°	361	11
10.5°	11.2°	332	8	10.4°	11.1°	303	9
14.2°	15.1°	219	10	14.2°	15.1°	249	11

B. NEUTRON CROSS SECTION SENSITIVITY STUDIES IN OXYGEN, NITROGEN, AND DRY AIR. (N. E. Banks and W. B. Beverly)

The perturbation code SAMCEP[1] is designed to investigate the sensitivity of neutron transport, through complex geometries, to errors or uncertainties in neutron cross sections. Investigations of N^{14} have been reported in NCSAC-38. Sensitivity studies[2] have been performed since that time for the transport of neutrons in oxygen and dry air. ENDF/B Round 1 and Round 2 cross section sets were used in the calculations. The $4\pi r^2$ integrated fast fluence results for a 12.2- to 15.0-MeV source differ at 12 mfp by about 20-30%, with Round 2 predicting the higher results. The spectral results using ENDF/B Round 1 are essentially the same as those predicted by Round 2 in the energy region below 5.0 MeV. Therefore, it is concluded that the spectral results below about 5.0 MeV can be predicted equally well with either cross section set. However, in the energy region between 5.0 and 15.0 MeV the two cross section sets predict differences in spectral results as large as a factor of two at 12 mfp. In weapon effects studies where the shape of the spectral fluence above 5.0 MeV is crucial, the uncertainty in the neutron cross sections used in the transport may be a very important input parameter. A sensitivity investigation[3] was also conducted in uniform nitrogen in which the basic set of cross sections were perturbed. This perturbation led to an increase of approximately 100% in the total fluence at ten mfp when the source of neutrons was monoenergetic at 14.0 MeV.

---

[1] S. Hui, et al., "SAMCEP: An Application of Correlated Monte Carlo to the Simultaneous Solution of Multiple, Perturbed, Time-dependent Neutron Transport Problems in Complex Three-dimensional Geometry", BRL Contract Report No. 62, MAGI MR 7020, January 1972.

[2] N. E. Banks, "Neutron Cross Section Sensitivity Studies for Oxygen, Nitrogen, and Dry Air", BRL Report No. 1583, March 1972.

[3] W. B. Beverly, "Correlated Sampling Monte Carlo Neutron Transport Using SAMCEP: Three Studies", BRL Report (to be published).

YALE UNIVERSITY

A. FAST NEUTRON POLARIZATION STUDIES (F.W.K. Firk, H.L. Schultz, R.J. Holt and R. Nath)

1. Differential Polarization of Neutrons in n-^{12}C Scattering Between 2 and 5 MeV

Measurements of the differential polarization of neutrons elastically scattered from ^{12}C at laboratory angles of 30^{o},50^{o},65^{o},90^{o},110^{o},130^{o} and 150^{o} have been completed at energies between 2 and 5 MeV. The true neutron double-scattering technique was used at angles of 30^{o},50^{o} and 65^{o} for which the energy loss is not too great. The generalized spin precession method was used throughout the energy range: for a fixed value of the solenoidal field, the angles of precession for all neutrons were determined from their measured energies. The angles are shown in Fig. 1 in which the yields of elastically scattered neutrons observed with and without the magnetic field are represented for one of the detectors (at 50^{o}). The reliability of the results derived from the true double-scattering method has been demonstrated by carrying out the following measurements:

i) double-scattering with $\theta_1=\theta_2=30^{o}$ giving the polarization $p(E,30^{o})$

ii) double-scattering with $\theta_1=\theta_2=65^{o}$ giving the polarization $p(E,65^{o})$

and iii) scattering with $\theta_1=65^{o}$ and $\theta_2=30^{o}$ giving the product $p(E,65^{o})\cdot p(E,30^{o})$

Here, θ_1 and θ_2 are the laboratory angles for scattering at the first and second targets, respectively. The results are shown in Fig. 2. It is seen that excellent agreement is obtained for the polarizations deduced in these independent experiments.

The present results are being analyzed using a multi-level reaction theory in order to obtain a definitive set of phase-shifts throughout their energy region.

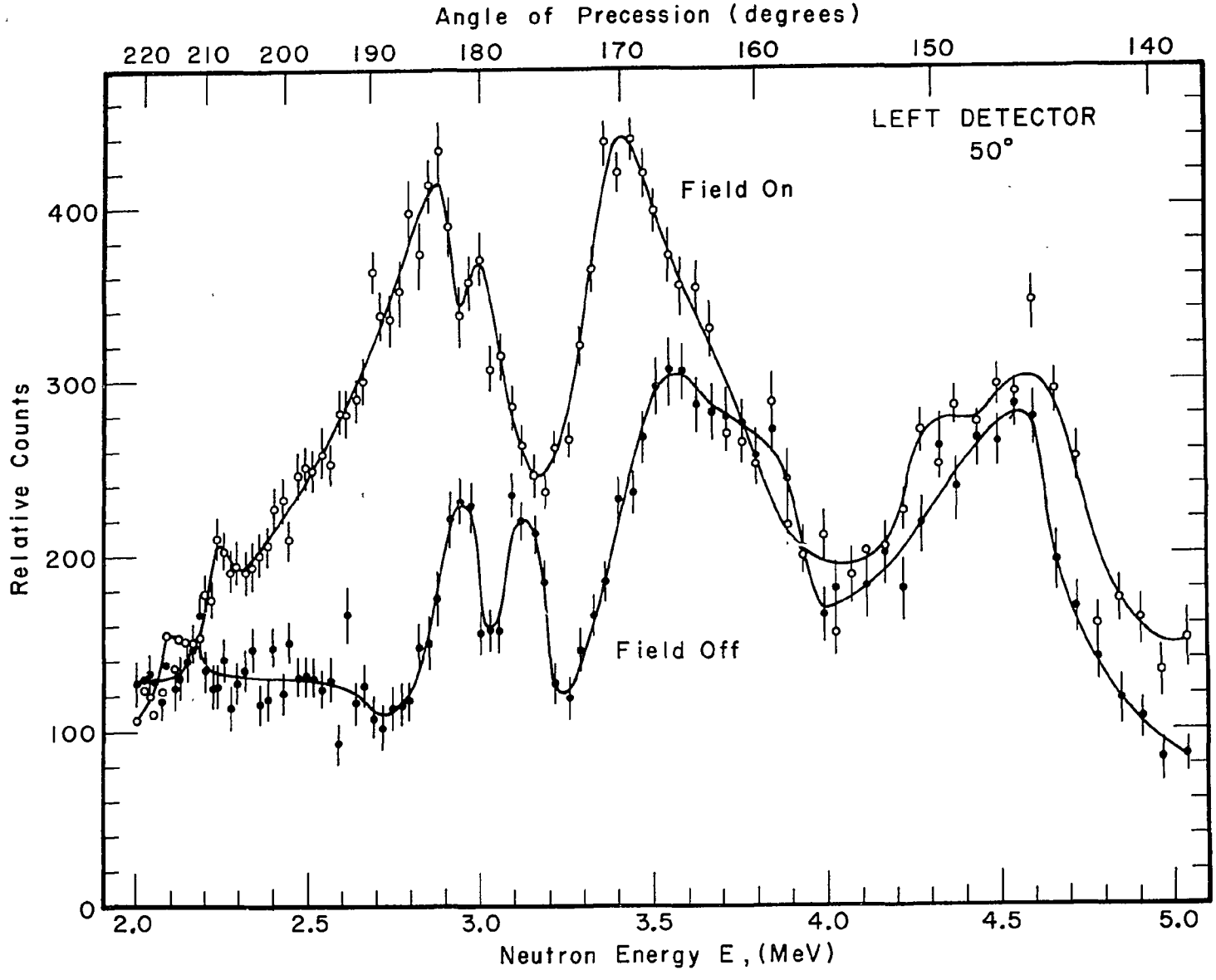
Angle of Precession (degrees)
220 210 200 190 180 170 160 150 140
LEFT DETECTOR
50°
Field On
Field Off
Relative Counts
0
100
200
300
400
2.0
2.5
3.0
3.5
4.0
4.5
5.0
Neutron Energy E, (MeV)

Fig A-1

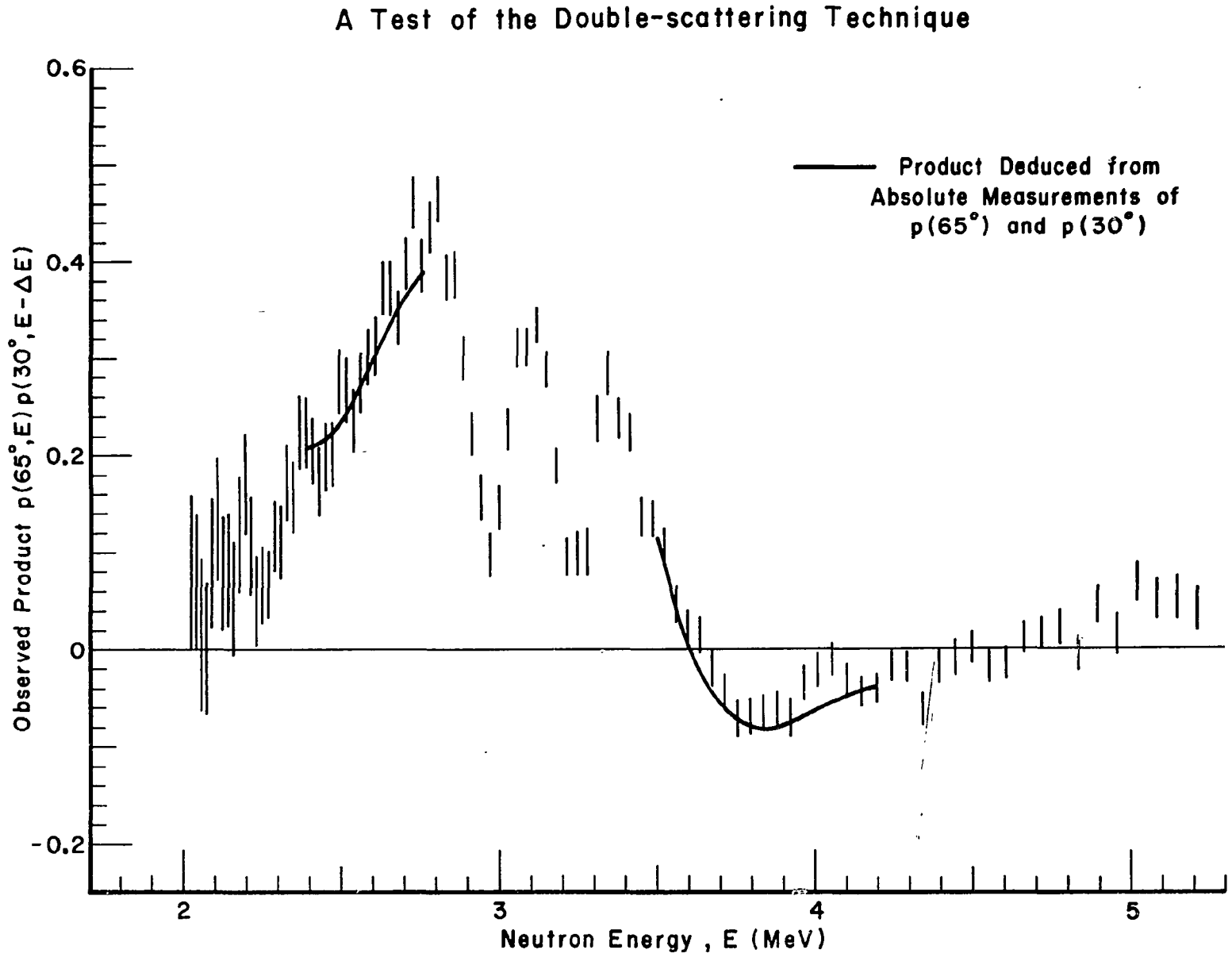
A Test of the Double-scattering Technique
Product Deduced from
Absolute Measurements of
p(65°) and p(30°)
Observed Product p(65°,E)p(30°,E-ΔE)
0.6
0.4
0.2
0
-0.2
2
3
4
5
Neutron Energy , E (MeV)

Fig A-2

2. Differential Polarization of Photoneutrons from the Reaction $^{12}C(\gamma,\vec{n})^{11}C$

Measurements of $d\vec{P}/d\Omega$ at 45^{o} and 90^{o} for the reaction $^{12}C(\gamma,\vec{n})^{11}C$ have been made in the region of the giant dipole states. The most interesting region corresponds to photoneutron energies between 2 and 5 MeV so that the $^{12}C(\vec{n},\vec{n})$ reaction provides a useful polarization analyzer. The results are being analyzed in conjunction with the measured angular distributions of photonucleons.

3. Polarization of Photoneutrons from Deuterium

Work on the polarization of neutrons from the reaction $D(\gamma,n)p$ at 45^{o} and 90^{o} in the photon energy range 7-30 MeV was completed and a paper has been submitted for publication in Nuclear Physics.

B. PHOTONUCLEAR REACTIONS-CHARGED PARTICLES* (J.E.E.Baglin**, R.W. Carr, E.J. Bentz, Jr.†)

1. The analysis of experimental data taken during a previous fiscal period at the Los Alamos EPA has been essentially completed.

i) A paper on $D(\gamma,p)n$ cross sections and angular distributions in the energy range E_γ=17-25 MeV was completed and is being submitted for publication.

ii) A paper on the reaction $^{14}N(\gamma,p_o)$, cross sections and angular distributions, has been submitted to the Physical Review.

iii) Analysis of the excited state cross sections for the reaction $^{14}N(\gamma,p_e)$ is nearing completion .

C. OTHER WORK

1. A table of angular distribution coefficients for (gamma,particle) and (particle,gamma) reactions was published in Nuclear Data Tables* (R.W. Carr and J.E.E.Baglin**)

* Work partially supported by Ames Laboratory-USAEC
** Now at Iowa State University
† Present address, Niels Bohr Institute

2. A paper on the response of the NBS "P-2" Standard Ionization Chamber in intense, pulsed X-ray beams has been submitted to Nuclear Instruments and Methods.* (J.E.E. Baglin**, E.J. Bentz,Jr.†, R.W. Carr and H.L. Schultz)

3. Measurements of the effects of narrow lead collimators on bremsstrahlung spectral shape were made using the $^{16}O(\gamma,n)$ reaction in conjunction with the fast neutron time-of-flight system as a photon spectrometer. The results are now being analyzed. This measurement has an important bearing on our previous absolute cross measurements on the photodisintegration of the deuteron, specifically the reaction $^{2}H(\gamma,p)n$. (R. Nath, F.W.K. Firk and H.L. Schultz)

* Work partially supported by Ames Laboratory-USAEC
** Now at Iowa State University
† Present Address, Niels Bohr Institute